DUST-LANES IN ELLIPTICAL AND LENTICULAR GALAXIES

Ray M. Sharples

Doctor of Philosophy

University of Edinburgh

1982

" If we indulge in fanciful imagination and build world's of our own, we must not wonder at our going wide from the path of truth and nature ..... On the other hand, if we add observation to observation, without attempting to draw not only certain conclusions, but also conjectural views from them, we offend against the very end for which only observations ought to be made "

- William Herschel

TABLE OF CONTENTS

STATEMENT OF ORIGINALITY

The work described in this thesis has not been submitted for any degree, diploma or other qualification at any other university. Some of the observations were carried out in collaboration with Dr. A.J. Longmore, Dr. T.G. Hawarden and Dr. D. Carter. The majority of this research is the author's own work.

Ray M. Sharples

ABSTRACT

A small proportion of elliptical and lenticular galaxies show evidence of well-defined dust-lanes when examined on deep survey plates. New near-infrared (JHK) observations of 46 dust-lane galaxies are presented and compared with those for a sample of 24 morphologically normal systems. Infrared excesses are found preferentially in galaxies which exhibit at least weak signs of a stellar disc ; the physics of the emission mechanism is discussed in the light of additional 3.5 μ observations and published optical spectra. The most extreme properties are those of the heavily obscured edge-on galaxy NGC7172. In this case, the infrared emission is variable on a timescale $\sim$ 0.5 yrs. New optical spectra are also discussed and support the identification of the hard X-ray source H2158-321 with this galaxy.

A restricted sample of 'elliptical-like' galaxies with dust-lanes, but containing no significant luminous disc, has been defined. It is demonstrated that these galaxies cannot be distinguished from a comparable sample of morphologically normal ellipticals on the basis of UBV colours or luminosity. Four examples have been selected for a detailed study of their structure and dynamics. Rotation curves and velocity dispersion profiles have been derived from long-slit spectra using Fourier analysis techniques ; surface photometry was obtained from large-scale photographic plates. The data reduction and analysis techniques are discussed in some detail. In three cases the angular momentum axis of the dust-lane is different from that of the stellar component, favouring an external origin for the dust and gas. Two of the galaxies rotate as rapidly as oblate models with isotropic velocity dispersions ; this property is characteristic of the luminous bulges in disc systems. The orientation of the dust-lane

favours a prolate geometry for one of these bulges. It is demonstrated that the kinematics are inconsistent with two recently published models of prolate galaxies.

CHAPTER 1

INTRODUCTION

The interstellar medium in galaxies plays an important role in their morphology and evolution. Elliptical and lenticular galaxies are particularly interesting in this respect, precisely because they contain very little interstellar matter. The deficiency of gas in these morphological types is a subject which has frequently been discussed in recent literature. As more sensitive surveys of their neutral hydrogen content have become available, the conflict with theoretical estimates of the ambient interstellar medium expected in an old stellar system has increased.

1.1 THE GAS CONTENT OF EARLY-TYPE GALAXIES

From an observational viewpoint, elliptical and lenticular galaxies share many common properties (e.g. Sandage and Visvanathan, 1978b). It is often convenient, therefore, to refer to both morphological types using the term 'early-type galaxies', because of their location at the start of the Hubble sequence.

Elliptical (E) galaxies are now thought to be extremely poor in neutral hydrogen when considered as a class. Upper limits of $M_{HI} < 5.10^6\ M_\odot$ have been placed in certain well-studied cases (Knapp et al, 1979). Nontheless, several examples are known which contain appreciable masses of neutral gas ($\sim 10^8$-$10^9\ M_\odot$), and it has been suggested that elliptical galaxies may have a bimodal distribution of neutral hydrogen content (Sanders, 1980). The deficiency of gas in ellipticals is a serious problem, since normal mass-loss processes (e.g. Cassinelli, 1979) in an old stellar population are expected to contribute 0.1 - 1 $M_\odot$ of gas per year to the ambient interstellar medium of a typical $10^{11}\ M_\odot$ galaxy. Faber and Gallagher (1976) have studied several methods by which this

material may be stored in some unobservable form or, alternatively, completely removed from the galaxy. They conclude that the most satisfactory explanation for the lack of neutral hydrogen in ellipticals is to remove the gas by a hot galactic wind (Matthews and Baker, 1971 ; Bregman , 1978). More recently, some authors have favoured residual star formation as a sink of interstellar material in elliptical galaxies (Oemler and Tinsley, 1979 ; Gunn, Strycker and Tinsley, 1981).

The lenticular (SO) galaxies also cover a wide range in neutral hydrogen content. Examples are known which have HI masses similar to those of late-type spiral and irregular galaxies (e.g. NGC 1553 : M(HI) $\sim 3.10^9 M_\odot$). Taken as a class, however, they are again gas poor (Gallagher et al, 1975 ; Van Woerden, 1977). The HI content of lenticular galaxies is closely related to the controversial problem of their origin. Ablation models (Gunn and Gott, 1972 ; Gisler, 1976), in which SO's are formed by stripping the interstellar material from spiral galaxies, now face several observational difficulties (Dressler, 1980), and it appears that any such mechanism must have occurred predominantly at early epochs (Larson, Tinsley and Caldwell, 1980).

A small proportion ($\sim$ 25%) of elliptical and lenticular galaxies have emission lines in their spectra (Humason, Mayall & Sandage, 1956), indicating the presence of ionized gas. In his study of the statistics of emission-line galaxies, Gisler (1978) also found evidence that the presence of nuclear emission line regions was dependent upon environment (being less frequent in rich clusters). However, the mass of gas implied by the emission-line strengths is small ($< 10^6 M_\odot$), even in the most prominent examples (Minkowski and Osterbrock, 1959 ; Osterbrock, 1960).

1.2 DUST IN EARLY-TYPE GALAXIES

In the Galaxy about 50% of interstellar matter is in the form of molecular hydrogen (Gordon and Burton, 1976). The sensitivities achievable using molecular line receivers are not yet sufficient to

routinely detect molecular gas in elliptical and lenticular galaxies (Johnson and Gottesman , 1979), so a useful additional test for the presence of cool interstellar components in early-type systems is to search for dark matter on optical photographs.

The detection of discrete absorption features in early-type galaxies is helped by the fact that normal systems are characterized by a more or less smooth light distribution. The luminosity profile of most ellipticals can be adequately fitted using a single component $r^{1/4}$ law (Kormendy, 1977) or King model (King, 1978) over a wide range in surface brightness. Lenticular galaxies contain an additional disk component whose brightness profile is approximately exponential (Burstein, 1979 b). Careful study of optical photographs reveals that a small fraction of early-type galaxies have brightness distributions which show evidence of dust absorption. These may have the appearance of well-defined lanes or isolated patches. The presence of weak absorption lanes between the bulge and disk components of SO galaxies has been well documented, and was used by Sandage (1961) as a parameter in his subclassification of the lenticular sequence. More recently, close attention has been paid to the identification of dust features in elliptical galaxies (Bertola and Galletta, 1978 ; Hawarden et al, 1981; Gallagher and Hunter, 1981). Aside from their intrinsic value in the study of interstellar matter in early-type systems, these peculiar galaxies are potentially able to shed light on several important problems in contemporary research.

The prototype dust-lane elliptical, NGC 5128, is associated with the powerful radio source Centaurus A (Bolton et al, 1949). Further observations have shown that the active nucleus in this galaxy is also a strong source of infrared, x-ray and γ-ray radiation (Grindlay,1975). Although this particular galaxy is undoubtedly an extreme example, several dust-lane galaxies are now known which are associated with non-thermal

radio sources. Kotanyi and Ekers (1979) have discussed seven examples in which a double-lobed radio source is orientated almost perpendicular to the dust lane. They infer that the radio source tends to form along the rotation axis of the dust-lane. In the beam model of radio jets proposed by Blandford and Rees (1974) the radio source lies close to the angular momentum axis of an accretion disk surrounding a central super-massive object. A mechanism through which the interaction of cool gas clouds with hot nuclear winds in an elliptical galaxy can fuel the accretion disk has been outlined by Gunn (1979).

Over the last decade a considerable body of photometric and kinematic data has been gathered on early-type galaxies. Contrary to previous expectations they have proved to be remarkably complex systems and no self-consistent picture of all their properties is available at the present time. Observations of the stellar kinematics of early-type galaxies (e.g. Illingworth, 1977 ;Schechter and Gunn, 1979) have demonstrated that most ellipticals cannot be axially symmetric systems flattened by rotation. The bulge components of lenticular galaxies, on the other hand, do appear to be consistent with oblate spheroidal models in which the distribution of random velocities is isotropic (Kormendy and Illingworth, 1981). Detailed surface photometry of ellipticals (Williams and Schwarzschild, 1979) has shown that several have pronounced twists in the orientation of their isophotes, which may be neatly explained if the figure of these galaxies is triaxial (Mihalas and Binney, 1981). Dynamical studies of equilibrium triaxial configurations have relied on numerical models such as those constructed by Schwarzschild (1979) and Miller and Smith (1979). The shape of these models is dominated by highly anisotropic velocity dispersions and in some cases the figure of the entire galaxy may be tumbling end-over-end in an inertial frame.

Gaseous material orbiting in a gravitational potential well will

rapidly settle onto closed orbits due to the dissipative effects of cloud-cloud collisions. The dust lanes in elliptical and lenticular galaxies can therefore be used as probes of the geometry and mass distribution of the stellar component in galaxies. The existence of 'preferred planes' of rotation in oblate and prolate potentials has been investigated by Tohline et al (1981). A combination of differential precession (Kahn and Woltjer, 1959) and frictional losses, tends to align the rotation axis of a gaseous disk with the symmetry axis of the potential. If the figure of the galaxy is rotating, Coriolis forces and resonances may also play an important role (van Albada et al, 1982; Binney, 1981).

The origin of the dust lanes in these galaxies is not fully understood and may be related to the more general problem of the gas content of early-type galaxies as a group. In NGC 5128 the angular momentum properties of the gas (and dust) are very different from those of the stellar component (Graham, 1979), which suggests that the dust lane is very unlikely to have formed from the mass lost by the evolving stars in the galaxy. Several authors have favoured the accretion of material from external sources (Graham, 1979 ; Shane, 1980 ; Raimond et al, 1981) as an alternative origin for the gas. However, sensitive searches for large ($> 10^8 M_\odot$) intergalactic clouds of neutral hydrogen have failed to find a sufficient number to explain the observed neutral hydrogen content of early-type galaxies by this process alone (Lo and Sargent, 1979 ; Haynes and Roberts, 1979). The accretion of gas-rich dwarf galaxies may prove to be a more satisfactory explanation (Silk and Norman, 1979). At the opposite extreme, the ejection of material from an active nucleus has also been proposed as a possible origin for the dust lanes (Rodgers, 1978; Morita and Sakashita, 1979). In principle, careful observations of the kinematics of the dust can distinguish between these two scenarios on angular momentum grounds.

Dusty early-type galaxies do not fit comfortably into the standard morphological classification schemes, and several prominent examples have been included in the IO (de Vaucouleurs et al, 1976) or Irr II (Sandage 1961) class. Krienke and Hodge (1974) found that many galaxies in this group have close companions, and it has been suggested that tidal capture of interstellar material from neighbouring galaxies may play an important role in some systems (Gottesman and Weliachew, 1977; Cottrell, 1977).

1.3 A SAMPLE OF EARLY-TYPE GALAXIES WITH DUST LANES

Early work on the identification of dust-lane galaxies arose from the association of several prominent examples with strong extragalactic radio sources, e.g. Centaurus A (Bolton et al, 1949), Cygnus A (Baade and Minkowski, 1954), Fornax A (Mills, 1954) and 3C272.1 (Wade, 1960). Since then, small surveys of dust-lane galaxies have been discussed by Bertola and Galletta (1978), Kotanyi and Ekers (1979) and Bertola (1981); the most comprehensive study, however, is that of Hawarden et al (1981) who identified 40 galaxies containing prominent dust lanes but no substantial luminous disk.

The source material on which this survey was conducted comprised the ESO/SRC III a J Survey in the south and the II a O Palomar Sky Survey north of declination -33°. The rigorous selection criteria applied to this sample were specifically designed to avoid a strong contamination by disk systems and excluded many of the possible candidates originally identified from the plates. A large fraction of the galaxies rejected from the lists were bona fide lenticular systems with strong dust lanes, and therefore interesting galaxies in their own right. These authors have kindly made the original list of candidates available, from which an independent classification into samples with and without luminous disks has been made.

Table 1.1 lists the restricted sample of 'elliptical-like' galaxies in which no evidence of a luminous disk component was found. The final

TABLE 1.1

The 'restricted' sample of elliptical-like galaxies with dust-lanes in which no evidence of a luminous disc component is found. Column 1 is the galaxy designation using either the standard IAU convention or the identification in the NGC/IC catalogues. This is followed by a P if the galaxy was found on the Palomer survey. Columns 5 and 6 give the (x,y) co-ordinates of the galaxy (measured in mm from the SE corner) on the survey field given in column 4. Major and minor axes (mm) are given in columns 7 and 8 with the position angle (N through E) of the major axis in column 9. Finally, the dust-lane morphology (c.f. Hawarden et al 1981) is in column 10 :

O (oblate) - Dust-lane lies along major axis

P (prolate)- Dust-lane lies along minor axis

S (sphere) - Isophotes appear circular

Sk(skew) - Dust-lane lies along neither symmetry axis

I (irregular)- Dust-lane is complex and/or contorted.

TABLE 1.1

GALAXY	RA	DEC	FIELD	X	Y	a	b	PA	TYPE
IC 1575 P	0 41 0.6	- 4 23 15	-06 0048	335	239	1.1	0.8	135	P
0147-269	1 47 5.6	-26 59 57	477	214	71	1.3	1.1	50	Sk
0151-498	1 51 17.4	-49 48 47	197	255	189	1.9	1.3	0	P
0219-345	2 19 10.5	-34 32 34	355	231	202	1.2	0.8	165	Sk
0418-583	4 18 3.1	-58 22 49	118	234	257	0.5	0.3	35	P
NGC 1947	5 26 29.0	-63 48 7	85	70	239	3.9	3.5	35	P
0609-331	6 9 50.0	-33 7 1	364	67	279	0.8	0.4	105	P
0632-629	6 32 52.4	-62 57 19	87	199	291	1.7	1.2	130	P
0641-412	6 41 52.2	-41 16 44	308	60	107	0.7	0.6	130	O
0711-604	7 11 20.8	-60 25 14	122	91	153	0.7	0.6	55	P
NGC 2534 P	8 8 55.9	55 49 16	+54 0814	268	296	1.1	1.0	-	S
0828+411 P	8 28 7.7	41 6 58	+42 0830	259	150	1.0	0.8	170	P/S
NGC 3108	9 59 28.0	-31 28 7	435	135	88	1.5	1.0	55	Sk
1029-459	10 29 3.0	-45 59 31	263	58	122	2.4	1.7	40	O
NGC 3302	10 33 26.7	-32 6 23	437	299	64	1.5	1.0	125	O
NGC 3528	11 4 49.8	-39 11 50	570	269	220	2.2	1.3	60	O
1118-291	11 18 25.4	-29 7 48	438	44	222	2.0	1.6	30	O
NGC 4583 P	12 35 36.3	33 43 49	+36 1236	230	86	0.5	0.4	90	Sk
NGC 4753 P	12 49 48.4	0 55 52	00 1248	220	157	5.0	2.8	65	I
1307-467	13 7 38.9	-46 43 29	269	147	87	3.0	1.7	60	Sk
1320-324	13 20 7.9	-32 28 21	444	232	45	1.4	1.1	-	S
NGC 5128	13 22 31.8	-42 45 30	270	273	299	39.0	28.0	45	P/Sk
NGC 5266	13 39 56.2	-47 54 49	220	91	290	4.3	2.5	45	P/Sk
IC 4320	13 41 15.5	-26 58 57	509	91	70	1.1	1.1	90	S
1352-336	13 52 37.4	-33 39 25	384	263	250	1.3	0.9	-	S
NGC 5363 P	13 53 36.5	5 29 58	+06 1400	321	171	5.0	2.8	135	P/I
NGC 5485 P	14 5 26.9	55 14 23	+54 1356	127	272	2.0	1.7	145	I
1409+554 P	14 9 34.7	55 25 25	+54 1356	96	286	0.5	0.4	130	O
NGC 5626	14 26 51.5	-29 31 34	447	263	203	1.6	1.2	90	S
1444-304	14 44 27.0	-30 26 9	447	58	153	1.5	0.9	45	Sk
1459-724	14 59 28.6	-72 25 12	67	113	47	1.0	0.8	90	O/Sk
NGC 5799	15 0 27.5	-72 14 17	67	109	56	1.6	1.2	105	Sk
2105-365	21 5 11.7	-36 35 40	402	251	92	0.8	0.6	125	P
NGC 7070A	21 28 34.2	-43 3 48	287	173	282	2.6	2.2	20	Sk
2248+368 P	22 48 44.9	36 49 15	+36 2252	261	193	0.9	0.7	125	P
NGC 7432 P	22 55 34.2	12 51 58	+12 2248	142	197	1.3	0.7	0	P
2350-297	23 50 44.8	-29 43 15	409	287	193	0.6	0.4	-	S
2357-287	23 57 56.8	-28 46 0	409	204	245	0.5	0.5	-	S

selection was based upon a visual inspection of all candidates on the survey plate material. As expected there is considerable overlap with the list of Hawarden et al (1981) since essentially the same selection criteria were used. The 14 galaxies which are not common to both samples are marginal cases and illustrate the necessarily subjective nature of such a classification at some level. A completeness limit for this morphologically-selected sample is difficult to define. Galaxies with diameters less than 0.5 mm ($\sim$ 35 arcsec) on the Schmidt plates have been rejected because of the difficulty in classifying small images (this corresponds to a magnitude cut-off at $m_B \sim$ 15-16 mag). Hawarden et al (1981) have noted that a more serious problem in obtaining complete samples, is the difference in resolution between the IIa O and III a J emulsions. In addition, the deeply exposed survey plates are saturated near the centres of bright galaxies and so small scale nuclear dust lanes like that discovered by Wade (1960) in NGC 4374 may be missed. No attempt was made to extend the survey of Hawarden et al (1981) closer to the galactic plane and the total area scanned remains at approximately 36,500 square degrees or 88% of the sky. That this selection is not a fair sample of the local population of galaxies can be seen in a plot of the apparent ellipticity distribution (Fig 1.1). Axial ratios have been taken from Hawarden et al (1981) or estimated directly from the photographic plates. The deficiency of apparently round galaxies may be attributed to a selection effect in which dust-lanes are difficult to detect if the orientation of the parent galaxy is unfavourable.

The lists have also been searched for the best examples of early-type disk galaxies with dust-lanes. This morphology is considerably more common than that discussed above and no attempt at completeness or homogeneity has been made in the small sample listed in Table 1.2. Most of these galaxies are lenticulars and would be classified as SO_3 or SO_{pec}

Figure 1.1

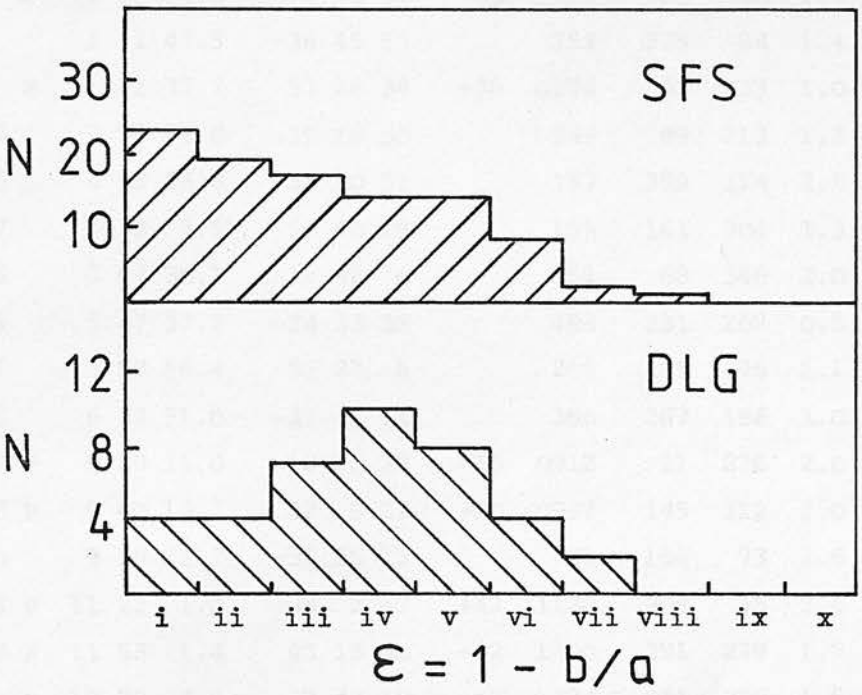

The distribution of apparent flattening for the dust-lane galaxies (DLG: Table 1.1) and a sample of bright ellipticals from Sandage, Freeman & Stokes (SFS : ApJ 160, 831). Values are binned according to the intervals selected by SFS.

Label	ε
i	0.00-0.09
ii	0.10-0.17
iii	0.18-0.26
iv	0.27-0.35
v	0.36-0.44
vi	0.45-0.53
vii	0.54-0.63
viii	0.64-0.72
ix	0.73-0.81
x	0.82-0.90

TABLE 1.2

(As for Table 1.1, but for 32 dust-lane galaxies with discs)

GALAXY		RA	DEC	FIELD	X	Y	a	b	PA	TYPE
0052-326		0 52 32.4	-32 17 53	351	129	323	1.0	0.6	180	SO
IC 1703	P	1 23 51.3	- 1 53 31	00 0112	80	50	1.5	0.6	135	SO
NGC 612		1 31 43.5	-36 45 13	353	225	84	1.4	0.9	165	SO
NGC 662	P	1 41 37.7	37 26 34	+36 0124	48	223	1.0	1.0	-	IO
NGC 1297		3 16 59.0	-19 16 50	547	89	213	1.2	1.1	10	SO
NGC 1546		4 13 33.8	-56 10 51	157	259	114	2.1	1.1	140	SO
0532-527		5 32 3.5	-52 40 29	159	161	304	1.3	1.0	5	SO
NGC 2076		5 44 30.1	-16 48 6	554	68	346	2.0	1.0	45	SO
0547-245		5 47 37.7	-24 33 39	488	231	202	0.5	0.3	50	SO
0557-524		5 57 56.4	-52 27 6	205	196	46	1.1	0.8	80	SO
0639-346		6 39 51.0	-34 41 41	366	267	196	1.0	0.6	135	SO
NGC 2907	P	9 29 15.0	-16 30 28	-18 0912	11	276	2.0	1.0	100	SO/a
NGC 2968	P	9 40 18.2	32 9 22	+30 0932	145	312	2.0	1.3	45	IO
NGC 3100		9 58 28.7	-31 25 13	435	154	73	2.6	1.2	155	SO
NGC 3665	P	11 22 1.0	39 2 12	+42 1130	308	45	2.4	1.5	130	SO
1153+433	P	11 53 1.4	43 19 20	+42 1200	291	279	1.5	0.8	40	SO
NGC 4370	P	12 22 23.2	7 43 13	+06 1224	265	299	1.5	0.8	85	SO
1310-301		13 10 10.1	-30 10 10	443	82	168	1.1	0.4	90	SO
1407-199		14 7 17.5	-19 58 35	578	86	179	0.7	0.4	25	SO
NGC 5525	P	14 13 14.2	14 31 8	+12 1400	66	340	2.2	1.2	30	SO
NGC 5691	P	14 35 19.2	- 0 11 1	00 1424	89	191	1.8	1.2	105	IO
NGC 5719	P	14 38 22.6	- 0 6 15	00 1424	48	196	3.5	1.3	100	Sa
NGC 5745	P	14 42 16.7	-13 44 5	-12 1448	319	107	1.7	0.8	85	SO
IC 5063		20 48 13.4	-57 15 15	144	220	326	2.6	1.9	125	SO
NGC 7066	P	21 23 50.8	13 58 10	+12 2112	84	261	1.0	1.0	-	IO
NGC 7172		21 59 7.2	-32 6 37	466	84	60	2.2	1.4	100	Sa:
NGC 7213		22 6 10.0	-47 24 27	288	85	47	3.6	3.2	40	SO
NGC 7225		22 10 19.6	-26 23 54	532	55	102	2.0	1.0	140	Sa
NGC 7625	P	23 17 59.7	16 57 12	+18 2312	160	95	1.3	1.3	35	SO/a
2323-400		23 23 30.7	-40 2 47	347	81	174	1.1	0.7	105	SO
NGC 7722		23 36 6.4	15 40 44	+18 2336	235	28	2.0	1.8	135	SO
2353-301		23 53 12.7	-30 9 10	409	258	170	0.9	0.4	170	SO

on the revised Hubble system. Some Sa spirals were also included if the dust-lane morphology appeared particularly interesting.

1.4 SUMMARY OF THE PRESENT WORK

Observational aspects of dust in early-type galaxies have previously been restricted to limited studies of individual objects (e.g. Demoulin, 1969 a, b, c; Chromey, 1973, 1974 a,b). Although these have served to illustrate the diversity of form which may be found in dusty galaxies, they have contributed comparatively little to our understanding of these peculiar systems. The availability of a substantial sample of dust-lane galaxies (§ 1.3) suggested that a more comprehensive survey of their observable properties would be most worthwhile. The kinds of problems which could be addressed by such a survey include the following questions : What are the global properties of early-type galaxies with dust lanes and how do they compare with morphologically normal systems ? What percentage of galaxies exhibit these peculiarities ? Do they occur preferentially in low luminosity galaxies where supernova-driven winds are weakest ? Is the active nucleus in NGC 5128 an isolated example or does the presence of interstellar matter in these galaxies somehow favour nuclear activity and in what form ? What are the dynamical properties of dust-lane galaxies ; in particular, is the presence of a minor axis dust lane indicative of minor axis rotation in these systems ? What inferences may be deduced from these observations regarding the origin of the dust lanes ? This thesis contains the results of such a survey carried out in the optical and infrared regions and attempts to answer some of these questions.

We begin in Chapter 2 with a discussion of the near-IR properties of the nuclear regions of a sample of 46 elliptical and lenticular galaxies with dust lanes. Further optical and infrared observations of the galaxy NGC7172 (whose extreme IR-excess was discovered in the course of this work)

follow in Chapter 3. Chapter 4 reviews the optical properties of the disc-less sample (Table 1.1), from which four galaxies have been selected for a detailed study of their kinematic properties (Chapter 5) and surface brightness profiles (Chapter 6). The implications of these observations to studies of the structure and dynamics of elliptical galaxies are discussed in Chapter 7. Finally, a summary of this work and the conclusions which may be drawn from it are given in Chapter 8.

CHAPTER 2

IR OBSERVATIONS OF EARLY TYPE-GALAXIES

WITH DUST LANES

Broad-band photometry of E and SO galaxies at 1.2, 1.65 and 2.2 μ (Johnson 1966a ; Frogel et al, 1975a,c) showed that the infrared flux is usually dominated by emission from late-type stars. Detailed studies of their stellar content have been made by Frogel et al (1975b , 1978) and Aaronson et al (1978a,b) using narrow-band observations of the luminosity-sensitive CO feature at 2.29μ , and the effective-temperature sensitive H_2O band at 1.87 μ. The strong CO and H_2O bands found in E/SO galaxies indicate that most of the light at near-IR wavelengths comes from late-type giants with a mean effective temperature close to that of K and M stars.

Ever since the first detection of the nearby Seyfert galaxy NGC 1068 at infrared wavelengths (Pacholczyck and Wisniewski, 1967), these objects have aroused tremendous interest due to their prodigious energy output in the infrared (Rieke and Low, 1972 ; Rieke 1978). The controversy over the nature of this emission is well-documented (Neugebauer et al, 1976; Stein and Weedman, 1976 ; Rieke and Lebofsky, 1979a). Strong infrared emission has also been detected from the giant radio galaxies Centaurus A (Becklin et al, 1971 ; Kleinmann & Wright 1974; Grasdalen and Joyce 1976) and Cygnus A(Rieke and Low, 1972). It was noted in the previous chapter that these are two of the most well-known examples of early-type galaxies with dust lanes.

Thermal-reradiation by dust grains can be a very efficient means of producing large infrared fluxes. Infrared observations have revealed intense emission from galaxies like M82 and NGC 253 which show evidence of

large amounts of dust on optical photographs. In general, these are spiral or irregular systems, however, and much remains to be learnt about non-stellar emission from the nuclei of early-type galaxies (Rieke and Lebofsky 1979a).

A program of infrared photometry of early-type galaxies with dust lanes was begun in 1979 in collaboration with Dr. A.J. Longmore (Royal Observatory, Edinburgh). The principal aims of this project were to obtain near-infrared colours for the nuclear regions of a sufficient number of these peculiar systems to determine whether the visible presence of dust is correlated with non-stellar infrared emission in early-type galaxies. These observations would be supplemented by longer wavelength studies of any infrared-excess objects, to investigate the nature of the emission mechanism. Suitable candidates were taken from the extended sample of dust-lane galaxies defined in Chapter 1 (i.e including some early-type disk systems).

2.1 OBSERVATIONS AND ERROR ANALYSIS

2.1.1 Observations

Near -IR observations of 46 early-type galaxies with dust-lanes were obtained using the 1.88 m telescope of the South African Astronomical Observatory (SAAO), and the 3.8m UK Infrared Telescope (UKIRT) in Hawaii, during three observing runs in November 1979 (SAAO), January 1980 (UKIRT) and May 1980 (UKIRT). Three separate cryostats were used, all of which employed InSb detectors cooled to pumped nitrogen temperatures. The filter characteristics (Table 2.1) were similar and there does not appear to be any systematic differences between the observations made with each system. Instrumental difficulties during the January 1980 run restricted the observations to J, H and K wavelengths.

TABLE 2.1 Filter characteristics for the UKIRT cryostats, λ_c is the central wavelength and $\Delta\lambda$ the bandwidth (in microns)

Name	λ_c	$\Delta\lambda$
J	1.25	0.3
H	1.65	0.3
K	2.2	0.4
L	3.45	1.05

Standard stars were observed frequently during each night to monitor changes in extinction or instrumental sensitivity. For the northern galaxies the California Institute of Technology (CIT) standards were adopted from Frogel et al (1978). In the south, a recent compilation from the Anglo-Australian Observatory (AAO) was used.

The CIT system has slightly different J filter characteristics than those in use at UKIRT and SAAO. Transformation equations were available from observations with the SAAO 0.75 m telescope during June 1979 and (less reliably) from the two UKIRT runs ; they are consistent with the relations found by Frogel et al (1978) and Jones and Hyland (1980) to within the errors (Figure 2.1). Beam profiles were determined from star drifts across the apertures and the telescope optics were carefully focussed to minimise any differences in the profiles between filters. The effective aperture, as determined from the FWHM (or the total area) of the profile, was approximately 95% of the nominal aperture size.

Since one of the principal aims of this survey was to isolate those galaxies with peculiar infrared colours, a comparison sample of 24

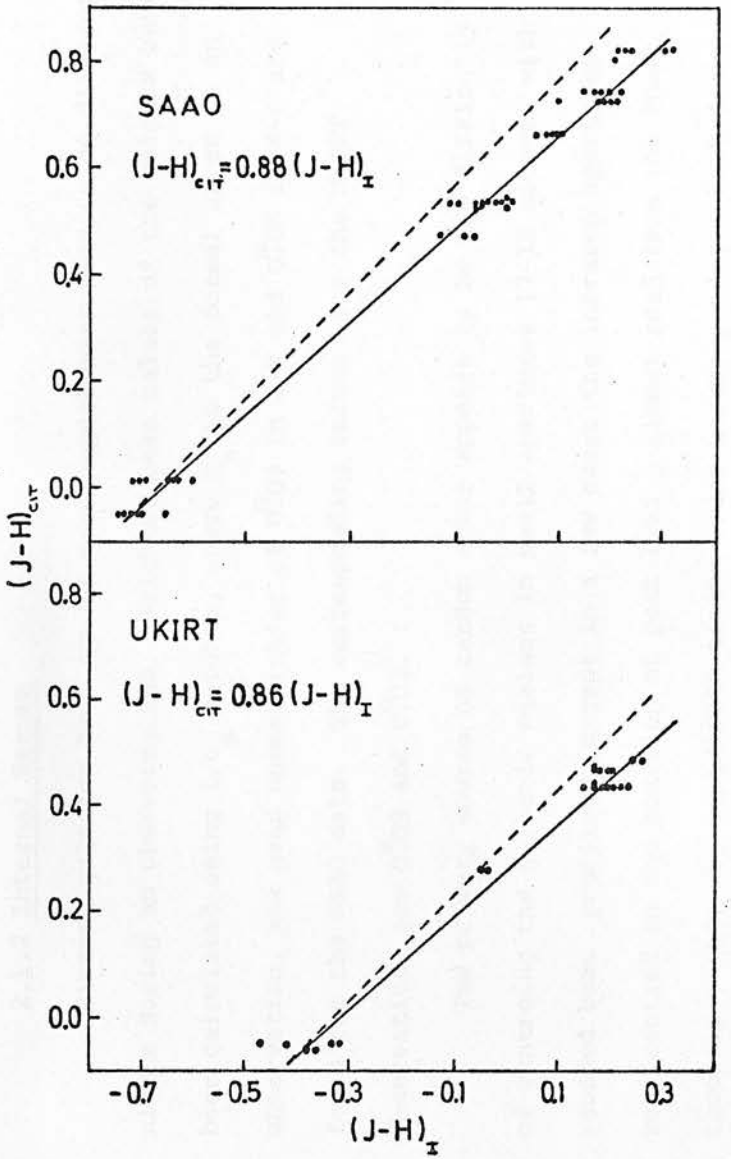

Figure 2.1

Transformation equations between the $(J-H)_{CIT}$ colours of Frogel et al (1978) and the instrumental colour systems at SAAO and UKIRT. The SAAO data were obtained using the Mk II photometer with the 0.75m telescope. Any differences between these filters and those in the Mk I version used on the 1.88m are expected to be negligible (Glass 1981). The solid line is a least squares fit to the data points ; the dashed line has a slope of 45°. Transformation equations to the Johnson (1966 b) system have also been determined by Frogel et al (1978) for the CIT system and Jones and Hyland (1980) for the Mt. Stromlo Observatory (MSO) system (which uses the Caltech filters) :

$$(J-H)_{CIT} = 0.92\ (J-H)_J$$

$$(J-H)_{MSO} = 0.93\ (J-H)_J$$

The similarity of these colour coefficients to those derived from the figure suggests that both the SAAO and UKIRT instrumental colours are on the Johnson system. There do not appear to be any colour-dependent terms in the transformation equations for the H & K filters.

morphologically normal E/SO galaxies was also observed with this same set up.

2.1.2 Internal Errors

Sixteen galaxies have one or more repeat measurements on different nights during an observing run. Weighted mean values of the colours have been calculated using $1/\sigma_s$ weights, where σ_s is the formal error in an observation, and mean uncertainties of $0^m.05$ in J-H and $0^m.06$ in H-K are found for the SAAO data. The corresponding values for the UKIRT observations are $0^m.03$ and $0^m.02$.

The primary source of random error appears to be the difficulty of centreing the galactic nucleus in small apertures (7-12 arcsec) with rounded beam profiles. Except in a few cases the infrared apertures were centred on the position of peak 1.65 μ signal read from the chart recorder ; this may contribute to the lower accuracy of the SAAO data, for which the signal-to-noise (S/N) on the traces and the atmospheric seeing, were both generally poorer. The telescope was mostly offset guided using nearby bright stars.

Four of the galaxies observed during January 1980 were re-observed during May to extend the wavelength baseline to 3.5 μ. The mean colour residuals between these runs were :

$$\langle \Delta(J-H) \rangle = 0.00 \pm 0.03 \ (1\sigma)$$

$$\langle \Delta(H-K) \rangle = 0.01 \pm 0.02 \ (1\sigma)$$

in good agreement with the internal error estimates above.

2.1.3 External Errors

Much of the aperture photometry of normal galaxies in the infrared has involved large beam sizes or relatively poor statistical accuracy (e.g. Grasdalen 1975 ; Glass 1973, 1976) so the estimation of external errors using standard methods is difficult. The mean residuals of four

galaxies in common with the sample of Frogel et al (1978) are :

$$\langle \Delta(J-H) \rangle = 0.00 \pm 0.007 \quad \text{and}$$

$$\langle \Delta(H-K) \rangle = -0.02 \pm 0.021$$

A more statistically significant result may be obtained using the mean colours of the comparison sample :

$$\langle J-H \rangle_o = 0.72 \qquad \langle H-K \rangle_o = 0.22 \qquad (24 \text{ gal})$$

Taking 36 galaxies with small aperture (A < 16".5) measurements from the data of Frogel et al (1978) one finds mean corrected colours of :

$$\langle J-F \rangle_F = 0.73 \qquad \langle H-K \rangle_F = 0.23$$

This close agreement suggests that there are no systematic colour differences between the two data sets.

A comparison of the K magnitudes of the four common galaxies (corrected for reference beam flux where appropriate) suggests that the uncertainty in magnitudes is $\pm 0^m.1$.

2.2 DATA REDUCTION

Several sources of possible systematic effects can be identified (c.f. Frogel et al, 1978).

2.2.1 Reference Beam Corrections

Corrections to the observed colours for the galactic flux in the reference aperture have not been applied. Evidence for radial gradients in the purely infrared colours of E and SO galaxies is currently somewhat ambiguous (Aaronson, 1977) and the implied corrections are in any event very small. In the case of galaxies with a nuclear infrared excess, these corrections would be expected to be less than $0^m.02$, in the sense of making the galaxies bluer.

2.2.2 Galactic Extinction

Galactic extinction corrections have been applied using the cosecant law (Sandage, 1973a) and the van de Hulst reddening curve No.15 (Johnson, 1968). The adopted reddening relations are listed in Table 2.2 ; because of the small size of the extinction at infrared wavelengths, uncertainties due to the choice of reddening law are less than $0^{m}.02$ for the galaxies considered here.

2.2.3 K-Corrections

The K-correction is the magnitude difference between a redshifted and non-redshifted spectral energy distribution, when observed through a fixed wavelength interval. Any program of broad-band filter photometry of distant galaxies must account for the effects of K-corrections if unbiased statements are to be made about their intrinsic parameters.

TABLE 2.2 Corrections for reddening and redshift, where C and C_o are the observed and corrected colours respectively, and

$$C_o = C - E_c - K_c$$

Reddening	Redshift
$A_V = 0.10\ (\mathrm{CSC}\ \lvert b\rvert - 1),\ \lvert b\rvert \lesssim 50^{\circ}$	$K_H = -0.23z$
$A_V = 0.0\ ,\ \lvert b\rvert > 50^{\circ}$	$K_{J-H} = 0.37z$
$E_{V-K} = 0.91\ A_V$	$K_{H-K} = 3.55z$
$E_{J-H} = 0.10\ A_V$	$K_{K-L} = -1.37z$
$E_{H-K} = 0.06\ A_V$	
$E_{K-L} = 0.04\ A_V$	

Derivations of the K-corrections to optical photometry of galaxies have relied on detailed spectrophotometry of the energy distributions of bright nearby galaxies (e.g. Whitford, 1971 ; Oke and Schild, 1971). The K-corrections to near-IR broad-band data are more difficult to determine because of the strong atmospheric absorption outside the filter band-passes. Detailed spectrophotometric observations throughout the 1-5μ region can only be obtained using balloons or aircraft to carry the equipment above most of the atmosphere , and current techniques limit such observations to relatively bright infrared sources. Frogel et al (1978) have used the stellar spectrophotometry from Woolf, Schwarzschild and Rose (1964) to derive K-corrections for broad-band JHK and narrow-band H_2O and CO filters. The availability of a new source of airborne stellar spectrophotometry (Strecker et al, 1979) from 1.2-5.5μ suggested that these corrections should be re-examined and extended to cover the L filter at 3.5μ.

The definition of the K-correction:

$$K_i(z) = 2.5 \log(1+z) + 2.5 \log \left\{ \int_0^\infty F(\lambda)\, S_i(\lambda)\, d\lambda \Big/ \int F\left(\frac{\lambda}{1+z}\right) S_i(\lambda)\, d\lambda \right\} \quad (2.1)$$

(Oke and Sandage, 1968) has been adopted ; $F(\lambda)$ is the (rest frame) energy distribution, $S_i(\lambda)$ the response function of the i^{th} filter and z the redshift. The differences in the computed K-corrections using the spectral energy distributions of αTau ($K5$ III), β And (MO III) and β Peg (M2 II-III) from Strecker et al (1979) are less than $0^m.01$ for $z < 0.03$, which is the range in redshifts of the galaxies in the sample with known velocities. The solution forβ Peg has been adopted, since this is appropriate to the mean spectral type determined from the H-K colours of the comparison sample of morphologically normal galaxies. The results can be adequately represented by linear functions of z over

the range of redshifts required, and are given in Table 2.2.

These corrections are clearly not applicable to a galaxy whose near -IR colours indicate the presence of non-stellar emission at long wavelengths. Studies of the K-corrections appropriate to a galaxy having a cool black-body component superimposed, indicate that K_{H-K} is substantially reduced and K_{K-L} may be reversed in sign. The most critical case for the galaxies with known redshift is NGC 612, whose velocity of 9115 km s^{-1} implies a reduction of the H-K colour from the observed value of $0^m.43$ to $0^m.32$ if the correction from Table 2.2 is adopted. If, however, the J flux from NGC 612 is considered to arise primarily from a stellar component whose near-infrared spectral energy distribution is characterized by the mean colours of the normal galaxy sample, then the excess radiation can be modelled with a black-body thermal spectrum having a colour-temperature of $T \sim 700^{\circ}$ K between 1.65 and 2.2μ, and contributing a maximum of 10% of the total flux in the K-band. The appropriate K-correction is then $K_{H-K} = 2.5z$ or $0^m.08$ in the case of NGC 612.

In general, the observed colours have been corrected using the prescription in Table 2.2, but for the two galaxies with both an infrared excess and $z > 0.015$ (i.e. NGC 612 and NGC 5745) the model-dependent approach described above has been adopted. In the case of galaxies with no published redshift, a value of $z = 0.01$ has been used in computing the corrections, based upon the distribution of known redshifts in the sample.

2.3 RESULTS

The final JHKL colours, corrected for reddening and redshift, are presented in Table 2.3 for 46 early-type galaxies with dust lanes. All measurements made on the AAO (Johnson) system have been transformed to the CIT system. Revised morphological types T have been taken from de Vaucouleurs, de Vaucouleurs and Corwin (1976, hereinafter RC2) where

TABLE 2.3 : Corrected JHKL colours for 46 early-type galaxies with dust lanes. Column 1 is the galaxy designation ; column 2 is a morphological-type parameter, following the RC2 ; columns 3 and 4 contain the galactic latitude and the redshift, taken from the RC2 when available ; column 6 is the nominal focal-plane aperture size in arcseconds. Uncertain quantities are denoted by a colon (:).

NEAR-INFRA-RED OBSERVATIONS OF DUST-LANE GALAXIES

Galaxy	T	$\|b^{II}\|$	Z	Tel	Aper (")	K	$(J-H)_o$	$(H-K)_o$	$(K-L)_o$	
IC1575	-5	67.0	0.0188[2]	SAAO	12.0	12.04	0.65 :	0.22:	-	
U0052-326	-1	55.0	-	SAAO	12.0	11.97	0.73	0.28	-	
IC1703	-1	63.1	0.0188	UKIRT	7.2	11.93	0.75	0.22	-	
NGC 612	-2	77.0	0.0304	SAAO	12.0	10.84	0.72	0.34	-	R
NGC 662	1	24.0	-	UKIRT	7.2	12.73	0.79	0.21	-	
U0147-270	-3	77.1	-	SAAO	12.0	12.02	0.66	0.24	-	
U0151-498	-5	64.3	0.0206[2]	SAAO	12.0	10.68	0.69	0.26	-	
U0219-345	-5	69.5	-	SAAO	12.0	11.43	0.68	0.25	-	
NGC 1297	-3	55.2	0.0052	SAAO	12.0	11.21	0.61	0.24	-	U
NGC 1546	-2	43.8	0.0038	SAAO	12.0	10.50	0.66	0.22	-	
U0418-583	-5	42.5	-	SAAO	12.0	12.84	0.75 :	0.21	-	
NGC 1947	-3	33.4	0.0030	SAAO	12.0	9.89	0.69	0.28	0.67:	
U0532-527	-2	32.9	-	SAAO	12.0	11.42	0.88	0.33	-	
NGC 2076	-1	21.5	-	UKIRT	7.2	10.68	0.97	0.35	0.41:	
U0547-245	-1:	23.8	-	UKIRT	7.2	12.65	0.71	0.18	-	
U0632-629	-5	26.0	-	SAAO	12.0	11.33	0.70	0.30	-	
P0828+411	-5	35.6	-	UKIRT	7.2	12.51	0.78	0.19	-	
NGC 2907	1	24.6	0.0069[1]	UKIRT	7.2	9.97	0.77	0.21	-	U
NGC 2968	0	49.0	0.0054	UKIRT	7.2	10.48	0.75	0.26	-	R
NGC 3528	-3	37.0	0.0123[2]	UKIRT	7.2	10.60	0.76	0.20	0.36	
NGC 3665	-2	32.9	0.0067	UKIRT	7.2	10.12	0.77	0.32	0.31	R
P1153+433	-2	70.5	-	UKIRT	7.2	11.93	0.76	0.36	0.88:	
NGC 4370	1	69.3	0.0026[2]	UKIRT	7.2	11.36	0.88	0.30	0.46:	U
NGC 4374	-5	33.1	0.0031	UKIRT	7.2	9.33	0.72	0.20	-	R
NGC 4583	-5	83.1	-	UKIRT	10.8	11.42	0.72	0.17	-	
NGC 4753	0	61.7	0.0042	UKIRT	10.8	9.52	0.86	0.28	0.25	

TABLE 2.3 (Cont'd)

Galaxy	T	$\|b^{II}\|$	Z	Tel	Aper (")	K	$(J-H)_o$	$(H-K)_o$	$(K-L)_o$	
U1310-302	-1:	32.2	-	UKIRT	7.2	11.80	0.80	0.27	-	
IC4320	-5	34.2	0.0225[2]	UKIRT	10.8	11.51	0.76	0.21	-	
U1352-336	-5	27.1	0.0152[2]	UKIRT	7.2	11.78	0.72	0.17	-	
NGC 5363	0	63.2	0.0038	UKIRT	10.8	9.16	0.83	0.26	0.25	R
NGC 5485	-2	59.0	0.0066	UKIRT	10.8	10.67	0.69	0.19	0.57:	U
U1407-199	-1	39.0	-	UKIRT	7.2	12.38	0.87	0.37	-	
NGC 5525	-1	66.6	-	UKIRT	10.8	11.01	0.77	0.27	0.25	
NGC 5626	-2:	28.4	0.0231[2]	UKIRT	10.8	11.14	0.76	0.19	-	
NGC 5691	0:	52.5	-	UKIRT	7.2	12.92	0.65	0.21	-	
NGC 5719	1	52.0	0.0059[2]	UKIRT	10.8	10.14	0.90	0.39	0.55	
NGC 5745	-1	40.6	0.0243[2]	UKIRT	10.8	10.94	0.81	0.33	0.31	
IC5063	-3	38.7	0.0116	SAAO	9.0	10.70	0.73	0.35	1.55	R
NGC 7066	0	25.3	-	UKIRT	10.8	11.39	0.72	0.22	0.22	
NGC 7070A	0	47.0	0.0077[2]	SAAO	12.0	11.33	0.70	0.26	-	
NGC 7172	1	53.0	0.0088	SAAO	12.0	9.79	0.91	0.71	-	
					9.0	10.03	0.97	0.74	1.33	
NGC 7213	1	52.6	0.0059	SAAO	12.0	9.12	0.73	0.37	0.93	R
NGC 7225	1	54.7	0.0160[2]	SAAO	12.0	10.45	0.83	0.39	0.48	
NGC 7432	-2	41.3	-	SAAO	12.0	11.52	0.65	0.35	-	
NGC 7625	1	40.5	0.0055	SAAO	12.0	11.00	0.68	0.35	-	R
NGC 7722	1	43.7	-	SAAO	12.0	11.62	0.75	0.26	-	

Notes:

1. Sandage A.J. 83, 709.
2. SAAO redshift (Chapter 4).

TABLE 2.4 : Corrected JHKL colours for 24 morphologically normal galaxies. Column 1 is the galaxy designation ; column 2 is a morphological-type parameter, following the RC2 ; columns 3 & 4 contain the galactic latitude and the redshift, taken from the RC2 when available ; column 6 is the nominal focal-plane aperture size in arcseconds. Uncertain quantities are denoted by a colon (:).

NEAR-INFRA-RED OBSERVATIONS OF MORPHOLOGICALLY NORMAL GALAXIES

Galaxy	T	$\lvert b^{II} \rvert$	Z	Tel	Aper (")	K	$(J-H)_o$	$(H-K)_o$	$(K-L)_o$
NGC 1167	-3	20.5	0.0157	UKIRT	7.2	11.07	0.76	0.18	-
NGC 2329	-3	22.8	0.0192	UKIRT	7.2	11.20	0.72	0.19	-
NGC 2911	-2	40.6	0.0106	UKIRT	7.2	10.67	0.80	0.22	-
NGC 4272	-5	82.4	0.0024	UKIRT	7.2	11.61	0.71	0.28	-
NGC 4278	-5	82.8	0.0022	UKIRT	7.2	9.49	0.70	0.21	-
NGC 4486	-4	74.9	0.0042	UKIRT	7.2	10.09	0.72	0.25	-
NGC 2749	-5	37.5	0.0141	UKIRT	7.2	10.80	0.67	0.20	-
NGC 4472	-5	70.2	0.0030	UKIRT	7.2	9.45	0.72	0.22	-
NGC 984	-1	33.6	-	UKIRT	10.8	10.71:	0.76	0.18	-
NGC 1497	-2	21.8	-	UKIRT	10.8	10.96	0.74	0.25	-
NGC 3078	-5	21.8	0.0084	UKIRT	10.8	9.63	0.71	0.18	-
NGC 3998	-2	60.1	0.0038	UKIRT	10.8	8.99	0.72	0.19	-
NGC 4552	-5	74.9	0.0008	UKIRT	10.8	8.93	0.73	0.20	-
NGC 1587	-5	30.5	0.0130	SAAO	12.0	10.09	0.68	0.20	-
NGC 1588	-5	30.5	0.0113	SAAO	12.0	10.76	0.68	0.22	-
NGC 1404	-5	53.6	0.0064	SAAO	12.0	9.00	0.66	0.21	0.12:
NGC 1399	-5	53.6	0.0048	SAAO	12.0	9.05	0.71	0.21	-
NGC 1052	-5	57.9	0.0048	SAAO	12.0	9.27	0.70	0.26	0.35
NGC 2332	-5	23.6	-	UKIRT	7.2	11.03	0.74	0.22	-
IC 708	-5	63.4	-	UKIRT	10.8	11.37	0.71	0.26	0.18:
NGC 4278	-5	82.8	0.0022	UKIRT	10.8	9.31	0.70	0.20	0.17:
NGC 5444	-3	72.7	0.0132	UKIRT	10.8	10.43	0.72	0.20	0.14
NGC 741	-5	53.7	0.0185	UKIRT	5.1	11.24	0.72	0.25	0.19[1]
NGC 7173	-5	53.1	0.0083	UKIRT	7.2	10.47	0.76	0.19	0.22

Notes: (1) L' : $\lambda_c = 3.82\ \mu$, $\Delta\lambda = 0.60$

possible, or estimated from the survey plates. Data for the comparison sample of 24 morphologically normal galaxies is listed in Table 2.4.

The properties of the dust lane galaxies can be usefully summarized in terms of the JHK and JKL two-colour diagrams (c.f. Glass 1976, 1979 ; Ward et al, 1981), and the distribution of galaxies in these two planes will now be discussed in turn.

2.3.1 JHK Colours

In Figure 2.2, galaxies from Tables 2.3 and 2.4 are plotted. A cursory examination of this figure indicates that the dust-lane galaxies form a very heterogeneous group in terms of their near-infrared colours. About two thirds of the sample are indistinguishable from normal galaxies in the JHK plane. The remaining galaxies with red colours are identified explicitly in Figure 2.2. Eight of them have residuals which are consistent with simple reddening estimates on the basis of the standard van de Hulst extinction curve. In one case, NGC 2076, this internal reddening reaches $A_V \simeq 2^m.5$. Redshifts are known for all of the very red galaxies except NGC 2076, UO532-527, NGC 7432 and P 1153 + 433. Uncertainties in the K-corrections therefore, cannot in general be responsible for the colour residuals. Many of these galaxies have at least one repeat measurement, and the colours are confirmed in each case.

Since most of the galaxies in the figure have been observed using a single aperture size, it is not possible to normalize the colours to a uniform effective aperture (i.e. one scaled to the apparent diameter of a galaxy) as for example Frogel et al (1978) have done. If the mean colour gradients from their work are adopted, however, the systematic effects for the range of diameters in the present sample are less than $0^m.05$ in J-H and $0^m.03$ in H-K. Galaxies containing nuclear infrared sources usually exhibit strong colour gradients (Aaronson, 1977 ; Glass, 1981) because the flux becomes increasingly dominated by the

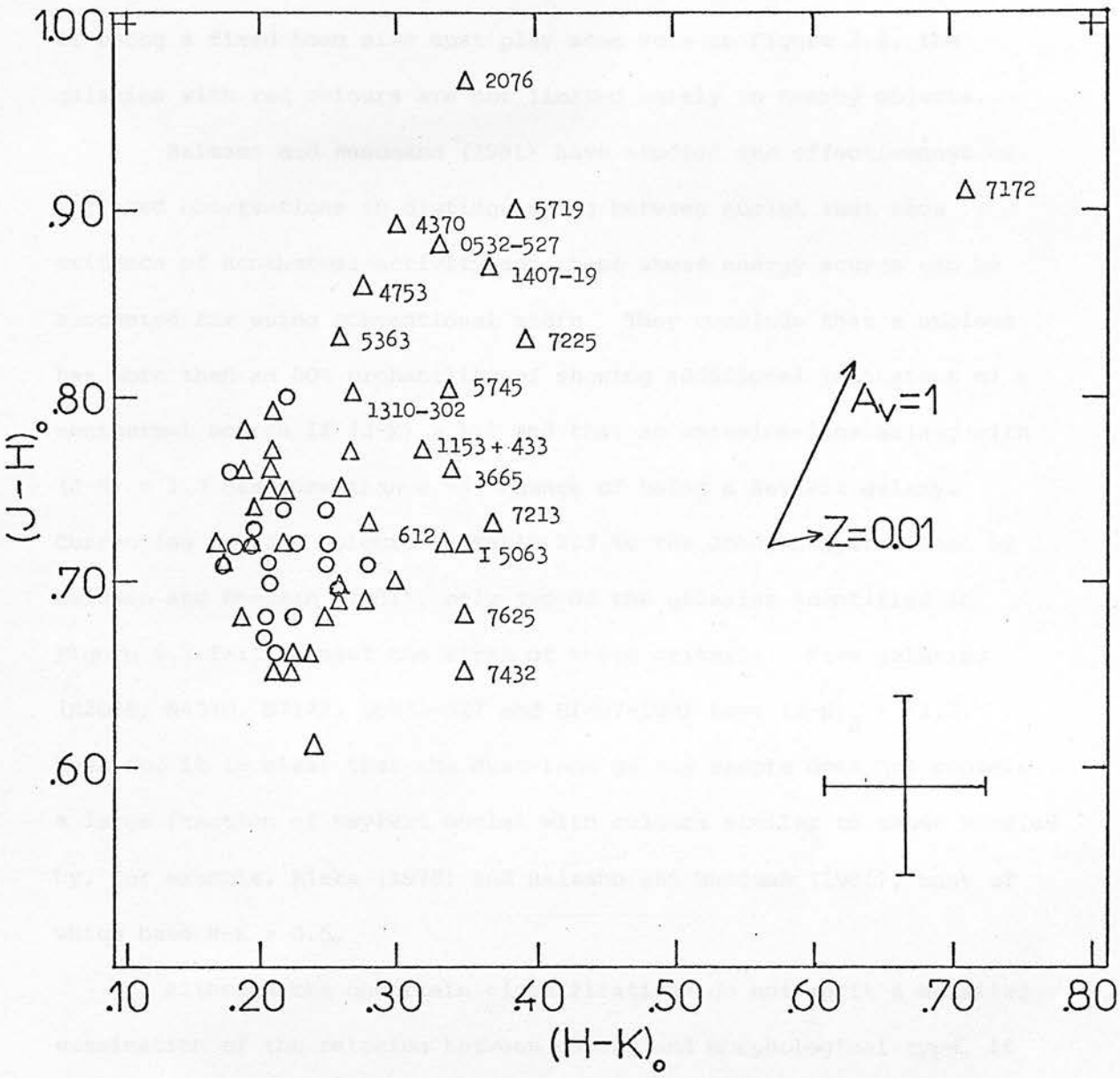

Figure 2.2

The distribution of early-type galaxies with normal (o) and dust-lane morphologies (Δ) in the JHK plane. Galaxies with large residuals from the distribution of normal galaxies are denoted explicitly. The arrows indicate the change in the observed colours of a galaxy when reddened with a van de Hulst ※15 law and $A_v = 1$, or redshifted by $\Delta_z = 0.01$. Error bars are the assigned nominal errors for a single observation of the SAAO galaxies only.

stellar population at large effective apertures. Although the effect of using a fixed beam size must play some role in Figure 2.2, the galaxies with red colours are not limited solely to nearby objects.

Balzano and Weedmann (1981) have studied the effectiveness of infrared observations in distinguishing between nuclei that show evidence of nonthermal activity and those whose energy source can be accounted for using conventional stars. They conclude that a nucleus has more than an 80% probability of showing additional indicators of a nonthermal source if (J-K) > 1.1 and that an emission-line galaxy with (J-K) > 1.3 has more than a 95% chance of being a Seyfert galaxy. Correcting the J-H colours in Table 2.3 to the Johnson system used by Balzano and Weedman (1981), only two of the galaxies identified in Figure 2.2 fail to meet the first of these criteria. Five galaxies (N2076, N4370, N7172, UO532-527 and U1407-199) have $(J-K)_J > 1.3$. Even so, it is clear that the dust-lane galaxy sample does not contain a large fraction of Seyfert nuclei with colours similar to those studied by, for example, Rieke (1978) and Balzano and Weedman (1981), many of which have H-K > 0.5.

Although the uncertain classifications do not merit a detailed examination of the relation between colour and morphological type, it is noticeable that all of the galaxies with large colour residuals are from the later types ($T \geq -3$) in the sample. An equivalent statement is that there are no disk-less systems with very red colours (assuming the dust-lane itself is not interpreted as constituting a disk). This is well-illustrated in Figure 2.3, where the frequency distribution histogram of H-K colours is plotted. Spheroidal (T = -5) and disk-systems are given separately - dust lane galaxies in Figure 2.3(b) and those from comparable studies of early-type systems (Aaronson, 1977 ; Frogel et al, 1978) in Figure 2.3(a).

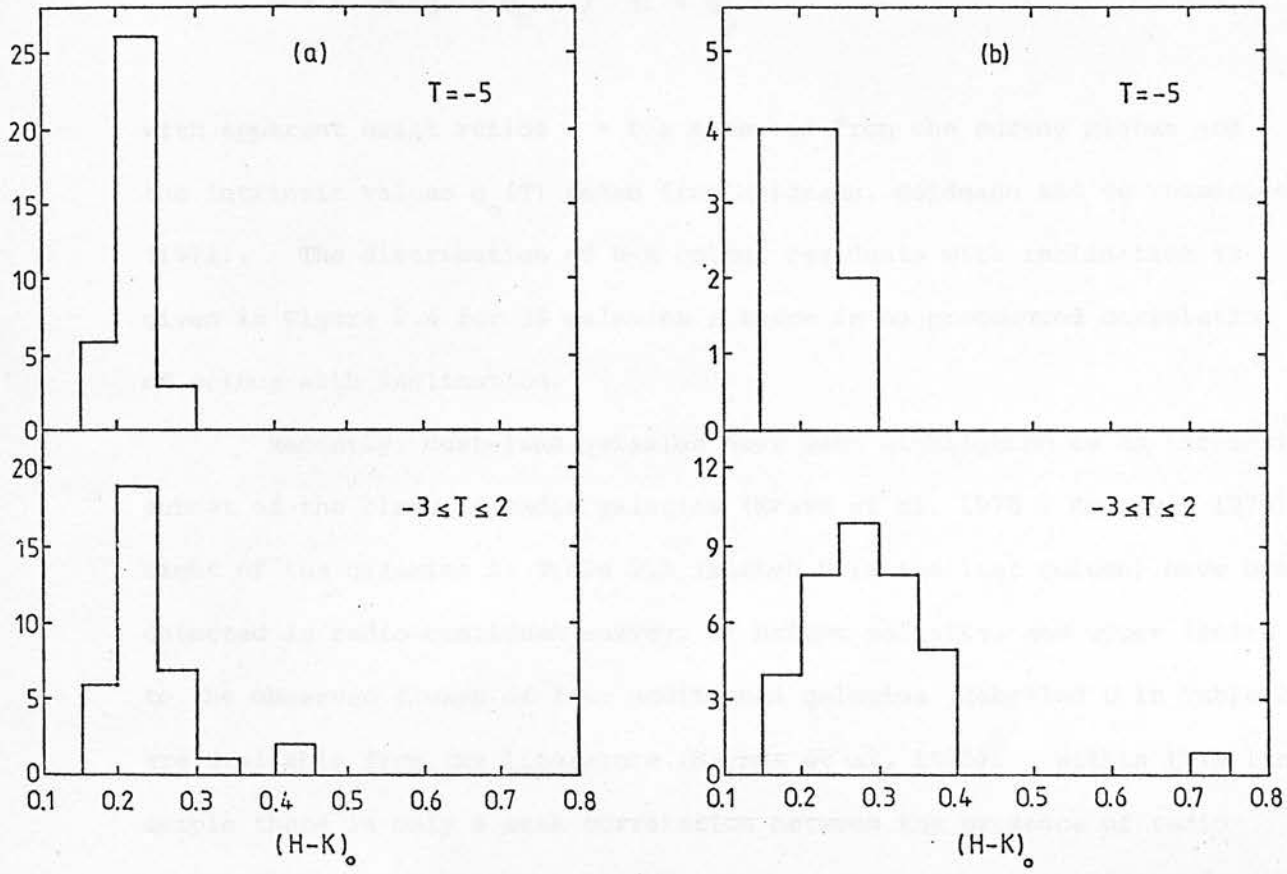

Figure 2.3

Frequency distribution histograms of (H-K) colour indices from

(a) the data of Aaronson (1977) and Frogel et al (1978) combined

(b) this work

Spheroidal (T = -5) and disk ($-3 \lesssim T \lesssim 2$) systems are plotted separately.

For the galaxies with disks, one may also look for correlations between infrared colour and inclination. The inclinations of all galaxies with $T \gtrsim -3$ have been estimated using the Hubble (1926) formula

$$\cos^2 i = (q^2 - q_o^2) / (1 - q_o^2) \qquad (2.2)$$

with apparent axial ratios $q = b/a$ measured from the survey plates and the intrinsic values $q_o(T)$ taken from Heidmann, Heidmann and de Vaucouleurs (1972). The distribution of H-K colour residuals with inclination is given in Figure 2.4 for 35 galaxies ; there is no pronounced correlation of colour with inclination.

Recently, dust-lane galaxies have been highlighted as an interesting subset of the class of radio galaxies (Ekers et al, 1978 ; Kotanyi, 1979). Eight of the galaxies in Table 2.3 (marked R in the last column) have been detected in radio continuum surveys of bright galaxies, and upper limits to the observed fluxes of four additional galaxies (labelled U in Table 2.3) are available from the literature (Haynes et al, 1975). Within this limited sample there is only a weak correlation between the presence of radio continuum emission and red JHK colours. Furthermore, several of the galaxies in the comparison sample (which all have normal near-infrared colours) contain compact radio cores (Condon and Dressel, 1978).

2.3.2 JKL Colours

It is not possible with JHK data alone to establish the nature of the very red galaxies. All of the observations illustrated in Figure 2.2 can be explained by combinations of reddening and thermal re-radiation by dust. In fact by varying the relative spatial distribution of dust and stars, much of Figure 2.2 can be reproduced by reddening alone. Longer wavelength observations enable further constraints to be placed on the astrophysical processes involved, and to this end 3.5μ measurements of

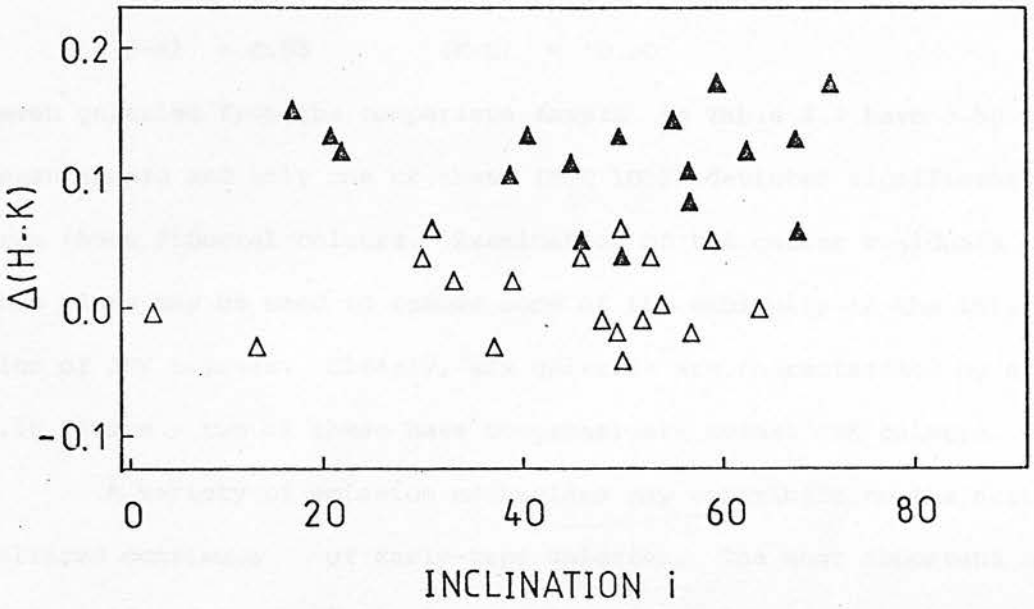

Figure 2.4

A colour-inclination plot for 35 galaxies with morphological type parameter $T \geq -3$. H-K is the [1.65μ] - [2.2 μ] colour corrected for redshift and galactic reddening and i is the inclination angle (i = 0 is face-on) described in the text. The galaxies labelled explicitly in Fig 2.2 are denoted ▲.

several galaxies in the sample were obtained. The L observations are considerably more difficult to make than those at shorter wavelengths, and the estimated mean error in the (K-L) colours is $0^m.1$. The distribution of galaxies in the JKL plane (Figure 2.5) is not representative, since it is heavily weighted by the galaxies with very red colours in the JHK sample. An old stellar population (appropriate to E/SO galaxies) would have (Johnson, 1966b) :

$$(J-K) = 0.95 \qquad (K-L) = 0.20$$

Seven galaxies from the comparison sample in Table 2.4 have 3.5μ measurements and only one of these (NGC 1052) deviates significantly from these fiducial colours. Examination of the colour residuals in this plane may be used to remove some of the ambiguity in the interpretation of JHK colours. Clearly, six galaxies are characterized by strong 3.5μ fluxes ; two of these have comparatively normal JHK colours.

A variety of emission mechanisms may contribute to the near-infrared continuum of early-type galaxies. The most important ones are considered in the following section along with some more general reddening models.

2.4 MODELLING AND INTERPRETATION

The information content of broad-band filter photometry is necessarily somewhat less detailed than that obtained using spectroscopic or panoramic instruments. The problem inherent to the interpretation of this data is therefore to construct a sufficiently general (possibly composite) model without introducing too many poorly-constrained free parameters. The approach adopted has been to investigate the systematic effects of a few of the most important physical processes on the infrared colours of a normal old stellar population characterized by the fiducial colours :

$$(J-H) = 0.72 \quad (H-K) = 0.23 \quad (K-L) = 0.20 \qquad (2.3)$$

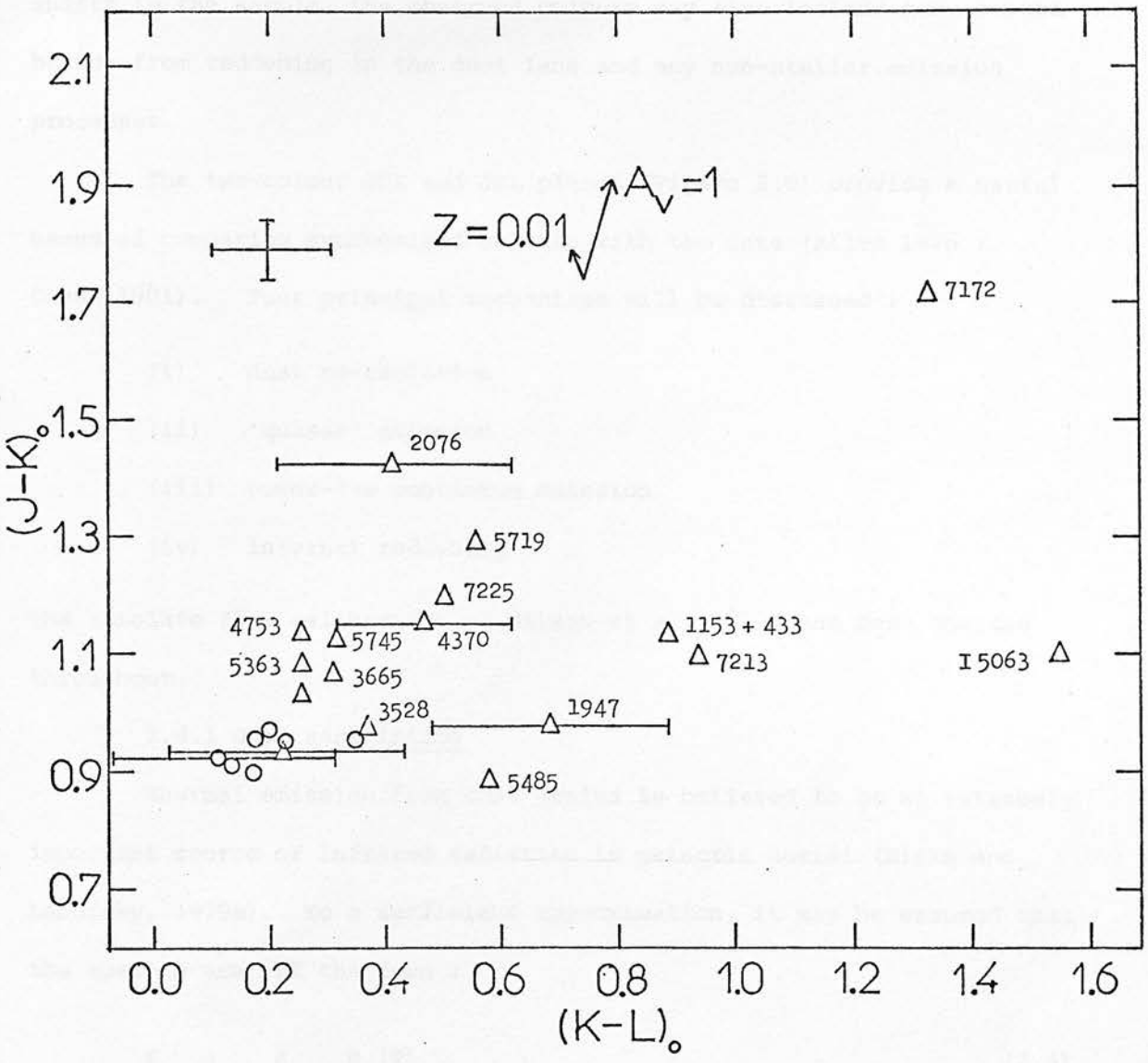

Figure 2.5

The distribution of early-type galaxies with normal (o) and dust-lane (Δ) morphologies in the JKL plane. The arrows and error bars have the same meaning as in Fig 2.2. Individual error estimates have been plotted when the statistical uncertainty in the (K-L) colour exceeds $0^m.1$.

Since the apertures are sampling the light from within a circle of radius 0.5 - 5 kpc (for H_o = 50 kms^{-1} Mpc^{-1}) over the range of redshifts in the sample, the observed colours may also include some contribution from reddening in the dust lane and any non-stellar emission processes.

The two-colour JHK and JKL planes (Figure 2.6) provide a useful means of comparing synthesized colours with the data (Allen 1976 ; Glass 1981). Four principal mechanisms will be discussed :

(i) dust re-radiation

(ii) 'quasar' emission

(iii) power-law continuum emission

(iv) internal reddening

The absolute flux calibration of Wilson et al (1972) has been adopted throughout.

2.4.1 Dust Reradiation

Thermal emission from dust grains is believed to be an extremely important source of infrared radiation in galactic nuclei (Rieke and Lebofsky, 1979a). To a sufficient approximation, it may be assumed that the spectra are of the form :

$$f_\nu \alpha \varepsilon_\nu B_\nu(T) \qquad (2.4)$$

where $\varepsilon_\nu \alpha \nu^n$, $B_\nu(T)$ is the Planck function and $0 < n < 2$ for commonly considered grains (e.g. Aannestad, 1975). Broad-band colours for two dust models (at $T = 600^o$ K and 1000^o K) with black-body emissivity have been calculated by convolving spectra of the form given by equation 2.4 with the transmission functions of the UKIRT JHKL filters.

The effect of adding these sources to a 'standard galaxy' component is shown in Figure 2.6, where the distance between the tick marks represents

Figure 2.6

The effects of non-stellar emission processes and internal reddening on the near-IR colours of a normal galaxy component with :

$$J-H = 0.72 \qquad H-K = 0.22 \qquad K-L = 0.20.$$

Two dust-reradiation models with black-body emissivities are shown, for T = 600 and 1000° K. Tick marks indicate an increase of 10% in the contribution of the source to the observed 2.2μ flux, and the arrow shows the change in colour if an emissivity of the form $\varepsilon_\nu \propto \nu^2$ is used. The effect of adding a quasar, with mean colours from Hyland and Allen (1981), to a normal galaxy is also given. The locus of power-law continua $f_\nu \propto \nu^\gamma$ contributing 50% of the observed 2.2 μ flux is shown by the long-dashed line, and is labelled by the value of γ. Two reddening models are illustrated:

A) a simple dust screen
B) an exponential distribution of stars and dust with scale lengths of 3 and 1.5 Kpc respectively.

The tick marks on these lines indicate $\tau_V^{\frac{1}{2}}$ - the optical depth at λ5600 Å to the centre of the galaxy. The effect of the covering factor on model B with $\tau_V^{\frac{1}{2}} = 10$ mag is shown by the short-dashed line, with a tick mark indicating the predicted colours when 50% of the observed K flux comes from the unreddened galaxy.

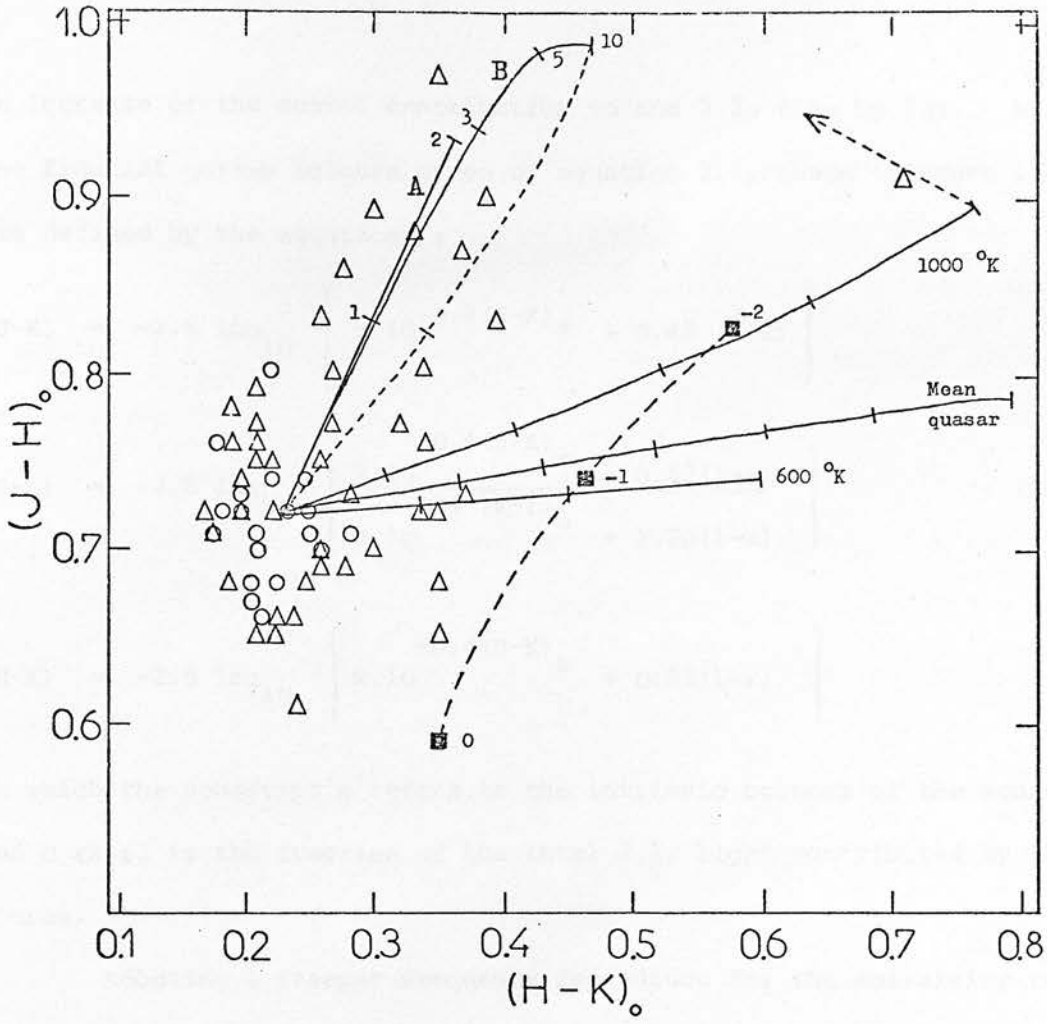
1.0
0.9
0.8
0.7
0.6
$(J-H)_o$
0.1
0.2
0.3
0.4
0.5
0.6
0.7
0.8
$(H-K)_o$
A
B
1
2
3
5
10
-2
-1
0
1000 °K
600 °K
Mean
quasar

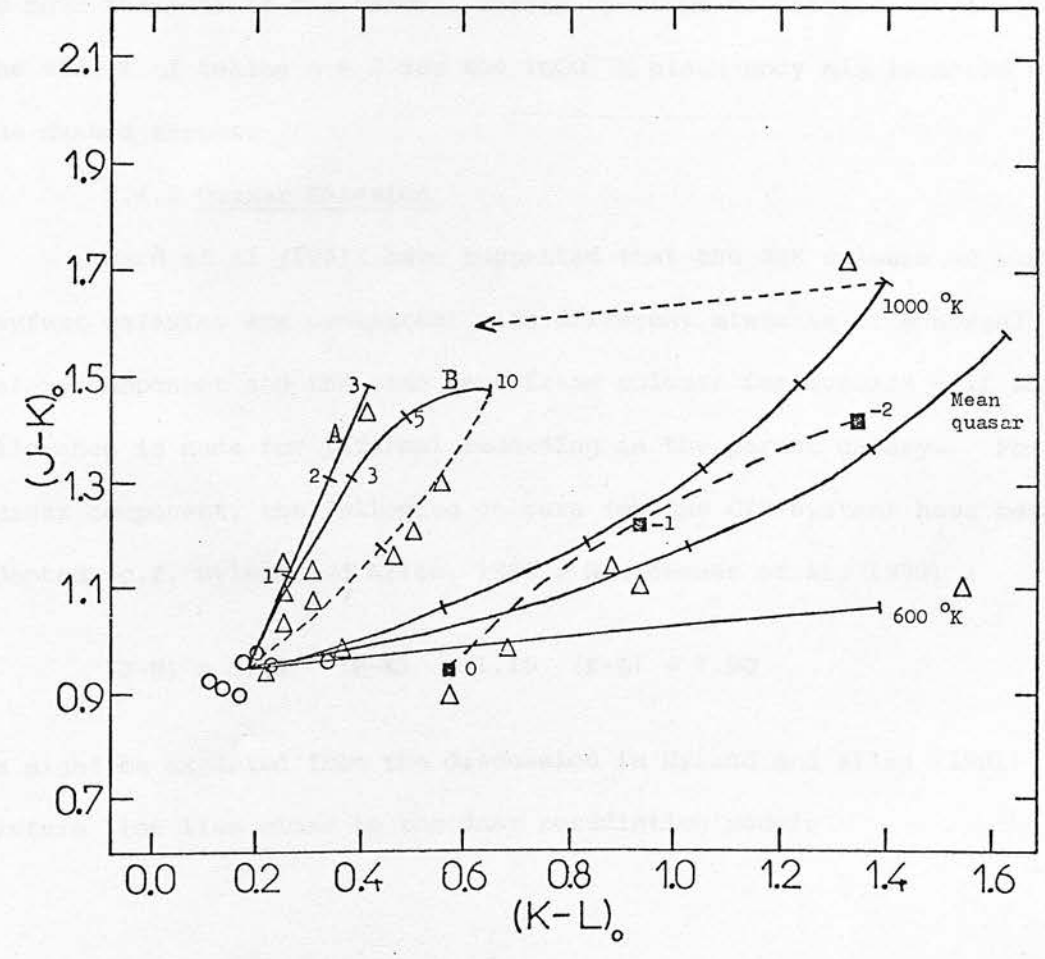
2.1
1.9
1.7
1.5
1.3
1.1
0.9
0.7
$(J-K)_o$
0.0
0.2
0.4
0.6
0.8
1.0
1.2
1.4
1.6
$(K-L)_o$
A
B
1
2
3
5
10
-2
-1
0
1000 °K
600 °K
Mean
quasar

an increase of the source contribution to the 2.2μ flux by 10%. With the fiducial galaxy colours given by equation 2.3, these 'mixture lines' are defined by the equations :

$$(J-K) = -2.5 \log_{10} \left\{ x.10^{-0.4(J-K)_s} + 0.42\ (1-x) \right\}$$

$$(J-L) = -2.5 \log_{10} \left\{ \frac{x.10^{-0.4(J-K)_s} + 0.42(1-x)}{x.10^{0.4\ (K-L)_s} + 1.20(1-x)} \right\} \qquad (2.5)$$

$$(H-K) = -2.5 \log_{10} \left\{ x.10^{-0.4(H-K)_s} + 0.82(1-x) \right\}$$

in which the subscript 's' refers to the intrinsic colours of the source and $0 \leq x \leq 1$ is the fraction of the total 2.2μ light contributed by the source.

Adopting a steeper frequency dependence for the emissivity tends to move the peak of the thermal energy spectrum to shorter wavelengths. The effect of taking n = 2 for the 1000^{o} K black-body mix is shown by the dashed arrows.

2.4.2 Quasar Emission

Ward et al (1981) have suggested that the JHK colours of many Seyfert galaxies are consistent with different mixtures of a normal galaxy component and the mean rest-frame colours for quasars - if some allowance is made for internal reddening in the parent galaxy. For the quasar component, the following colours (on the CIT system) have been adopted (c.f. Hyland and Allen, 1981 ; Neugebauer et al, 1979) :

$$(J-H) = 0.87 \quad (H-K) = 1.15 \quad (K-L) = 1.90$$

As might be expected from the discussion in Hyland and Allen (1981) , the mixture line lies close to the dust reradiation models.

2.4.3 Power-law Continuum Emission

Power-law continua of the form $f_\nu \alpha \nu^\gamma$ have been found in some Seyfert 1 and BL Lac objects (McAlarey et al, 1979, Allen and Hyland, 1981). The long-dashed line in Figure 2.6 is the locus of models in which half the 2.2μ flux arises from a normal galaxy component and half from a power-law continuum.

The near-infrared JHKL colours of ionized gas are largely unaffected by line emission (Willner et al, 1972). Since an optically thin free-free continuum can be approximated by $f_\nu \sim$ constant, the thermal bremsstrahlung from an ionized nebula is therefore only a special case of a power-law continuum with $\gamma \sim 0$.

2.4.4 Internal Reddening

The optical evidence for dust in each of the galaxies in Table 2.3 obviously requires that careful attention be paid to extinction effects. Straightforward reddening estimates based on any reasonable determination of the Galactic extinction law (e.g. Whitford, 1958) cannot reproduce many of the observed colours in Figure 2.6. It seems probable, however, that the dust in these galaxies will be distributed in some form through the stellar component, so that simple dust-screen models are unlikely to be appropriate. The effective absorption in the near-infrared due to arbitrarily distributed dust has been calculated from the expression

$$I_T(\nu) = \int_{-\infty}^{\infty} I_\nu(x)\, e^{-\tau_\nu(x)}\, dx \qquad (2.6)$$

where $\tau_\nu(x) \int_x^{\infty} K_\nu \rho(x')\, dx'$

The relative values of the extinction coefficient K_ν were adapted from Savage and Mathis (1979). Two specific models, that of a simple dust screen and of uniformly mixed dust, can be evaluated analytically (Jones and Stein, 1975) and serve as a check on the accuracy of the numerical techniques employed.

Since most of the galaxies with red colours in Figure 2.6 contain an obvious stellar disk, the model adopted is characterized by exponential density distributions (Freeman 1970 ; Burton 1976) for both the absorption (dust) and emission (stars) :

$$I_\nu(x) = I_\nu(0)\ e^{-|x|/x_s}$$

$$\rho(x) = \rho(0)\ e^{-|x|/x_D}$$

with x_s = 3 kpc and x_D = 1.5 kpc. The frequency dependence of the stellar emissivity function $I_\nu(0)$ was calculated from equation 2.3. Addition of either a molecular ring component to the absorption or an $r^{\frac{1}{4}}$ bulge to the stellar flux, moves the reddening line closer to that of the simple dust-screen.

Because the aperture sizes used are generally larger than the apparent thickness of the dust lanes, the observed flux arises partly from the reddened material associated with the dust and partly from the surrounding bulge and disk. The variation of this covering factor is represented by the short-dashed line in Figure 2.6, which is the mixture locus for an unreddened galaxy component and one in which the visual optical depth to the centre of the galaxy ($\tau_V^{\frac{1}{2}}$) is 10 magnitudes.

2.4.5 Discussion

It is evident from Figure 2.6 that even using only the simple models discussed above, an unambiguous interpretation of the two-colour diagrams is not possible.

The addition of black-body thermal components affects mainly the 2.2μ and 3.5μ fluxes, and galaxies with red J-H colours therefore require very hot grains. Dust temperatures much greater than $T \sim 1\text{-}1.5\ 10^3\ ^oK$ seem unlikely in view of the relevant condensation temperatures (Martin, 1979), although the effects on the spectra of increasing the temperature can be qualitatively reproduced by assuming a grain material such as graphite whose absorption efficiency varies steeply with frequency. Internal reddening appears to play an important role in determining the colours of galaxies such as NGC 4370, NGC 2076 and NGC 5719, which exhibit moderate colour residuals in the JHK plane, but do not have large K-L excesses. The positions of NGC 7213 and IC 5063 in the JHK plane indicate that the colour residuals in this case are produced by an infrared excess at 2.2μ. This is confirmed by the large 3.5μ fluxes found in these galaxies.

Two of the dust- lane galaxies with normal JHK colours (NGC 5485 and NGC 1947) show strong non-stellar emission at longer wavelengths in the JKL plane. The weak 3.5μ excess in the morphologically normal galaxy NGC 1052 (which also has standard JHK colours)may be related to the strong 10μ source found by Rieke and Low (1972). More detailed studies of this galaxy have recently been made by Rieke, Lebofsky & Kemp (1982) and Wynn-Williams et al (1982).

2.5 INDIVIDUAL GALAXIES

It is to be expected that in a study of almost 50 galaxies, a few systems of particular interest on an individual basis will be encountered. NGC 7172 is clearly the most extreme object in the present sample so a more extensive discussion of this galaxy is given in Chapter 3.

NGC 612 (PKS 0131-36)

This southern galaxy was identified with the radio source PKS 0131-36 by Westerlund and Smith (1966), who also noted the presence of the dust lane and a strong spheroidal component. Ekers et al (1978)

obtained a detailed 1.4 GHz map and showed that the radio source consisted of a wide double (orientated approximately along the minor axis of the light distribution) and a compact core. The radio morphology is particularly interesting since most double radio sources are thought to reside in elliptical galaxies, whilst there is clear evidence of a stellar disk in this galaxy on the survey plates. Goss et al (1980) find an upper limit to the mass of $M < 1.1\ 10^{12}\ M_{\odot}$ within 40 kpc of the nucleus, from observations of weak emission lines along the major axis. The velocity field is characteristic of a massive early-type disk system, and substantial rotation is also found in the stellar component. Since no strong, high-excitation emission lines are observed at the position of the compact nuclear radio source, these authors also suggest that the optical nucleus may be effectively obscured by dust.

The infrared observations reveal a weak excess at 2.2μ. A close similarity between this galaxy and IC5063 makes further observations at longer wavelengths extremely desirable.

IC 5063 (PKS 2048-57)

Detailed studies of the optical emission line spectrum in IC 5063 have been made by Caldwell and Phillips (1981) and Danziger et al (1981). The distribution of ionized gas is dominated by a bright nuclear emission region for which an electron temperature of $T_e \sim 20{,}000^{\circ}$ K is found from the [O III] 5007/4363 ratio. Danziger et al (1981) argue that the energy input comes predominantly from photo-ionization, but that the ionizing continuum is significantly hotter than that produced by normal OB stars. Assuming a value of $n_e \sim 680\ cm^{-3}$ for the electron density they derive a diameter of $D \sim 40\ \varepsilon^{-1/3}$ pc for the nuclear emission region, where ε is the filling factor for the Balmer-line gas. Taking $\varepsilon \sim 0.01$ as a characteristic value for active nuclei (Osterbrock, 1977), the apparent size of the emitting region is then 0.6 arcsec at an adopted distance of d = 66 Mpc.

The near-infrared excess can be adequately fitted by a $T = 600^{\circ}$ K black-body which contributes 12% of the observed flux in the 2.2μ band. The total infrared luminosity of this component (extrapolated to longer wavelengths) would be $L_{IR} \sim 7.10^{43}$ ergs s^{-1} $(2.10^{10} L_{\odot})$ of which about 10% is observed at $\lambda < 3.5\mu$. This is likely to be a severe underestimate if any cooler grains are also present.

From the optical spectrophotometry, one may estimate using simple models whether Lyman α heating is sufficient to explain this infrared luminosity or whether higher dust-gas ratios and heating by Lyman continuum photons are required.

For a pure hydrogen nebula the Hβ flux is given by :

$$4\pi d^2 F(H\beta) = \alpha_{\beta}(T_e) \; h\nu_{\beta} \; n_e^2 \; V \; e^{-\tau_{\beta}} \qquad (2.7)$$

where $\alpha_{\beta}(T_e)$ is the volume recombination coefficient for Hβ and τ_{β} is the effective optical depth to the H II at $\lambda = 4861$ Å. The luminosity of the ionizing continuum is therefore :

$$L_{UV} = \beta_2(T_e) \; n_e^2 \; V\langle h\nu\rangle = \frac{\beta_2(T_e)}{\alpha_{\beta}(T_e)} \; \frac{4\pi d^2 F(H\beta) e^{\tau_{\beta}} \langle h\nu \rangle}{\nu_{\beta}} \qquad (2.8)$$

where $\beta_2(T_e)$ is the recombination coefficient summed over all but the first principal quantum level and $\langle h\nu \rangle$ is the average energy of ionizing photons. Assuming that the observed Balmer decrement (Danziger et al, 1981) is due to the effects of reddening on the Case B recombination value (Brocklehurst, 1971), then $\tau_{H_{\beta}} \sim$ 1.2-3.2 depending on whether the dust is internal or external to the emitting region. At an electron temperature of $T_e = 20{,}000^{\circ}$ K the ionizing photons have a characteristic energy of

$$\langle h\nu \rangle \sim 13.6 + 3/2 \; kT_e \sim 16.2 \text{ eV}.$$

Taking $F(H\beta) = 1.45\ 10^{-14}$ ergs $cm^{-2}\ s^{-1}$ (Danziger et al, 1981), $\alpha_\beta = 1.03 \cdot 10^{-14}\ cm^{-3}\ s^{-1}$ and $\beta_2 = 1.43\ 10^{-13}\ cm^{-3}\ s^{-1}$ (Osterbrock, 1974), the ionizing continuum has

$$L_{UV} \sim 0.6 - 4.4\ 10^{9}\ L_\odot .$$

i.e. somewhat less than the estimated infrared luminosity. If the absorbing grains are those responsible for the reddening, this suggest that the grains compete effectively with the gas to absorb the UV flux, as is the case in some compact galactic H II regions (Wynn-Williams and Becklin, 1974).

NGC 7213 (PKS 2206-47)

Recent observations with the HEAO-A2 experiment have suggested the identification of NGC 7213 with the X-ray source H2209-471 (Marshall et al, 1979). At a distance of 35 Mpc, the 2-10 keV luminosity is $L_x = 3.5\ 10^{42}$ ergs s^{-1}. The intrinsic 3.5μ flux of $F_{3.5} = 2.3\ 10^{29}$ ergs $s^{-1}\ Hz^{-1}$ (Table 2.3) places this galaxy close to the proposed correlation between X-ray and infrared luminosities (e.g. McAlarey et al, 1979 ; Chapter 3).

Sersic (1968) classified NGC 7213 as E1 with a light absorption lane, but Phillips (1979) favoured a lenticular morphology and showed that the optical spectrum was similar to some Seyfert 1 and broad-line radio galaxies, with extremely strong Hα emission and a steep Balmer decrement. The infrared colours lie close to those of the dust re-radiation models. A $T = 800^{\circ}$ K black-body contributing 15% of the 2.2μ flux has colours (cf Table 2.3) :

(J-H) = 0.75 (H-K) = 0.37 (K-L) = 1.01

Additional infrared observations have recently been made by Glass (1981) and Ward et al (1981). After correcting for the non-stellar

TABLE 2.5 Optical and infrared aperture colours of NGC 7213. The infrared data are on the CIT system and have been corrected for reference beam flux as described in the text. Effective apertures for SAAO data are taken as 95% of the nominal aperture size.

Infrared Photometry

Aper.	Source	J	H	K	L
5.7"	G	10.71	10.01	9.41	8.24
7.0"	W	10.70	9.88	9.33	8.35
8.6"	G	10.22	9.48	9.01	8.20
11.4"	G	9.92	9.21	8.81	8.20
11.4"	S	9.98	9.25	8.90	8.09
17.1"	G	9.58	8.82	8.44	-

Optical Photometry

Aper	Source	V	B-V	U-B	V-R
29.4"	SA	11.41	0.90	0.45	-
30.1"	SV	11.37	0.97	0.45	0.92
35.3"	SA	11.21	0.90	0.45	0.91
35.3"	LS	11.28	0.95	0.48	-
54.7"	SA	10.90	0.93	-	0.91
75.5"	LS	10.74	0.94	0.39	-
80.9"	SA	10.68	0.90	-	0.89
106.7"	SA	10.52	0.92	-	0.89

Ref: G- Glass 1981 ; W - Ward et al, 1981 ; S- this work ;
SA - Sandage 1975 ; SV - Sandage and Visvanathan 1978a;
LS - Chapter 4.

flux using the above model, the 2.2μ observations in Glass (1981) (obtained with both 12 and 66 arcsec beam separations) may be used to define an empirical correction for the galaxy flux in the reference aperture. As noted by Glass, the principal effect of these corrections is to make the (K-L) colours slightly bluer than the observed values (Table 2.5). Since there is no evidence of temporal variations, all of the data may then be used to derive the source spectrum more accurately. Assuming that the 1.2μ flux in the largest aperture arises primarily from a stellar component with normal colours, the contamination at smaller aperture sizes may be estimated by extrapolating using a mean growth curve (from Frogel et al, 1978, extended using data for the M31 bulge from Aaronson et al, 1980 and Aaronson 1977). The zero-point of the effective-aperture scale was determined by normalizing this growth curve to the magnitude-aperture slope of the V photometry of NGC 7213 (Table 2.5), since there is no evidence in the UBV colours of a non-thermal optical continuum. The stellar contributions were then subtracted from the observed values in each aperture to determine a mean and standard deviation for the source flux as a function of frequency (Figure 2.7).

As was expected from the normal (J-H) colour of NGC 7213, only upper limits could be placed on the non-stellar component at 1.2 and 1.65μ. A 10 μ flux of 190 $\pm$ 20 mJy has recently been detected from NGC 7213 by Frogel and Elias (unpublished, but quoted by Phillips 1979), and a 2700 MHz flux of 230 mJy is given in the Parkes catalogue (Bolton et al, 1979). The emission from T = 800° K black-body grains does not continue to fit the derived energy distribution out to 10μ, and in fact no single Planck function or power-law spectrum is adequate.

Observations at GHz radio frequencies and at longer IR wavelengths would help to constrain any incoherent synchroton model, but it is easy to show that the best method for distinguishing between non-thermal and

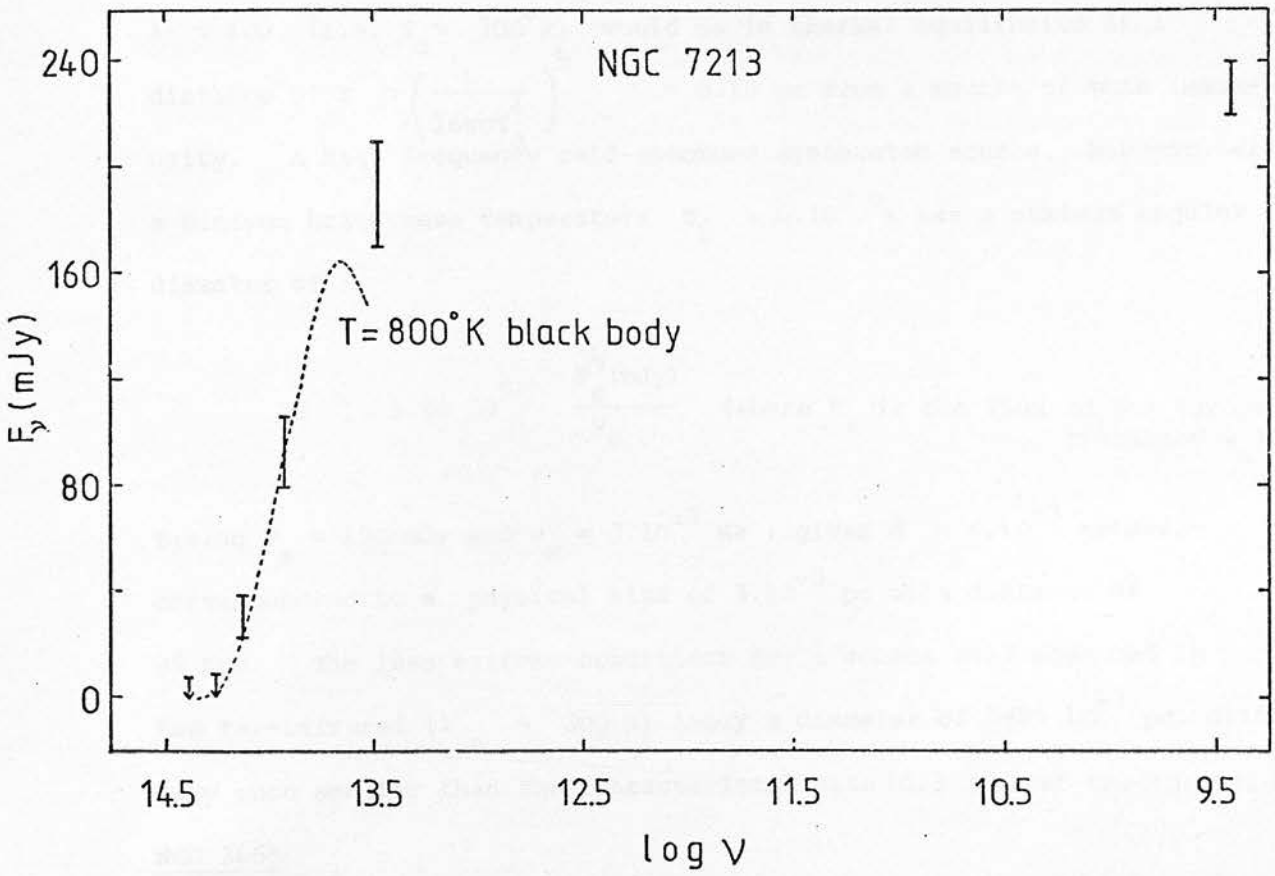

Figure 2.7

The energy db^n of the non-stellar radiation from NGC7213 between near-IR and radio wavelengths. A T = 800°K black-body model contributing 50% of the total observed 2.2 μ flux in an 11.4 arcsecond aperture is illustrated by the dashed line.

thermal IR emission in NGC 7213 would be to monitor the IR flux for variability. Since the absolute luminosity in Hα is 2.10^{41} ergs s^{-1} (Phillips, 1979), a Lyman continuum of approximately 3.10^{42} ergs s^{-1} is required to ionize the gas. Black-body grains re-emitting at $\lambda \sim 10\mu$ (i.e. $T_d \sim 300^{\circ}K$) would be in thermal equilibrium at a distance of $r \sim \left(\frac{L}{16\pi\sigma T_d^4}\right)^{\frac{1}{2}} \sim 0.15$ pc from a source of this luminosity. A high frequency self-absorbed synchroton source, however, with a minimum brightness temperature $T_b > 6.10^9\ ^{\circ}K$ has a maximum angular diameter of :

$$\theta \simeq 3.84\ 10^5 \frac{F_s^{\frac{1}{2}}(mJy)}{\nu_s}$$ (where F_s is the flux at the turnover frequency ν_s)

Taking F_s = 190 mJy and $\nu_s = 3.10^{13}$ Hz ; gives $\theta \sim 4.10^{-3}$ arcsec, corresponding to a physical size of 3.10^{-5} pc at a distance of 35 Mpc. The less extreme conditions for a source self absorbed in the far-infrared ($\lambda_s \sim 300\ \mu$) imply a diameter of 5-25 10^{-3} pc, still very much smaller than the characteristic size (0.3 pc) of the thermal model.

NGC 3665

Radio observations of NGC 3665 have been made by Kotanyi (1979), who favoured an elliptical classification since the luminosity profile could be adequately fitted by an $r^{\frac{1}{4}}$ law. The radio emission comes from a compact nuclear source and an outer component elongated at PA $\sim 135^{\circ}$. On short exposure plates a dust lane $\sim$ 5kpc in diameter can be seen near the nucleus, orientated at PA $\sim 33^{\circ}$.

Jenkins (1981) has studied the stellar kinematics of NGC 3665 and found a rapidly rotating system in which the ratio of maximum rotational velocity to central velocity dispersion is $V_m/\sigma_c > 0.6$. Since most luminous ellipticals appear to have only a small fraction of their kinetic energy in ordered rotational motions (e.g. Illingworth,1981) the kinematic evidence supports the SO classification of Nilsson (1973) and de Vaucouleurs et al (1976).

If the infrared aperture is assumed to be centred on the compact nuclear radio source (which is also the optically brightest point) the covering factor for the dust lane may be estimated using the short exposure photograph in Kotanyi (1979). Even without this constraint, however, the JHKL colours cannot be accurately reproduced by extinction effects using a standard reddening law, unless the unreddened stellar population has (H-K) $\sim$ 0.28. Thermal emission from hot ($T > 1000^{\circ}$ K) dust may also reproduce the observed colours, but any contribution from cool grains is severely restricted by the (K-L) colour of 0.31 (e.g. less than a 2% contribution at 2.2μ from $T = 600^{\circ}$ K dust).

NGC 7625

The JHK colours of this galaxy are unusual in that (J-H) has a blue colour residual, whilst (H-K) is somewhat redder than the nominal galaxy colours given by equation 2.3. A contribution from optically thin free-free emission cannot be ruled out with the available data, but seems unlikely to be the dominant mechanism in view of the large Hβ luminosity ($\sim 10^{42}$ ergs s^{-1}) which would be implied by the 2.2μ excess.

A more acceptable model is one where the long wavelength excess again arises from thermal re-radiation by dust grains, but in which the mean stellar population colours are slightly bluer than those given by equation 2.3. Spectroscopic evidence for a young stellar population in NGC 7625 has been discussed by Demoulin (1969a), who showed that the Balmer series is seen in absorption shortward of Hβ. A model in which 5% of the K flux arises from BO stars would have infrared colours :

J-H = 0.65 H-K = 0.20 K-L = 0.19

As expected, the addition of young blue stars affects mainly the short wavelength band passes and a small contribution from thermal dust emission can then easily reproduce the observed colours in Table 2.3.

The broad band optical colours of this galaxy are also bluer than the mean values for early-type galaxies, with :

$(U-B) = 0.15 \quad (B-V) = 0.70$

(de Vaucouleurs et al, 1976).

2.6 SUMMARY

New near-infrared (JHK) observations of 46 early-type galaxies with dust lanes have been obtained. About one third of these have red broad band colours when compared with a sample of 24 morphologically normal galaxies. IR excesses are found preferentially in systems exhibiting at least weak signs of a luminous disk. The prototype dust-lane galaxy NGC 5128 (which if observed at z = 0.01 would have J-H $\sim$ 1.1 H-K $\sim$ 0.4 in a 12" aperture) must clearly be anomalous in this respect. Longer wavelength observations (at 3.5 μ) have been obtained for 24 galaxies and provide additional constraints on the origin of the IR excess. Although a unique interpretation cannot be given for individual cases, the distribution of galaxies in the JKL plane suggests that internal reddening plays an important role in about half of this sample. Eleven galaxies have published radio continuum fluxes or upper limits. Within this small subset, there is no indication of a strong correlation between infrared excess and radio flux density. Two of the galaxies with infrared excesses lie within X-ray error boxes from HEAO-A2 observations.

CHAPTER 3

NGC 7172 : FURTHER OBSERVATIONS OF AN EXTREME IR-EXCESS GALAXY

3.1 INTRODUCTION

The near-infrared survey described in the previous chapter showed that NGC 7172 has the most extreme JHK nuclear colours in a sample of 46 early-type galaxies with dust lanes. At the effective apertures used in the survey this infrared excess is comparable with those in many active galaxies, as observed for example by McAlarey et al (1979), Balzano and Weedman (1981) and Glass (1981).

NGC 7172 (Sab pec : ; De Vaucouleurs et al, 1976) is a member of a small group containing NGC 7173 (E2), NGC 7174 (Sb pec :) and NGC 7176 (EO). The spectra and morphologies of these galaxies were first discussed by Rubin (1974). NGC 7172 shows no sign of the bright star-like nucleus which characterizes many classic Seyfert galaxies (Weedman, 1977). It is an edge-on system heavily obscured by a strong equatorial dust lane, with a morphology similar to that of the narrow emission-line galaxy NGC 5506 (see Wilson (1979) and Fig 3.2).

Keel (1980) has interpreted an apparent deficiency in the number of edge-on Seyferts as a selection effect, due to internal absorbing material in these galaxies. This picture has been extended by Lawrence et al (1981) to include narrow emission-line galaxies like NGC 5506 which show evidence of energetic activity in the hard X-ray and infrared regions, but whose relatively weak optical spectra are assumed to have been severely modified by dust absorption. Although the optical spectrum of NGC 7172 was described by Rubin (1974) as "typical of the low-excitation present in early-type spirals", the large infrared excess of the nucleus suggested

that such effects might be important for this galaxy also.

3.2 OPTICAL OBSERVATIONS

Photoelectric aperture photometry of NGC 7172 from various sources is listed in Table 3.1. The UBV colours are not unusual for an early-type system, which suggests that only a small fraction of the optical flux arises from the reddened material behind the dust lane.

Photographic surface photometry has been obtained from a 30 minute UK Schmidt telescope plate using hypersensitized III a J emulsion and a GG 395 filter. A description of the digitization and reduction methods used to analyze the plate will be deferred until Chapter 6. Calibration was available from a 16-element stepwedge exposed simultaneously onto the plate and the zero-point established using the B photoelectric photometry in Table 3.1. The small colour terms between the 'J' passband and the Johnson B system (e.g. Kron, 1980) can be considered negligible for the present purposes. Inspection of the uncalibrated image indicated that the galaxy was not saturating either the PDS microdensitometer on which the plates were measured or the III a J emulsion itself. The mean sky brightness derived from a comparison of Table 3.1 with simulated aperture photometry of the intensity-calibrated image is B = 22.55 $\pm$ 0.1 mag/sq. arcsec.

The isophote structure of NGC 7172 is reproduced in Figure 3.1(a). The contour levels are at intervals of 0.5 mag/sq arcsec with the outermost contour at B = 24.0 mag/sq arcsec or 25% of the sky background. The asymmetries due to absorption by the dust lane can be seen in the central parts of this figure, and more clearly in a density profile taken along the minor axis (labelled 'B' in Fig.3.1(b)). Photographic plates taken in the ultraviolet (III a J + UG1) and far-red (IVN + RG 695) confirm that the nucleus is largely obscured at optical wavelengths by the dust lane (Figure 3.2). Direct evidence for obscured nuclei (on the basis of

TABLE 3.1 : Photoelectric Aperture Photometry of NGC7172

Log D(0.1)	V	(B-V)	(U-B)	Source
0.56	13.61	1.07	0.59	G
0.71	13.22	1.11	0.57	BP
0.77	13.11	1.07	0.51	LS
0.78	13.05	1.07	0.45	G
0.79	12.95	1.07	0.49	G
0.87	12.84	1.09	0.51	BP
0.92	12.74	1.07	0.50	VM1
1.00	12.49	1.03	0.51	G
1.03	12.41	1.04	0.44	VM1
1.05	12.24	1.03	0.49	BP
1.18	12.14	-	-	G
1.28	12.11	0.93	0.40	VM1
1.35	12.01	-	-	G
1.43	11.94	0.94	0.56	VM1

Ref:

BP - Bucknell & Peach (1976)

G - Griersmith (1980a)

LS - Longmore & Sharples (unpublished data)

VM1- de Vaucouleurs & de Vaucouleurs (1972).

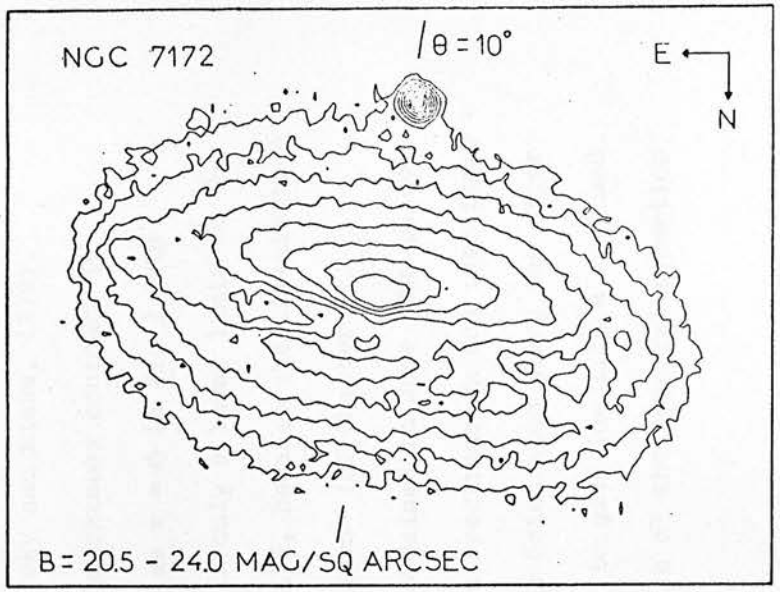

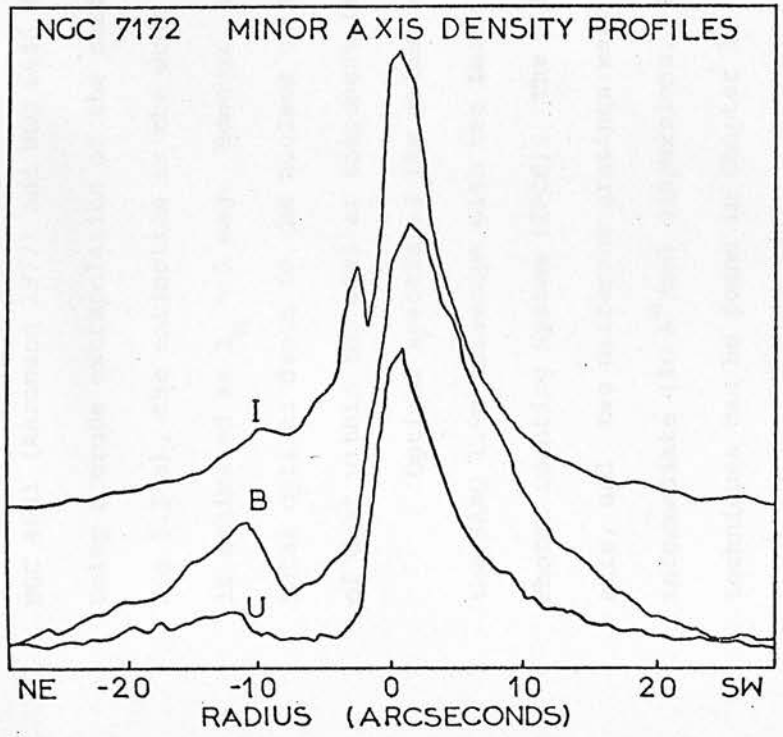

Figure 3.1

(a) Isophotal contours of NGC7172 in the 'B' system. A foreground star to the SW of the galaxy is easily identifiable, and lies close to the minor axis of the galaxy at position angle $\theta = 10^{\circ}$.

(b) Density profiles along the minor axis in the U, B and I passbands :

U λ_{eff} = 3580 Å

B λ_{eff} = 4725 Å

I λ_{eff} = 7780 Å

The radial distances are measured from the centre of symmetry of the outer (unobscured) parts of the galaxy.

infrared maps) has previously been found for at least two other galaxies: NGC 4631 (Aaronson 1977) and NGC 6946 (Lebofsky and Rieke, 1979). Using a crude extrapolation of the surface brightness contours in Fig 3.1(a), the extinction in the dust lane at r = 0 in Fig 3.1(b) is estimated as $A_B \sim 1$ mag. However, this is only a lower limit to the total optical depth to the nucleus of NGC 7172, because the distribution of dust within the stellar component is unknown (cf Chapter 2).

Optical spectra of the galaxy were obtained in June 1980 using the SAAO 1.9m telescope with the Image Tube Spectrograph and the Image Photon Counting System (IPCS). The slit was orientated along the major axis, and two different gratings were used to give low (210 A^{o}/mm) and intermediate (40 A^{o}/mm) dispersions. Details of the spectral reduction techniques can be found in Chapter 5.

Since the low dispersion spectrum had poor spatial resolution, it was subsequently reduced to a 1-D format by co-adding the increments containing the galaxy and subtracting the sky from the ends of the slit. Weak emission lines of [N II] 6584/6548, Hα , [O III] 5007/4959 and [O II] 3727 were detected, superposed on a strong stellar continuum with prominent NaD and Mgb absorption lines. Because of the narrow slit used (1".8) and the generally non-photometric weather, only a crude relative flux calibration could be obtained from observations of spectrophotometric standards. However, a comparison of the relative continuum fluxes with an average E/SO energy distribution taken from Pence (1976), did not reveal any signs of the 'blue continuum' referred to by Rubin (1974). Furthermore there is no supporting evidence for this component in the available optical photometry (Table 3.1).

The intermediate dispersion spectra were processed in full 2-D format (2000 x 25 pixels) to study the kinematics of the emission-line regions along the major axis. Separate grating angles were necessary to

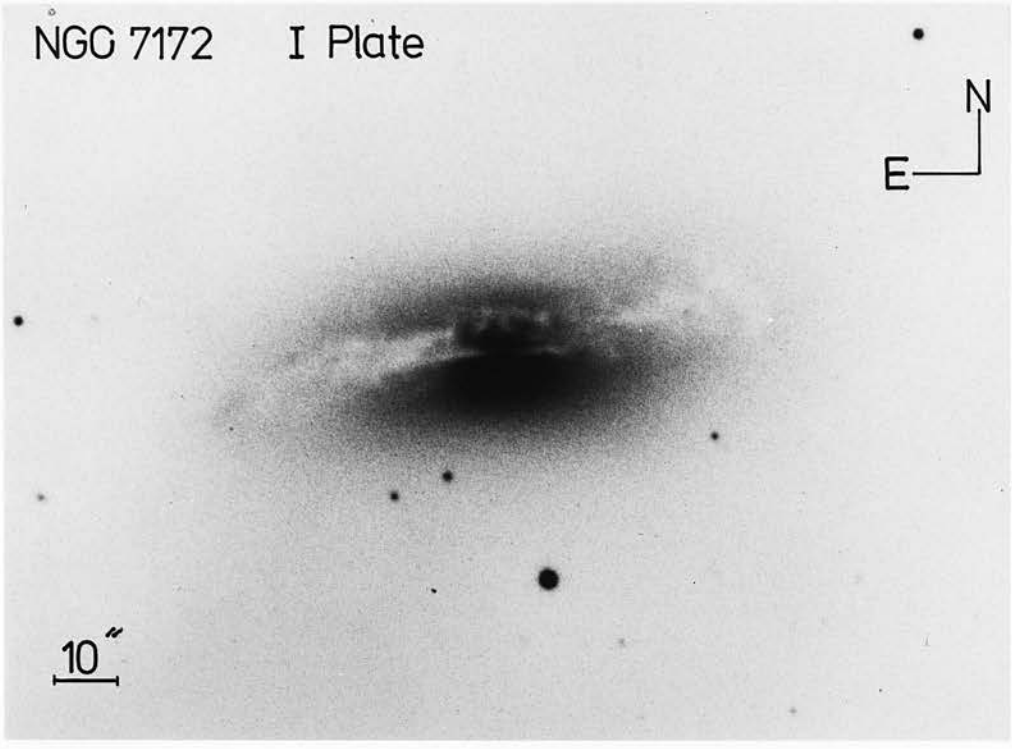
NGC 7172 I Plate
N
E
10″

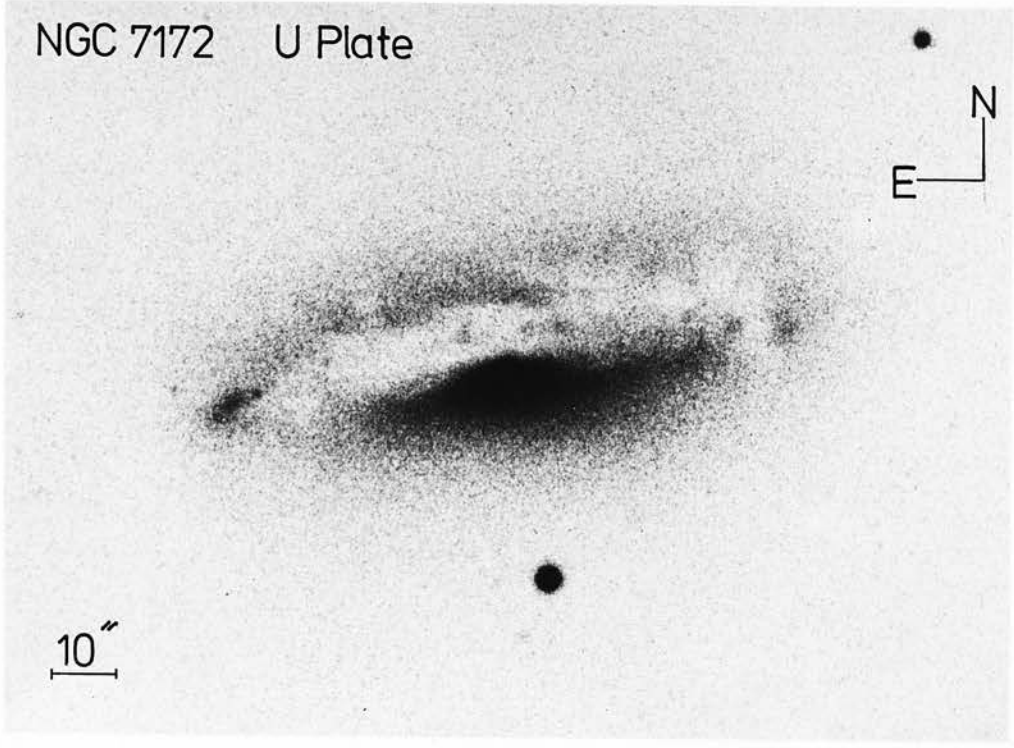
NGC 7172 U Plate
N
E
10″

Figure 3.2

AAT prime focus plates of NGC7172 in the U and I passbands. The scale and orientation are the same for both prints. Over this wavelength baseline there is a striking change in morphology due to obscuration by the dust lane. On the far-red plate, the nucleus can be seen between two thin dust features which cross the bright central bulge. This whole region is much more effectively obscured by dust on the ultraviolet plate. A further interesting feature is the very blue knot at the SE extremity of the galaxy. However, there is no evidence of organized spiral patterns on either plate and the dust distribution is noticeably chaotic.

provide coverage of the [O III] lines and the Hα/ [N II] lines, so two 6000 sec exposures were obtained on different nights. The spectra were flat-fielded in the usual way to remove the high frequency components of the detector response, but the results of this procedure were generally imperfect due to drifts in the IPCS and constitute a major source of noise in the measurement of line positions. A cross-correlation technique (basically the same as that employed in Chapters 4 and 5 for determining absorption-line redshifts, but with a restricted wavelength range including only the emission features) was used to determine a rotation curve for each spectrum. The results are plotted in Figure 3.3, where the error bars indicate the formal error estimates (c.f. Tonry and Davis, 1979). Since the exposures of each wavelength region were obtained independently on separate nights, the absolute positioning of the the slit on the galaxy is not necessarily the same for both spectra. The radial distances in Fig 3.3 have therefore been measured relative to the position of the peak in the continuum counts in each case. This involves a relative spatial shift of the two frames by approximately one increment (3".6) and assumes that the galaxy profiles peak at the same point on the sky in both bandpasses. A simple zero-point error in the spatial or velocity scales cannot, however, explain the differences between the two velocity fields in the figure. Each increment along the slit has been calibrated independently using frequently taken 2-D arc frames and the r.m.s. residual in the fit of wavelength vs. channel number was typically 0.25 channels ($\sim$ 8 kms^{-1}). A similar figure can be placed on the residual S-distortion along the slit, as measured from the λ5890 and λ6300 night-sky lines on the red spectrum.

Information about the velocity fields in individual emission lines is lost using thistype of correlation analysis, so the wavelengths have

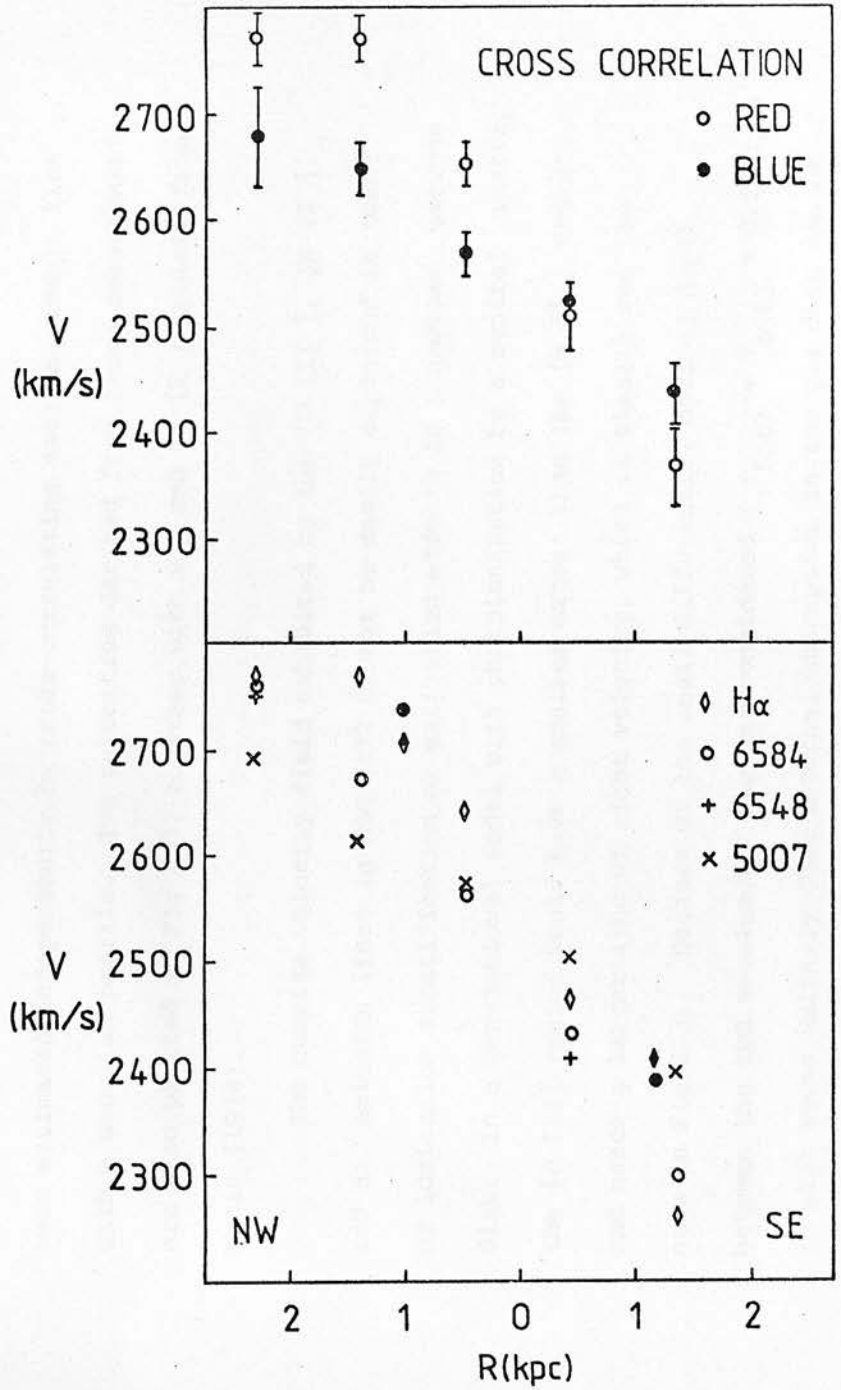

Figure 3.3 : Emission line rotation curves along the major axis of NGC7172. In the upper diagram are the relative velocities from cross-correlation analyses of the red (Hα + [NII] λλ 6548,6584) and blue ([OIII] λλ 4959, 5007) spectra. Velocities from measurements of individual line positions are given in the lower diagram. The radial distances are measured from the peak in the continuum counts on each spectrum assuming that the galaxy is at a distance of 51.8 Mpc. Filled symbols in the lower diagram are data from Rubin (1974).

been estimated independently by cross-correlating each measurable line with a Gaussian profile. The velocities derived from these measurements are also plotted in Fig 3.3, together with Hα and [N II] points from Rubin (1974).

The complex velocity field exhibited by the [O III], [N II] and Hα emission lines in NGC 7172 cannot be easily explained in terms of ionization stratification or extinction effects in a nuclear gaseous disk. In a conventional model with photoionization by a central source, the [O III] region would have a smaller extent than the [N II] region and hence a larger line of sight velocity, which is clearly not the case in Fig 3.3. Because of the small differential optical depth between the two wavelength regions considered ($\tau_{5007} - \tau_{6563} = 0.33\ \tau_V$), it also seems unlikely that internal absorption in the gas disk can be entirely responsible for the observed rotation curves. A similar phenomenon has been found by Westin (1980) who noted that the tilts of the Hα and [N II]λ 6584 lines across the nucleus of the Seyfert galaxy NGC 7469 are different ; unfortunately the velocity fields in both lines are peculiar and the significance of his result is not clear. A major uncertainty in this study of NGC 7172 is the possibility that one of the spectra were taken with the slit offset slightly along the minor axis of the galaxy. The observations, at present, do not warrant a detailed model. Seeing and scattering effects may well have to be considered when higher quality data become available.

The mean heliocentric redshift from Figure 3.3 is V = 2545 kms^{-1}, corresponding to a distance of D = 51. 8 h^{-1} Mpc (where $h = H_o/50$, and H_o is the Hubble constant in kms^{-1} Mpc^{-1}). In the red spectrum the velocity gradient is 148 h kms^{-1} kpc^{-1}, which may be compared with 145 (± 15) derived from the data given by Rubin (1974). The estimated

nuclear mass is therefore 3-4 10^9 $M_\odot$ within 1 kpc of the centre, depending on the adopted flattening.

The emission lines are resolved on the intermediate dispersion spectra, and have a mean FWHM of 245 $\pm$ 50 kms^{-1}, after correcting for instrumental broadening and the effects of rotation. This value is near the lower end of the distribution of line widths for Seyfert 2 galaxies and narrow-line radio galaxies found by Koski (1978). Important astrophysical information is also contained in the relative line strengths. The flux-calibrated low dispersion spectrum gives a lower limit for the Balmer decrement of $H\alpha/H_\beta > 8.5$. If this ratio is interpreted as due to the effects of extinction on an intrinsic recombination value of 2.86 (from Brocklehurst [1971] for case B, $T_e = 10^4$, $N_e = 10^2$), then the optical depth derived using a Whitford (1958) reddening law (as parametrized by Miller and Matthews [1972]) is $A_v > 2.7$ mag. Baldwin et al (1981, hereafter BPT) have outlined the use of two-dimensional diagnostic diagrams, based upon emission-line intensity ratios, to isolate the principal excitation mechanism in extragalactic objects. Figure 3.4 is the BPT diagram for the emission lines of Hα(6563), Hβ(4861), O III (5007) and N II (6584). The logarithmic line ratios for NGC 7172 :

$$[6584/6563] = 0.08 \qquad [5007/4861] > 0.69$$

have been derived from the nuclear spectra taken at intermediate dispersion in which the signal-to-noise (S/N) is very good. Reddening corrections have been applied (using $A_v = 2^m.7$) but one of the merits of using this particular diagram is the relative insensitivity to extinction effects. The position of NGC 7172 in Fig 3.4 is clearly indicative of a non-thermal (power-law) excitation source for the nuclear emission lines. Well outside the nucleus the relative intensities are more like H II region

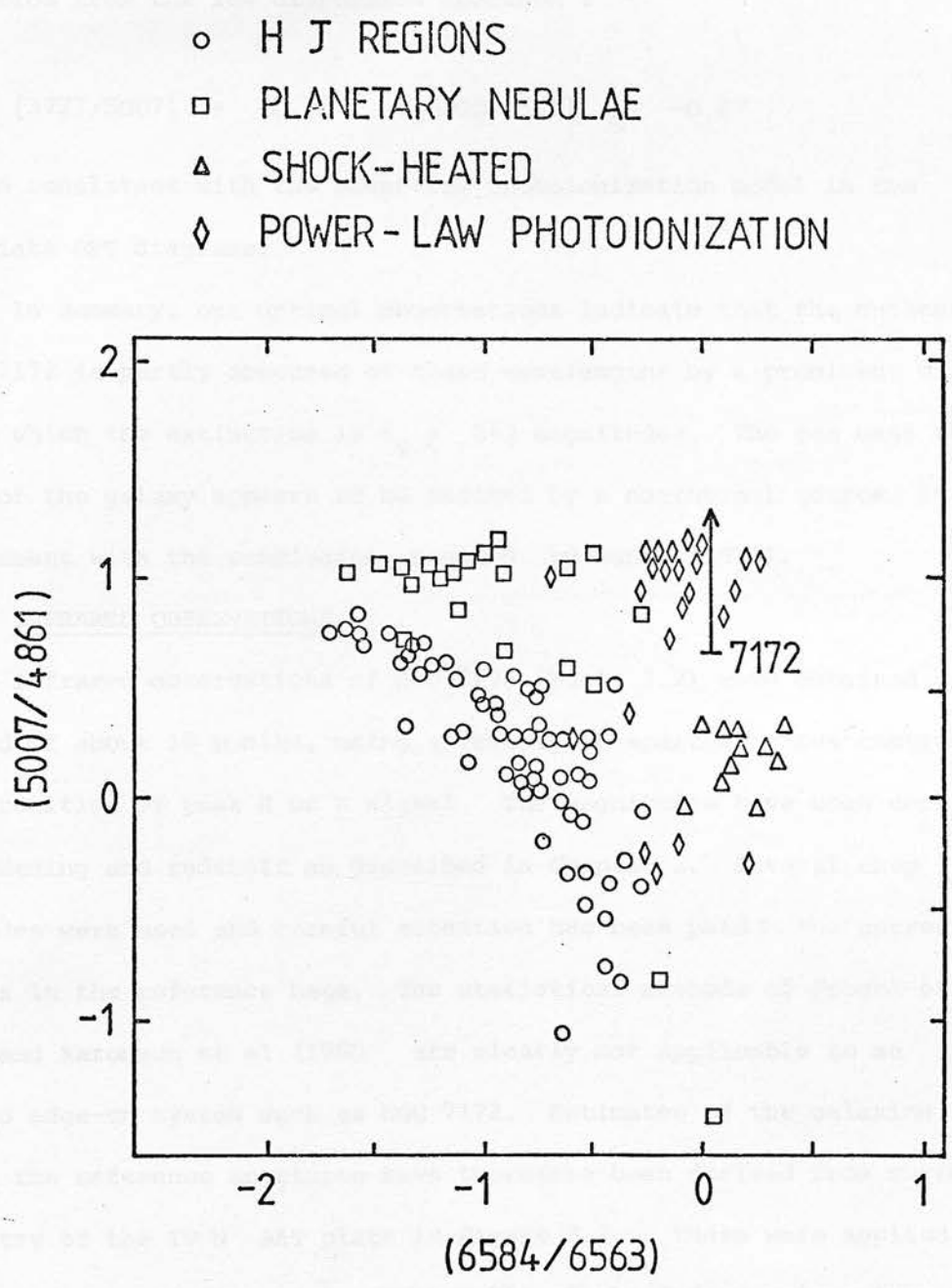

Figure 3.4

Emission-line intensity ratios for the nucleus of NGC7172. The upward arrow indicates a lower limit for the [OIII]λ5007/Hβ ratio. Other symbols are taken from Baldwin et al (1981).

emission, although the S/N is very much poorer. The reddening-corrected line ratios from the low dispersion spectrum :

$$[3727/5007] \simeq -0.18 \qquad [6300/6563] \lesssim -0.27$$

are also consistent with the power-law photoionization model in the appropriate BPT diagrams.

In summary, our optical observations indicate that the nucleus of NGC 7172 is partly obscured at these wavelengths by a prominent dust lane in which the extinction is $\tau_V \gtrsim$ 2-3 magnitudes. The gas near the centre of the galaxy appears to be excited by a nonthermal source, in disagreement with the conclusions reached by Rubin (1974).

3.3 INFRARED OBSERVATIONS

Infrared observations of NGC 7172 (Table 3.2) were obtained over a period of about 18 months, using a variety of aperture sizes centred on the position of peak H or K signal. The magnitudes have been corrected for reddening and redshift as described in Chapter 2. Several chop amplitudes were used and careful attention has been paid to the corrections for flux in the reference beam. The statistical methods of Frogel et al (1978) and Aaronson et al (1980 are clearly not applicable to an obscured edge-on system such as NGC 7172. Estimates of the galaxian flux in the reference apertures have therefore been derived from surface photometry of the IV N AAT plate in Figure 3.2. These were applied to the data using a simple model in which 75% of the J flux arises from the stellar component, which is assumed to have the colours appropriate to a normal early-type galaxy (Chapter 2) reddened by A_V = 3 magnitudes. The early observations were made by offset-guiding on nearby bright stars since the galaxy could not be seen directly. After December 1980, an integrating TV system became available for acquisition and guiding, which could be used to view the optical image. The IR nucleus (defined to be

TABLE 3.2 : Infrared Observations of NGC 7172

Date (UT)	Aperture (")	Telescope (m)	Chop (")	J	H	K	L	J	H	K	L
				(uncorrected)				(corrected)			
10.11.79	12.0	1.9	15	11.47	10.54	9.79	-	11.34	10.40	9.72	-
10.11.79	9.0	1.9	15	11.83	10.77	10.00	8.68	11.74	10.68	9.97	8.67
11.11.79	12.0	1.9	66	11.28	10.30	9.65	-	11.28	10.30	9.68	-
11. 5.80	10.8	3.8	14	11.66	10.72	9.97	8.74	11.55	10.60	9.91	8.72
11. 5.80	7.2	3.8	14	12.22	11.11	10.29	8.89	12.14	11.04	10.27	8.89
7. 9.80	5.1	3.8	39	12.60	11.33	10.38	8.96[4]	12.60	11.33	10.41	8.98
7.12.80	3.8	3.8	45	12.62	11.11	9.96	-	12.62	11.11	9.99	-
4. 6.81[1]	10.8	3.8	50	11.58	-	9.70	8.19	11.58	-	9.73	8.21
4. 7.81[2]	12.0	1.9	120	11.26	10.28	9.45	-	11.26	10.28	9.48	-
9. 7.81[3]	10.8	3.8	40	11.58	-	9.65	8.25	11.58	-	9.68	8.27
9. 7.81[3]	7.2	3.8	40	11.86	-	9.88	8.29	11.86	-	9.91	8.31
13. 9.81[3]	5.1	3.8	80	12.23	10.99	9.99	8.28	12.23	10.99	10.02	8.30

1 observations kindly provided by M. Stewart

2 " C.P.Blackman

3 " A.J.Longmore

4 L' : corrected by $0^{m}.35$ to standard filter

the position of peak H or K signal) was found to lie 2-3 arcseconds N of the optically brightest point, as might be expected from the discussion in § 3.2.

A low resolution map of the galaxy was made during September 1980 in the J and K wavebands. The major and minor axis profiles in Figure 3.5 were obtained by integrating at discrete points in the galaxy using a 5" beam and a 40" N-S chop. The shape of the profiles may be used to estimate the difference in the position of peak integrated flux between the J and K wavebands. This value is always < 1 arcsecond for the aperture sizes in Table 3.2, and indicates that no systematic errors are introduced by the choice of wavebands (always H or K) used to centre the galaxy nucleus in the apertures. The asymmetries in the profiles are readily identified with the distribution of dust in Fig 3.2, which is more dense to the N and E of the nucleus. The relatively wide peak of the J profile reflects the extended distribution of the old stellar component, whose spectral energy distribution peaks in the shorter wavelength bandpass. It is not possible to determine from this data whether the non-stellar component is also extended.

The multiaperture photometry in Table 3.2 exhibits a marked discontinuity between the September 1980 and December 1980 observing runs. This is most clearly illustrated by the growth curves in Figure 3.6, where the data taken up to and including the September 1980 run are plotted as filled symbols and that since the December 1980 run as open symbols. The decrease in the magnitude-aperture slopes with increasing wavelength is characteristic of a galaxy with a point-like souce of IR radiation in the nucleus. These curves become flatter after December 1980 because only the compact IR source can vary on such short timescales.

Variability in the IR flux from galaxies has always been a subject of much controversy (Stein, Gillett, and Merrill, 1974 ; Rieke

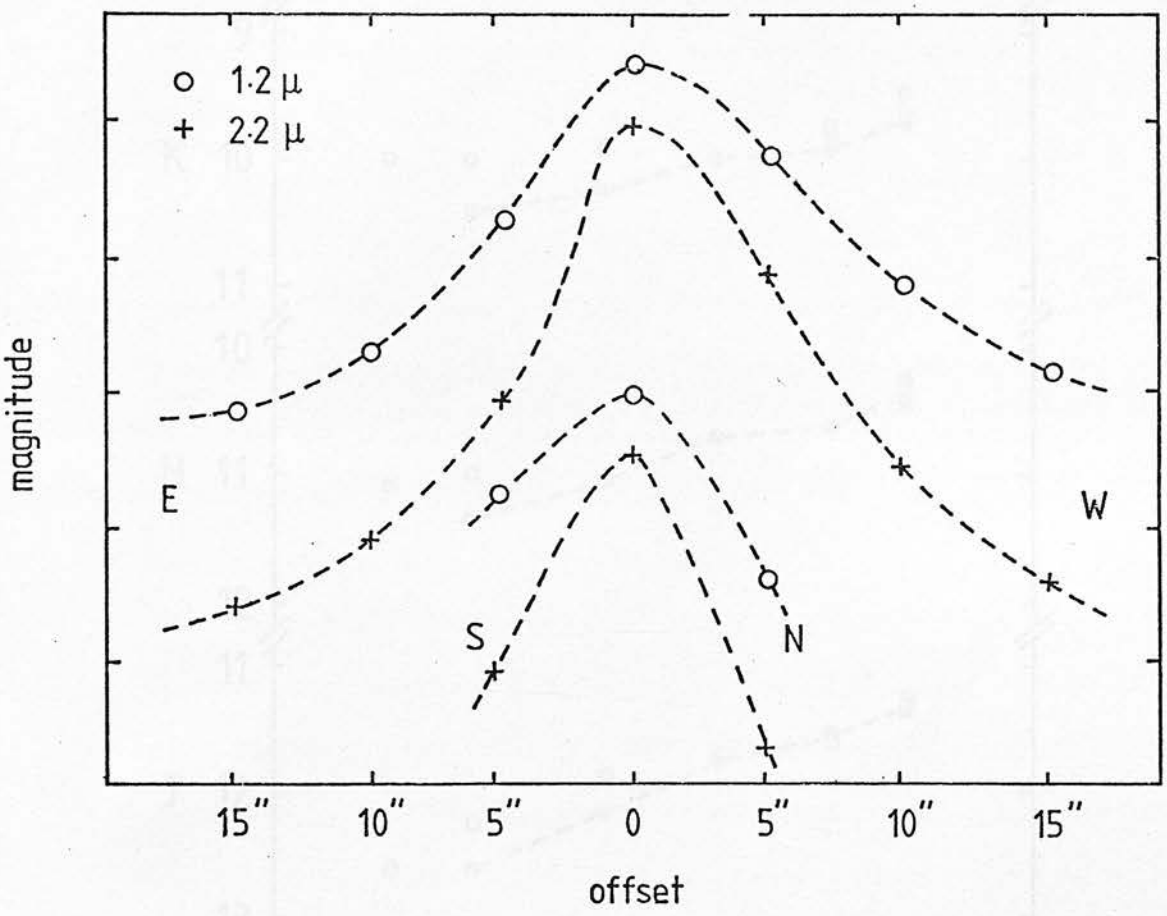

Figure 3.5

Infrared surface brightness profiles, obtained from spot measurements with a 5".1 beam, along the major (PA = 100°) and minor (PA = 10°) axes in the J & K bandpasses. Tick marks on the ordinate are at intervals of one magnitude and the mean central surface brightnesses are:

J = 15.88 mag/□"
K = 13.68 mag/□"

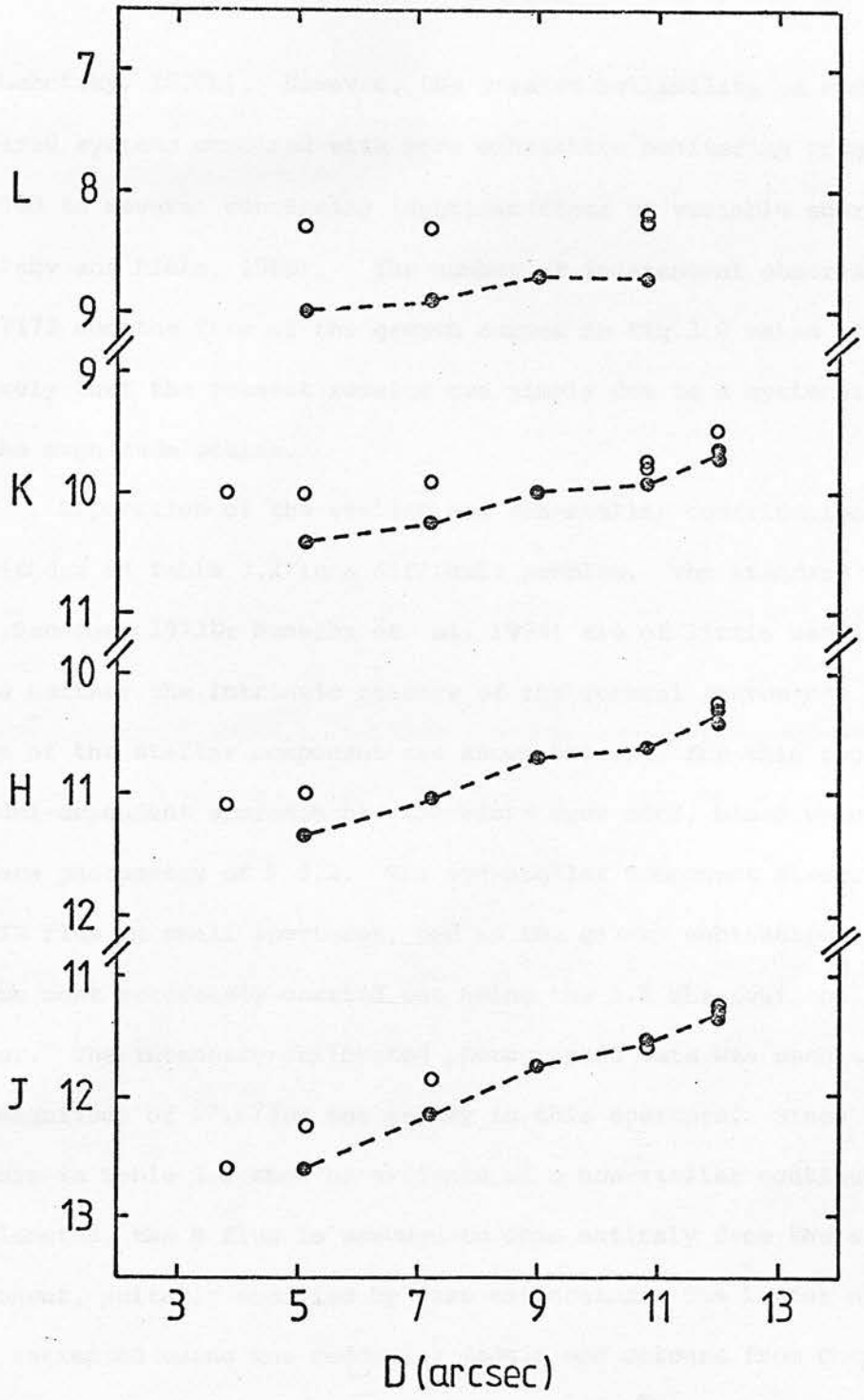

Figure 3.6 : Multiaperture infrared photometry of NGC7172. Observations made prior to Sept 1980 are denoted by filled circles; those made since Dec 1980 are plotted as open circles. The data have been corrected for Galactic extinction, redshift and reference beam corrections as described in the text.

and Lebofsky, 1979b). However, the greater reliability of modern infrared systems combined with more exhaustive monitoring programs, has led to several convincing identifications of variable sources (e.g. Lebofsky and Rieke, 1980). The number of independent observations of NGC 7172 and the form of the growth curves in Fig 3.6 makes it extremely unlikely that the present results are simply due to a systematic error in the magnitude scales.

Separation of the stellar and non-stellar contributions to the magnitudes in Table 3.2 is a difficult problem. The standard methods (e.g.Sandage, 1973b; Penston et al, 1974) are of little use in this case, since neither the intrinsic colours of the central source nor the growth curve of the stellar component are known reliably for this peculiar galaxy. A model-dependent approach has therefore been used, based upon the optical surface photometry of § 3.2. The non-stellar component clearly dominates the IR flux in small apertures, and so the galaxy subtraction procedure can be most accurately carried out using the $5\overset{''}{.}1$ observations in each colour. The intensity-calibrated photographic data was used to estimate a B magnitude of 17.17for the galaxy in this aperture. Since the UBV colours in Table 3.1 show no evidence of a non-stellar continuum at these wavelengths, the B flux is assumed to come entirely from the stellar component, suitably modified by dust extinction. The latter effect has been estimated using the reddening models and colours from Chapter 2, with a uniform distribution of dust and $\tau_V \sim 2\overset{m}{.}5$. The colours of the reddened stellar component :

U-B = 0.61 B-V = 1.12 V-J = 2.87

J-H = 0.87 H-K = 0.33 K-L = 0.33

are relatively insensitive to the distribution of dust (provided it is fairly well mixed) and the visual optical depth appears to be a reasonable

estimate given the discussion in § 3.2. The optical colours of this model are also consistent with the small aperture UBV data in Table 3.1.

The intrinsic spectrum of the nuclear source has been derived for two epochs using the IR observations from Sept 1980 and Sept 1981. The spectral energy distributions are plotted in Figure 3.7 using the flux calibration of Wilson et al (1972). Because the instrumental configuration was similar for both observations, the differential changes in the spectra are well determined, and indicate that the source had brightened by approximately 0.5 magnitudes over this 12 month period (Table 3.3). Any comparison with observations at different aperture sizes is severely limited at short wavelengths by the accuracy of the model adopted. The $3\overset{''}{.}8$ observations are, however, generally consistent with the conclusion that the majority of the change in brightness of the nuclear component took place between Sept 1980 and the Dec 1980, giving a characteristic variability timescale $\tau \sim (\partial \mathcal{E} n f_\nu / \partial t)^{-1} \sim 0.5$ yr. If the nuclear spectrum is dereddened using a standard Whitford (1958) extinction curve and $A_V = 2\overset{m}{.}5$ from the model, the intrinsic spectrum can be well-approximated over the 1-4 μ region by a power-law :

$$f_\nu \sim \nu^{-1.8} \quad (\pm 0.1)$$

TABLE 3.3: Spectral decomposition of NGC 7172

Component	J	H	K	L
Galaxy (5"1)	13.18	12.31	11.98	11.65
Source: 7/9/80	13.56	11.89	10.70	9.14
13/9/81	12.82	11.37	10.22	8.35
Dereddened (A_V=2.5)	12.18	10.99	10.00	8.26

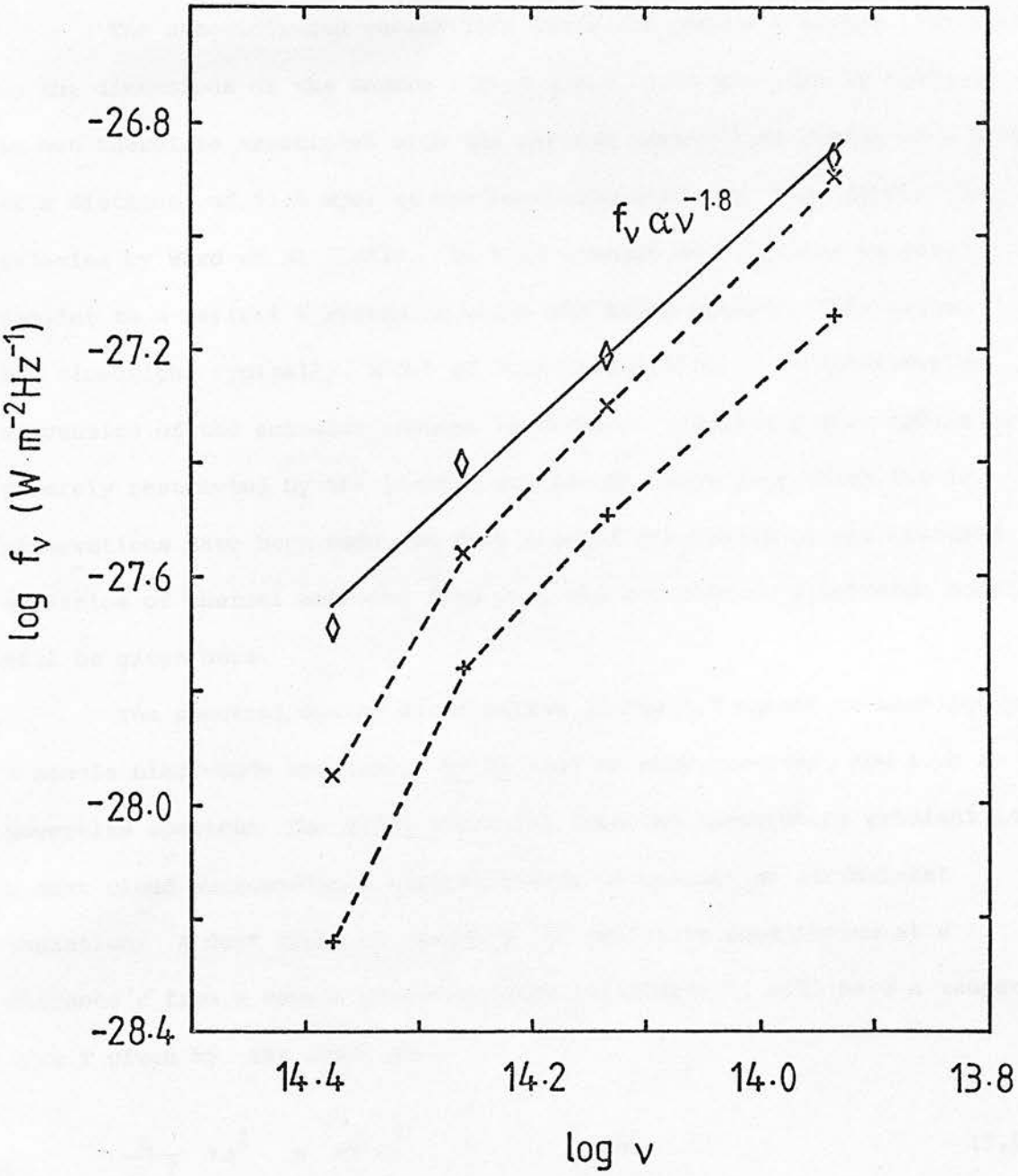

Figure 3.7 : Near-infrared spectra of the nuclear source in NGC7172, after subtraction of the stellar component. The data are plotted for two epochs : 1980.7 (+) and 1981.7 (x). Open diamonds are the most recent of these observations dereddened by $A_v = 2^m.5$. The straight line is a linear least squares fit to these points and has a slope of 1.8.

3.4 NON-THERMAL vs THERMAL MODELS

The near-infrared variability timescale places a strong constraint on the dimensions of the source : $D < c\tau \sim 0.15$ pc. The IR emission is not therefore associated with the optical narrow-line region ($D \sim 2$ kpc at a distance of 51.8 Mpc) as has been suggested for some Seyfert 2 galaxies by Ward et al (1981). In this respect NGC 7172 may be more similar to a Seyfert 1 system,in which the broad emission-line region has dimensions typically ~ 0.1 pc (Osterbrock,1979). A quantitative discussion of the emission process in terms of specific source models is severely restricted by the limited wavelength range over which the IR observations have been made, so only a brief discussion of the standard scenarios of thermal emission from dust and non-thermal synchroton models will be given here.

The spectral energy distribution in Fig 3.7 cannot be modelled by a single black-body spectrum. It is easy to show, however, how such a power-law spectrum can arise naturally from the temperature gradient in a dust cloud surrounding a central source of optical or ultraviolet radiation. A dust grain of radius 'a' in radiative equilibrium at a distance 'r' from a source of ultraviolet luminosity L, will have a temperature T given by the equation :

$$\frac{L}{4\pi r^2}\,\pi a^2 = 4\pi a^2 \int B(\nu,T)\, d\nu \qquad (3.1)$$

where the grains have been treated as black-bodies whose emission spectrum is given by the Planck function $B(\nu,T)$. Most of the IR emission arises from grains within one optical depth of the central source, so the attenuation of the incident radiation arises chiefly from the inverse

square law effect. Equation 3.1 may be integrated to give :

$$T \quad \alpha \quad r^{-\frac{1}{2}} \tag{3.2}$$

and so

$$\frac{dT}{dr} \quad \alpha \quad r^{-3/2} \tag{3.3}$$

If the density of grains at radius r is given by

$$\rho(r) \quad \alpha \quad r^{-x} \tag{3.4}$$

then the number of grains between r and r + dr is (assuming spherical symmetry) :

$$N(r)\ d(r) \quad = \quad 4\pi r^2 \quad \rho(r) \quad dr$$

or

$$N(r) \quad \alpha \quad r^{2-x} \tag{3.5}$$

From (3.2) and (3.3) :

$$N(T) \quad = \quad N(r) \quad \frac{dr}{dT} \quad \alpha \quad T^{2x-7} \tag{3.6}$$

The flux of radiation received at frequency ν is

$$F_\nu \quad \alpha \quad \int \quad B(\nu,T) \quad N(T) \quad dT \tag{3.7}$$

and to a first approximation it may be assumed that all the black-body flux is emitted at the frequency ν_m:

$$B(\nu,T) \quad \sim \quad C_1 \ T^4 \ \delta(\nu-\nu_m) \tag{3.8}$$

where $\nu_m = C_2 T$ is given by the Wien law ; C_1 and C_2 are constants. Substituting in (3.7) :

$$F_\nu \alpha \int T^{2x-7} \quad T^4 \quad \delta(\nu - C_2 T)\, dT$$

i.e. $$F_\nu \alpha \nu^{2x-3} \tag{3.9}$$

For a power-law slope of -1.8, a modest degree of central concentration is therefore required :

$$x \sim 2/3 \tag{3.10}$$

In practice, equation 3.9 is only valid up to a frequency $\nu_m = C_2 T_{max}$, where $T_{max} \sim 1000\text{-}1500^{\circ}$ K is the evaporation temperature of the grains. Real grain materials with emissivity $\varepsilon \alpha 1/\lambda^{\beta}$ and $0 \lesssim \beta \lesssim 3$ (Werner and Salpeter, 1969), would be hotter at a given distance r from the source than a black-body at the same distance, and the modified Planck function $\varepsilon_\nu B(\nu,T)$ would also peak at a shorter wavelength. A satisfactory fit to Figure 3.7 can only be obtained with $\beta > 2$ if $T_{max} < 1500^{\circ}$K. The degree of central concentration is then somewhat larger than that given by equation (3.10).

If the thermal emission mechanism is to be a satisfactory model for the source in NGC 7172, then the physical size implied by equation 3.1 must be less than the upper limit inferred from the variability timescale in § 3.3. The ultraviolet luminosity of the central source cannot be determined directly but a lower limit to L can be obtained by integrating the reradiated IR spectrum over the 1-4 μ region:

$$L_{IR} \sim 7.5\ 10^9\ L_\odot$$

This is likely to be a severe underestimate if the spectrum continues

to rise steeply into the far-IR (see for example Telesco and Harper 1980). Assuming the 3.5 μ radiation arises predominantly from grains at T ≃ 850° K, equation 3.1 requires

$$\tau \sim 1.22 \frac{L_{45}^{\frac{1}{2}}}{T_2} \gtrsim 0.15 \text{ yr}$$

which is just compatible with the IR observations in Table 3.2. The dependence of thermal variability timescales on wavelength $\tau \propto \lambda^{2.5}$ is not evident in the present data ; however, the constraints are rather weak because of the limited wavelength range of the observations. Puschell (1981) has suggested that the observed 1-10μ variations in the broad-line radio galaxy 3C382 are consistent with the predictions of the thermal models. Further observations of NGC7172 at longer infrared wavelengths are clearly desirable to test this hypothesis.

The case for a non-thermal origin of the IR radiation in Seyfert 1 nuclei has been put by Stein and Weedman (1976) and Neugebauer et al (1976). In the following section the analysis will be restricted to a simple discussion on the basis of incoherent synchroton theory (e.g. Ginsberg and Syrovatski, 1965). More general treatments can be found in Jones et al (1974a,b).

Optically thin synchroton emission from a relativistic electron energy distribution $N(E) \propto E^{-p}$ has a flux distribution of the form

$$f_\nu \propto \nu^{-\alpha}$$

where $\alpha = \frac{p-1}{2}$. The observed spectral index in NGC7172 ($\alpha = 1.8$) requires a moderately steep electron spectrum with $p = 4.5$. The equipartition field (Moffet, 1975) is given by :

$$B_{min} = 2.3 \, (a \, AL/V)^{0.29} \qquad (3.11)$$

where (a-1) is the ratio of the energy density in energetic baryons to

that in relativistic electrons, L is the luminosity and V the emitting volume of the source. $A = A(\alpha,\nu_1,\nu_2)$ is a numerical constant depending on the slope and cut-off frequencies of the spectrum. Taking $\nu_1 = 8.6\ 10^{13}$ (3.5 μ), $\nu_2 = 2.5\ 10^{14}$ (1.2μ), $L > 2.8\ 10^{43}$ ergs s^{-1}, $a = 2$ and $D = 0.15$ pc implies

$$B_{min} > 0.1 \text{ Gauss}$$

The critical frequency for synchroton emission from electrons of energy E is

$$\nu_c = 6.3\ 10^{18}\ B\ E^2 \tag{3.12}$$

which at the frequencies ν_1, ν_2 give $E_1 < 7$ GeV, $E_2 < 12$ GeV. The decay time due to synchroton losses for a 12 GeV electron is

$$T_{\frac{1}{2}} = (2.37\ 10^{-2}\ B^2\ E)^{-1} < 0.1 \text{ yrs} \tag{3.13}$$

which is comparable with the variability timescale. Inverse Compton losses will also generally be present in strong sources of small angular size. In the Thompson limit, the ratio of Compton to synchroton luminosity

$$L_{c/L_s} \simeq \frac{U_{ph}}{U_B} \tag{3.14}$$

where $U_{ph} = L/4\pi r^2 c$ is the photon energy density and $U_B = B^2/8\pi$ is the energy density in magnetic fields. For the equipartition field

$$L_{c/L_s} \sim 1.3$$

Inverse Compton scattering of the IR radiation would produce gamma-ray

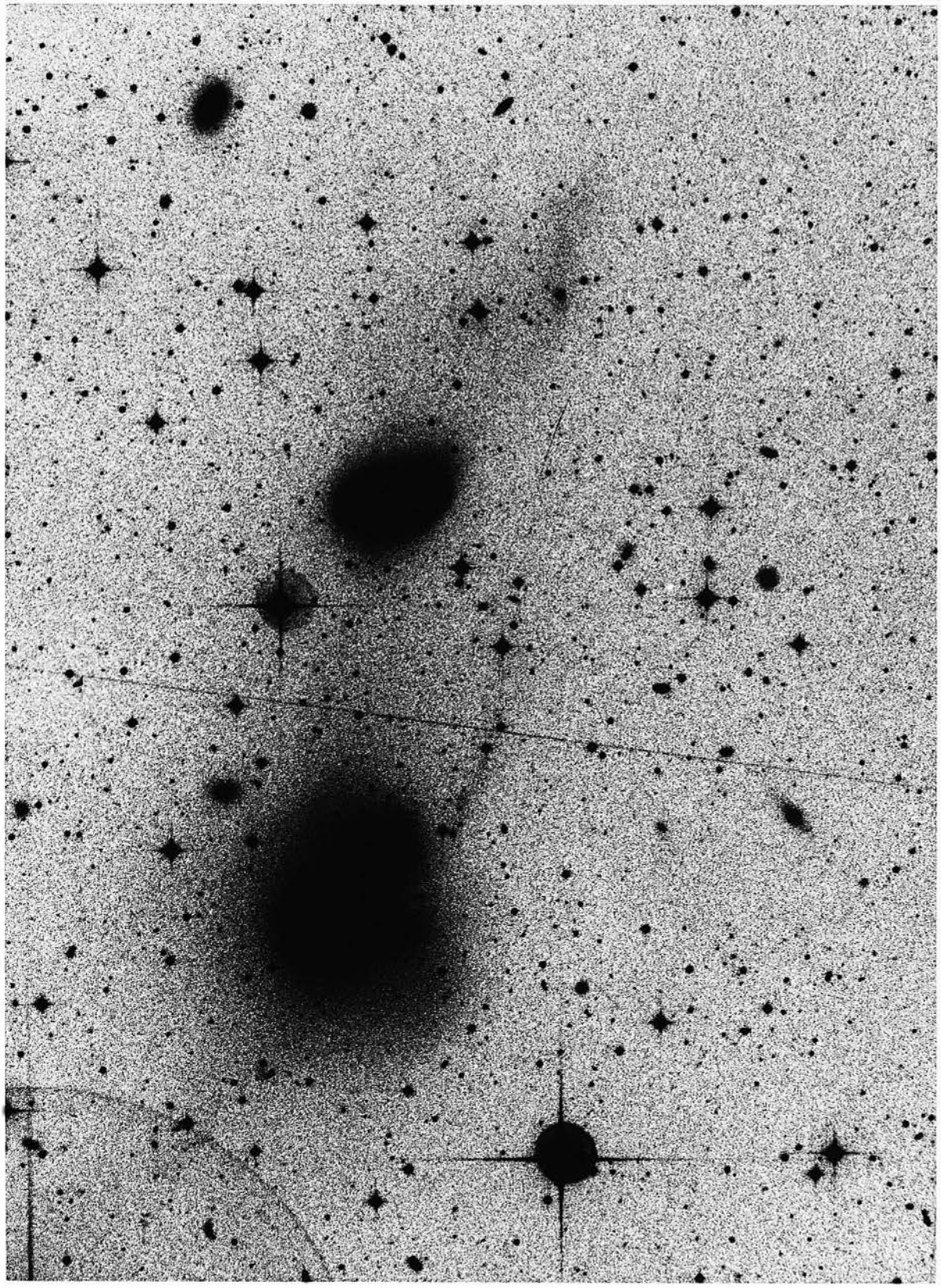

Figure 3.8 : A high contrast UK Schmidt plate of the NGC7172-group. North is up and East to the left. NGC7172 is the central galaxy with a very distorted bulge and a faint tidal tail extending to the NW. NGC7173, 7174 and 7176 are in the tightly-packed group to the South, which is burnt out on this deep photograph.

photons, since

$$\nu_{IC} \sim 4/3 \quad \gamma^2 \quad \nu_s \qquad (3.15)$$

where $E = \gamma m_o c^2$ is the electron energy, and m_o the electron rest mass. The synchroton source will also become optically thick at a frequency

$$\nu_{ss} \sim 8.10^{10} \text{ Hz}$$

which is consistent with the fact that NGC7172 is not known to be a strong radio source.

3.5 DISCUSSION

An upper limit to the mass of neutral hydrogen in NGC7172 has been measured by Bottinelli et al (1980) :

$$M_{HI} < 7.4\ 10^8\ h^{-1}\ M_\odot$$

This galaxy was one of only 2 which were not detected in a survey of 40 Sa/Sab morphological types. The majority of these early-type spirals form a homogeneous group, with $< M_{HI}/L_{opt} > \sim 0.15\ M_\odot/L_\odot$ and a dispersion of only 0.4 in $\log(M_{HI}/L_{opt})$. The much lower value of M_{HI}/L_{opt} (<0.03) found for NGC7172 is close to the upper limits established for many E and SO galaxies. The absence of spiral structure in Fig 3.2 raises the possibility that NGC7172 may be a pure lenticular system whose peculiar morphology is due to the irregular dust lane. Deep optical photographs (Fig 3.8) show that the galaxy is also severely affected by its nearby companions. A long tail ($\sim$ 80 h^{-1} kpc) is seen extending to the NW together with a gross distortion of the outer bulge. These features are characteristic of tidal interactions involving galaxies of approximately equal mass (Toomre and Toomre, 1972).

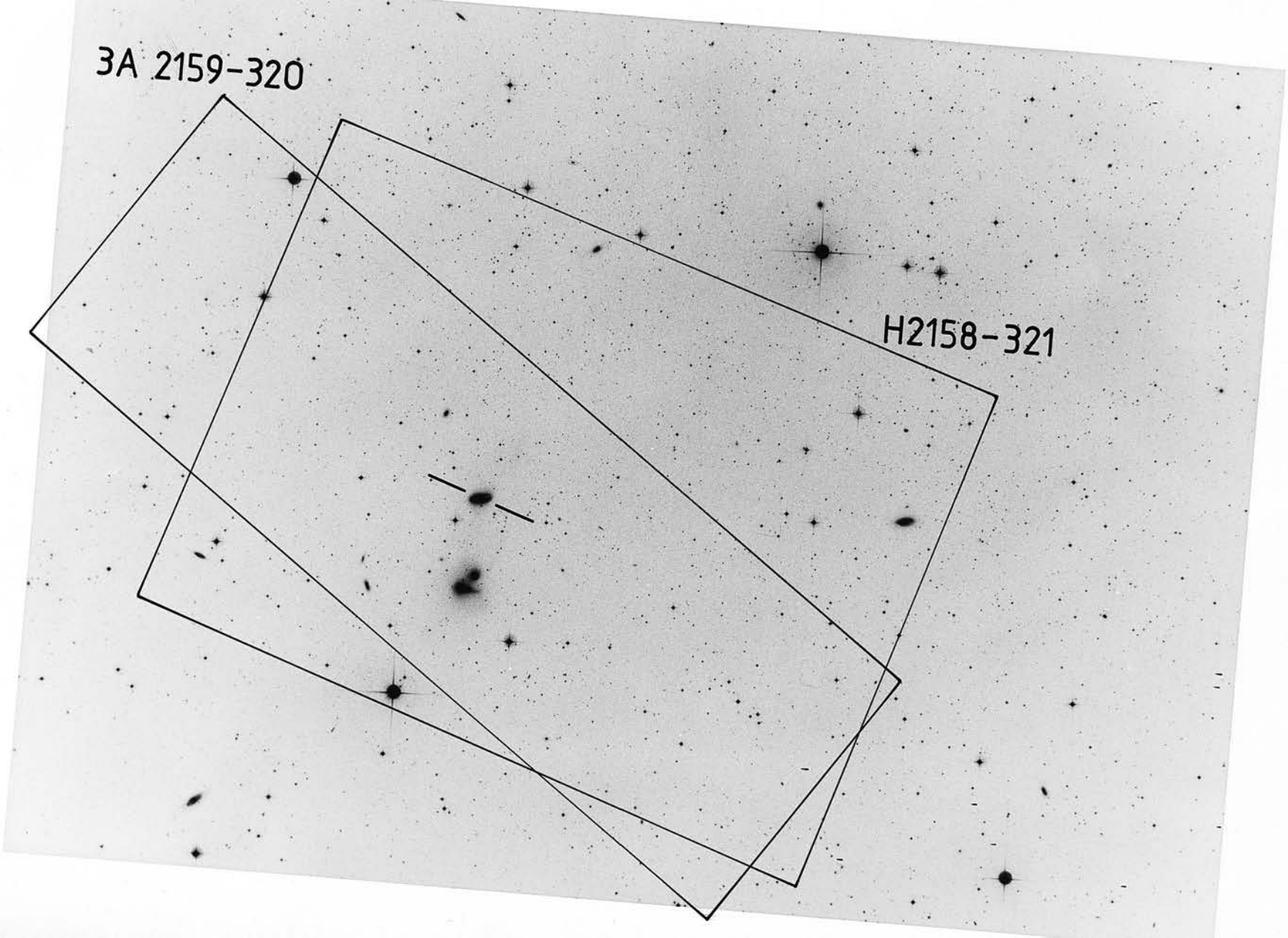
3A 2159-320
H2158-321

Figure 3.9: The 90% confidence contours for the hard X-ray sources H2158-321 (HEAO-A2) and 3A2159-320 (ARIEL V). Co-ordinates for the rectangle approximations were taken from Marshall et al (1979) and McHardy et al (1981). NGC7172 is marked with a bar. Assuming a conversion factor of

1 SSI ct/sec = 2.1 R15 cts/sec

the two experiments give slightly different values for the source flux :

HEAO-A2	1st scan	0.9 ± 0.1 SSI cts/sec
	2nd scan	0.7 ± 0.1 SSI cts/sec
ARIEL V		0.5 ± 0.07 SSI cts/sec

Although this might be taken as weak evidence for X-ray variability, the uncertainties in the conversion factors are large.

Marshall et al (1979) have proposed a tentative identification of the HEAO-A2 hard X-ray source H2158-321 with NGC7172. The uncertainty was largely due to Rubin's (1974) observations of a 'normal' optical spectrum. New evidence in favour of this identification is provided by the nuclear emission-line ratios discussed in section 3.2 and the survey at similar X-ray energies by the Ariel V satellite (Figure 3.9). Further support may also be found from the infrared observations in section 3.3. Several authors (Elvis et al, 1978, McAlarey et al 1979, Glass 1979) have proposed a correlation between the 3.5μ IR flux and the X-ray flux in active galaxies. Figure 3.10 shows that NGC7172 also fits this relation remarkably well. The correlation could arise naturally from inverse Compton scattering of infrared photons by low energy (∿ 60 MeV) electrons.

No sensitive searches for radio emission from NGC7172 appear to have been made up to the present time. On the basis of the observed correlation between radio and IR fluxes in Seyfert galaxies (de Bruyn and Wilson 1978 ; Ward et al 1981) the predicted radio flux would be :

$$S_\nu \text{ (21 cm)} \sim 10\text{-}1000 \text{ mJy}$$

The higher values are probably excluded by the non-detection of NGC7172 in southern radio source surveys (e.g. Large et al,1981).

3.6 CONCLUSIONS

NGC7172 has been found to be a particularly interesting example of the subset of early-type disk galaxies with dust. The true nucleus of the galaxy is partially obscured by the strong dust lane, and a lower limit for the extinction to the source of the optical line-emission and near-IR continuum of $A_V \sim 2\text{-}4$ mag. has been derived. Observations of variability in the nuclear infrared source limit the size of the

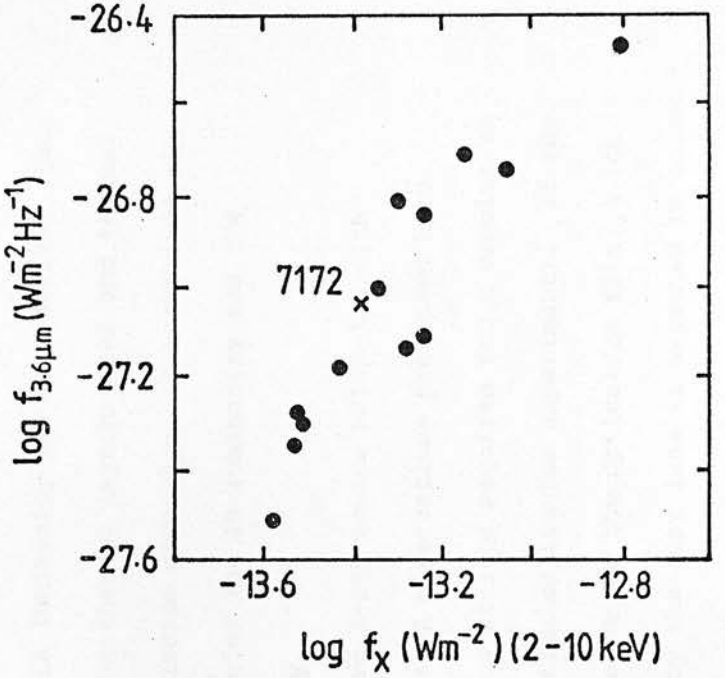

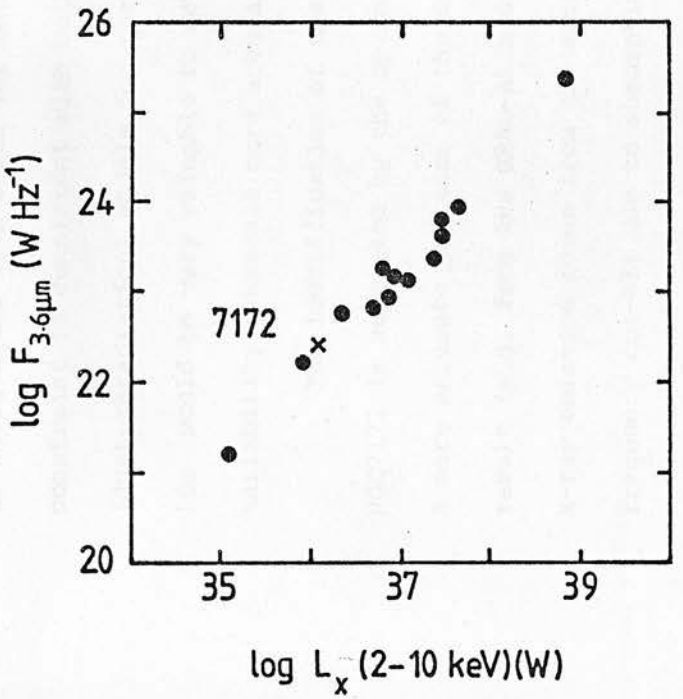

Figure 3.10: The correlation between infrared and X-ray flux for NGC7172 and a sample of X-ray galaxies from Elvis et al (1978). The X-ray flux is based on a calibration of

$$1\text{SSI}\quad \text{ct/sec} = 5.4\ 10^{-11}\ \text{ergs}\ s^{-1}\ cm^{-2}$$

in the 2-10 KeV band. NGC7172 lies close to the mean relations for both the observed (upper diagram) and intrinsic (lower diagram) fluxes. The first of these comparisons is important because of the spurious correlations which can arise between distance-dependent parameters in incompiete samples.

emission region to less than $\sim$ 0.15 pc. Because of the limited range of wavelengths from which the total IR luminosity has been derived, this constraint is consistent with both non-thermal (synchroton) and thermal (dust-reradiation) models for the emission mechanism. Observations at 10μ would be very valuable to determine the IR luminosity and the variability timescale more accurately.

The identification of the hard X-ray source H2158-321 with NGC7172 is supported by the optical & IR observations presented here. A more accurate position of the source will be required for a conclusive result (e.g. from the HEAO-A1 modulation collimator experiment). If the X-ray emission comes from the same region as the optical/IR flux, a low frequency cut-off due to absorption by the dust lane is expected to occur at E $\sim$ 1.2 keV. Observations of the soft X-ray flux from NGC7172 would be required to determine the optical depth to the X-ray emitting region directly. Lawrence et al (1981) have suggested that the large absorbing columns required to explain the 1-10 keV spectra of several narrow emission-line galaxies may be responsible for the lack of strong broad emission lines in their optical spectra. Unfortunately, the spectroscopic data presented in § 3.2 are not of sufficient quality to detect the presence of weak broad wings on the permitted lines, like those which have been found in several X-ray emission-line galaxies by Shuder (1980) & Veron et al (1980). Ward et al (1978) have remarked upon the tendency for these galaxies to be members of interacting groups and contain considerable quantities of dust, both of which are clearly the case for NGC7172.

CHAPTER 4

OPTICAL PROPERTIES OF THE DISCLESS GALAXY SAMPLE

The restricted sample of elliptical-like galaxies with dust-lanes identified in Chapter 1 (Table 1.1) clearly exhibits a wide variety of optical morphological peculiarities. Hawarden et al (1981) have discussed in some detail how these galaxies deviate from the conventional classification schemes outlined by de Vaucouleurs (1959) and Sandage (1961). An interesting problem which remains to be discussed is whether these galaxies exhibit any further anomalous optical properties which would isolate them from a comparable sample of morphologically normal ellipticals.

4.1 UBV PHOTOELECTRIC PHOTOMETRY

4.1.1 Observations

Multiaperture UBV photometry of a selection of galaxies from Table 1.1 was obtained in November 1979 with the Peoples Photometer on the 0.5 m telescope at SAAO. The EMI 6256 (S13) tube was operated at -10^{o}C, giving a mean dark count of 30 (10 sec)$^{-1}$. Both dark counts and β-source counts were taken each night to monitor the tube performance. Since the UBV system in use at SAAO closely approximates the Johnson system, mean colour equations for this tube were adopted throughout. The observations were reduced w.r.t. Cousins (1973) E-region standards using mean extinction co-efficients, and the aperture sizes were taken from Smyth and Stobie (1980). The mean internal errors estimated from repeat observations on separate nights are :

$$\sigma_V = 0.03 \qquad \sigma_{B-V} = 0.03 \qquad \sigma_{U-B} = 0.04$$

Several well-observed galaxies were also included in the program as a check on possible systematic errors. Additional observations of some of the dust-lane galaxies were available from the literature and from Hawarden (private communication), so Table 4.1 lists measurements in at least one aperture size for 21 galaxies or 55% of the sample identified in Table 1.1.

4.1.2 Standard Diameter System

The use of a fixed aperture size or range of aperture sizes inevitably introduces some redshift-dependent systematic effects into Table 4.1. These may be quantified by defining effective aperture sizes with respect to a uniform system of galaxy diameter measurements. De Vaucouleurs et al (1976, hereafter RC2) have adopted an isophotal diameter system based on the B = 25 mag/arcsec^2 isophote, and present formulae to reduce the diameters from several catalogues to this homogeneous system. Of particular relevance to the present work are the relations :

$$\log D_{25}^{RC2} = 0.22 + 0.88 \log D^{UGC} \quad (4.1)$$

$$\log R_{25}^{RC2} = 0.95 \log R^{UGC} \quad (4.2)$$

where D^{UGC} is the diameter (in units of 0.1) and R^{UGC} is the axial ratio, as measured by Nilsson (1973) from the Palomar Survey blue plates. Eight galaxies from Table 4.1 have diameter estimates in the RC2. Using equation (4.1) to correct these values back to the survey-plate based system of the UGC for comparison with the measurements in Table 1.1, the mean difference (in the sense RC2 - this work) is :

$$< \Delta \log D > = -0.14 \quad (4.3)$$

with a standard deviation of $\sigma(\Delta \log D) = 0.15$.

TABLE 4.1 : Optical photometry of the discless galaxy sample

Galaxy	Log D(O)	Aperture	Source	V	(B-V)	(U-B)	B_T
IC1575	1.15	35.2	LS	13.93	1.14	0.55	14.3
0147-269	1.01	35.2	LS	14.75	1.01	-	15.1
		75.3	LS	14.25	1.00	-	
0151-498	1.13	20.9	TGH	13.57	1.14	0.64	13.6
		30.1	TGH	13.27	1.12	-	
		35.2	LS	13.21	1.11	0.59	
		59.6	TGH	12.81	1.08	0.60	
		75.3	LS	12.70	1.07	0.57	
		84.6	TGH	12.62	1.07	0.52	
0219-345	0.95	20.9	TGH	14.48	1.12	0.54	14.8
		35.2	LS	14.20	1.09	0.56	
		42.6	TGH	14.04	1.07	0.52	
		75.3	LS	13.96	1.07	-	
0418-583	0.74	30.1	TGH	14.92	0.92	0.22	15.4
		42.6	TGH	14.58	0.94	0.20	
NGC1947	1.43	10.5	W	13.68	1.03	0.59	12.0
		14.3	W	13.14	1.10	0.58	
		22.6	WW	12.79	1.09	0.66	
		55.0	WW	11.66	1.04	0.52	
		110.0	WW	11.15	1.05	0.66	
0609-331	0.77	35.2	LS	14.54	1.12	-	15.3
0632-629	1.09	20.9	TGH	14.72	1.18	0.53	14.8
		30.1	TGH	14.44	1.16	0.60	
		35.2	LS	14.38	1.12	-	
		42.6	TGH	14.23	1.15	0.53	
		75.3	LS	13.98	0.96	-	
0711-604	0.77	20.9	TGH	14.51	1.15	0.54	15.0
NGC2534	1.17	15.0	WE	14.29	0.91	0.34	13.7
		41.0	HU	13.55	0.85	0.32	
0959-314	1.04	20.9	TGH	12.90	1.11	0.68	13.1
1029-314	1.22	20.9	TGH	13.06	1.20	0.78	13.1
NGC3302	1.04	20.9	TGH	13.64	1.08	0.55	13.7
NGC3523	1.17	20.9	TGH	13.37	1.13	0.67	13.4
NGC4753	1.70	49.9	VM1	11.18	1.06	0.62	10.6
		114.3	VM1	10.41	0.99	0.52	
		161.5	VM1	10.19	0.99	0.49	
NGC5128	2.29	20.0	K	13.47	1.69	0.95	-
		30.0	VB	12.68	1.64	0.92	
NGC5266	1.43	15.1	W	12.82	1.18	0.70	12.0
		33.8	W	12.14	1.13	0.69	

Galaxy	Log D(O)	Aperture	Source	V	(B-V)	(U-B)	B_T
NGC5363	1.70	49.9	VM1	11.36	1.13	0.45	11.0
		64.3	VM1	11.23	1.08	0.39	
		114.3	VM1	10.66	1.05	-	
NGC5485	1.39	84.0	B	11.94	0.89	0.54	12.3
		134.0	B	11.74	0.98	0.59	
NGC7070A	1.27	35.2	LS	13.55	1.00	0.52	13.3
		75.3	LS	12.71	0.97	0.44	
		99.6	VM1	12.47	1.02	0.52	
NGC7432	1.18	35.2	LS	13.86	1.10	-	14.1

REF:

B - Bigay J.H. 1964 Pub.Obs. Haute Provence, 7.

HU - Huchra J.P. 1977 Ap.J.Supp 35, 171.

K - Kunkel W.E. & Bradt H.V. 1971. Ap.J. 170,L1.

LS - this work.

TGH- T.G. Hawarden, private communication.

VB - van den Bergh S. 1976 Ap.J. 208, 673.

VM1- de Vaucouleurs G. & de Vaucouleurs A. 1972 Mem. RAS 77, 1.

W - Wegner W.G.1979. Aph.Sp.Sci 60, 15.

WE - Weedman D.W.1973 Ap.J 183, 29.

WW - Westerlund B.E. & Wall J.V. 1969 A.J.74, 335.

An important effect in any comparison of this kind is the fainter limiting isophote of the UK Schmidt plates, which leads to systematically larger visual diameter estimates. This can be seen most clearly by comparing with the measurements from the Palomar (POSS) and UK Schmidt (UKS) plates independently :

$$\text{POSS (4 gals)} : \quad \langle \Delta \log D \rangle = -0.03 \quad \sigma(\Delta \log D) = 0.09 \tag{4.4}$$

$$\text{UKS (4 gals)} : \quad \langle \Delta \log D \rangle = -0.27 \quad \sigma(\Delta \log D) = 0.06 \tag{4.5}$$

To reduce the diameter estimates from Table 1.1 to the RC2 system, therefore, the UK Schmidt measurements only have been corrected by -0.25 (in log D) before applying equation 4.1. A comparison of axial ratios R (= a/b) gives

$$\langle \Delta \log R \rangle = 0.02 \qquad \sigma(\Delta \log R) = 0.06 \tag{4.6}$$

with no dependence on the source of the measured values. The axial ratios have therefore been reduced to the RC2 system directly using equation 4.2. Isophotal diameters also depend on the inclination of the galaxy. Although this correction is somewhat arbitrary in a sample whose three-dimensional shape is very uncertain, the data have been further reduced to "face-on" diameters following the RC2 :

$$\log D(o) = \log D_{25} - 0.235 \log R_{25} \tag{4.7}$$

A comparison of the eight galaxies in common with the RC2 then gives :

$$\langle \Delta \log D(o) \rangle = 0.02 \quad \sigma(\Delta \log D(o)) = 0.06 \tag{4.8}$$

Because of the small sample involved and the bias towards brighter galaxies, a conservative estimate of 0.1 has been adopted for the mean error in both log D(o) and log R_{25}.

4.1.3 Optical Colours

Photoelectric photometry of large samples of galaxies has revealed several important properties of their UBV colours. An overall correlation with Hubble type is found, in the sense that late-type galaxies have generally bluer colours which are attributed to an increasing population of young stars. Early-type galaxies also exhibit a correlation (particularly of U-B colour) with absolute magnitude (Visvanathan and Sandage 1977, Griersmith 1980c). Because of the observed variations in absorption-line strengths (Faber 1977), this effect is usually interpreted as a change in metal-abundance (which affects the U-band mainly through line-blanketting) with luminosity. Finally, a variation of colour with effective aperture size is observed (being redder at smaller apertures). In E/SO galaxies this has been attributed to the same cause as the colour-absolute magnitude effect, because of the similarity of the two relations when plotted in colour-colour diagrams (Strom et al, 1976).

At least the last two effects would be expected to play a role in determining the colours of the dust-lane galaxies in Table 4.1. A detailed comparison with previously published data on morphologically normal ellipticals would require complete redshift information and mean colour-aperture growth curves (e.g. Sandage and Visvanathan 1978b), but a more rudimentary approach can be made using colour distributions. Figures 4.1 & 4.2 show the U-B and B-V histograms for the dust-lane galaxies (DLG), where unweighted mean colours have been adopted if observations at more than one aperture size were available. The upper histograms were derived from a comparable survey by Wegner (1979) of 42 elliptical galaxies.

The two samples are seen to be remarkably similar in their mean UBV properties. NGC5128 (U-B =0.93, B-V = 1.66) is clearly anomalous,

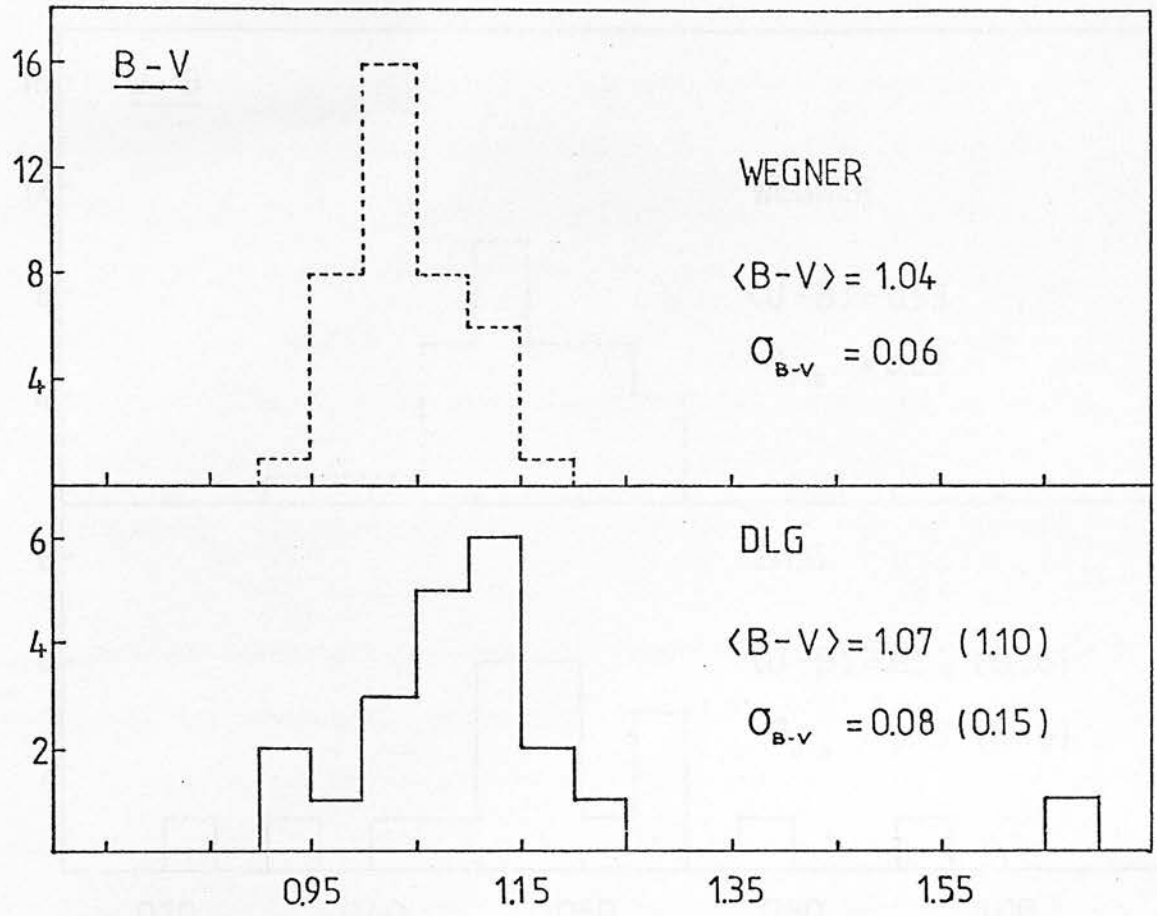

Figure 4.1 : Histogram of B-V colours for the dust-lane galaxies (DLG) and a sample of normal ellipticals from Wegner (1979). No corrections for reddening or redshift have been applied. The mean and standard deviation of the two distributions is given, with NGC5128 omitted from the DLG sample (values including this galaxy are enclosed in parentheses).

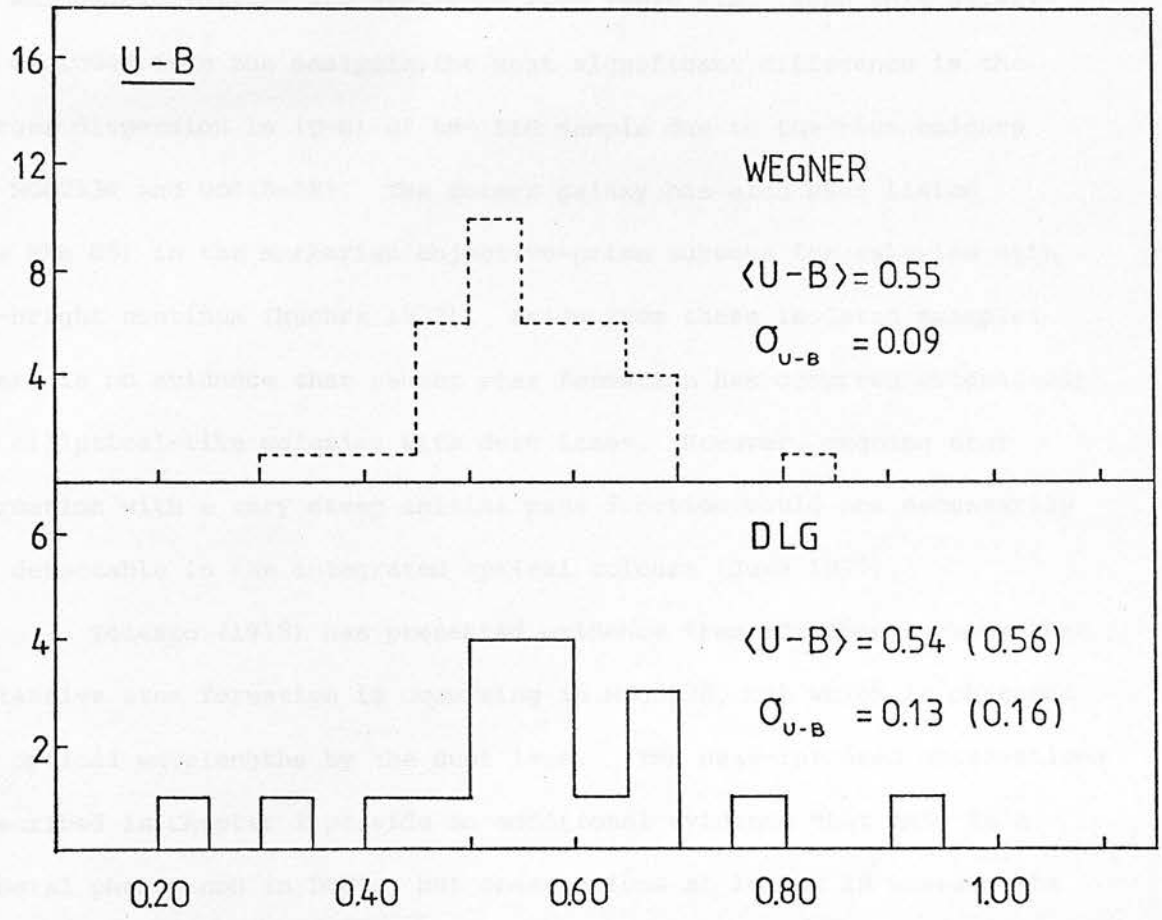

Figure 4.2 : Histogram of U-B colours for the dust-lane galaxies (DLG) and a sample of normal ellipticals from Wegner (1979). No corrections for reddening or redshift have been applied. The mean and standard deviation of the two distributions is given, with NGC5128 omitted from the DLG sample (values including this galaxy are enclosed in parentheses).

but this is partly an artifact of the very small effective apertures at which observations are available from Table 4.1. When this galaxy is excluded from the analysis,the most significant difference is the larger dispersion in (U-B) of the DLG sample due to the blue colours of NGC2534 and UO418-583. The former galaxy has also been listed (as Mkn 85) in the Markarian objective-prism surveys for galaxies with UV-bright continua (Huchra 1977). Aside from these isolated examples, there is no evidence that recent star formation has occurred extensively in elliptical-like galaxies with dust lanes. However, ongoing star formation with a very steep initial mass function would not necessarily be detectable in the integrated optical colours (Jura 1977).

Telesco (1978) has presented evidence from 10μ observations that extensive star formation is occurring in NGC5128, but which is obscured at optical wavelengths by the dust lane. The near-infrared observations described in Chapter 2 provide no additional evidence that this is a general phenomenon in DLG's, but observations at longer IR wavelengths are probably necessary for a satisfactory test.

It has been noted in previous sections that the integrated optical colours of DLG's would not necessarily be expected to show the effects of internal reddening, since the covering factor of the dust lanes is generally small for the aperture sizes listed in Table 4.1, so the flux becomes dominated by the unobscured regions of the galaxy.

4.1.4 Total Magnitudes

Using the isophotal diameters listed in Table 4.1, total magnitudes (B_T) may be derived for each galaxy from standard magnitude-aperture growth curves (c.f. de Vaucouleurs and Corwin 1977). Because only a limited number of aperture sizes are available for most of these galaxies, a simple extrapolation using the mean E/SO growth curve from de Vaucouleurs and de Vaucouleurs (1964, hereafter RCBG) has been

adopted, after applying a zero-point correction of $0^m.3$ to the RCBG diameters to bring them onto the RC2 system (see RC2). Where more than one aperture magnitude is available the internal scatter in the total magnitudes is typically $0^m.15$. Mean values have been obtained by weighting the larger apertures more heavily. A comparison of 5 galaxies which also have B_T magnitudes in the RC2 gives :

$$<\Delta B_T> = 0.10 \qquad \sigma(B_T) = 0.20 \tag{4.9}$$

Again, because of the small size of this sample, a conservative estimate of $0^m.5$ has been adopted for the mean error in the B_T magnitudes given in Table 4.1.

4.2 SPECTROSCOPIC OBSERVATIONS

Optical spectroscopic observations of a sample of galaxies from Table 1.1 were obtained in June 1980, using the same instrumental configuration as for the low dispersion spectra of NGC7172 (see section 3.2). The primary objectives of this program were to increase the number of known redshifts in the sample and to search for galaxies with strong emission-line spectra. Additional galaxies from the infrared sample in Chapter 2 were also observed as time permitted.

Absorption-line redshifts were determined for 15 galaxies using standard cross-correlation techniques described in Chapter 5. A further 5 have radial velocity measurements available from the literature (Table 4.2). To estimate the external errors in the SAAO redshifts, they have been compared with values from the literature or from higher dispersion AAT observations obtained in July 1980. The number of objects available for this comparison was increased to 10 by including those galaxies in the IR (disk) sample with independent redshift estimates. Figure 4.3 shows the results of this analysis. A mean error of 60 kms^{-1}

TABLE 4.2 : Redshift data for the restricted sample of elliptical-like galaxies with dust lanes. Column 1 is the galaxy identification ; column 2 the total blue absolute magnitude corrected for Galactic extinction ; column 3 lists the independent redshift estimates from the sources in column 7 ; column 4 is the SAAO heliocentric velocity from the present work, with the cross-correlation error parameter in column 5 ; the presence or absence of emission lines is noted in column 6.

Galaxy	$M_{B_T^o}$	V_c	V_s	r	Emission	Ref
IC1575	-21.2	-	5637	4.3	N	-
U0151-498	-22.1	6172	6315	3.7	Y	1
NGC1947	-19.2	902	-	-	N	2
NGC2534	-20.8	3580	-	-	N	3
U1029-459	-21.2	-	2882	4.6	Y	-
NGC3302	-20.8	-	3556	3.6	N	-
NGC3523	-21.1	-	3516	5.2	N	-
U1118-291	-	-	8800	3.5	N	-
NGC4753	-21.2	1255	-	-	N	2
NGC5128	-21.6	541	-	-	Y	2
NGC5266	-22.5	3040	3107	7.6	Y	4
IC4320	-	-	6739	3.2	N	-
U1352-336	-	-	4569	3.7	N	-
NGC5363	-20.7	1121	1182	3.1	Y	1
NGC5485	-21.0	1985	-	-	N	2
NGC5626	-	6849	6895	4.1	N	1
U1459-724	-	-	4460	3.9	N	-
NGC5799	-	-	2968	5.2	N	-
NGC7070A	-20.3	2392	2358	4.7	N	1
U2350-297	-	-	8496	3.0	N	-

Ref:

Sources of comparison velocities (V_c) :

1 : AAT observations

2 : RC2

3 : Sargent 1972 ApJ 173, 7

4 : Martin 1976 MNRAS 175, 633.

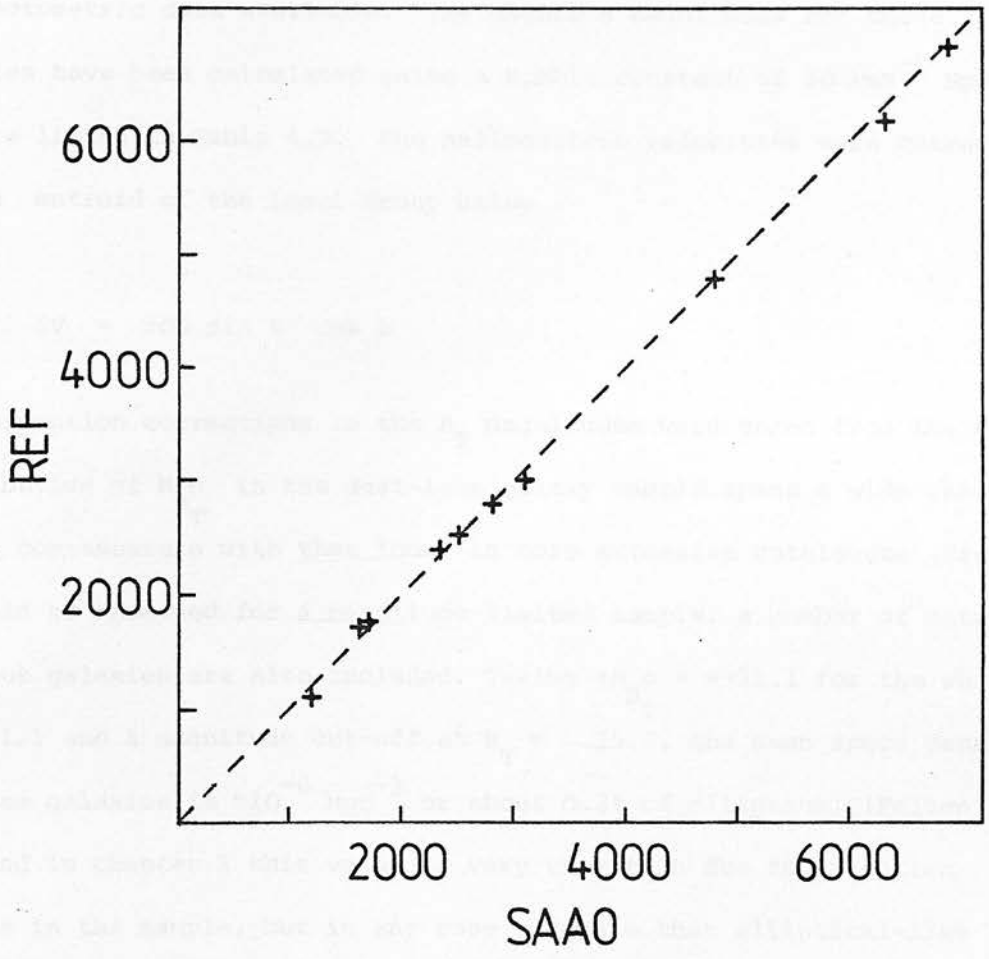

Figure 4.3 : A comparison of SAAO cross-correlation redshifts with velocities from other sources listed in Table 4.2. The dotted line has a slope of 1, and the rms residual is 60 kms^{-1}. Four of the galaxies in this diagram (NGC5719, NGC7172, NGC7213 & NGC7225) were observed to obtain redshifts for the infrared sample discussed in Chapter 2 ;their velocities are listed in Table 2.3.

has been adopted for all the SAAO heliocentric velocities in Table 4.2, since there is no correlation of the velocity residuals with the formal error parameter r (c.f. Chapter 5). This uncertainty is comparable with the formal error in the wavelength calibration, which for these low-dispersion data had an rms residual (in the fit of arc line positions vs wavelength) of 50 kms^{-1}.

A total of 13 galaxies from Table 1.1 have both spectroscopic and photometric data available. The absolute magnitudes for these galaxies have been calculated using a Hubble constant of 50 kms^{-1} Mpc^{-1}, and are listed in Table 4.2. The heliocentric velocities were corrected to the entroid of the Local Group using :

$$\Delta V = 300 \sin \ell \cos b$$

and absorption corrections to the B_T magnitudes were taken from the RC2. The distribution of $M_{B_T}^o$ in the dust-lane galaxy sample spans a wide range, but is commensurate with that found in more extensive catalogues (Fig.4.4). As would be expected for a magnitude-limited sample, a number of extremely luminous galaxies are also included. Taking $\langle M_{B_T}^o \rangle = -21.1$ for the whole of Table 1.1 and a magnitude cut-off at $B_T = 15.5$, the mean space density of these galaxies is $\sim 10^{-6}$ Mpc^{-3} or about 0.2% of ellipticals (Felten 1977). As noted in Chapter 1 this value is very uncertain due to selection effects in the sample, but in any case suggests that elliptical-like galaxies with large-scale dust features are very rare objects.

4.3 ISOPHOTE STRUCTURE

The resurgence of interest in elliptical galaxies in recent years has prompted several careful studies of their optical structure (e.g. King 1978 ; Williams and Schwarzschild 1979 ; Leach 1981). Luminosity profiles are particularly difficult to determine accurately, because of

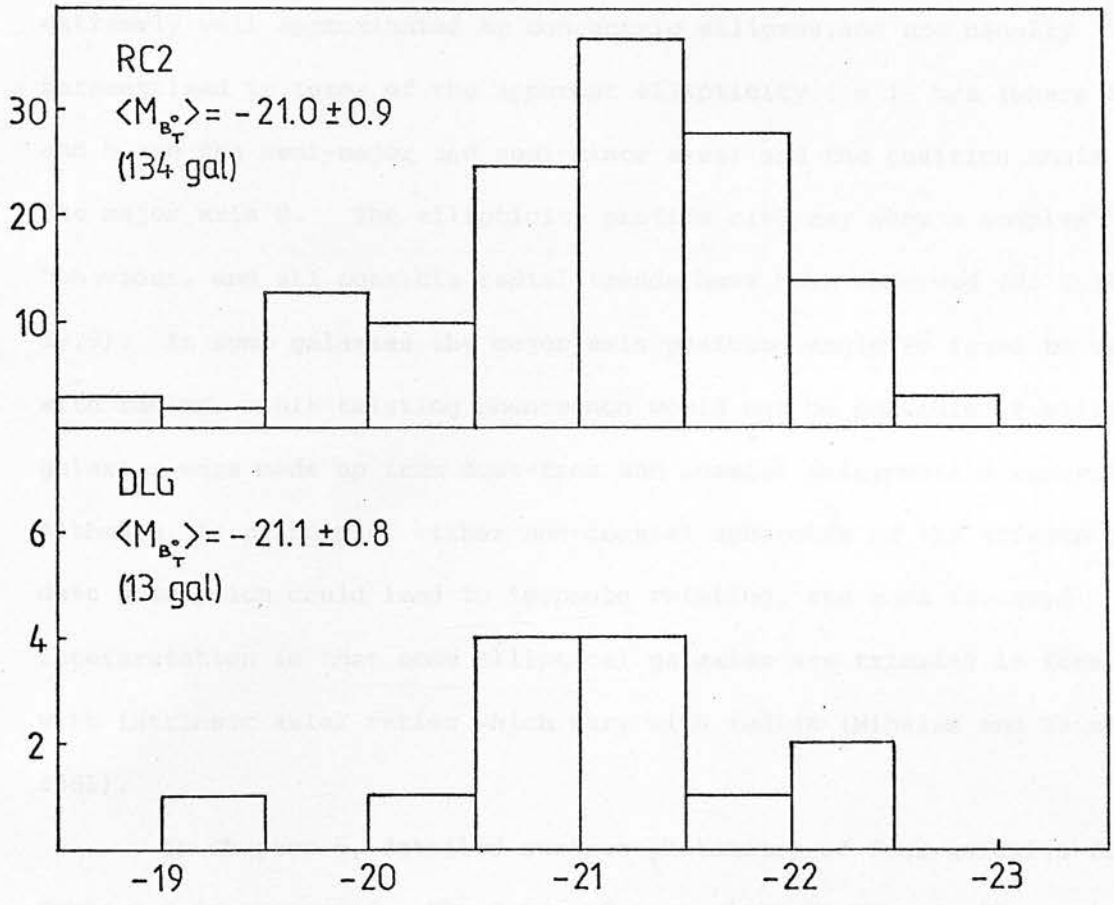

Figure 4.4 : The distribution of absolute magnitudes for the 13 galaxies with photometry and redshifts. Values of $M_{B_T^o}$ have been calculated from the B_T magnitudes of Table 4.1 (corrected for extinction following the RC2) using $H_o = 50$ kms^{-1} Mpc^{-1}. The upper diagram shows a sample of 134 elliptical galaxies with velocities and B_T magnitudes taken from the RC2.

uncertainties in calibrating the non-linear response of photographic emulsion and in estimating the local sky-background intensity. In the centres of galaxies, the effects of atmospheric seeing may also play a dominant, but currently somewhat controversial, role (Schweizer 1979;1981)

The geometric properties of elliptical galaxy isophotes can be rather more reliably determined. In general, their shapes can be extremely well approximated by concentric ellipses,and are usually parametrized in terms of the apparent ellipticity $\varepsilon = 1 - b/a$ (where a and b are the semi-major and semi-minor axes) and the position angle of the major axis θ. The ellipticity profile $\varepsilon(r)$ may show a complex behaviour, and all possible radial trends have been observed (di Tullio 1979). In some galaxies the major axis position angle is found to vary with radius. This twisting phenomenon would not be possible if elliptical galaxies were made up from dust-free and coaxial axisymmetric subsystems. Although, in principle, either non-coaxial spheroids or the effects of dust absorption could lead to isophote twisting, the most favoured interpretation is that some elliptical galaxies are triaxial in form, with intrinsic axial ratios which vary with radius (Mihalas and Binney 1981).

In Chapter 6, detailed surface photometry of four galaxies from Table 1.1 is presented. The range of morphology in that small sample is,however, necessarily very restricted. Figure 4.5 shows the ellipticity profiles and major axis position angles for eight dust-lane galaxies, obtained by manually fitting elliptical contours to isodensity maps of each galaxy on the survey plates. The maps were produced using a Joyce-Loebel isodensitracer, with a magnification of 105x and a step size of 5μ. In the case of U 0151-498 the accuracy of this procedure may be estimated by comparing with the more objective results obtained in Chapter 6 from a numerical least-squares fit for the same parameters. The

Figure 4.5: Isophote shapes and orientations for eight galaxies

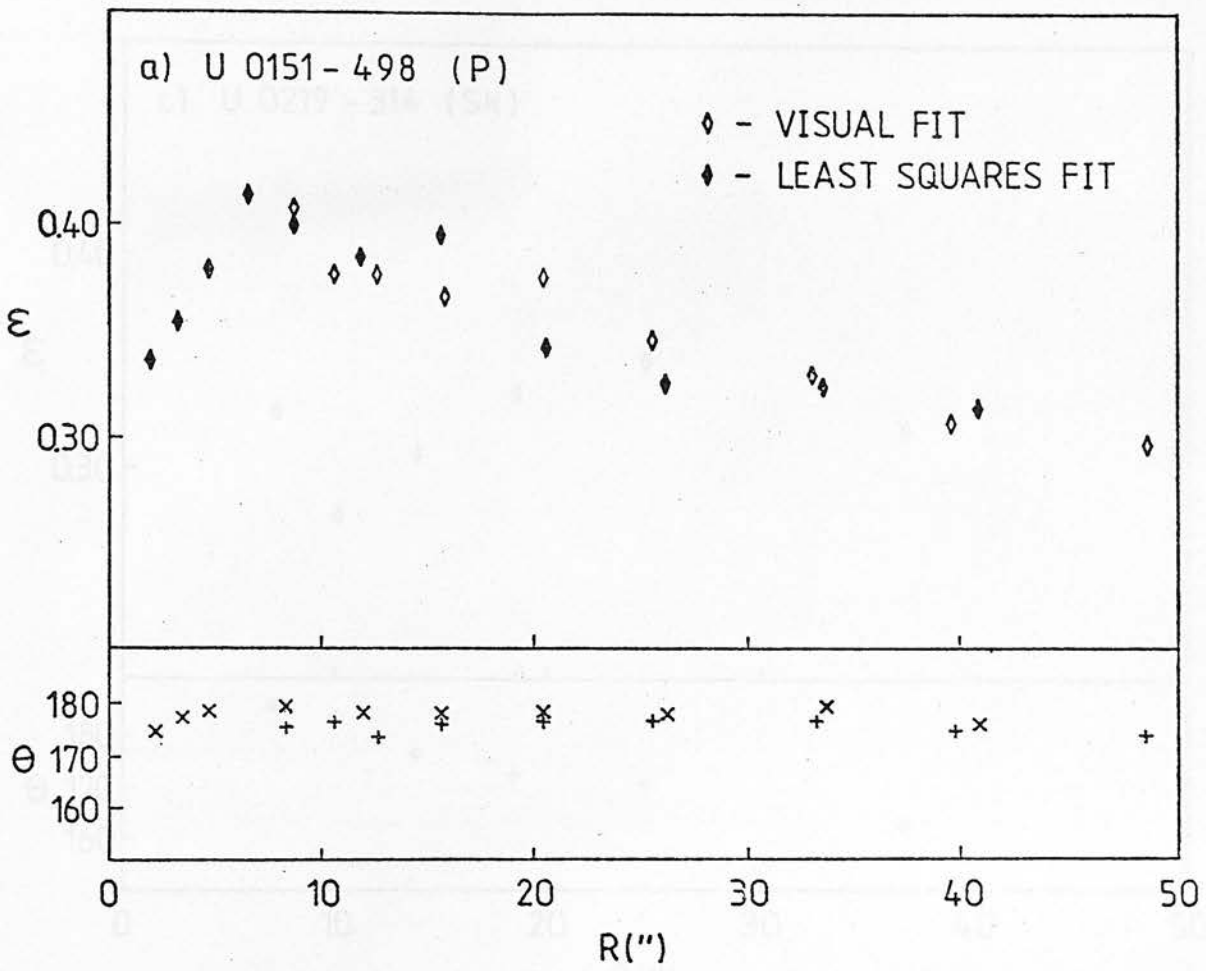

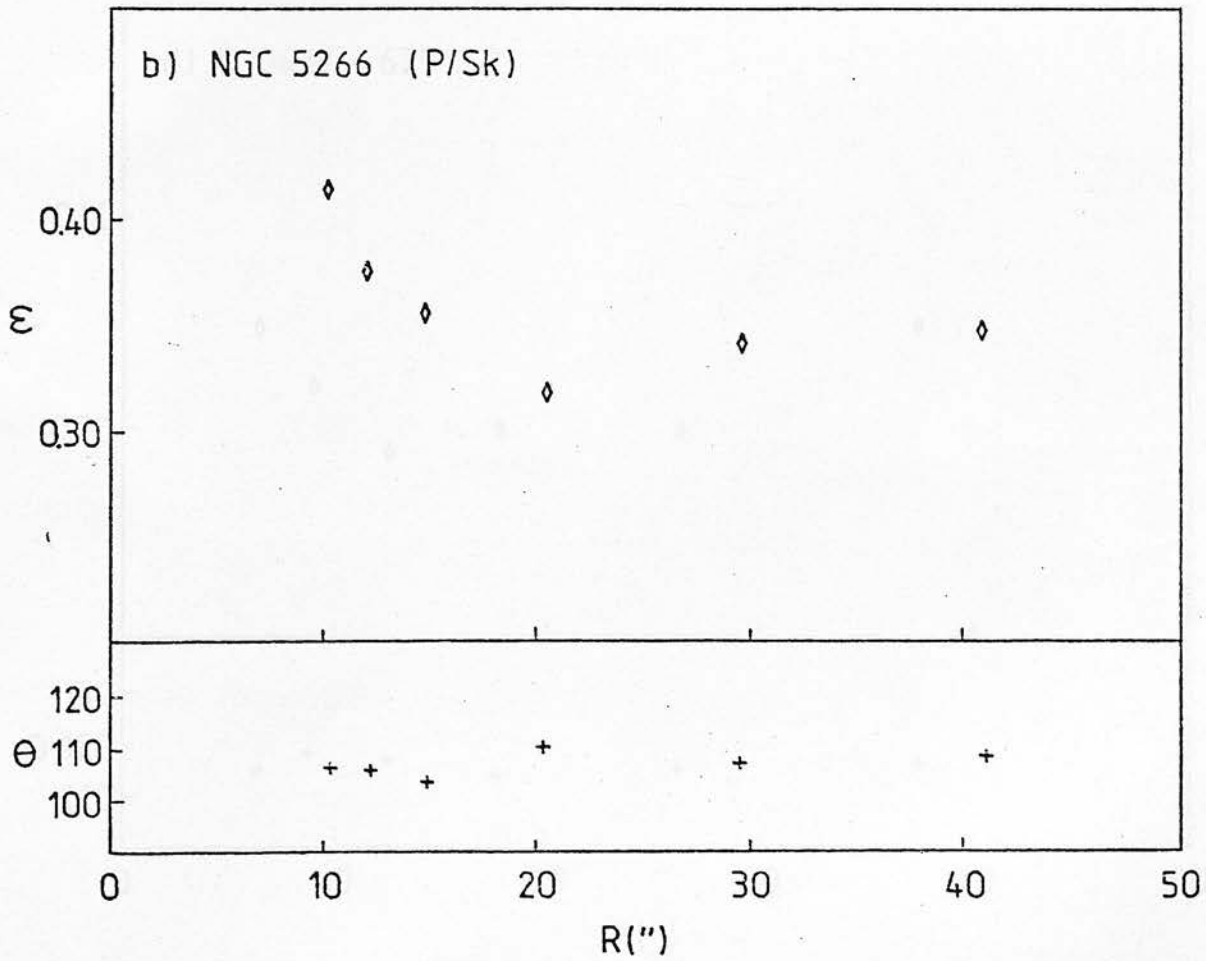

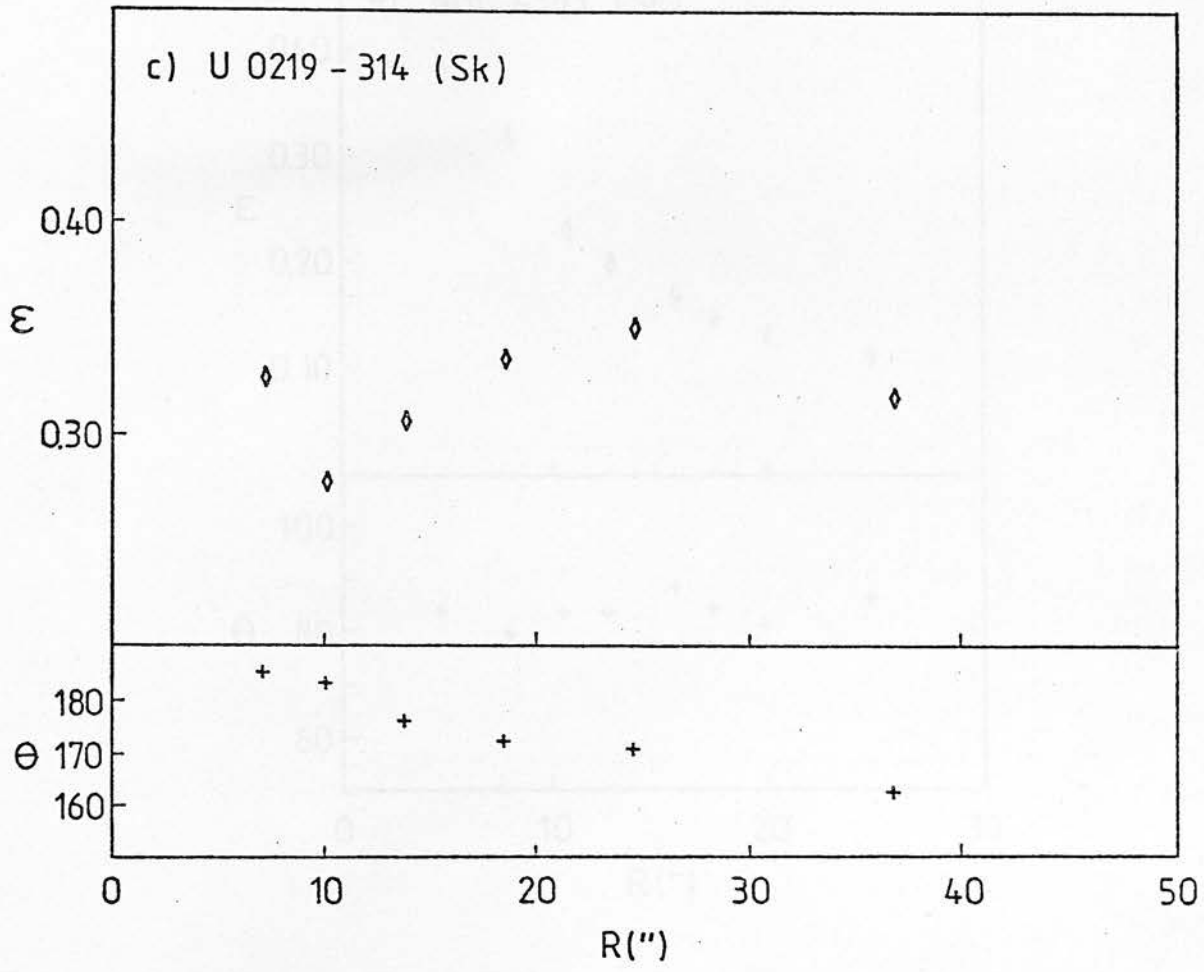
c) U 0219 - 314 (Sk)
0.40
ε
0.30
180
Θ 170
160
0
10
20
30
40
50
R(")

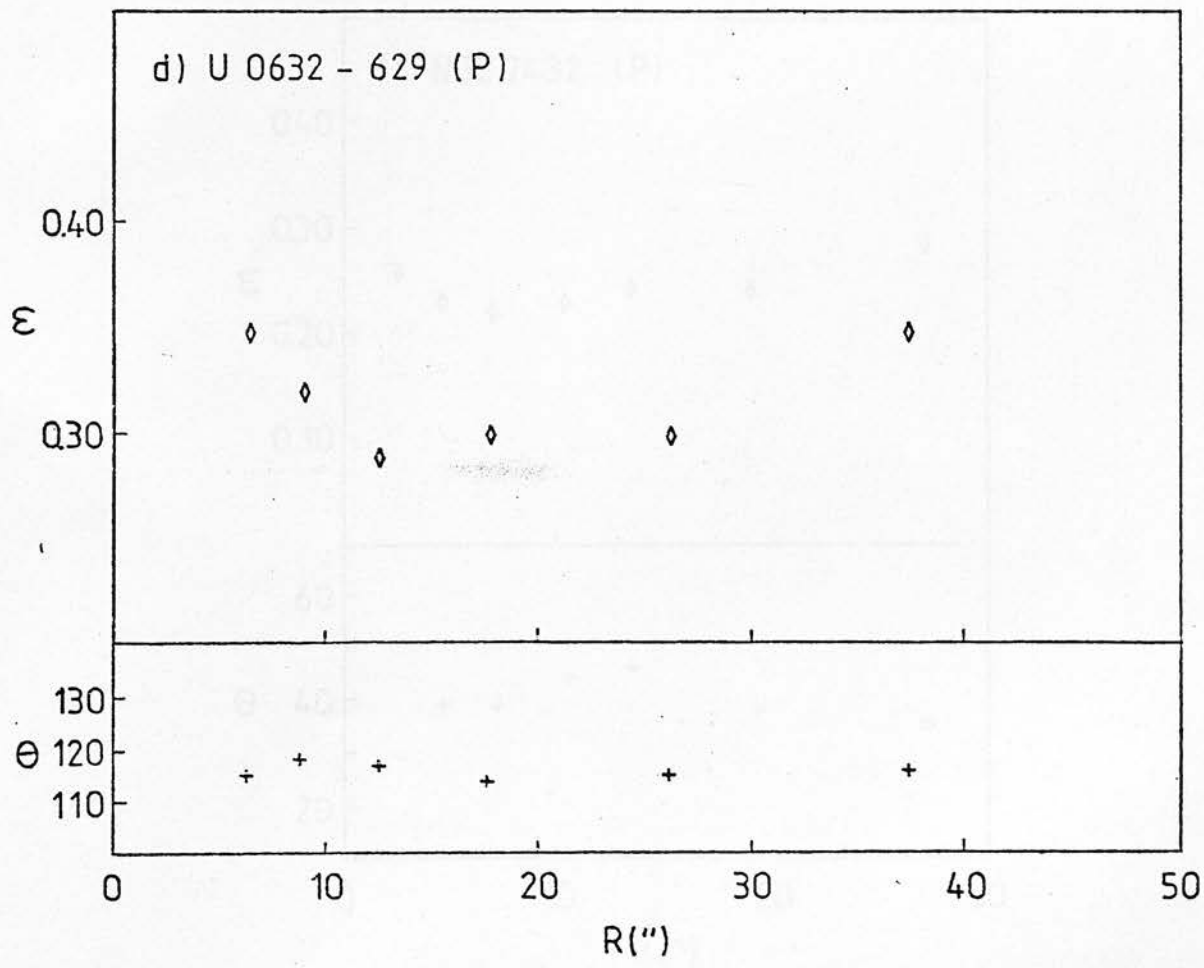
d) U 0632 - 629 (P)
0.40
ε
0.30
130
Θ 120
110
0
10
20
30
40
50
R(")

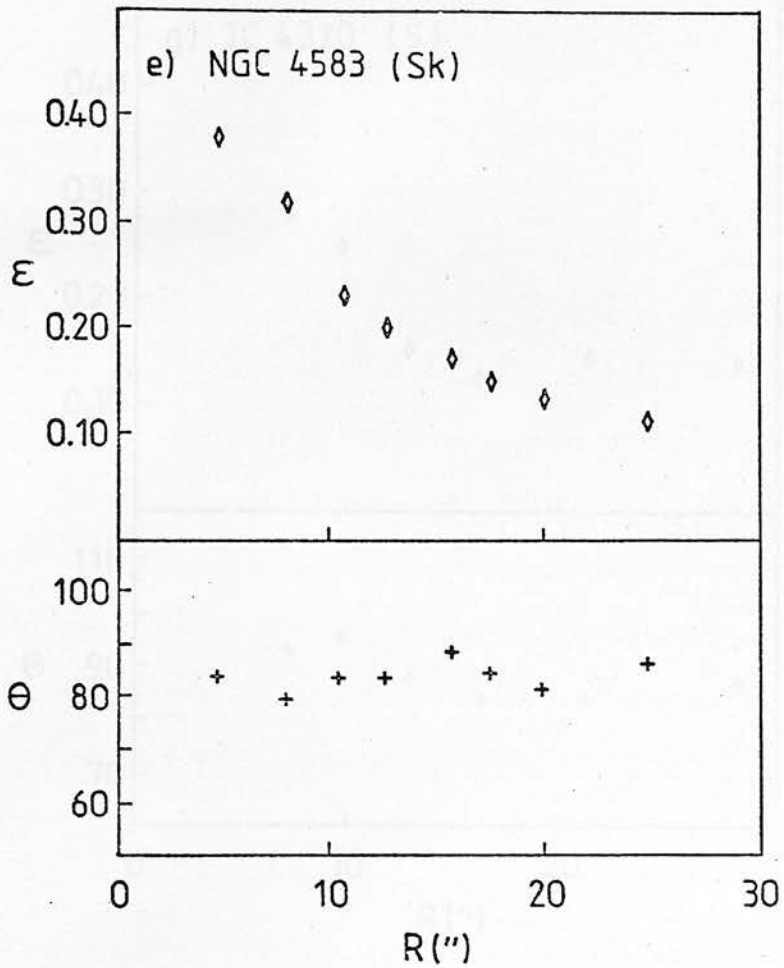
e) NGC 4583 (Sk)
0.40
0.30
ε
0.20
0.10
100
Θ 80
60
0
10
20
30
R(")

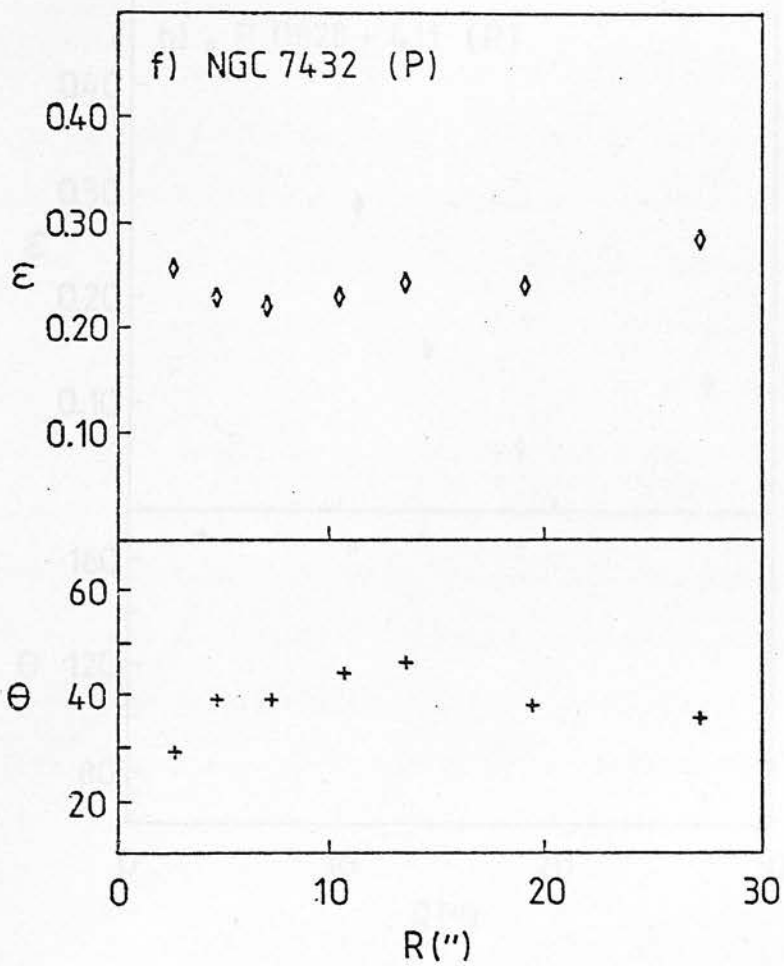
f) NGC 7432 (P)
0.40
0.30
ε
0.20
0.10
60
Θ 40
20
0
10
20
30
R(")

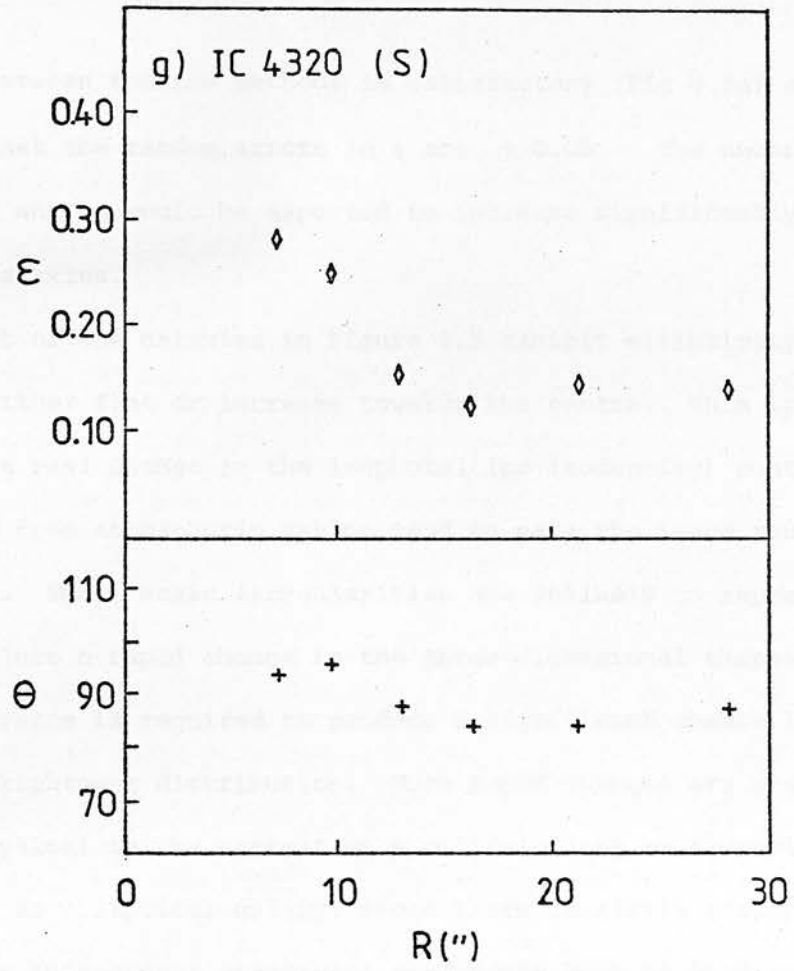
g) IC 4320 (S)
0.40
0.30
ε
0.20
0.10
110
Θ 90
70
0
10
20
30
R(")

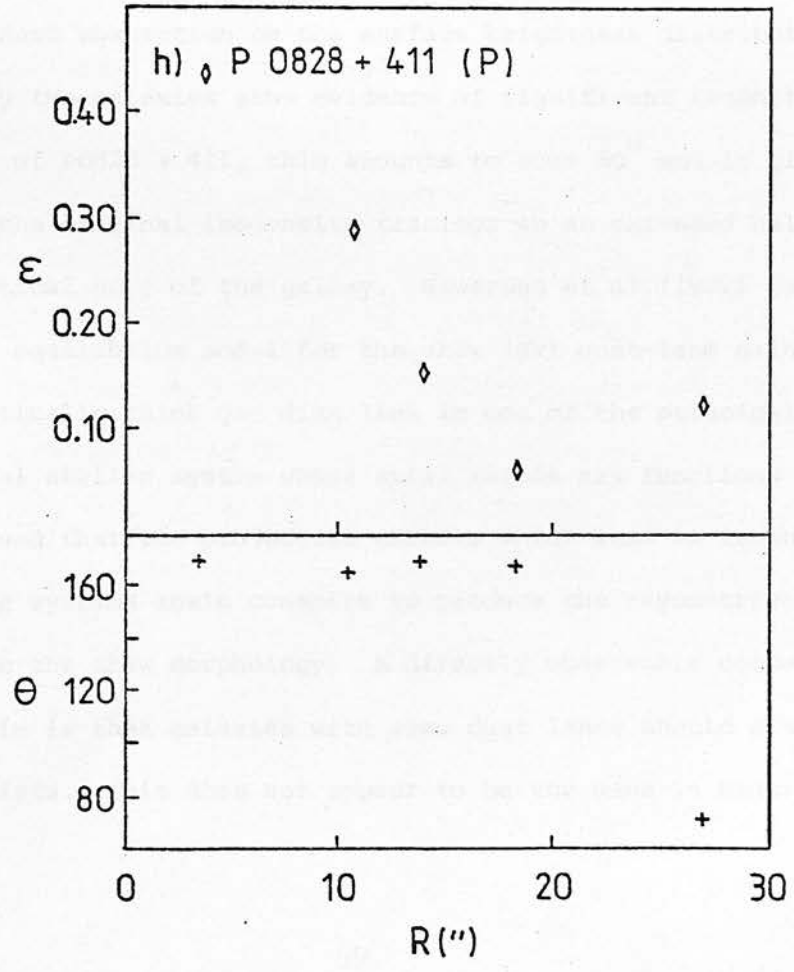
h) ◊ P 0828 + 411 (P)
0.40
0.30
ε
0.20
0.10
160
Θ 120
80
0
10
20
30
R(")

agreement between the two methods is satisfactory (Fig 4.5a) and indicates that the random errors in ε are ~ 0.05. The uncertainty in position angles would be expected to increase significantly for less flattened galaxies.

Most of the galaxies in Figure 4.5 exhibit ellipticity profiles which are either flat or increase towards the centre. This is likely to reflect a real change in the isophotal (or isodensity) contours, since any effects from atmospheric seeing tend to make the image rounder at small radii. Small scale irregularities are unlikely to represent real features, since a rapid change in the three-dimensional shapes of isodensity surfaces is required to produce a significant change in the projected brightness distribution. Such rapid changes are probably rather unphysical in the context of a collisionless self-gravitating system like an elliptical galaxy, where there is little morphological evidence for independent structural components such as bars or lenses. For the galaxies in Figure 4.5, some noise may also be contributed by the effects of dust absorption on the surface brightness distributions.

Only two galaxies show evidence of significant isophotal twisting. In the case of P0828 + 411, this amounts to some 80° and is clearly evident on the original isodensity tracings as an extended halo around the main optical body of the galaxy. Hawarden et al (1981) have proposed a tentative equilibrium model for the skew (Sk) dust-lane galaxies in which an optically thick gas disk lies in one of the principal planes of a triaxial stellar system whose axial ratios are functions of radius. It is proposed that the projection effects which lead to isophote twists in dust-free systems again conspire to produce the asymmetries which characterize the skew morphology. A directly observable consequence of this scenario is that galaxies with skew dust lanes should also exhibit isophote twists. This does not appear to be the case in Figure 4.5, where

neither NGC4583 (Sk) or NGC5266 (P/Sk) have significant variations in the orientation of their major axes. A more pronounced twist is, however, found in UO219-314 (Sk).

4.4 SUMMARY

A survey of the optical properties of the discless galaxy sample defined in Chapter 1 has revealed the following points :

(i) The U-B and B-V colour distributions of the DLG's at large effective apertures are very similar to those derived from a comparable sample of morphologically normal ellipticals. This result suggests that recent star formation cannot have occurred extensively in these galaxies unless the initial mass function is heavily weighted by low-mass stars.

(ii) There is no evidence from the distribution of absolute magnitudes in this survey that the luminosity function is significantly different from that of a magnitude-limited sample of morphologically normal galaxies.

(iii) A study of the shapes and orientations of the isophotes in eight selected examples does not reveal any preferred radial trend in the ellipticity profiles. The absence of pronounced twists in two examples with 'skew' dust lanes, suggests that projection effects in triaxial systems cannot account for all cases of this peculiar morphology.

Within the limitations of this survey, therefore, one may conclude that the discless galaxies with dust-lanes are not distinguishable from any comparable sample of morphologically normal galaxies on the basis of colour, luminosity or isophote structure.

CHAPTER 5

2-D SPECTROSCOPY: OBSERVATIONS AND DATA REDUCTION

5.1 INTRODUCTION

The study of the kinematics of stellar systems using spectroscopic observations has advanced rapidly in recent years. Particular attention has been paid to the problem of elliptical galaxies. Prior to 1975 there had been some conviction that elliptical galaxies could be adequately modelled by relaxed quasi-isothermal spheroids (King 1966) whose apparent flattening was attributed to rotation about the symmetry axis (Wilson 1975). However, simple arguments suggested that the maximum rotational velocity should then be of the same order as the velocity dispersion. Observations of the rotation curve of NGC4697 by Bertola and Cappaccioli (1975) indicated that this galaxy possessed less than one third of the rotational kinetic energy expected on the basis of the simplest oblate spheroidal models. Further observations by Illingworth (1977), Schechter and Gunn (1979) and Davies (1981) have revealed low rotation velocities in the majority of elliptical galaxies.

Binney (1976) has put forward an explanation for this discrepancy in terms of residual velocity anisotropy produced in the violent relaxation of protogalaxies from aspherical initial conditions. As a natural extension of Binney's approach, however, one is led to ask whether the 'classical' picture of elliptical galaxies as simple oblate spheroids has any continued justification. In principle the initial conditions could equally favour a prolate or generally triaxial geometry. Indeed several studies have demonstrated that the observed distribution of ellipticities is consistent with any of these three alternatives (Contopoulos 1956 ; Binggelli 1980 ; Binney and de Vaucouleurs 1981).

Attempts to determine the intrinsic geometry observationally via a correlation of mean surface brightness with apparent ellipticity (Marchant and Olsen 1979 ; Richstone 1979) have proved equally inconclusive.

Bertola and Galletta (1978) have interpreted the presence of dust lanes on the projected minor axes of five early-type galaxies as evidence for a prolate geometry. A prolate stellar system whose velocity distribution function depends only on the classical integrals of angular momentum and total energy, should show rotational motions along its shortest axis (Lake 1981 a,b). Although most elliptical galaxies appear to have very little minor axis rotation (Schechter and Gunn 1979 ; Efstathiou,Ellis and Carter 1980), none of the galaxies for which suitable observations have been made were included in the Bertola and Galletta (1978) sample.

In view of these considerations, a program was formulated in collaboration with Dr.T.G. Hawarden (R.O.E) and Dr. D. Carter (A.A.O) to study the kinematics of a subsample of four elliptical-like galaxies with a range of dust-lane types. The primary objectives of this program were to determine the rotation curves along the major and minor axes of these galaxies, and to establish the form of the velocity dispersion profiles where possible. Observations of the velocity fields in the dust lanes would also be obtained for comparison with the stellar kinematics.

5.2 SPECTROSCOPIC OBSERVATIONS

In order to study the kinematics of galaxies out to a substantial radius, a detector with a linear response is extremely desirable. A differential study of regions with a wide range of surface brightnesses can then be undertaken without further calibration, and accurate sky subtraction is available in the faint outer regions. A large

8127501

(AAT PLATE)

8127501

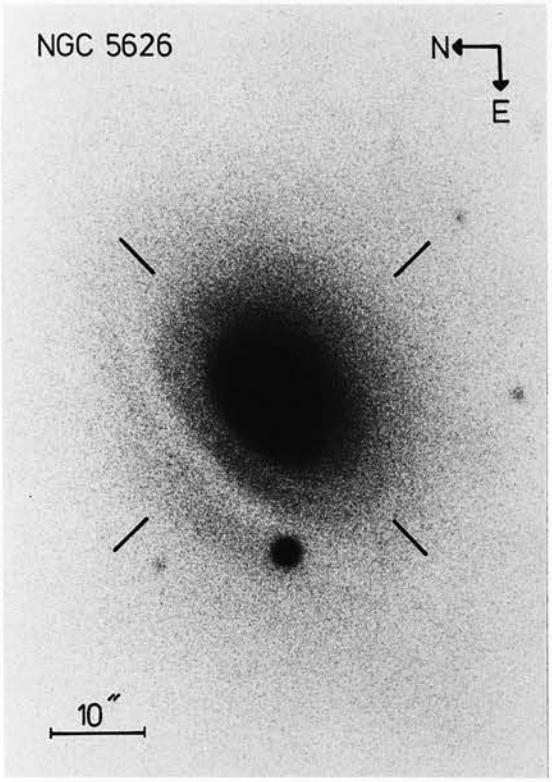
NGC 5626
N
E
10″

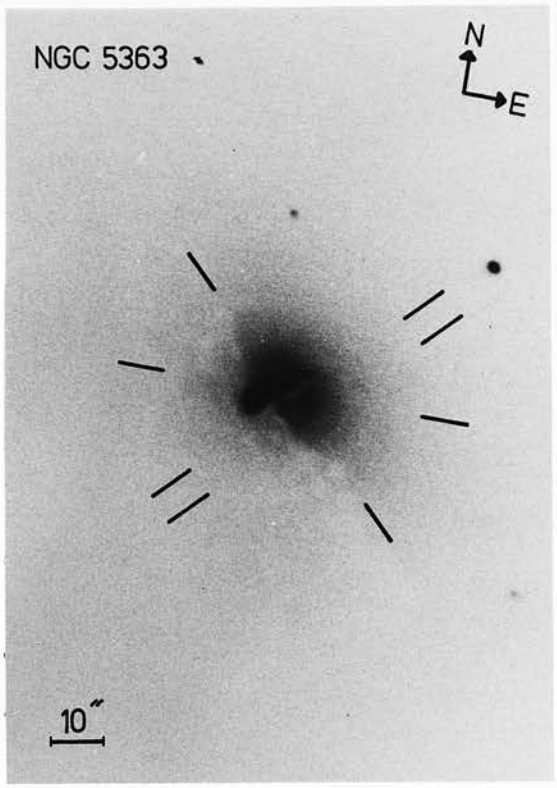
NGC 5363
N
E
10″

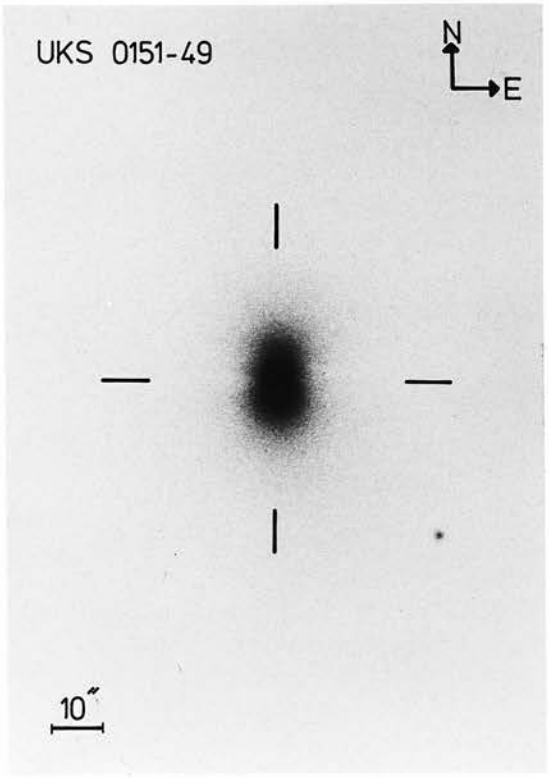
UKS 0151-49
N
E
10″

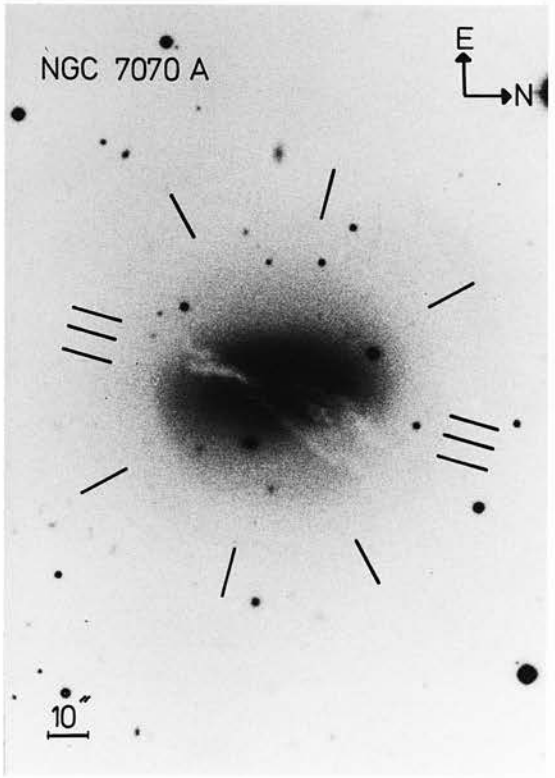
NGC 7070 A
E
N
10″

Figure 5.1 : AAT prime focus plates of the four galaxies :- (a) NGC5363 - III a J emulsion UG1 filter. The bright image to the south west of the centre of the galaxy is a foreground star ; (b) NGC7070A-III a J emulsion GG385 filter ; (c) NGC5626 - III a J emulsion GG385 filter ; (d) UKSO151-498 - III a J emulsion GG385 filter. This high quality photographic material was obtained subsequently to the spectroscopic observations. Certain morphological details in the figures were not evident from the survey plate material on which the galaxies were selected. In particular, dust absorption is seen along the major axis of NGC5363, in addition to the minor axis feature referred to by Bertola and Galletta (1978). The dust lane in NGC7070A appears much more complex with filaments extending into the NW envelope. Finally, the increased resolution in NGC5626 leads us to suspect that the faint envelope referred to by Hawarden et al (1981), may be a coplanar stellar disc in which the dust lane is embedded. The slit positions on each galaxy are marked and refer to the position angles in Table 5.2 (measured N thorugh E).

telescope is needed to reach low surface brightnesses ($B \sim 21\text{-}22^{m}$ arcsec^{-2}) whilst maintaining adequate spatial and spectral resolution.

Observations with the 3.9m Anglo-Australian Telescope were made over three nights in July 1980, using the RGO spectrograph with the Image Photon Counting System (IPCS: Boksenberg 1972 ; Boksenberg and Burgess 1973) as a detector. The IPCS is a panoramic intensified-TV system which is capable of detecting individual photon events, positioning them via hard-wired logic circuits, and counting them into an external memory. The active area of this detector (and hence the spatial and spectral coverage) is defined by a 'data window' consisting of a number of channels along the direction of the dispersion, and a number of increments along the spectrograph slit. A wavelength baseline from 4800-6050 Å was chosen to cover the strong absorption lines of Mgb(λ5173) and NaD(λ5890) and also any emission lines of Hβ(λ4861) and [O III] ($\lambda\lambda$ 5007, 4959), which it was hoped would be associated with the diffuse matter in the dust lane. This could only be achieved, however, at the expense of introducing some extra distortion into the wavelength scale of the IPCS. The slit width was chosen to be 350μ (2".3) which gave a projected slit of 50 μ or 2.6 channels on the IPCS. The observing set-up is summarized in Table 5.1.

The program galaxies were chosen from the restricted set of elliptical-like galaxies with dust lanes identified in Chapter 1. Observations were made of two 'prolate' forms (NGC5363 and UKS0151-498), one 'skew' (NGC7070A), and one spherical (NGC5626). Each galaxy was observed with the spectrograph slit in at least two position angles in order to map out the velocity and velocity dispersion fields as comprehensively as possible. The slit positions are indicated in Figure 5.1 and the observations are summarised in Table 5.2.

TABLE 5.1 : Instrumental Settings for the AAT Observations

RGO Spectrograph :

25 cm Camera

Grating 1, 1200 lmm^{-1}, blaze 4650 Å

blaze-to-collimator giving 33 Å/mm

Slit width : 350 μ = 2.3 arcsec

IPCS :

Scan format : 2048 x 66

Data window : 2040 (channels) x 56 (increments)

Slit length : 2.4 arcmin at 2.6 arcsec/increment

Wavelength baseline : 1290 Å at 0.63 Å/channel

Frame time : 37 ms (c.f.max count rate: 0.5 cts/s/pixel in 5363)

Y gain = 6 X gain = low

Focus : FWHM 2.5 channels

Rotation : Residual < 0.03 channels

Scan correction : Residual < 0.04 increments

TABLE 5.2 : Spectroscopic Observations

Galaxy	Grating Angle	Dust-lane Type	P.A.of Slit	Axis Label	Exposure(sec)
NGC5363	6.5o	Prolate	135	Major	3000
			45	Dust-lane	4000
			45	Offset	4000
			90	Skew	5000
NGC7070A	6.24	Skew	209	Major	5000
			299	Minor	4000
			346	Dust-lane	6000
			346	Bright-Edge	4000
			346	Faint-Edge	4000
			256	Skew	5000
UKS0151-49	5.88	Prolate	270	Dust-lane	5000
			180	Major	5000
NGC5626	5.88	Spherical	45	Minor	4000
			135	Major	4000

Template	Spectral Type	Magnitude	Total Counts(10^6)	Exposure(sec)
SAO 099805	F8	8.1	0.77	2000
HD 219509	KO	9.2	0.33	1200
HD 101266	G5	9.2	0.84	1000
HD 8779	gKO	6.5	1.9	3000
SAO 119413	G8	6.4	0.55	1000

The possibility of drifts in the camera electronics and flexure in the spectrograph/detector assembly makes it extremely important to take calibration arc spectra at regular intervals in order to monitor these changes. The duty cycle employed consisted of a 100 second arc exposure followed by a 1000 second exposure of the galaxy. The telescope was then offset by approximately 10 arcmin to an area of blank sky, and a sky exposure taken for 100 seconds, followed by another 100 second arc exposure at the position of the galaxy. This cycle was repeated as often as required. The galaxy nuclei were always centred in the middle of the slit.

Twilight time was used to obtain spectra of template stars for use in determining velocities and velocity dispersions. The stars were selected on the basis of spectral type and are listed in Table 5.2. Because of the generally good seeing it was necessary to trail the star continuously across the width of the slit to ensure a similar instrumental profile for the template and galaxy spectra. Observations were also made of the spectrophotometric standard Van Maannen 2(Oke 1974).

In order to maximize the region of overlap in the rest frame spectra of templates and galaxies, one of three grating angles was used for the galaxy observations depending on the redshift of the system. These were $6^{\circ}.50$, $6^{\circ}.24$, and $5^{\circ}.88$, which corresponded to central wavelengths of 5422.0, 5477.6, and 5576.8 Å respectively. All template observations were taken at grating angle $6^{\circ}.50$. Before and after each night's observing flat-field spectra were obtained using 10,000 second exposures of a tungsten continuum source.

5.3 CALIBRATION AND REDUCTION OF SPECTRA

The study of velocity and velocity dispersion profiles in galaxies obviously requires very accurate wavelength calibration procedures over the entire data window. The spectra were all reduced using the Edinburgh

Spectral Processing system written by Dr. B.D.Kelly at R.O.E. specifically for the reduction of IPCS data. Because this new package had only recently been finished, and had never before been used for the reduction of long slit spectroscopy, considerable effort was made during the early stages of this work to check its reliability and to optimize the routines for efficient processing of large 2-D data sets. A brief discussion of the reduction procedures follows.

5.3.1 Flat-field Calibration

Small scale inhomogeneities in the image tube photocathode lead to a very non-uniform detector response to incident light. The extent of this effect can be mapped using the flat-field calibration exposures. It is necessary to take very long flat-field exposures in order to reduce the photon noise to a minimum without saturating the IPCS. In practice, this limits the taking of flat-fields to the beginning and end of the night, which are coadded to produce a mean exposure of 20,000 secs.

The success of flat-fielding is critically dependent on the stability of the IPCS camera electronics and on the degree of flexure between the camera and image tube. Cross-correlation of flat-field exposures taken at the beginning and end of the night indicated a mean shift of $\sim$ 0.2 channels. Night to night variations were of order 0.8 channels. However, all flat-field exposures were taken with the same telescope orientation which tends to reduce the effects of flexure. Fortunately, the AAO image tube has a fairly uniform photocathode ($\sim$ 6% r.m.s) and residual flat-field noise is only expected to dominate the signal-to-noise characteristics in the nuclei of the brightest galaxies, where the photon noise intrinsic to the data becomes negligible.

5.3.2 Wavelength Calibration

Wavelength calibration was achieved using the frequently taken Cu-Ar comparison arc spectra. Neutral density filters were necessary to prevent saturation in the strongest lines but the short (100 second) arc exposures were then found to be of poor signal-to-noise, particularly in the 5200-5400 Å range where the argon lines are rather weak. Each galaxy/sky pair was calibrated using the sum of the two arc frames taken immediately before and afterwards. The residual shift between these arc frames was found to be typically 0.25 channels ($\sim$ 10 kms^{-1}). Adjacent arcs in a given frame shifted by less than 0.1 channels in the mean,so each arc was box-smoothed in the direction of the slit by three increments, and Gaussian smoothed in the direction of the dispersion by one channel. No systematic effects appeared to be introduced by this procedure, which greatly improved the stability of the 2-D wavelength calibration.

An approximate set of calibration coefficients (3rd order) for the first increment were obtained using the positions of five lines identified interactively with a cursor. This approximate solution was then used with an automatic line-finding algorithm to locate the positions of up to 30 user-defined arc lines. The line identification process involved a pattern-search over a restricted range and used the centre of gravity of the line as the position datum. This augmented list of wavelengths vs. channel numbers was then used to define the ('scrunch') coefficients of a higher (up to 9th) order calibrating polynomial, which could be used to rebin the data onto a linear wavelength scale (the process referred to as 'scrunching'). The remaining increments were processed automatically, using the scrunch coefficients from the previous increment for the trial solution. The use of a line-finding algorithm at each stage ensured that the increments were effectively calibrated independently.

As noted previously, the extended wavelength baseline introduced large distortions in the wavelength scale at the ends of the spectra. In order to fit these distortions high order (7th or 9th) polynomials were required. A typical fit was then found to have an r.m.s. residual of 0.20 channels (7 kms^{-1}) and a maximum residual of 0.4 channels. Similar values could be obtained using lower order fits by excluding the ends of the spectra. No obvious trends of r.m.s. residuals along the slit were noted. The internal consistency of the wavelength calibration was tested by scrunching arc spectra with their own scrunch coefficients and examining the residuals between measured line positions and their adopted wavelengths. For a typical increment the mean residual was $0.03 \pm 0.11 (1\sigma)$ Å. The stability of the 2-D scrunching procedure was estimated from the variation in position of the strong OI λ 5577 night-sky line along the slit. For an average sky frame, the mean wavelength was 5577.35 ± 0.10 Å over 56 increments with no systematic trends. An identical frame reduced independently using the SDRSYS software at the Anglo-Australian Observatory gave $\langle\lambda\rangle = 5577.32 \pm 0.08$ Å. These lengthy procedures confirmed that there were no systematic errors either in the zero point or scale of the wavelength calibration, and enabled independently calibrated spectra to be added without the introduction of relative shifts or broadening.

5.3.3 Sky Subtraction

Individual sky frames (100^s) were taken for each galaxy exposure, excepting those of NGC5626. Although taken in blank (down to $m_v \sim 20$) regions of sky, these exposures are not uniform, primarily because of low frequency sensitivity variations in the IPCS, and vignetting in the spectrograph optics. Parallel to the slit this variation could be corrected for using the total counts in each increment of a sky frame to define a calibration curve. This normalisation was then applied to every frame at the same time as the flat field correction.

The sky subtraction was initially done using the sky frames for each individual galaxy and position angle. However, this approach appeared to be introducing unnecessary noise into the velocities and velocity dispersions derived from the spectra. This is most probably accounted for by a combination of the faintness of the sky continuum ($\sim$ 0.004 cts/sec/chan) introducing photon noise, and the non-photometric conditions which were known to be present occasionally during the observing run.

Close inspection of the frames for each galaxy revealed that only in one case (NGC5363) was the galaxy still contributing significantly at the ends of the slit. In the three remaining systems the outer increments were used to form a mean sky spectrum which was effectively simultaneous with the galaxy exposure. A mean sky frame (2400s total exposure) was eventually used for sky subtraction in the case of NGC5363. Tests of the method based on the residual strength of the λ 5577 emission line, indicated that sky subtraction was generally good to 5-8%. More significantly, a marked improvement was found for the scatter within the velocity and velocity dispersion profiles.

Examples of fully reduced spectra of a template and a galaxy are given in Figure 5.2, with identifications taken from Davies (1981).

5.4 DATA ANALYSIS TECHNIQUES

The possibility of accurate measurement of radial velocities and velocity dispersions from absorption-line spectra attracted considerable attention when the first good spectra of elliptical galaxies became available. Early attempts by Minkowski (1954, 1962), Morton and Chevalier (1973) and Morton and Elmergreen (1976) using visual comparison with artificially broadened stellar spectra led to large discrepancies between different authors (Faber and Jackson 1976). More objective methods became available with the introduction of Fourier techniques (Simkin 1974)

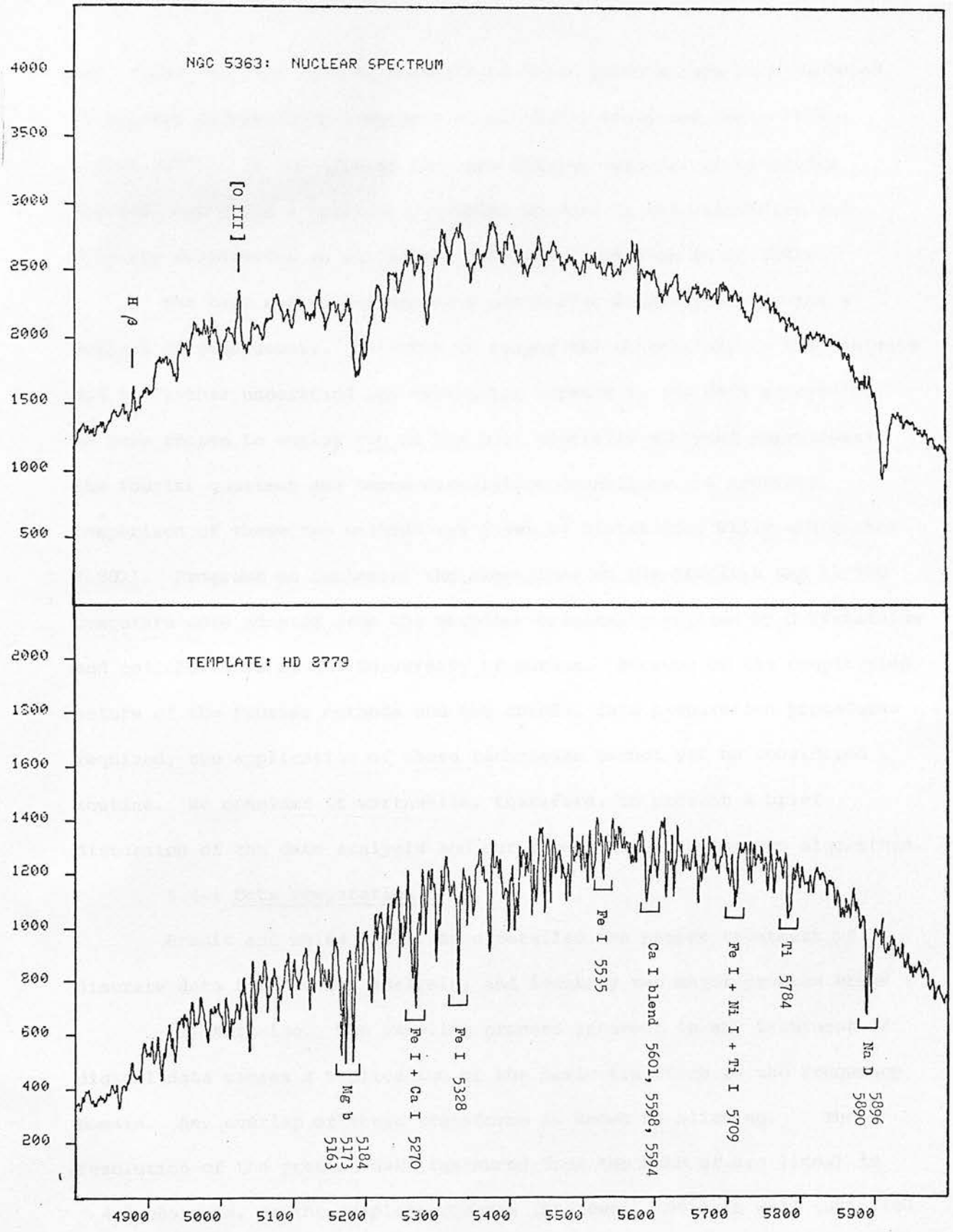

Figure 5.2 : Wavelength calibrated spectra of the nucleus of NGC5363 and a template star. The total exposure times were 3000 seconds in each case, and the ordinates are in IPCS counts. The spectrum of NGC5363 is built up from four increments and includes both the [OIII]λ 5007 and Hβ emission lines. Absorption line identifications have been taken from Davies (1981).

and in recent years several variants of these methods have been employed (Faber and Jackson 1976 ; Sargent et al 1977 ; Tonry and Davis 1979 ; Davies 1981). It now appears that the Fourier methods, if carefully applied, can yield a reasonably precise measure of the velocities and velocity dispersions in elliptical galaxies (Terlevich et al 1981).

The best method for use in a particular application remains a subject of some debate. In order to reduce the uncertainty in the analysis and to further understand any systematic effects in the data processing, we have chosen to employ two of the most generally accepted approaches: the Fourier quotient and cross-correlation techniques. A previous comparison of these two methods was given by Efstathiou, Ellis and Carter (1980). Programs to implement the algorithms on the Starlink VAX 11/780 computers were adapted from the versions originally written by G.Efstathiou and collaborators at the University of Durham. Because of the complicated nature of the Fourier methods and the careful data preparation procedures required, the application of these techniques cannot yet be considered routine. We consider it worthwhile, therefore, to present a brief discussion of the data analysis and our experience with the two algorithms.

5.4.1 Data Preparation

Brault and White (1971) have detailed the proper treatment of discrete data for Fourier analysis, and identify two major problem areas :

(i) Aliasing. The sampling process inherent in any treatment of digital data causes a replication of the basic transform in the frequency domain. Any overlap of these transforms is known as aliasing. The resolution of the present data (measured from the FWHM of arc lines) is $\sim$4.5 channels, so the sampling theorem (Bracewell 1965) is well satisfied (as was verified by visual inspection of the raw power spectra).

(ii) Leakage. The use of a finite data window results in the convolution of the basic transform with a resolution function. In the

case of a simple data string of length L the resolution function is the sinc function $\frac{\sin(\pi Ls)}{\pi Ls}$. Leakage is particularly detrimental if the basic transform has a strong low-frequency spike, which is then redistributed over the remaining Fourier components. The effect can be minimised by removing the low frequency components ('continuum') in the calibrated spectra. Polynomial fits to the continuum are not generally satisfactory because of the complex continuum shapes so a digital filtering technique (Martin and Lutz 1979) has been adopted. This method is equivalent to high pass filtering the data and removes the low frequency components below $\sim$ 0.025 cycles/channel. In practice this was achieved by dividing the computed continuum (from a low pass digital filter) into the original spectrum. (This method was adopted in favour of continuum subtraction, which may introduce line shifts when the continuum is sharply varying. However, both methods have their disadvantages). Finally, the ends of the spectrum are masked using a cosine-bell of 204 channels in order to produce a resolution function whose sidelobes are less severe than those of the sinc function.

Prior to Fourier transformation, the calibrated sky-subtracted spectra were rebinned onto a logarithmic wavelength scale using linear interpolation. Radial velocity shifts are then linear in these co-ordinates.

5.4.2 Fourier Quotient (SSBS) Method

The Fourier Quotient method was introduced by Sargent et al (1977, hereafter SSBS) for the purpose of measuring the central velocity dispersions in elliptical galaxies. It has been subjected to rigorous testing (SSBS ; Sargent et al 1978) and gives formally accurate results. Its wider applications have been exploited by several authors with slight modifications to the basic algorithm (Schechter and Gunn 1979 ; Davies 1981 ; Efstathiou, Ellis and Carter 1980).

In common with all of the Fourier methods, the SSBS approach relies on the representation of the galaxy spectrum as the convolution integral of some template spectrum S(v) with a suitable broadening function B(v):

$$G(v) = S(v) * B(v) \tag{5.1}$$

Defining the discrete Fourier transform of F(v), v = 1,2,....,N by

$$\tilde{F}(k) = \sum_{v=1}^{N} F(v) \exp\left(\frac{2\pi i v k}{N}\right) \quad k = 0,1,\ldots,N-1 \tag{5.2}$$

we have, by the Fourier convolution theorem (Bracewell 1965) :

$$\tilde{G}(k) = \tilde{S}(k) . \tilde{B}(k) \tag{5.3}$$

SSBS use a Gaussian broadening function of the form :

$$B(v) = \frac{\gamma}{(2\pi)^{\frac{1}{2}}\sigma} \exp\left\{\frac{(v - v_o)^2}{2\sigma^2}\right\} \tag{5.4}$$

where v_o is the systematic velocity, σ the velocity dispersion and γ a normalisation factor which measures the mean strength of the galaxy lines with respect to the template lines. The Fourier transform of this function is :

$$\tilde{B}(k) = \gamma \exp\left\{-\frac{1}{2}\left(\frac{2\pi k\sigma}{N}\right)^2 + \frac{2\pi i v_o k}{N}\right\} \tag{5.5}$$

Because of noise in the spectra and mismatch between the template and galaxy spectra, equation (5.3) will, in general, not be exact and it is necessary to use a least squares procedure to find the values of

γ, σ and v_o . In the Fourier quotient method this is achieved by minimising the residuals

$$\left| \tilde{G}(k) \Big/ \tilde{S}(k) - \tilde{B}(k) \right|^2$$

SSBS assume that the errors in the quotient $\tilde{Q}(k) = \tilde{G}(k)/\tilde{S}(k)$ are normally distributed, and minimise the χ^2 statistic :

$$\chi^2 = \sum_{k_L}^{k_u} \left| \frac{\tilde{Q}(k) - \tilde{B}(k)}{\Delta\tilde{Q}(k)} \right|^2 \qquad (5.6)$$

where

$$\frac{\Delta\tilde{Q}(k)}{\tilde{Q}(k)} = \left\{ \left| \frac{\Delta\tilde{G}(k)}{\tilde{G}(k)} \right|^2 + \left| \frac{\Delta\tilde{S}(k)}{\tilde{S}(k)} \right|^2 \right\}^{\frac{1}{2}} \qquad (5.7)$$

However, Davies (1981) has pointed out that the errors in the quotient are in fact Cauchy distributed and notes that erroneously large contributions to χ^2 will be obtained when $\tilde{S}(k) \simeq 0$. Very high S/N template spectra are required to minimise this problem. Because the variance of a Cauchy distribution is infinite, the definition of a suitable χ^2 function is somewhat arbitrary ; an alternative method of weighting the Fourier quotient has been discussed by Williams (1981).

In the present implementation a weighting function of the form (5.7) was adopted and a simplex minimisation routine (Nelder and Mead 1965) was used for the 3-parameter least-squares fit. This fit was restricted to the spatial frequency range $k_L = 0.005$: $k_u = 0.1$ cycles/channel in order to reduce the effects of noise and residual continuum variations ; as noted by several authors, no systematic dependence on reasonable values of these parameters was found.

Because of the uncertainties in the appropriate weighting for the SSBS χ^2 statistic, formal error estimates using the covariance matrix are unsatisfactory. The method of Lampton et al (1976) was therefore used to determine the range in parameter space defined by a 1σ reduced χ^2 contour.

5.4.3 Cross-Correlation Method

The cross-correlation method introduced by Simkin (1974) and favoured by Tonry and Davis (1979, hereafter TD) is closely related to the Fourier quotient methods, although conceptually much more simple.

Following TD, we define the normalised cross-correlation function:

$$C(v) = \frac{1}{N \sigma_S \sigma_G} \sum_m G(m) \quad S(m-v) \tag{5.8}$$

where $\sigma_S = \frac{1}{N} \sum_v S(v)$ and $\sigma_G = \frac{1}{N} \sum_v G(v)$

If G(v) is identical to S(v), but shifted by n channels, then C(v) will have a peak of 1 at v = n. Fourier transforming the formula for C(v) we have :

$$\tilde{C}(k) = \frac{1}{N \sigma_G \sigma_S} \quad \tilde{G}(k) \cdot \tilde{S}^*(k) \tag{5.9}$$

Let $\tilde{G}(k) \simeq \tilde{S}(k) \cdot \tilde{B}(k)$, where $\tilde{B}(k)$ is given by the usual Fourier broadening function :

$$\tilde{B}(k) = \gamma \quad \exp \left\{ - \frac{1}{2} \left(\frac{2\pi k \sigma}{N} \right)^2 + \left(\frac{2\pi i \, v_o k}{N} \right) \right\} \tag{5.10}$$

and suppose that $\tilde{S}(k)$ is modelled as a Gaussian with random phases

(ϕ_k) and a dispersion appropriate for a typical feature in S(v) to have width τ:

$$\tilde{S}(k) = C_1 \exp\left\{ -\frac{1}{2}\left(\frac{2\pi k\tau}{N}\right)^2 \right\} e^{i\phi_k} \qquad (5.11)$$

We have from 5.9 :

$$\tilde{C}(k) \simeq \frac{1}{N\,\sigma_G\,\sigma_s}\ \tilde{B}(k)\ \left|\tilde{S}(k)\right|^2$$

And so substituting from 5.10 and 5.11 :

$$\tilde{C}(k) \simeq C_2 \exp\left\{ -\frac{1}{2}\left(\frac{2\pi k\mu}{N}\right)^2 \right\} \exp\left\{ \frac{2\pi i v_o k}{N} \right\} \qquad (5.12)$$

where $\mu^2 = \sigma^2 + 2\tau^2$

The inverse transformation then gives :

$$\tilde{C}(v) \simeq C_2 \exp\left\{ -\frac{(v-v_o)^2}{2\mu^2} \right\} \qquad (5.13)$$

where C_1, C_2 and C_3 are constants.

Thus the displacement of the peak in the cross-correlation function from the origin yields the redshift v_o, and the width of the peak μ gives the quadratic sum of the two stellar widths (τ) and the velocity broadening width (σ). TD prove in some mathematical detail that fitting to the highest peak of the correlation function in this way is equivalent to minimising the χ^2 statistic :

$$\chi^2 = \sum_k \left| \tilde{G}(k) - \tilde{S}(k)\ \tilde{B}(k) \right|^2 \qquad (5.14)$$

This form of χ^2 weights the strong lines quadratically.

The cross-correlation function was computed from equation 5.9 and, as in the previous section, the data rebinned onto a ln λ scale, continuum divided and endmasked, prior to Fourier transformation. Because the cross-correlation function is affected by noise in the spectra and template mismatch, the spectra were bandpass filtered before correlation using a filter of the form :

$$\left.\begin{aligned} Q_k &= 0 && k < k_1 \\ Q_k &= (k-k_1)/(k_2-k_1) && k_1 \leq k \leq k_2 \\ Q_k &= 1 && k_2 < k < k_3 \\ Q_k &= (k_4-k)/(k_4-k_3) && k_3 \leq k \leq k_4 \\ Q_k &= 0 && k > k_4 \end{aligned}\right\} \qquad (5.15)$$

After testing various filters on template spectra, a compromise between the elimination of unwanted noise and the introduction of artificial broadening was achieved with :

$$k_1 = 0.005; \quad k_2 = 0.01 \; ; \; k_3 = 0.1 \; ; \; k_4 = 0.15 \text{ cycles/chan}$$

The instrumental response is approximately a Gaussian of dispersion 2.1 lnλ bins, so most of the information in the spectra is at spatial frequencies less than 0.075 cycles/channel and almost all at less than 0.15 cycles/channel. The range of velocity dispersions found in published studies of early-type galaxies (60-400 kms^{-1}) indicated that the interval $0.015 < k < 0.09$ would be the most relevant.

A second order polynomial was fitted to the highest peak in the correlation function (within a restricted redshift range) to determine its position and width. A relationship is then required between the FWHM of the fitted parabola and the assumed Gaussian cross-correlation

peak. This was generated empirically by fitting parabolas to filtered Gaussians and approximated by a third order polynomial.

TD have derived an elegant method for the analysis of errors in cross-correlation techniques. The basic figure-of-merit is given by the parameter :

$$r = h/\sqrt{2}\sigma_a \tag{5.16}$$

where h is the height of the cross-correlation peak, and σ_a is the r.m.s. of the antisymmetric (noise) component of C(n). The errors in the position (v_o) and width (w_o) of the maxima are then given by :

$$\Delta v_o \simeq \Delta w_o \simeq \frac{\Delta\varepsilon}{1+r} \tag{5.17}$$

where $\Delta\varepsilon = 2048/8B$, and B is the half-maximum point of $|\tilde{C}(k)|$. Examination of plots of $\tilde{C}(k)$ suggested an effective $B \sim 40$. However, the plots are very noisy and the half-maximum point is difficult to determine.

A much less subjective method of determining $\Delta\varepsilon$ is to normalise the error estimates with respect to independently determined velocities as TD have done. This approach is not feasible for the present program, however, because of the limited number of objects concerned. A similar analysis has therefore been carried out using template spectra. Cross-correlation of a pair of good signal-to-noise templates was used to produce a very accurate estimate of their relative velocity v_o. One of the templates was then degraded by the addition of random noise and a new cross-correlation function computed, from which the apparent relative velocity v and error parameter $r = h/\sqrt{2}\sigma_a$ were derived. The velocity error was taken to be the difference $\Delta v = v_o - v$ between these two values,

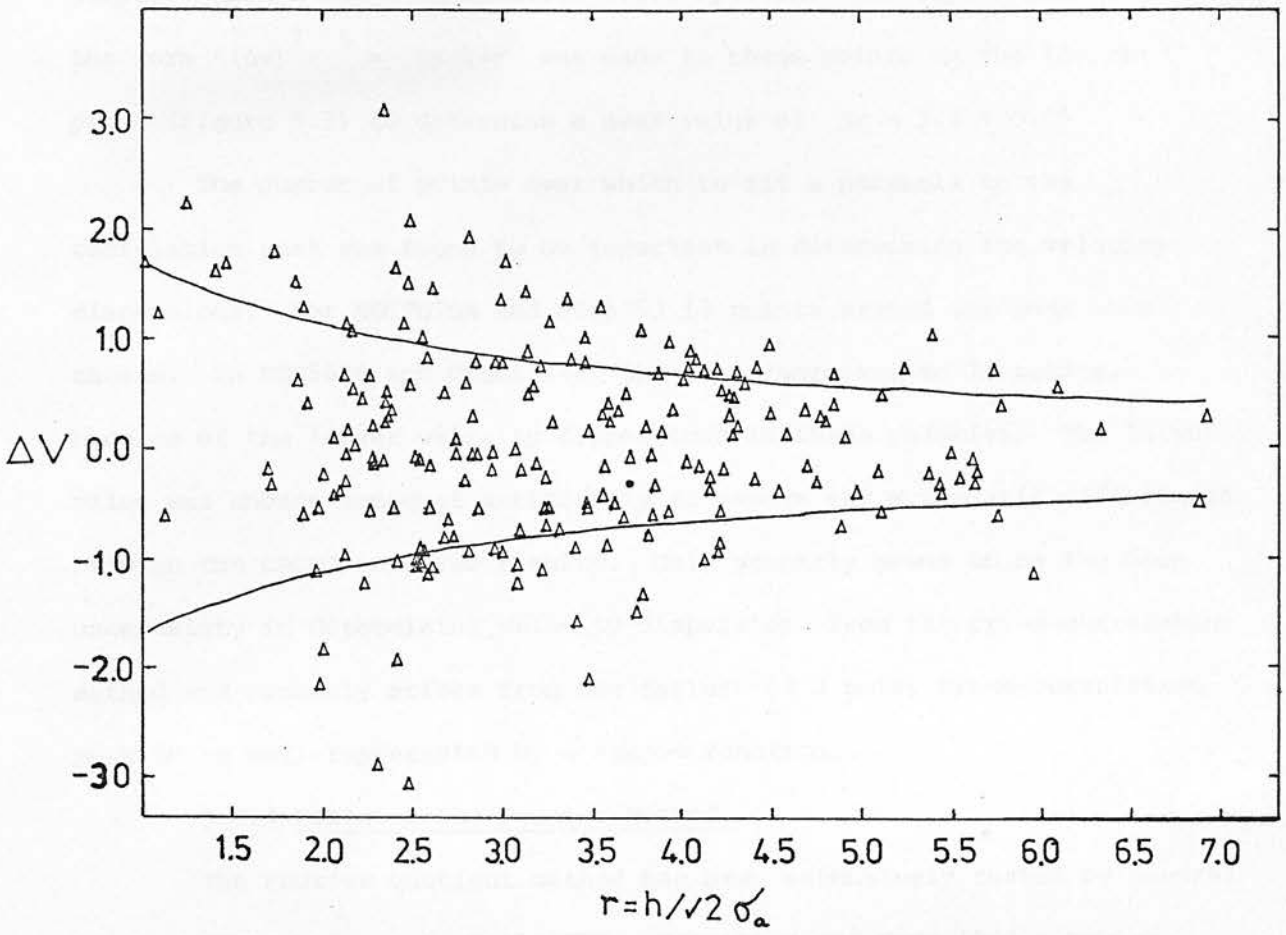

Figure 5.3 : Velocity error ΔV versus the cross-correlation error parameter r, for artificially degraded template spectra. The solid lines show the relation :

$$(1 + r) \; |\Delta V| = 3.4$$

which provides an estimate of the rms value of ΔV as a function of r.

and could be plotted against r. This test was repeated for each template with a range of additive noise spectra. Finally, a fit of the form $<(\Delta v)^2>^{\frac{1}{2}} = \Delta\varepsilon/1+r$ was made to these points in the $(\Delta v, r)$ plane (Figure 5.3) to determine a mean value of $\Delta\varepsilon = 3.4 \pm 0.95$.

The number of points over which to fit a parabola to the correlation peak was found to be important in determining the velocity dispersions. For NGC7070A and NGC5363 15 points around the peak were chosen. In NGC5626 and UKS0151-49 this was increased to 21 points, because of the larger velocity dispersions in these galaxies. The latter value was chosen somewhat arbitrarily to remove any systematic differences between the CRCOR and SSBS results. This property seems to be the main uncertainty in determining velocity dispersions from the cross-correlation method and probably arises from the failure of a noisy cross-correlation peak to be well-represented by a simple function.

5.4.4 Tests of the Fourier Methods

The Fourier quotient method has been extensively tested by several authors (SSBS ; Sargent et al 1978 ; Schechter and Gunn 1979 ; Davies 1981). The potential of the method, and its weaknesses, appear to be well defined. It remains, however, to ensure that the particular algorithm used to implement the method is performing adequately. This is most easily achieved using tests with artificially broadened stellar templates. Figure 5.4 shows the estimated velocity dispersion (σ_{out}) obtained using the method on various template stars broadened by fixed amounts (σ_{in}). A suitable 'mean template' for use as a reference spectrum was obtained by shifting individual templates to the radial velocity of SAO 099805, using linear interpolation between channels. Estimates of the relative shifts required were obtained by cross-correlation of all of the templates with each other. The procedure did not appear to introduce any significant artificial broadening into the mean template.

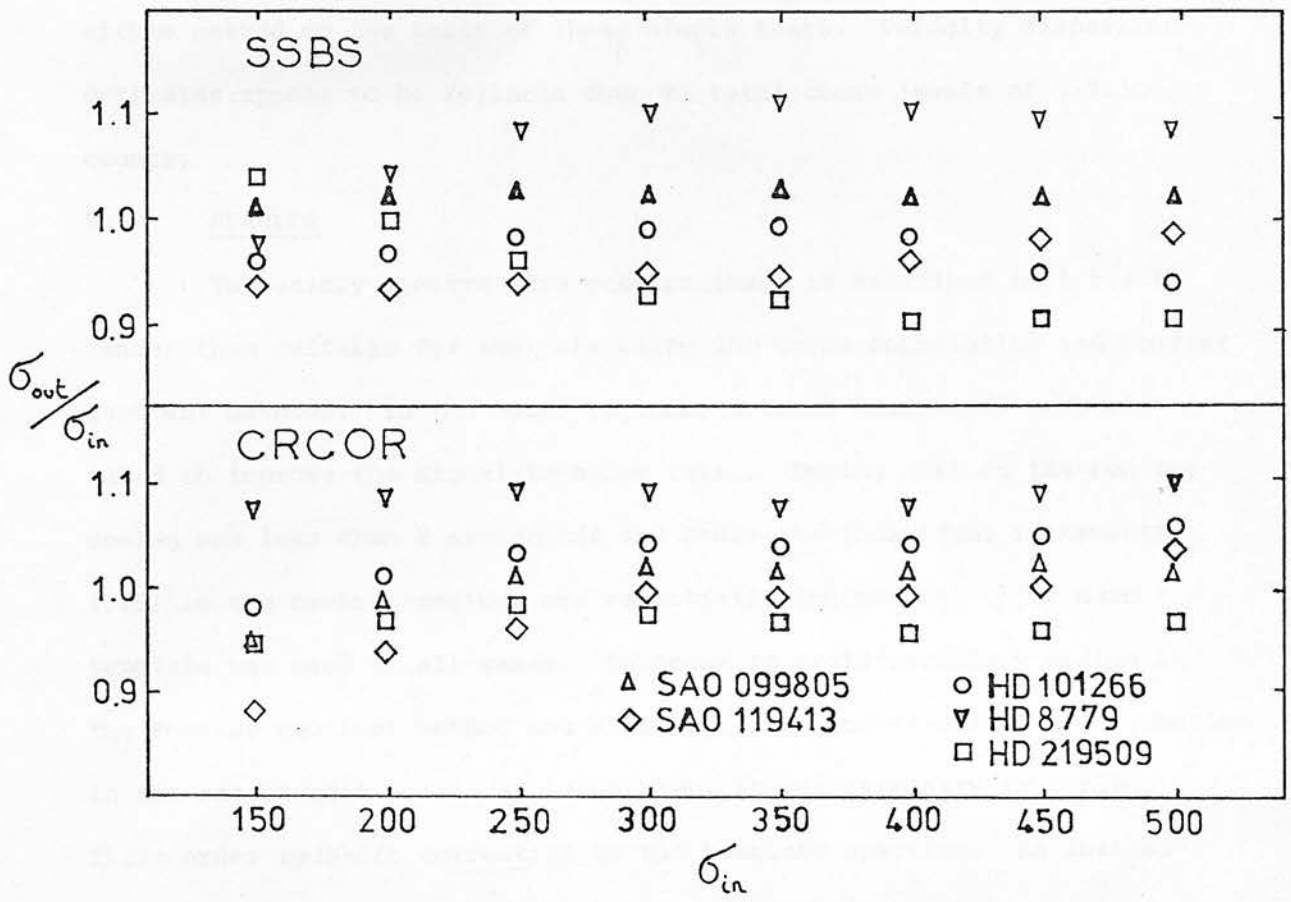

Figure 5.4 : Broadening tests for the Fourier quotient (SSBS) and cross-correlation (CRCOR) methods. σ_{out} is the dispersion estimate from one of these algorithms when a template spectrum is artificially broadened by an amount σ_{in} and compared with a mean template. The results are given for each template separately and indicate that errors due to spectral mismatch and other effects are <10% over a wide range of input broadenings.

The cross-correlation method was also tested in the same way. An examination of Figure 5.4 does not show any strong preference for either method on the basis of these simple tests. Velocity dispersion estimates appear to be reliable down to total count levels of $\sim 2.10^5$ counts.

5.5 RESULTS

The galaxy spectra were pre-processed as described in § 5.4 to render them suitable for analysis using the cross-correlation and Fourier quotient methods. In the outer regions, several increments were co-added to improve the signal-to-noise ratio. During most of the run the seeing was less than 2 arcseconds and hence the individual increments (2".6) in the central regions are essentially independent. The mean template was used in all cases. In order to avoid secondary minima in the Fourier quotient method and aliasing of the cross-correlation function in the measurement domain at large lags, it was necessary to apply a first order redshift correction to the template spectrum. An initial estimate of the galaxy redshift was obtained via the cross-correlation method, and the template spectrum was then shifted to this approximate value using linear interpolation.

Figure 5.5 shows the velocity dispersions and line strengths along the major axis of NGC5363, derived using the cross-correlation (□) and Fourier quotient (◇) methods. Error bars are taken from the cross-correlation estimates where appropriate, although little difference would be found using the Fourier quotient values instead. The agreement between the two methods is good.

Final rotation velocities V, dispersions σ and line strengths γ are tabulated for each slit position in Appendix I. Radial distances have been measured from the photometric centres, as defined by the peak in the

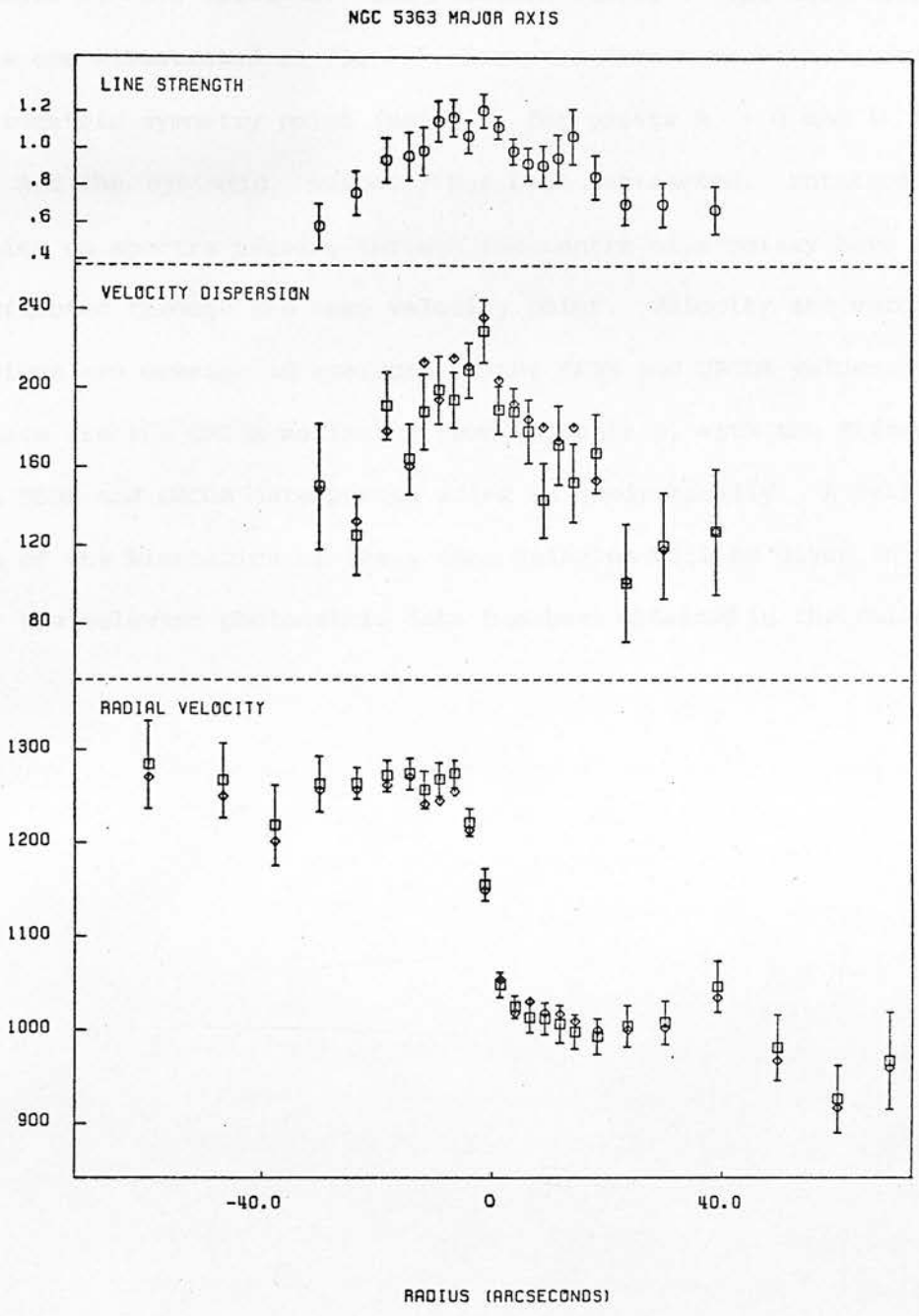

Figure 5.5 : Major axis rotation curve, velocity dispersion profile and line strength profile for NGC5363. Velocities and velocity dispersions have been measured using both the cross-correlation and Fourier quotient methods. Cross-correlation values are given as open squares, Fourier quotient results as open diamonds. The error bars are from the cross-correlation method using equation 5.17 with $\Delta\varepsilon = 3.4$. The line strength parameter is obtained entirely from the Fourier quotient method.

IPCS counts on each spectrum. The rotation curves & velocity dispersion profiles are illustrated in Fig 5.6 where the data have been folded about the photometric symmetry point (using ◊ for points R < 0 and □ for R ≥ 0) and the systemic velocity has been subtracted. Rotation velocities on spectra passing through the centre of a galaxy have also been reflected through the zero velocity point. Velocity and velocity dispersions are unweighted averages of the SSBS and CRCOR values. The error bars are the CRCOR estimates from Appendix I, with the difference between SSBS and CRCOR data points added in quadratically. A full discussion of the kinematics of these four galaxies will be given in Chapter 7 after the relevant photometric data has been obtained in the following chapter.

Figure 5.6 : Kinematics of the stellar components of the four galaxies :

NGC5363 (a) major axis;(b) inner (minor axis) dust lane;(c) parallel to inner dust lane but offset 7" SE;(d) at PA = 90°, i.e. 45° to major axis and dust lane;(e) same as (b) but excluding the NaD feature.

NGC7070A (a) major axis;(b) minor axis;(c) parallel to dust lane but offset 5" E;(d) dust lane; (e) perpendicular to dust lane;(f) parallel to dust lane but offset 5" W.

NGC5626 (a) minor axis;(b) major axis

0151-498(a) minor axis;(b) major axis

Rotation, velocity dispersion and line strength parameters are plotted as a function of radius, measured from the centroid of the IPCS counts along the slit. For relative compactness the profiles have been folded about this photometric symmetry point. In addition, the rotation curves at slit positions passing through the nucleus have had their mean value subtracted and been folded through the zero velocity axis. The velocity zero-point at offset slit positions is determined by subtracting the mean recession velocity of the galaxy taken from Appendix I. Velocity and velocity dispersions from the Fourier quotient and cross-correlation methods have been averaged. The error estimates allow for the formal errors in the cross-correlation technique and the disagreement between the two methods.

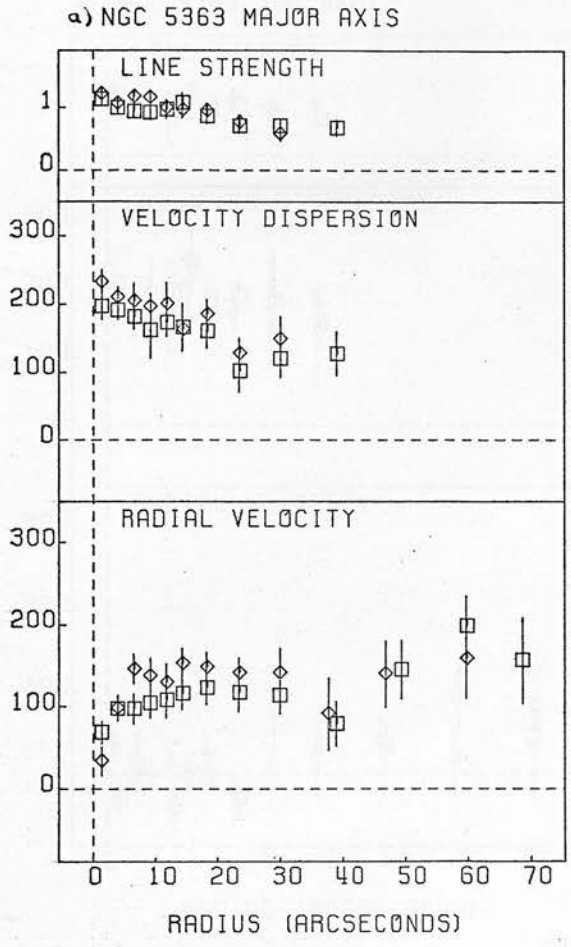
a) NGC 5363 MAJOR AXIS
LINE STRENGTH
VELOCITY DISPERSION
RADIAL VELOCITY
RADIUS (ARCSECONDS)

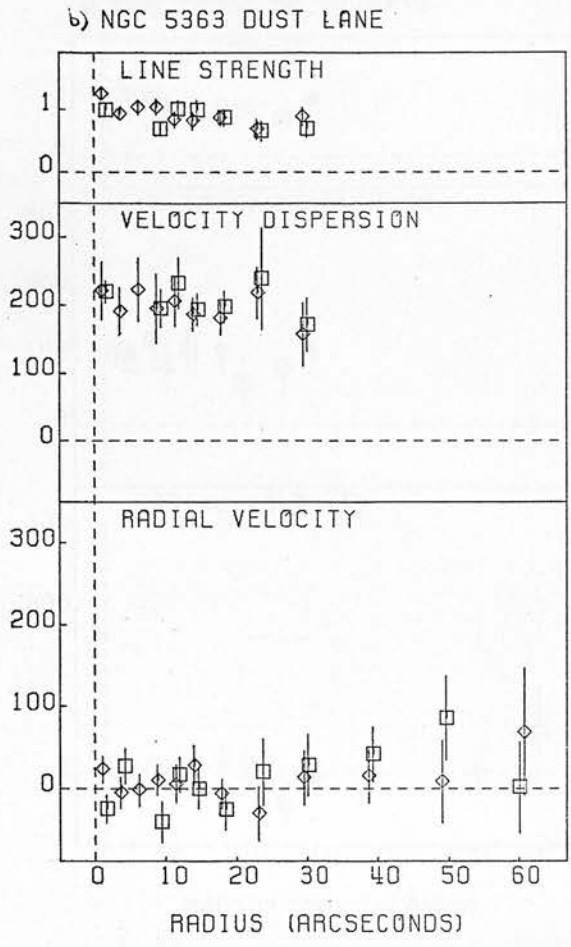
b) NGC 5363 DUST LANE
LINE STRENGTH
VELOCITY DISPERSION
RADIAL VELOCITY
RADIUS (ARCSECONDS)

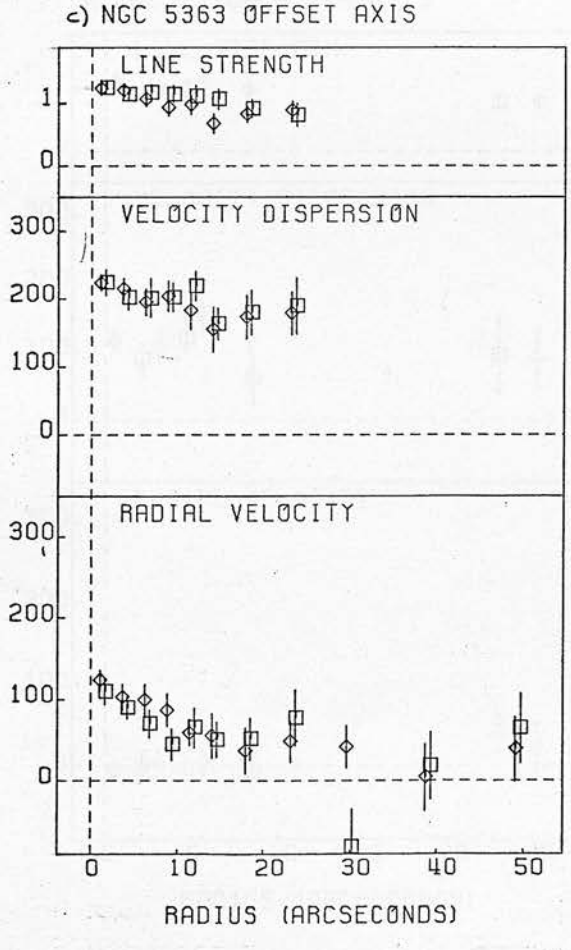
c) NGC 5363 OFFSET AXIS
LINE STRENGTH
VELOCITY DISPERSION
RADIAL VELOCITY
RADIUS (ARCSECONDS)

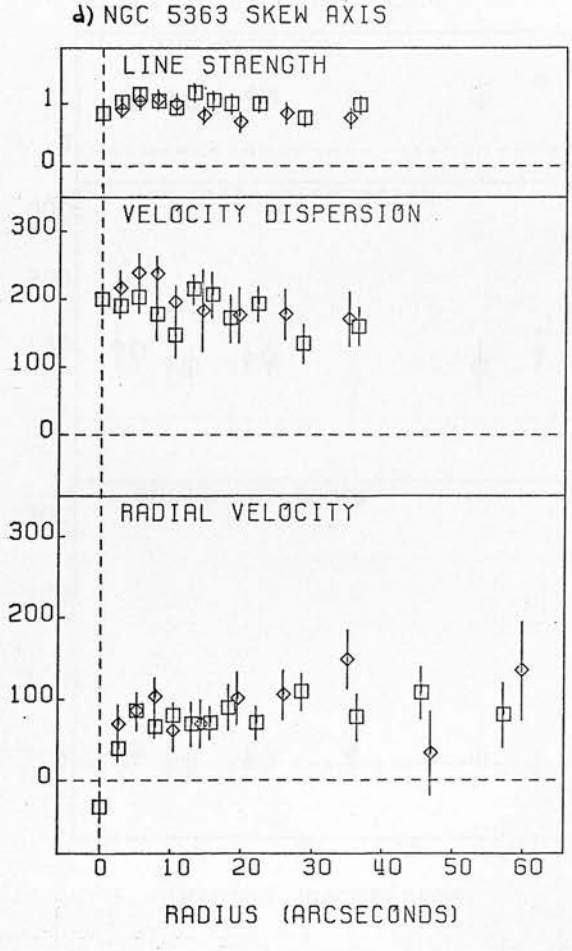
d) NGC 5363 SKEW AXIS
LINE STRENGTH
VELOCITY DISPERSION
RADIAL VELOCITY
RADIUS (ARCSECONDS)

e) NGC 5363 (NØ NaD)

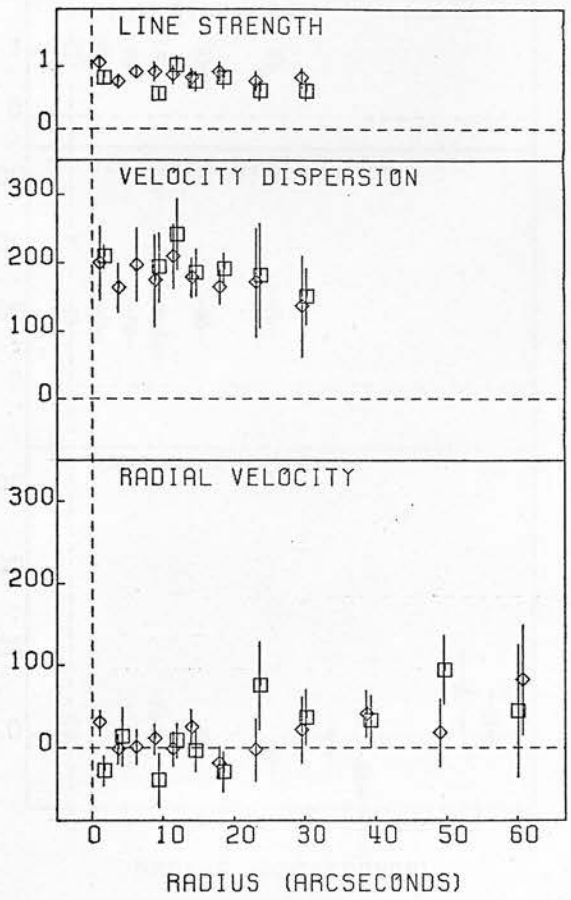

a) NGC 7070A MAJOR AXIS

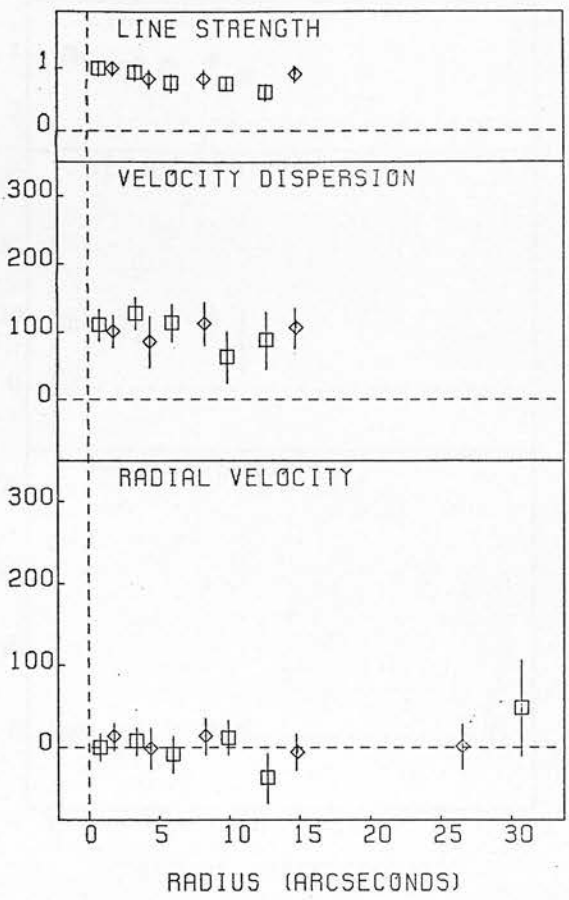

b) NGC 7070A MINOR AXIS

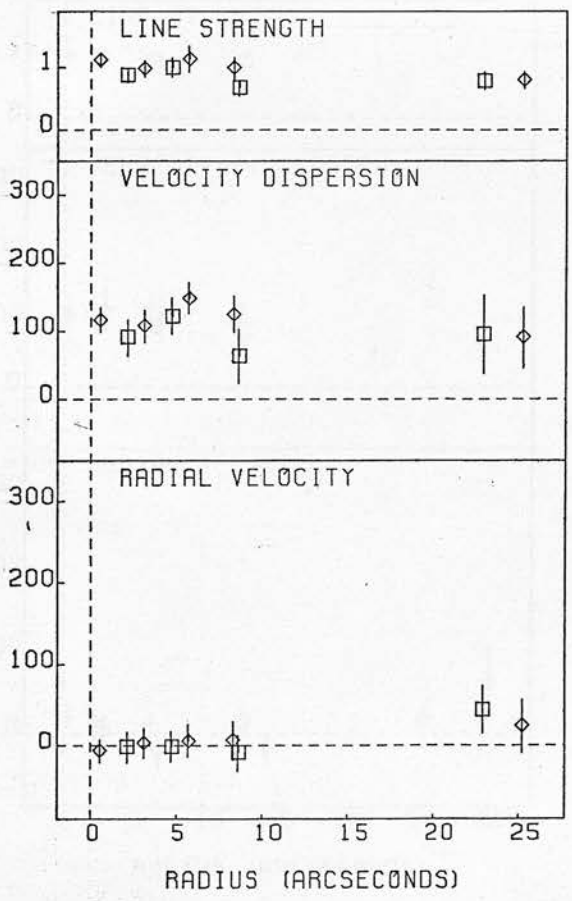

c) NGC 7070A BRIGHT EDGE

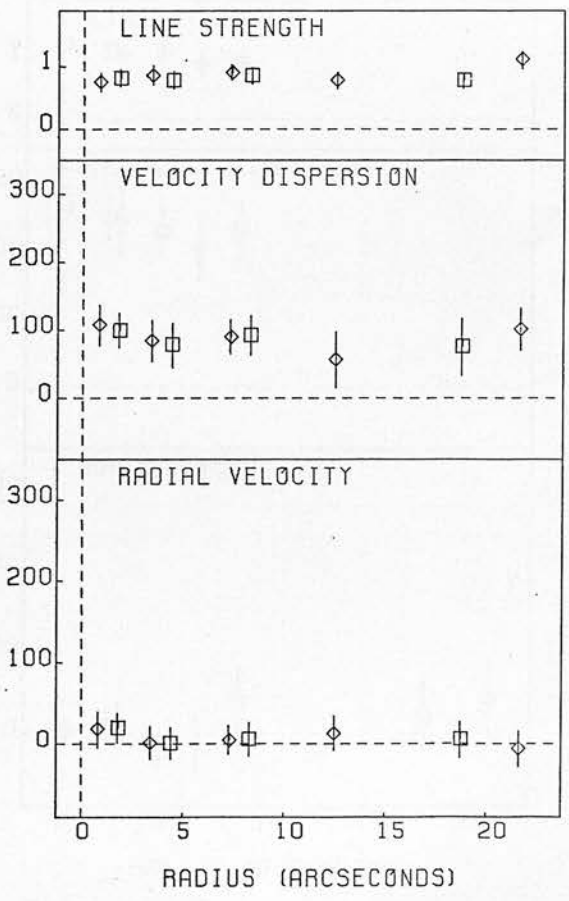

d) NGC 7070A DUST LANE

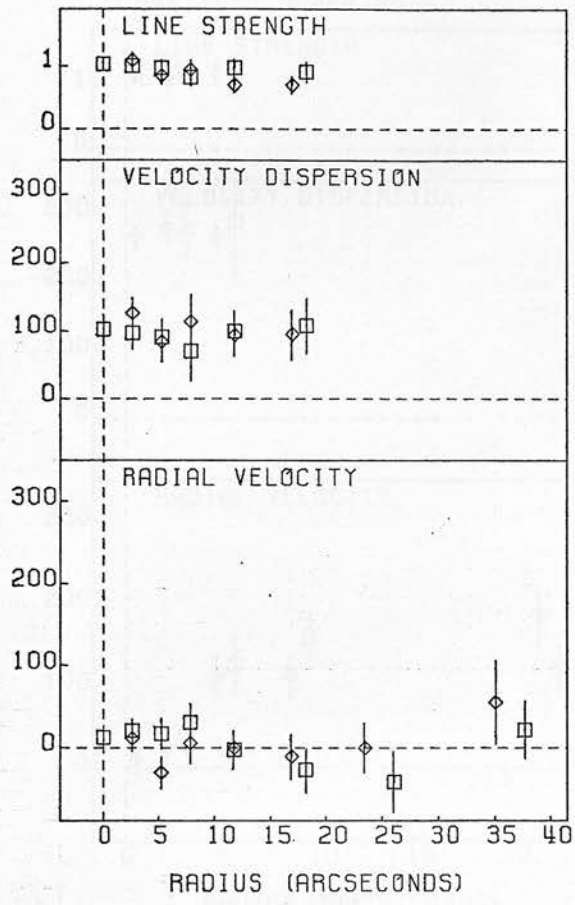

e) NGC 7070A SKEW AXIS

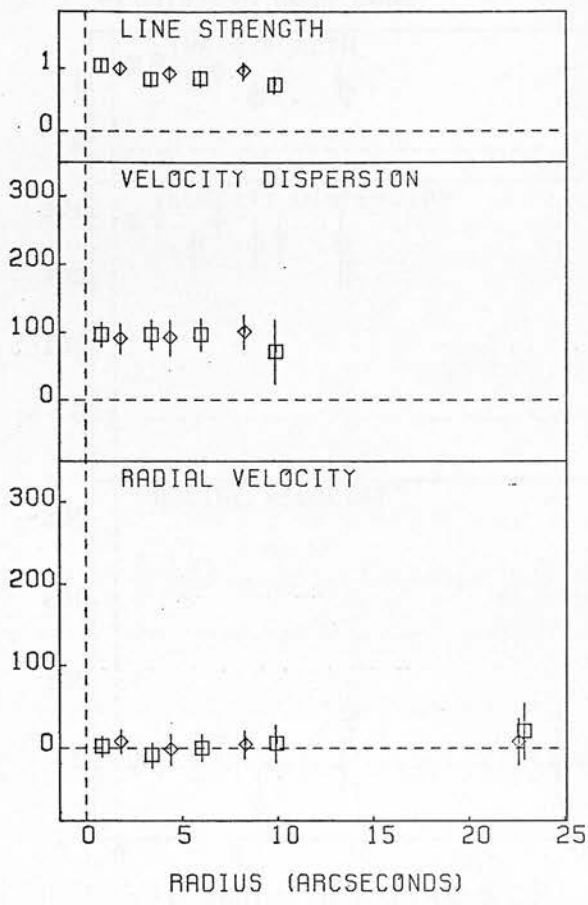

f) NGC 7070A FAINT EDGE

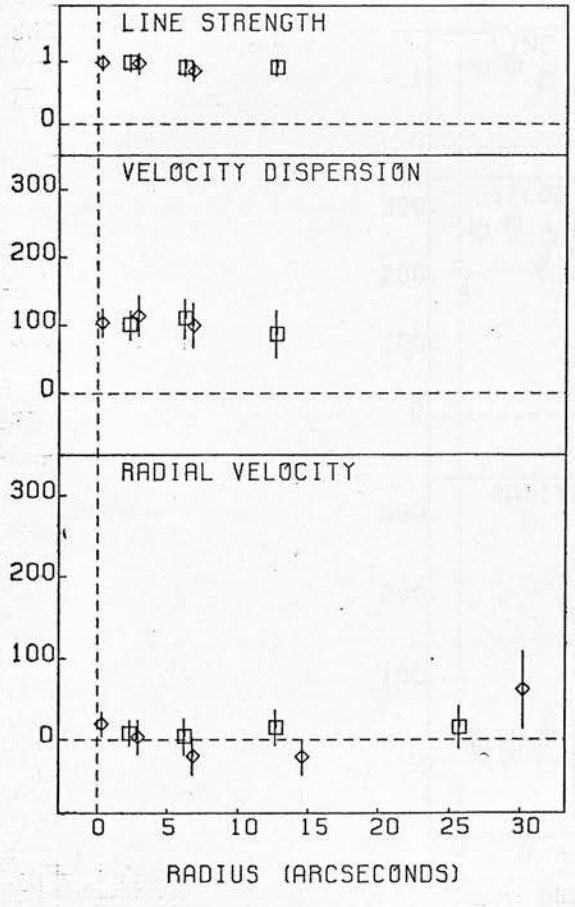

a) NGC 5626 MINOR AXIS

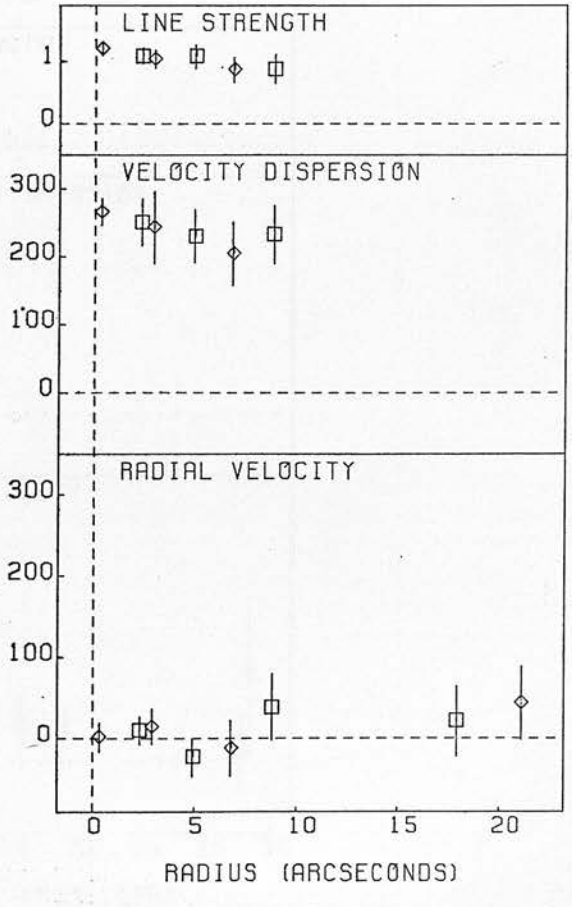

b) NGC 5626 MAJOR AXIS

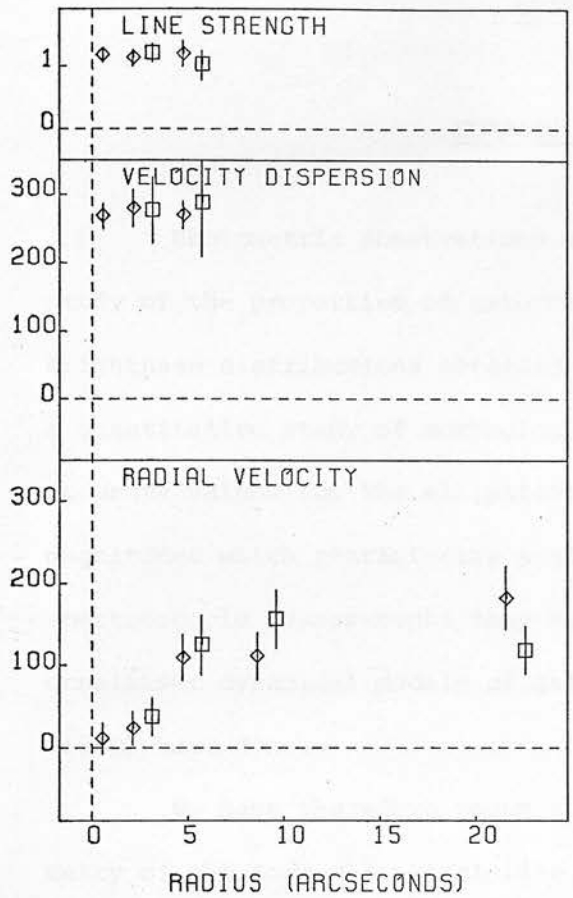

a) U0151-49 DUST LANE

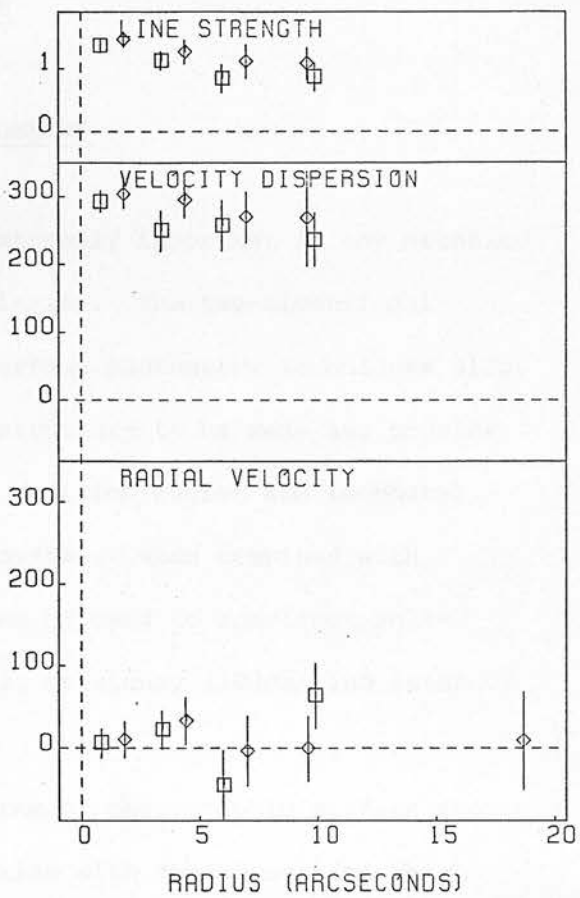

b) U0151-49 MAJOR AXIS

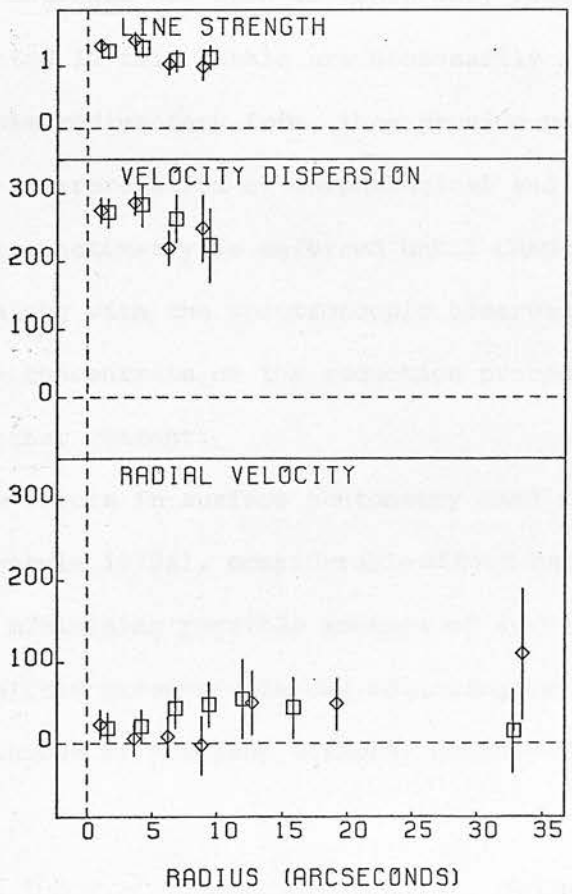

CHAPTER 6

SURFACE PHOTOMETRY

Photometric observations are extremely important in any detailed study of the properties of external galaxies. The two-dimensional brightness distributions obtained by surface photometry techniques allow a quantitative study of morphological structure to be made and provide accurate values for the ellipticities, position angles and isophotal magnitudes which characterize a given system. When combined with spectroscopic measurements they may also be used to construct self-consistent dynamical models of galaxies, as Binney (1980a) and Satoh (1980) have done.

We have therefore begun a program of photographic surface photometry of the four elliptical-like galaxies with dust lanes for which spectroscopic data were discussed in the previous chapter. Because the photographic plate material has been obtained only recently, the reduction and analysis presented in this thesis are necessarily rather preliminary. However, even in this rudimentary form, they provide useful additional constraints on the interpretation of morphological and kinematical data. The analysis of this photometry is deferred until Chapter 7, where it will be discussed along with the spectroscopic observations presented in Chapter 5. Here we concentrate on the reduction procedures and give the results without further comment.

Because the errors in surface photometry tend to be systematic in nature (e.g. Burstein 1979a), considerable effort has been expended in recent years on minimising possible sources of systematic effects. The reduction techniques presented in the following sections are firmly based on the experiences of previous workers, notably Godwin (1976),

Carter (1977, 1978) and Blackman (1979). Several programs have been adopted wholesale from these previous implementations, others have been written by the author.

6.1 OBSERVATIONS

The photographic plate material for this study was obtained in July 1981 at the f/3.3 prime focus of the Anglo- Australian Telescope. A doublet corrector was used with standard 10 x 10 inch plates, giving an unvignetted field of 25 arcmin and a platescale of 16.4 arcsec/mm. All plates were hypersensitized (Babcock, 1976) to improve their detective quantum efficiency, and developed for 5 minutes in Kodak D19 at 20° C. During the exposure dry nitrogen gas was flushed across the plate to prevent desensitization of the emulsion by water vapour, and a calibration wedge was projected onto the plate using the AAO 16-spot sensitometer. Only a few of the total number of plates taken are required for the discussion in Chapter 7. Details of the emulsion/filter combinations and exposure times for these plates are given in Table 6.1.

6.2 DATA REDUCTION

The data reduction process can be divided into five well-defined steps :

(i) Digitization of the plate

(ii) Conversion from density to relative intensity

(iii) Subtraction of the sky background

(iv) Determination of the intensity zero-point

(v) Extraction of the image parameters - luminosity profiles, isophote structure, etc.

each of which is discussed briefly in the following subsections.

TABLE 6.1

AAT PRIME FOCUS PHOTOGRAPHY

Galaxy	Emulsion	Filter	Spectral Range (nm)	Hypersensitization	Exposure
NGC 5363	III a J	GG 385	385 - 500 (B)	6^h N_2 bake at 65^o + 7^h H_2 at 20^o	15^m
	IV N	RG 695	695 - 900 (I)	4^m soak $AgNO_3$ sol^n (0.125 gm/l)	40^m
NGC 7070A	II a D	RG 495	495 - 600 (V)	1^h N_2 bake at 65^o + 7^h H_2 at 20^o	30^m
NGC 5626	III a F	RG 630	630 - 700 (R)	3^h N_2 bake at 65^o + 2^h N_2 at 20^o	40^m
0151-498	III a J	GG 385	385 - 500 (B)	6^h N_2 bake at 65^o + 7^h H_2 at 20^o	15^m
	III a F	RG 630	630 - 700 (R)	3^h N_2 bake at 65^o + 2^h N_2 at 20^o	15^m

6.2.1 Plate Digitization

All plates were digitized using a PDS microdensitometer (Wray and Benedict 1974) at the Anglo-Australian Observatory. Depending on the size of the galaxy, a square matrix of either 512 x 512 or 1024 x 1024 pixels was mapped at the centre of each plate. Both the spot size and pitch were standardized at 25 μ (0.4 arcsec). The total area mapped was therefore either 12.24 or 48.96 square arcminutes. Calibration spots were measured by scanning a 128 x 128 matrix, with a pitch size of 50 μ, centred individually on each spot. Because of the possibility of electronic drifts in the photomultiplier amplifier and mechanical drifts in the optics, the calibration spots were scanned both immediately before and after the galaxy scan. Such drifts were in fact detected and are discussed further in the following section.

6.2.2 Intensity Calibration

Since the photographic emulsion has a non-linear response to incident light, a transformation to relative intensities must be made using the calibration spot measurements. Scattered light in the emulsion and inhomogeneities in the iconel wedges can give rise to non-uniformity within the spot area. To eliminate these effects from the measurements a histogram of the number of pixels versus density was constructed for each spot. The peak of this histogram was approximately Gaussian in form, so all points with $>2\sigma$ residuals from the peak were rejected and the centroid of the truncated distribution adopted as the true spot density. The higher order moments of the histograms were also examined, so that badly contaminated spots could be excluded from the calibration curve. Due to the limited dynamic range of the PDS, only about 12 of the spots were found to be useful on any single plate. Improvements in the definition of the characteristic curve could probably be achieved by adding the spot sets from different plates in the same batch, as

Kormendy (1976) and Burstein (1979a) have done.

The fit to the characteristic curve was made in the conventional density vs log (intensity) plane. Polynomial approximations were found to be unsatisfactory, because the high orders required to fit the high-density saturation region and the under-exposed 'toe' of the H-D curve, became unstable on the linear section. Cubic splines gave much more reliable fits to the curve, using either one or two knots whose positions were chosen interactively. Relative spot intensities were taken from Malin and Peterson (1981) or Malin (1981, private communication).

Inspection of the two spot sets for each plate often showed that a drift had taken place between measurements (Figure 6.1). The skewness of the curves suggested that electronic problems were responsible, but unfortunately these were found to persist even after a substantial (> 24 hr) warm-up period was allowed. In the absence of any indication that the drift was non-linear, mean values of the two spot measurements were adopted for the spline-fitting procedure. That this does not introduce any significant errors for the present work is demonstrated in § 6.3.

6.2.3 Background Subtraction

Accurate background subtraction is required for studies of the faint outer regions of galaxies. We follow closely the procedure of Godwin (1976) in using density histograms on a 16 x 16 grid over the measured area to define the background. The peak of each histogram is determined iteratively, in a similar way to that for the calibration spots, which effectively removes the contamination by small images. Two-dimensional polynomial fits to these background levels are used to reject areas containing large images. Because the size of the scans is comparatively small and well within the unvignetted region of the

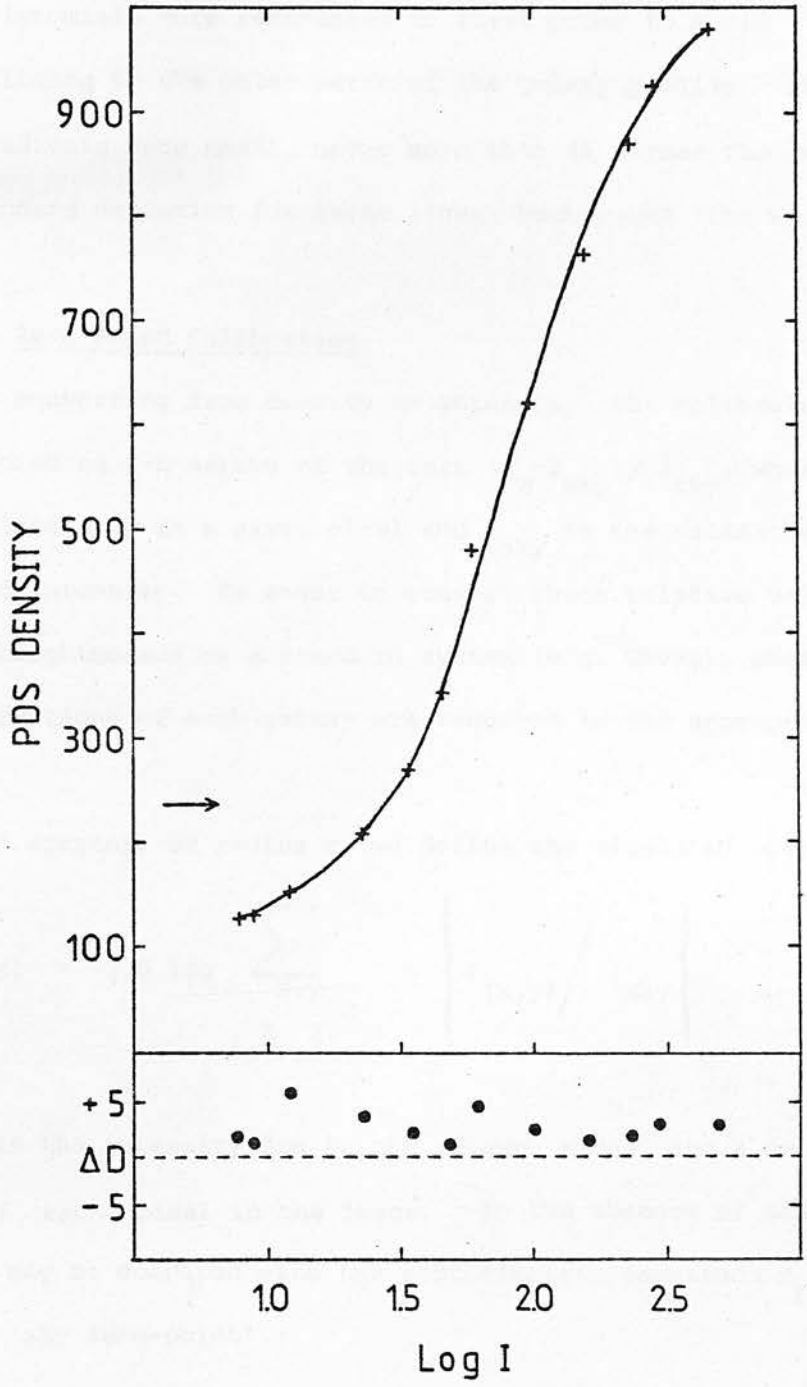

Figure 6.1: Mean calibration curve for a 15 minute R plate of 0151-498. The solid line is a cubic-spline fit using one knot at the position of the arrow. ΔD is the difference in mean density between each spot measurement before and after the galaxy scan. PDS densities are measured on an arbitrary scale from 0 to 1024 corresponding approximately to ANS1 diffuse densities in the range 0 to 4.

plate, the polynomials were restricted to first order to avoid erroneously fitting to the outer parts of the galaxy profile. Sky background gradients were small, never more than 4% across the measured area. The standard deviation for these linear background fits was typically 1%.

6.2.4 Zero-Point Calibration

After converting from density to intensity, the calibrated galaxy scans were stored as 2-D arrays of the form $(I_T - I_{sky}) / I_{sky}$, where I_T is the total intensity in a given pixel and I_{sky} is the estimated local sky background intensity. In order to convert these relative values into surface brightnesses on a standard system (e.g. UBVRI), photoelectric observations of each galaxy are required in the appropriate bandpass.

For an aperture of radius r, we define the simulated aperture magnitude :

$$m_{sim}(r) = -2.5 \log \sum_{\substack{x,y \\ |x^2+y^2|<r^2}} a \left\{ I_{(x,y)} \Big/ I_{sky} \right\}$$

where $I_{(x,y)}$ is the intensity due to the galaxy alone, and 'a' is the area of each pixel in the image. In the absence of saturation effects, this may be compared with the photoelectric magnitude $m_{pe}(r)$ to derive the 'sky zero-point' :

$$m_{sky} = -2.5 \log \langle I_{sky} \rangle = m_{pe} - m_{sim}$$

Saturation effects in the cores of bright galaxies can in principle be avoided using annular magnitudes or estimated directly from a comparison of photoelectric and photographic magnitudes at several aperture sizes (Smyth 1980). In practice, this was not a serious problem for the

TABLE 6.2 : Zero-Point Photoelectric Photometry

NGC 5363 $b^{II} = 63^{o}$ z = 0.0037 B_{sky} = 22.06 ± 0.06

Aperture "	U	B	V	R	I	Source	Notes
16.1	13.57	12.89	11.86	-	-	T	1
25.8	13.15	12.48	11.35	-	-	T	1
38.7	12.80	12.15	11.04	-	-	T	1
49.9	12.94	12.49	11.35	-	-	VM1	2
59.5	12.51	11.89	10.92	9.94	-	SV	3
61.9	12.45	11.87	10.90	-	-	V	
64.3	12.70	12.31	11.23	-	-	VM1	2
64.5	12.42	11.78	10.77	-	-	T	1
83.7	12.22	11.64	10.68	9.70	-	SV	3
114.3	-	11.71	10.66	-	-	VM1	2

NGC5626 $b^{II} = 28^{o}$ z = 0.0220 R_{sky} = 19.9[4] ± 0.3

NGC7070A $b^{II} = -47^{o}$ z = 0.0080 V_{sky} = 21.48 ± 0.11

Aperture "	U	B	V	R	I	Source	Notes
25.6	-	14.94	13.91	-	-	E	
35.2	15.07	14.55	13.55	-	-	LS	
39.1	-	-	13.34	-	-	E	
55.2	-	-	12.99	-	-	E	
75.3	14.12	13.68	12.71	-	-	LS	
99.6	14.01	13.49	12.47	-	-	VM1	

U0151-498 $b^{II} = -64^{o}$ z = 0.0206 B_{sky} = 22.16 ± 0.02

Aperture "	U	B	V	R	I	Source	Notes
20.9	15.35	14.71	13.57	12.92	12.24	TGH	
30.1	-	14.39	13.29	12.68	11.96	TGH	
59.6	14.49	13.89	12.81	-	-	TGH	
84.6	14.21	13.69	12.62	-	-	TGH	

Notes: 1 - Aperture centred 3" SW of nucleus
2 - corrected for field star with V = 12.11, B-V = 0.89, U-B=0.90
3 - corrected from ubVr to UBVR system
4 - estimated from infrared photometry in Chapter 2, assuming that NGC5626 has the same (R-K) colour as the EO galaxy NGC4552.

Ref:
E - E.Sadler, private communication
LS - this work
SV - Sandage A. & Visvanathan 1978, Ap.J.223, 707.
T - Tifft W.G. 1969 AJ.74, 354.
TGH - T.G.Hawarden, private communication.
VM1 - de Vaucouleurs G. & de Vaucouleurs A.1972 Mem RAS 77, 1.

relatively short exposure plates in this study.

Photoelectric observations of the program galaxies and the adopted sky zero-points are given in Table 6.2. Because no observations were available for NGC5626 (in any colour) or for NGC5363 in the I band, we continue to work for the present in units of the sky brightness. Further photoelectric work would be very desirable to strengthen these zero points and would provide a means of checking the characteristic curve adopted from § 6.2.2.

6.2.5 Image Parameters

Using the intensity-calibrated sky-subtracted arrays, a wide variety of information can be extracted about the galaxy image. For the present work, however, we shall be primarily interested in the luminosity (surface brightness) profiles and the isophote shapes and orientations.

To improve the signal-to-noise at large radii, radial profiles were taken using a wedge-shaped cross section of opening angle 20^{o}. The radial bins were constrained to have a constant aspect ratio (arc length/ radial length), and the profiles were truncated in the innermost regions where the number of pixels per bin was less than four.

The shapes and orientations of the isophotes were determined using the ellipse-fitting algorithm described by Carter (1978). This program extracts the largest isophotal contour at a given level and approximates it with an ellipse by minimising the function :

$$\sum_{i} \left\{ \frac{\left[(x_i-x_o)\cos\theta+ (y_i-y_o)\sin\theta\right]^2}{a^2} + \frac{\left[(y-y_o)\cos\theta- (x_i-x_o)\sin\theta\right]^2}{b^2} -1 \right\}^2$$

with respect to x_o, y_o, a, b, and θ.

Using a Fourier analysis of the residuals, the accuracy of the fit and any systematic deviations from ellipticity may also be investigated

Figure 6.2 : Isophote maps and ellipse-fitting for the B plate of 0151-498. The upper diagram is a contour map in intensity space of the unsmoothed calibrated image. In the lower diagram the longest contour has been extracted from each isophote level and approximated with an ellipse using the algorithm discussed in the text. The isophote levels are selected at constant intervals in logarithmic intensity to obtain a more even distribution over the brightness profile. Both maps are plotted to the same scale and orientation.

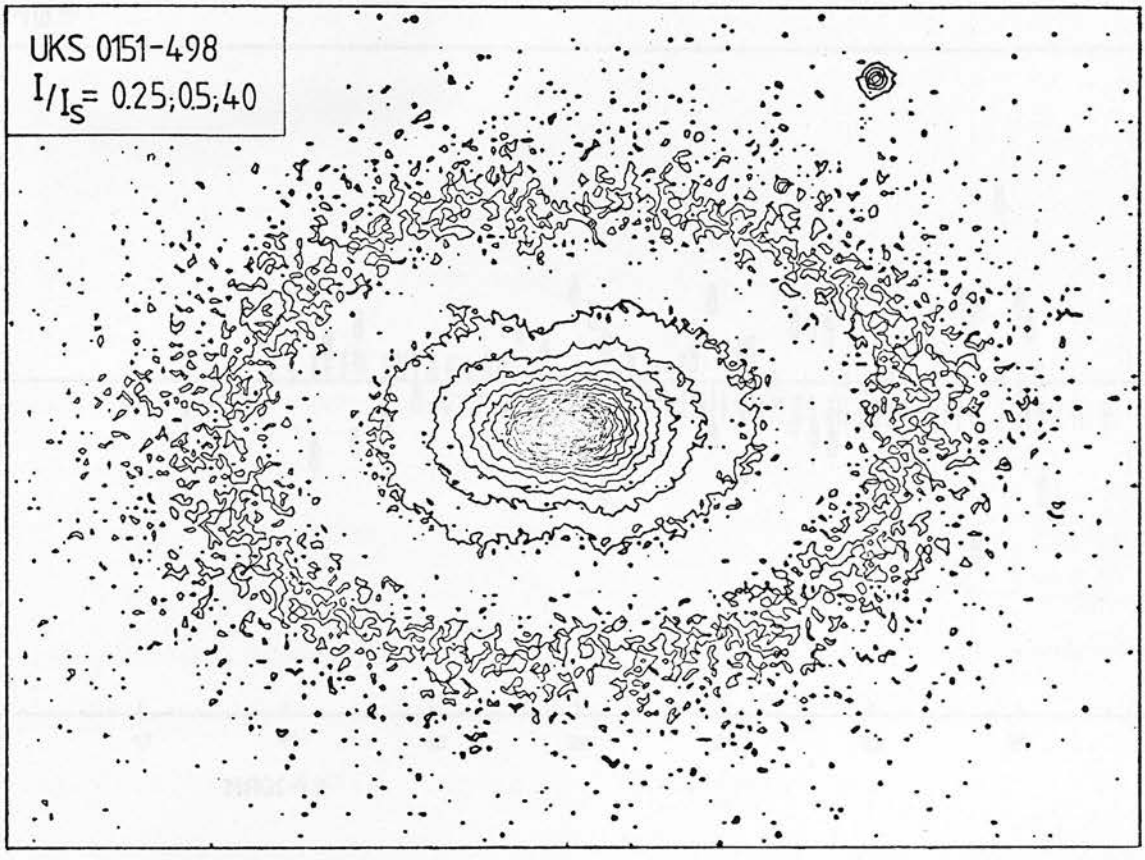
UKS 0151-498
I/I_S= 0.25;0.5;40

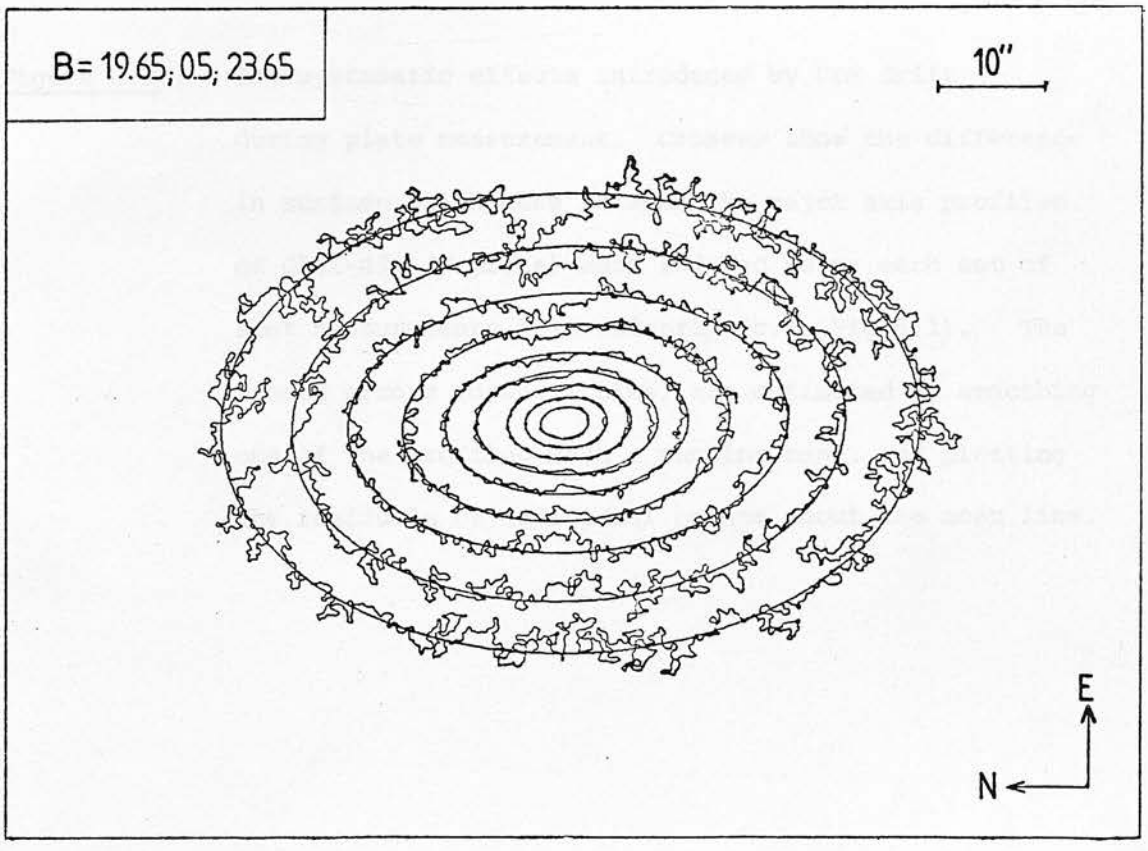
B= 19.65; 0.5; 23.65
10''
E
N

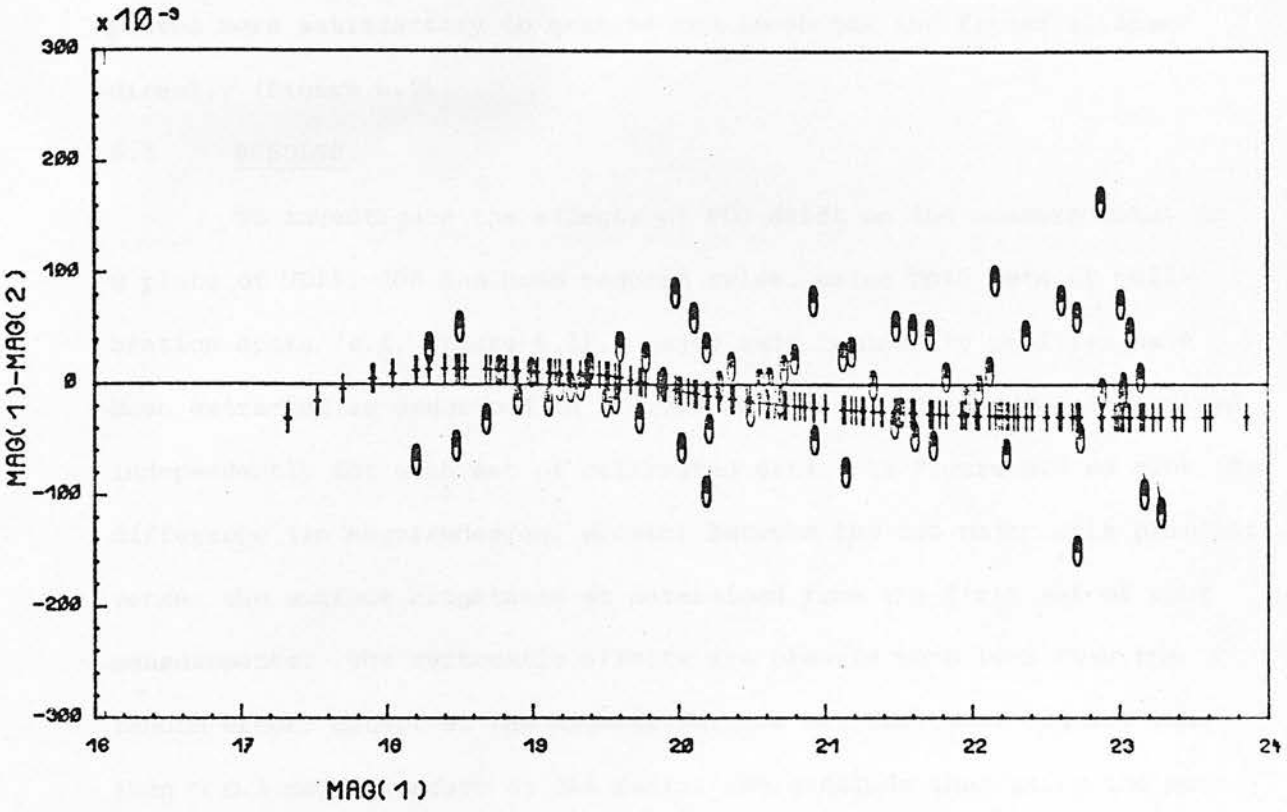

Figure 6.3 : The systematic effects introduced by PDS drift during plate measurement. Crosses show the difference in surface brightness between the major axis profiles of 0151-498 (R plate) when reduced using each set of spot measurements independently (c.f. Fig 6.1). The random errors (open circles) are estimated by smoothing one of the profiles with a running mean, and plotting the residuals of individual points about the mean line.

(c.f. Carter, 1978). However, for the dusty galaxies in this study it proved more satisfactory to examine the isophotes and fitted ellipses directly (Figure 6.2).

6.3 RESULTS

To investigate the effects of PDS drift on the measurements, an R plate of UO151-498 has been reduced twice, using both sets of calibration spots (c.f. Figure 6.1). Major axis luminosity profiles have been extracted as described in § 6.2.5 and the sky zero-point determined independently for each set of calibrated data. In Figure 6.3 we plot the difference (in magnitudes/sq. arcsec) between the two major axis profiles versus the surface brightness as determined from the first set of spot measurements. The systematic effects are clearly much less than the random errors except at the highest surface brightnesses, and are less than $\sim$ 0.1 mag/sq.arcsec at all radii. We conclude that using the mean calibration curve from the two spot sets does not introduce any significant discrepancies for the present work.

Major and minor axis luminosity profiles for each galaxy are given in Figure 6.4, using the following plate material :

NGC 5363 B plate

NGC 7070A V plate

NGC 5626 R plate

UO151-498 B plate

Isophote ellipticities and position angles are given in Figure 6.5. The position angles have been measured N. through E. in the usual sense. A discussion of these figures is presented in the following chapter.

Figure 6.4 : Luminosity profiles along the principal axes of the four galaxies. Surface brightnesses are given in terms of the local sky background I_{sky}. These may be converted to units of magnitudes per square arcsecond using :

$$\mu \text{ (mag/sq arcsec)} = m_{sky} - 2.5 \log I/I_{sky}$$

where m_{sky} is the appropriate sky zero-point from Table 6.2. The profiles have been folded about the intensity-weighted centroid of the entire image.

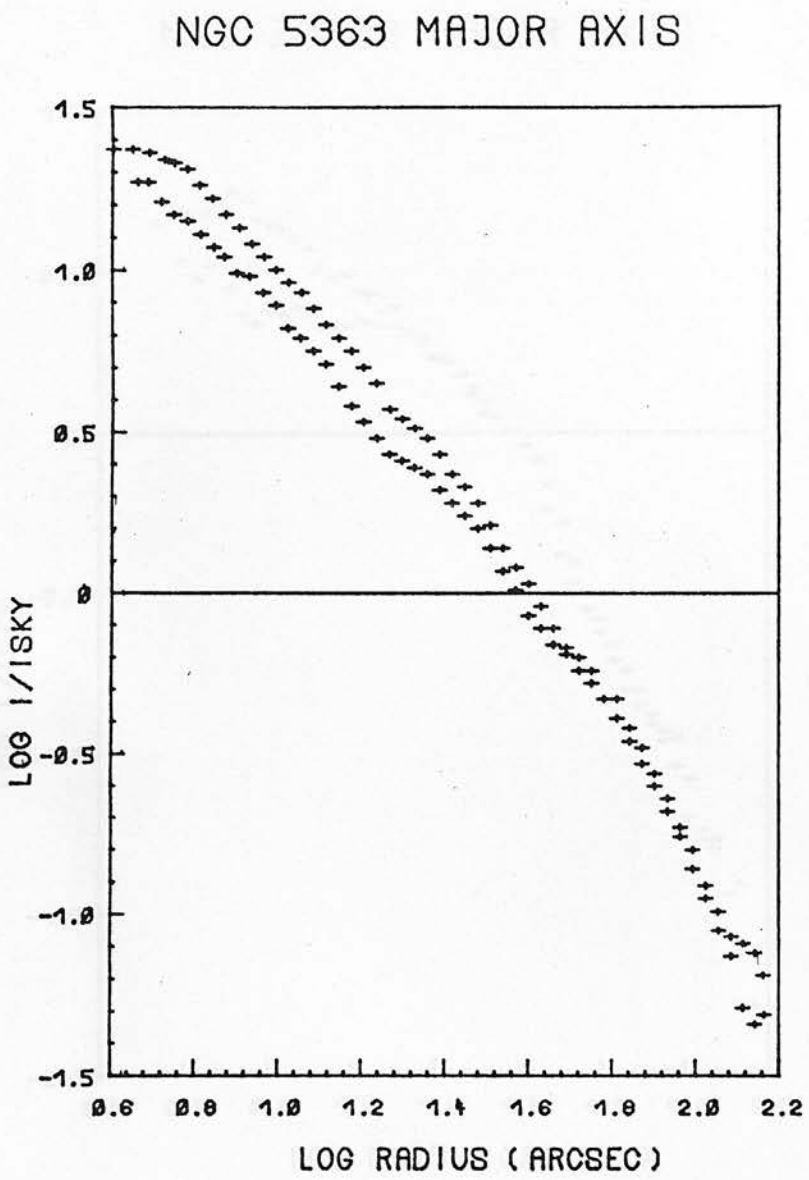
NGC 5363 MAJOR AXIS
LOG I/ISKY
LOG RADIUS (ARCSEC)
1.5
1.0
0.5
0
-0.5
-1.0
-1.5
0.6
0.8
1.0
1.2
1.4
1.6
1.8
2.0
2.2

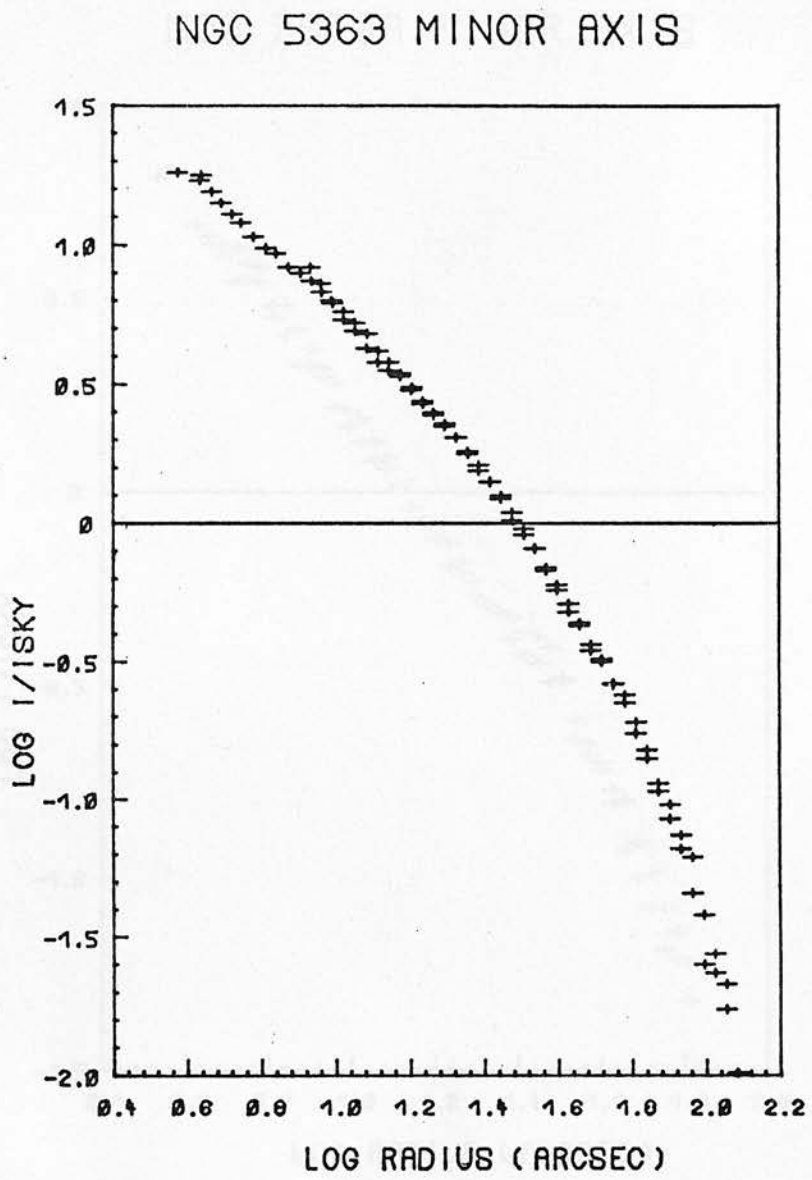
NGC 5363 MINOR AXIS
LOG I/ISKY
LOG RADIUS (ARCSEC)
1.5
1.0
0.5
0
-0.5
-1.0
-1.5
-2.0
0.4
0.6
0.8
1.0
1.2
1.4
1.6
1.8
2.0
2.2

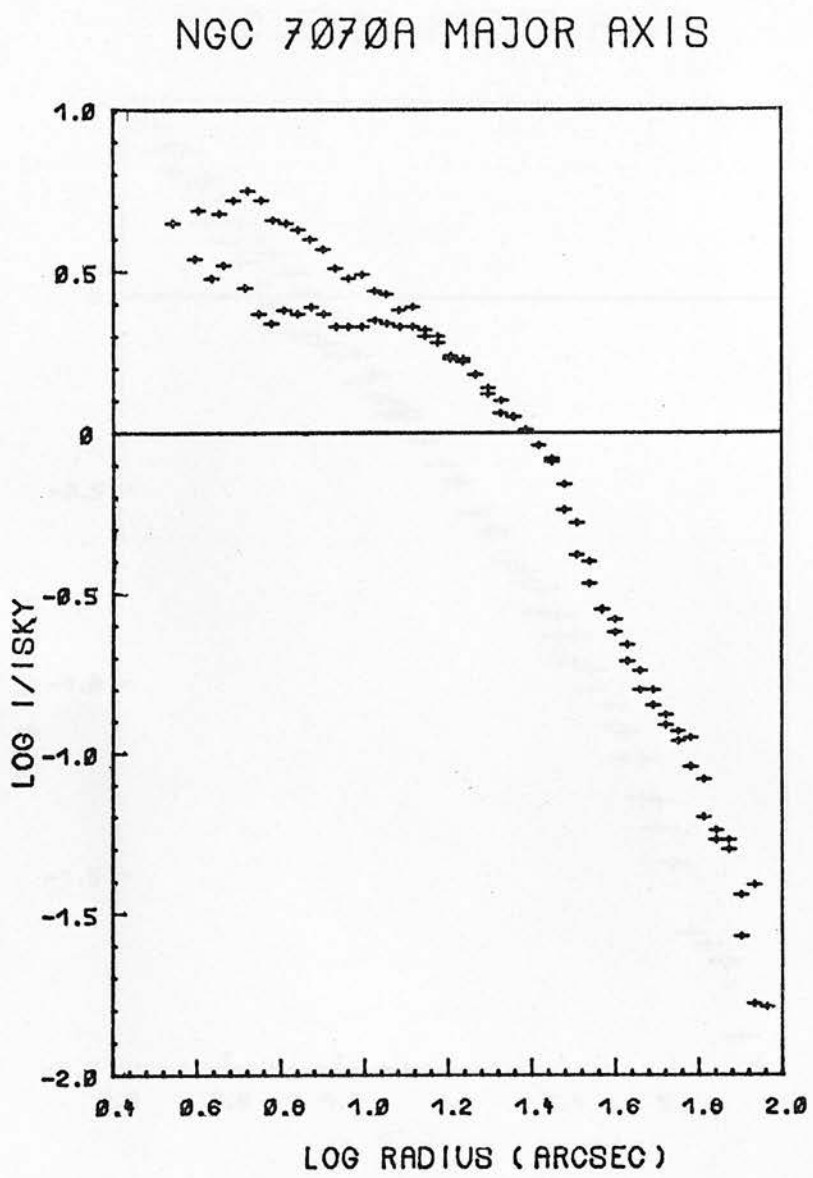
NGC 7070A MAJOR AXIS
1.0
0.5
0
-0.5
-1.0
-1.5
-2.0
LOG I/ISKY
0.4
0.6
0.8
1.0
1.2
1.4
1.6
1.8
2.0
LOG RADIUS (ARCSEC)

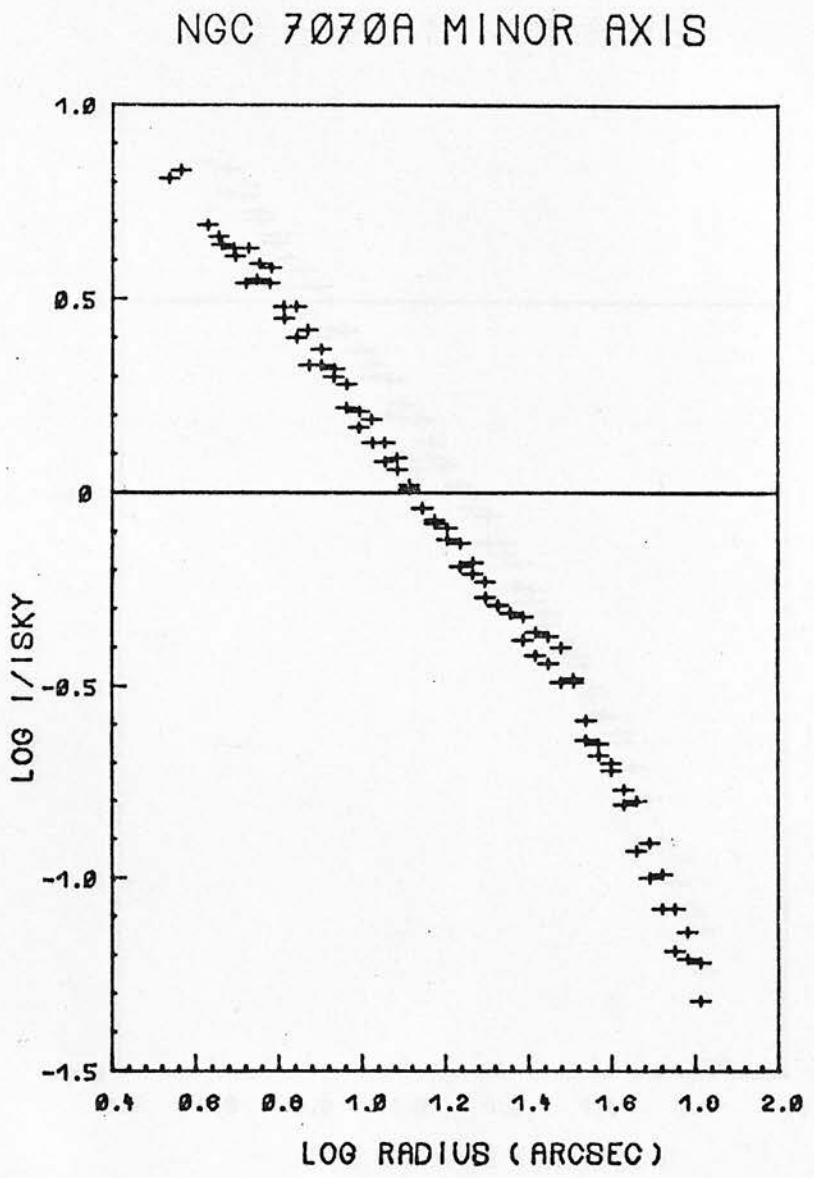
NGC 7070A MINOR AXIS
1.0
0.5
0
-0.5
-1.0
-1.5
LOG I/ISKY
0.4
0.6
0.8
1.0
1.2
1.4
1.6
1.8
2.0
LOG RADIUS (ARCSEC)

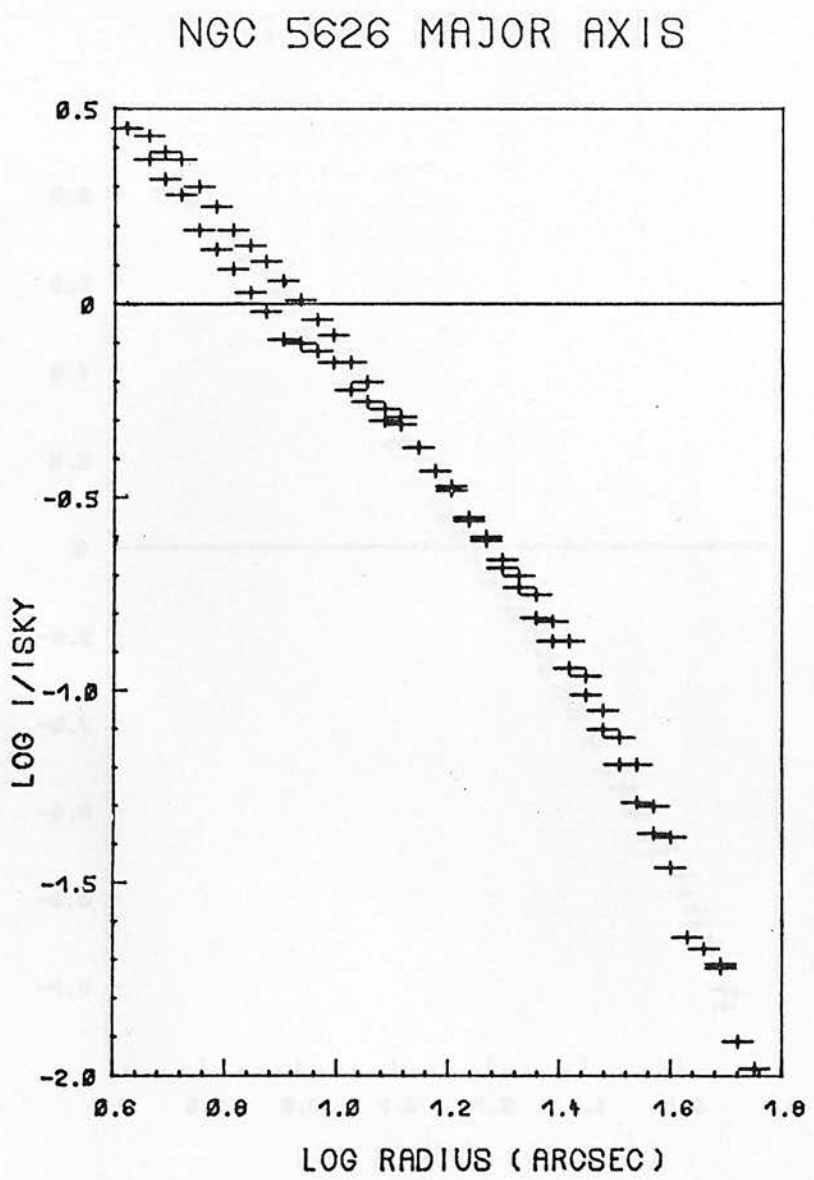
NGC 5626 MAJOR AXIS
0.5
0
-0.5
-1.0
-1.5
-2.0
LOG I/ISKY
0.6
0.8
1.0
1.2
1.4
1.6
1.8
LOG RADIUS (ARCSEC)

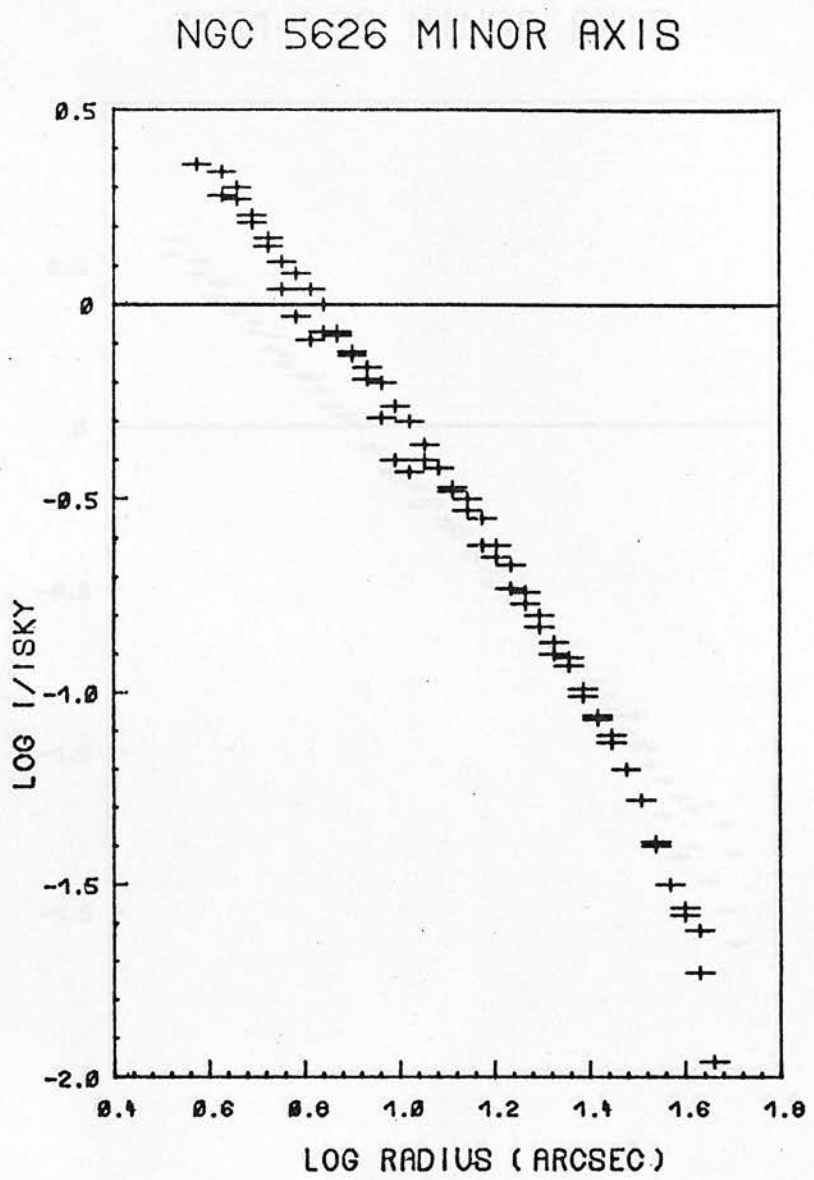
NGC 5626 MINOR AXIS
0.5
0
-0.5
-1.0
-1.5
-2.0
LOG I/ISKY
0.4
0.6
0.8
1.0
1.2
1.4
1.6
1.8
LOG RADIUS (ARCSEC)

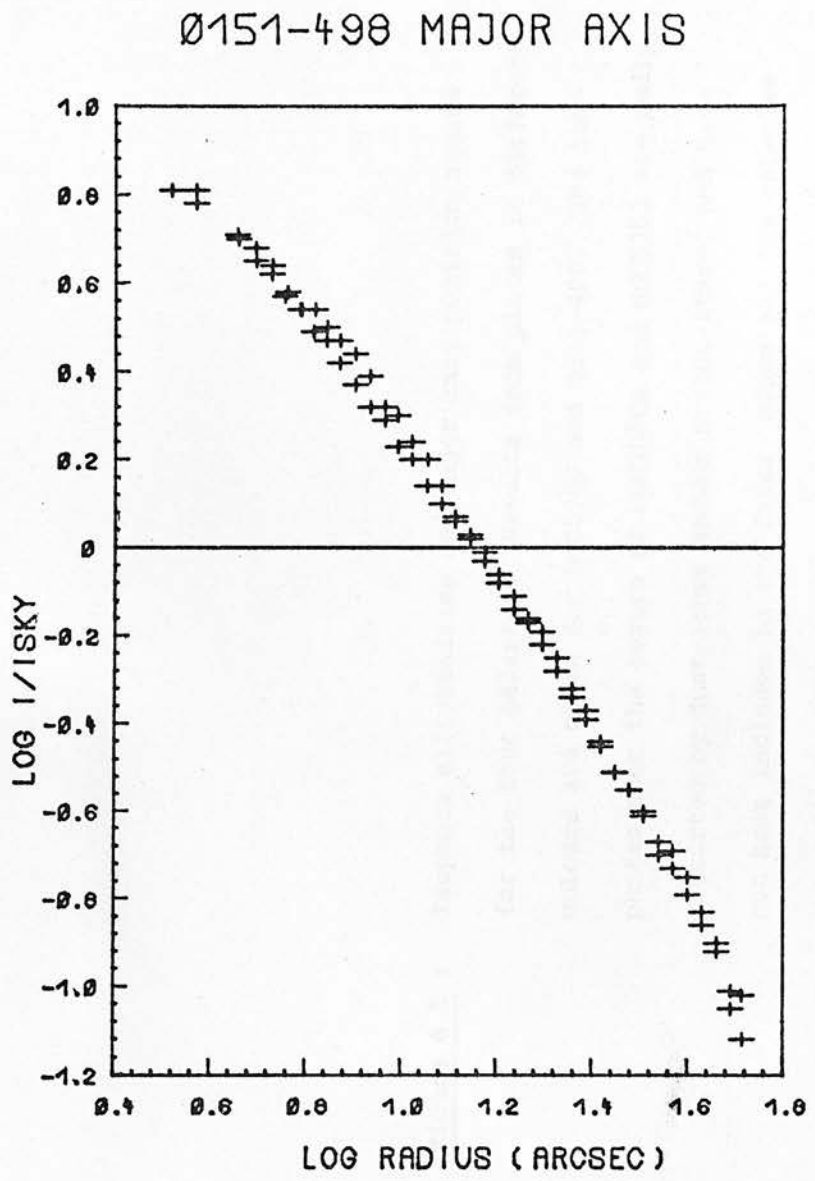
Ø151-498 MAJOR AXIS
LOG I/ISKY
LOG RADIUS (ARCSEC)
1.0
0.8
0.6
0.4
0.2
0
-0.2
-0.4
-0.6
-0.8
-1.0
-1.2
0.4
0.6
0.8
1.0
1.2
1.4
1.6
1.8

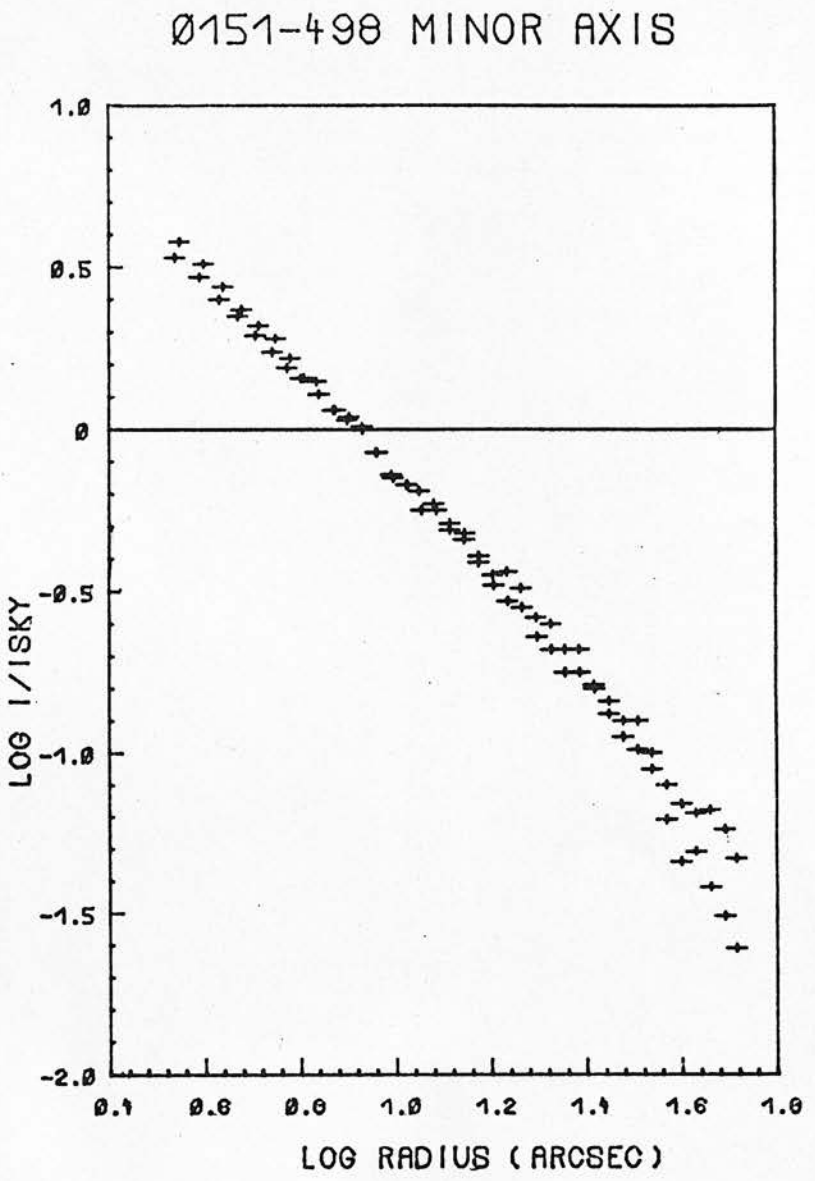
Ø151-498 MINOR AXIS
LOG I/ISKY
LOG RADIUS (ARCSEC)
1.0
0.5
0
-0.5
-1.0
-1.5
-2.0
0.4
0.6
0.8
1.0
1.2
1.4
1.6
1.8

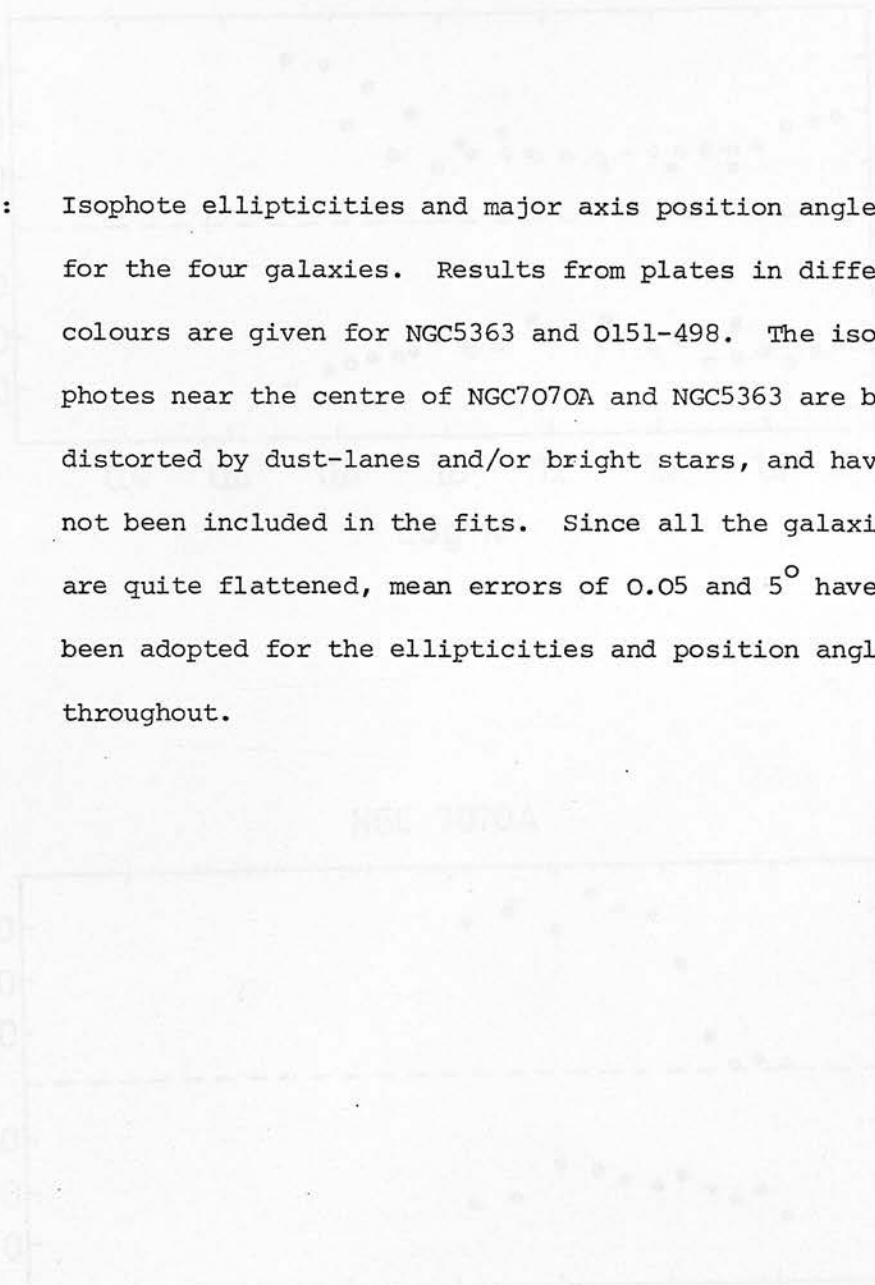

Figure 6.5 : Isophote ellipticities and major axis position angles for the four galaxies. Results from plates in different colours are given for NGC5363 and 0151-498. The isophotes near the centre of NGC7070A and NGC5363 are badly distorted by dust-lanes and/or bright stars, and have not been included in the fits. Since all the galaxies are quite flattened, mean errors of 0.05 and 5^{o} have been adopted for the ellipticities and position angles throughout.

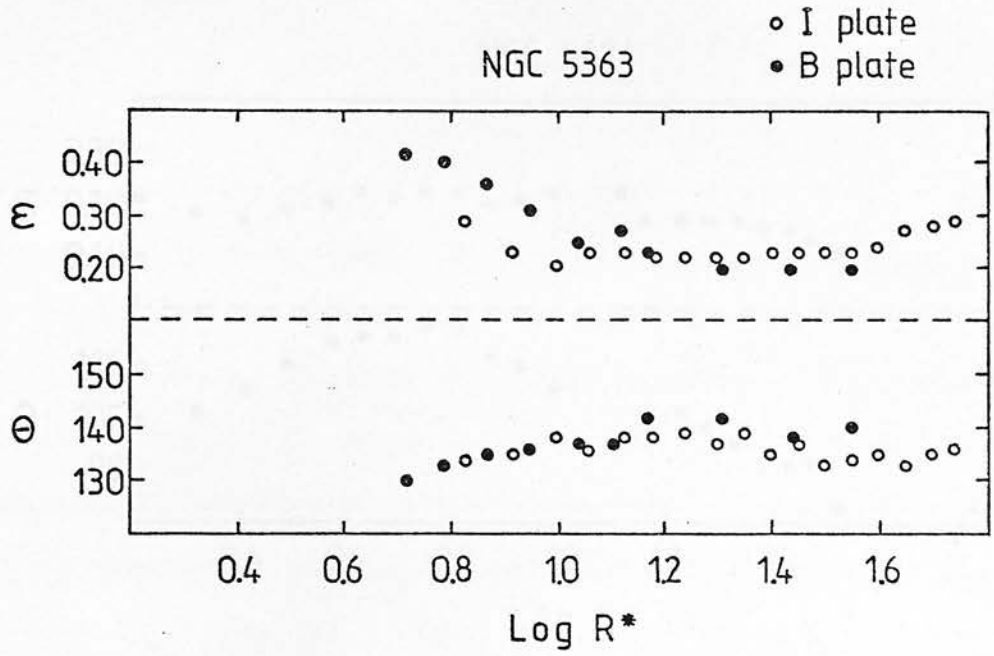
o I plate
• B plate
NGC 5363
ε
0.40
0.30
0.20
Θ
150
140
130
0.4
0.6
0.8
1.0
1.2
1.4
1.6
Log R*

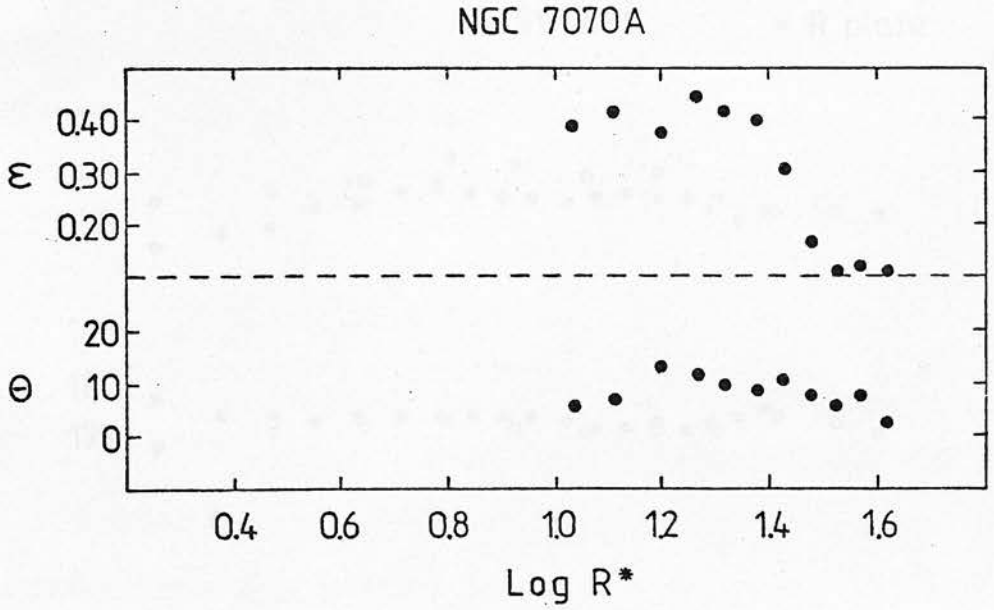
NGC 7070A
ε
0.40
0.30
0.20
Θ
20
10
0
0.4
0.6
0.8
1.0
1.2
1.4
1.6
Log R*

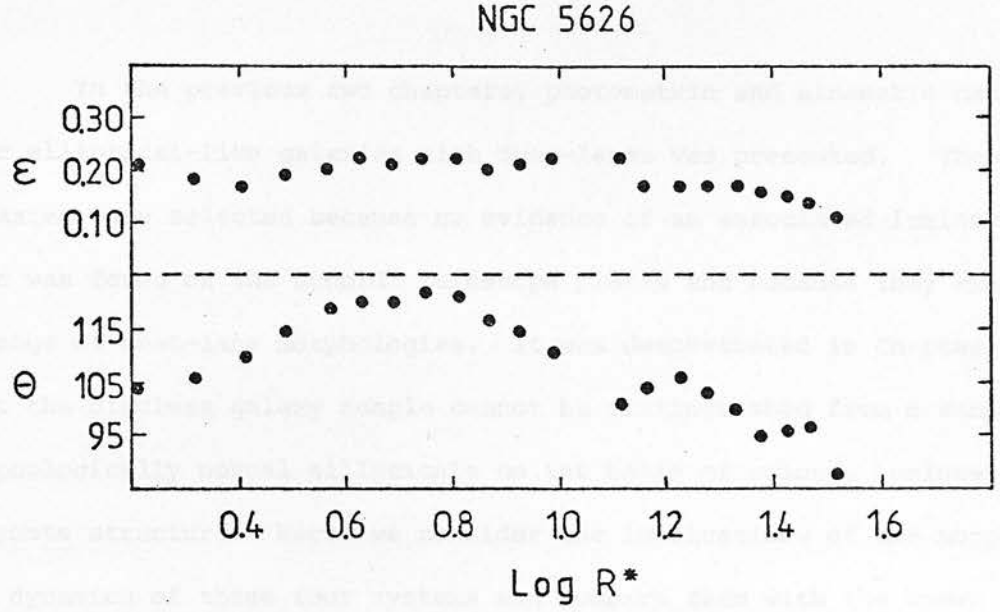
NGC 5626
0.30
ε 0.20
0.10
115
Θ 105
95
0.4
0.6
0.8
1.0
1.2
1.4
1.6
Log R*

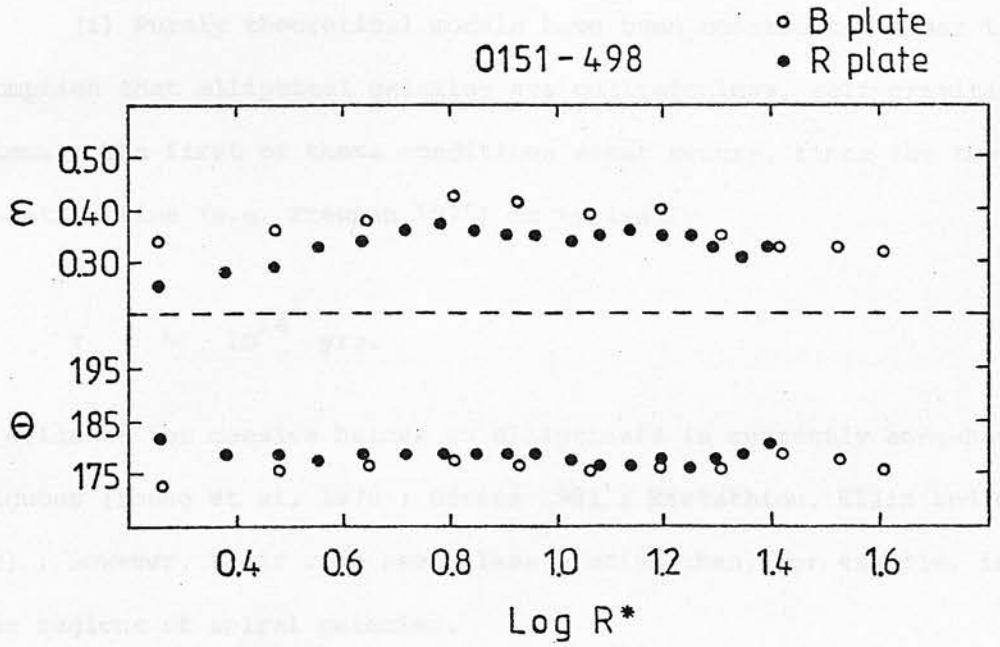
o B plate
• R plate
0151-498
0.50
ε 0.40
0.30
195
Θ 185
175
0.4
0.6
0.8
1.0
1.2
1.4
1.6
Log R*

CHAPTER 7

THE STRUCTURE AND DYNAMICS OF FOUR SELECTED GALAXIES

In the previous two chapters, photometric and kinematic data on four elliptical-like galaxies with dust-lanes was presented. These galaxies were selected because no evidence of an associated luminous disc was found on the Schmidt telescope plates and because they exhibit a range of dust-lane morphologies. It was demonstrated in Chapter 4, that the discless galaxy sample cannot be distinguished from a sample of morphologically normal ellipticals on the basis of colour, luminosity or isophote structure. Here, we consider the implications of the morphology and dynamics of these four systems and compare them with the known properties of normal galaxies.

Dynamical studies of elliptical galaxies have relied on two distinct approaches : analytical models and numerical simulations.

(i) Purely theoretical models have been constructed under the assumption that elliptical galaxies are collisionless, self-gravitating systems. The first of these conditions seems secure, since the two-body relaxation time (e.g. Freeman 1975) is typically

$$\tau \sim 10^{14} \text{ yrs.}$$

The evidence for massive haloes in ellipticals is currently somewhat ambiguous (Young et al, 1978 ; Davies 1981 ; Efstathiou, Ellis and Carter 1982) ; however, their role seems less crucial than, for example, in the outer regions of spiral galaxies.

The most direct approach to the dynamical properties of stellar systems is via the distribution function $f(\underline{x},\underline{v})$, which specifies the mass density of stars at the point $(\underline{x},\underline{v})$ in phase space. By choosing a form of the distribution function which satisfies both the steady-state collisionless Boltzmann equation :

$$\underline{v} \cdot \frac{\partial f}{\partial x} - \frac{\partial \phi}{\partial \underline{x}} \cdot \frac{\partial f}{\partial \underline{v}} = 0 \qquad (7.1)$$

and the Poisson equation :

$$\frac{\partial^2 \phi}{\partial x^2} = - 4 \pi G \rho(\underline{x}) \qquad (7.2)$$

where $\rho(\underline{x}) = \int f(\underline{x},\underline{v}) \, d^3(\underline{v})$, one may construct a self-consistent dynamical model (e.g. Michie 1963, Wilson 1975 ; Lake 1981a). The disadvantage of this method has always been the difficulty of choosing an appropriate form for $f(\underline{x},\underline{v})$, which can generate realistic density profiles and rotation curves (Wilson 1975, Lake 1981b). Furthermore, with increasing evidence for the existence of third integrals in axisymmetric systems, one must question whether the distribution function in real galaxies can necessarily be expressed in closed form.

In the absence of a detailed knowledge of the distribution function one may also proceed using the first moments of the Boltsmann equation - the so-called equations of stellar hydrodynamics. Under certain assumptions about the form of the velocity ellipsoids and the symmetries of the potential, these equations may be solved for the velocity and velocity dispersion fields in a model galaxy whose mass distribution is matched to surface photometry. At present these models have only been applied to a restricted class of oblate spheroidal systems (Satoh 1980 ; Binney 1980a ; Efstathiou,

Ellis and Carter 1982).

(ii) An alternative approach to stellar dynamics is through the use of N-body simulations (Miller and Smith 1979 ; Hohl and Zang 1979 ; Schwarzschild 1979 ; Wilkinson and James 1982). The numerical methods have the advantage that stability of the models can also be followed over periods of the order of a Hubble time. However, practical difficulties in modelling large systems remain a substantial problem. In particular, no N-body simulations have adequately reproduced the density contrasts found in real galaxies. It is also unclear to what extent the evolution found in some N-body calculations is governed by small number effects.

A considerable amount of accurate photometric and kinematic data has now been accumulated on elliptical galaxies. These improvements on the observational side have so far not been complemented, however, by a comparable theoretical effort, and no self-consistent picture of elliptical galaxies has yet emerged. Because of the inadequacies of the available models, it is doubtful whether much progress can be made by using detailed fits to the data presented in Chapters 5 and 6. Instead, we take a phenomenological approach and use the observed properties to infer the most important physical processes which characterize these four galaxies and the morphologically normal systems studied by previous workers.

7.1 GLOBAL PROPERTIES

Previous studies of the kinematics of elliptical and lenticular galaxies have shown the importance of linking this information to the photometric properties. In this section we investigate three of the most extensively used approaches.

7.1.1 Mass-to-Light (M/L) Ratios

The masses of early-type galaxies (and hence their M/L ratios) can only be derived in a model-dependent way. Core M/L ratios, based on King's (1966) lowered isothermal sphere models, require high spatial

resolution photometry to avoid being dominated by the effects of atmospheric seeing (Schechter 1980 ; Davies 1981). At the distances of 0151-498 and NGC5626, the method becomes impractical.

Poveda's (1958) method, although widely applied (e.g. Faber and Gallagher 1979 ; Tonry and Davis 1981a), is not based upon a self-consistent dynamical model. In particular, the assumed flat velocity dispersion profile is not compatible with an $r^{1/4}$ projected mass distribution ; this leads to an overestimate of the mass by a factor ~ 2. Binney (1980b) and Bailey and MacDonald (1981) have used the equations of stellar hydrodynamics to derive a relation between the central velocity dispersion and the total mass for a spherically symmetric model with an $r^{1/4}$ law of surface brightness. Further generalizations to rotationally flattened models (Michard 1980 ; Petrou 1981) introduce only second order changes in the final M/L values and require uncertain assumptions to be made about the intrinsic geometry, inclination etc. We have therefore computed M/L ratios for each of the four galaxies from the formula (c.f. Bailey and MacDonald 1981) :

$$\left(M/L\right)_T = 1.1\ 10^6 \ \frac{R_e^* \text{ (kpc)} \ \sigma_o^2 \text{ (kms}^{-1}\text{)}}{L(L_\odot)} \ \frac{M_\odot}{L_\odot} \qquad (7.3)$$

where R_e^* is the equivalent radius of the isophote containing half the light and σ_o is the central velocity dispersion. Two of the four galaxies show rapid rotation, so σ_o should be corrected for the fraction of the total energy in non-random motions. A simple estimate of the ratio of rotational kinetic energy (T_{rot}) to random kinetic energy (T_{ran}) is :

$$T_{rot}/T_{ran} = \frac{1}{3}\left(\frac{V_m}{\sigma_o}\right)^2 \qquad (7.4)$$

where V_m is the peak rotation velocity.

We may then define a corrected velocity dispersion :

$$\hat{\sigma}_o = \sigma_o \left\{ 1 + T_{rot}/T_{ran} \right\}^{\frac{1}{2}} \qquad (7.5)$$

The adopted values for these parameters and the final M/L ratios are given in Table 7.1.

Tonry and Davis (1981a) have measured central velocity dispersions for a total of 160 elliptical galaxies. Using equation 7.3 we find $\langle M/L \rangle = 7\ hM_\odot/L_\odot$ for this sample ($h = H_o/50$), with a dispersion of 0.25 in log (M/L). Three of the galaxies in Table 7.1 have M/L ratios close to this mean value, whilst the fourth (NGC7070A) lies near the lower end of the distribution. Isotropic velocity dispersions have been implicitly assumed in the above discussion, since the derived masses of spherical systems are relatively insensitive to radial anisotropy (Binney 1980b ; Efstathiou, Ellis and Carter 1980).

TABLE 7.1 : Global parameters for the four galaxies

Galaxy	V_o (kms^{-1})	D (Mpc)	B_T^o	R_e^* (")	L ($h^{-2}10^{10}L_\odot$)	σ_o kms^{-1}	Mg_2	M/L ($hM_\odot/L_\odot$)	V_m kms^{-1}
NGC5363	1125	22.4[1]	10.97	25	3.20	215[3]	0.32	5	135
NGC7070A	2392	47.7	13.06	26	2.11	99	0.22	3	<30
NGC5626	6845	134.0	13.67[2]	12	9.51	255[4]	0.28	7	145
0151-498	6170	120.8	13.38	15	10.1	257	0.27	6	50

Notes:

1. Group velocity 1164 kms^{-1} from Haynes (1981).
2. $\pm\ 0^m.3$
3. $\hat{\sigma}_o = 229\ kms^{-1}$
4. $\hat{\sigma}_o = 270\ kms^{-1}$

However, truly round galaxies are likely to be comparatively rare (Sandage, Freeman and Stokes 1970 ; Binney and de Vaucouleurs 1981) and spectroscopic observations indicate that pressure anisotropy must play a dominant role in determining the shapes of flattened galaxies. For a typical oblate E4 galaxy, the fractional excess pressure in the plane of the galaxy over that along the symmetry axis is (see Fig 1 of Binney 1980c):

$$\delta = 1 - \pi_{zz}/\pi_{xx} \sim 0.3 \qquad (7.6)$$

i.e. $\sigma_{z}/\sigma_{x} \sim 0.84$

The error in using $\sigma_o = \sigma_z$ in equation 7.3 would then be $\sim$ 20%. This effect could in principal account for the low velocity dispersion in NGC7070A if the galaxy were a very flattened system observed almost face-on.

7.1.2 $L \propto \sigma^4$ Relation

A number of previous studies (e.g. Faber and Jackson 1976 ; Whitmore et al 1979 ;Schechter and Gunn 1979) have examined the correlation between luminosity (L) and central velocity dispersion (σ_o) in early-type galaxies. A weaker correlation was also known to exist between luminosity and the strengths of certain absorption features (Faber 1977 and references therein). Terlevich et al (1981) have studied both these relations for a carefully chosen sample of ellipticals, and found that the residuals of individual galaxies about the two regression lines are strongly correlated. A corrected velocity dispersion can therefore be calculated for which the scatter in the L-σ diagram is substantially reduced.

The Mg_2 index as defined by Faber, Burstein and Dressler (1977) and Mould (1978), was determined for each galaxy using flux-calibrated

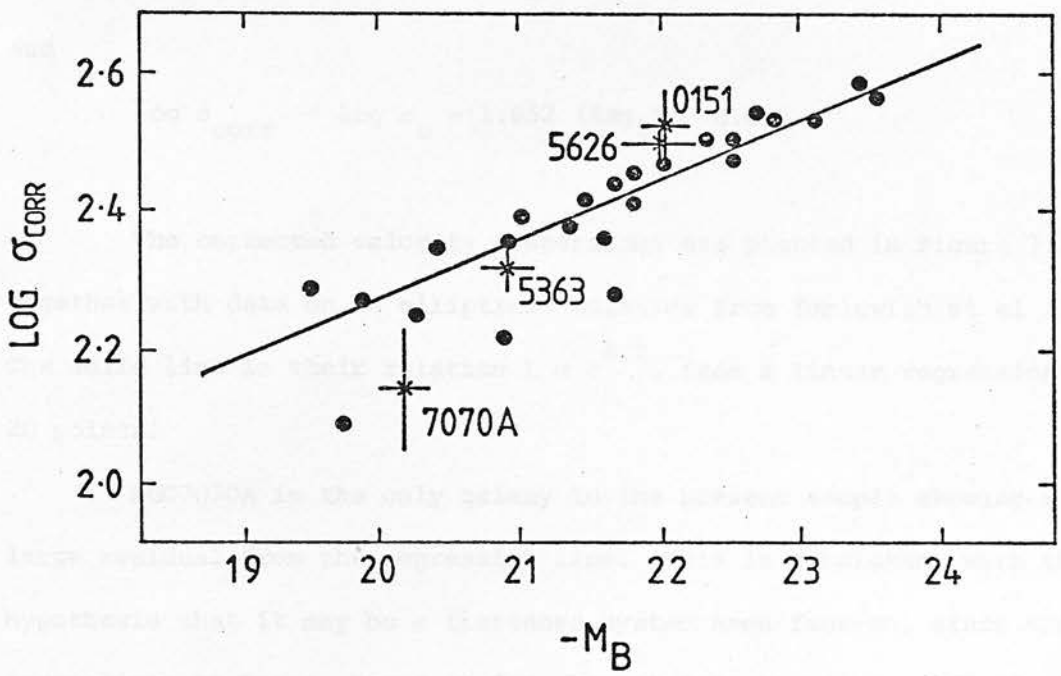

Figure 7.1 : Central velocity dispersion versus absolute magnitude. Crosses are dust-lane galaxies ; filled circles are ellipticals from Terlevich et al (1981). Metallicity corrections advocated by Terlevich et al have also been applied to the four new points, which have total absolute magnitudes corrected for absorption following the precepts of de Vaucouleurs et al (1976). NGC1172 is the point at $M_B = -19.74$, $\log \sigma_o = 2.094$.

spectra of the nuclear regions only, and is listed in Table 7.1. Following Terlevich et al (1981) we then define :

$$\delta Mg_2 = Mg_2 - 0.0130\ (-M_B) - 0.039 \qquad (7.7)$$

and

$$\log \sigma_{corr} = \log \sigma_o - 1.852\ (\delta Mg_2) - 0.015 \qquad (7.8)$$

The corrected velocity dispersions are plotted in Figure 7.1, together with data on 24 elliptical galaxies from Terlevich et al (1981). The solid line is their relation $L \alpha \sigma^{4.2}$, from a linear regression on 20 points.

NGC7070A is the only galaxy in the present sample showing a large residual from the regression line. This is consistent with the hypothesis that it may be a flattened system seen face-on, since the corrections to log σ based on δMg_2 cannot take anisotropy effects into account. A similar explanation has been put forward by Terlevich et al (1981) for NGC1172, which lies close to NGC7070A in Fig 7.1. However, Tonry (1981) has suggested that the mean relation for all galaxies in fact becomes steeper at low luminosities.

7.1.3 $V_{m/\sigma}$ vs. ε Diagram

It is convenient to discuss the rotation of early-type galaxies in terms of the ratio $V_{m/\sigma}$ of the maximum line-of-sight rotation velocity to the mean velocity dispersion. Binney (1978) has used the tensor virial theorem (Chandrasekhar 1964) to derive a relationship between $V_{m/\sigma}$ and ellipticity for oblate and prolate spheroidal models. Since the tensor virial theorem describes the global properties of a galaxy, we have used a mean luminosity-weighted velocity dispersion to locate the positions of the four dust-lane galaxies in Figure 7.2 (in practice, the dispersion profiles of three of the galaxies are flat and only

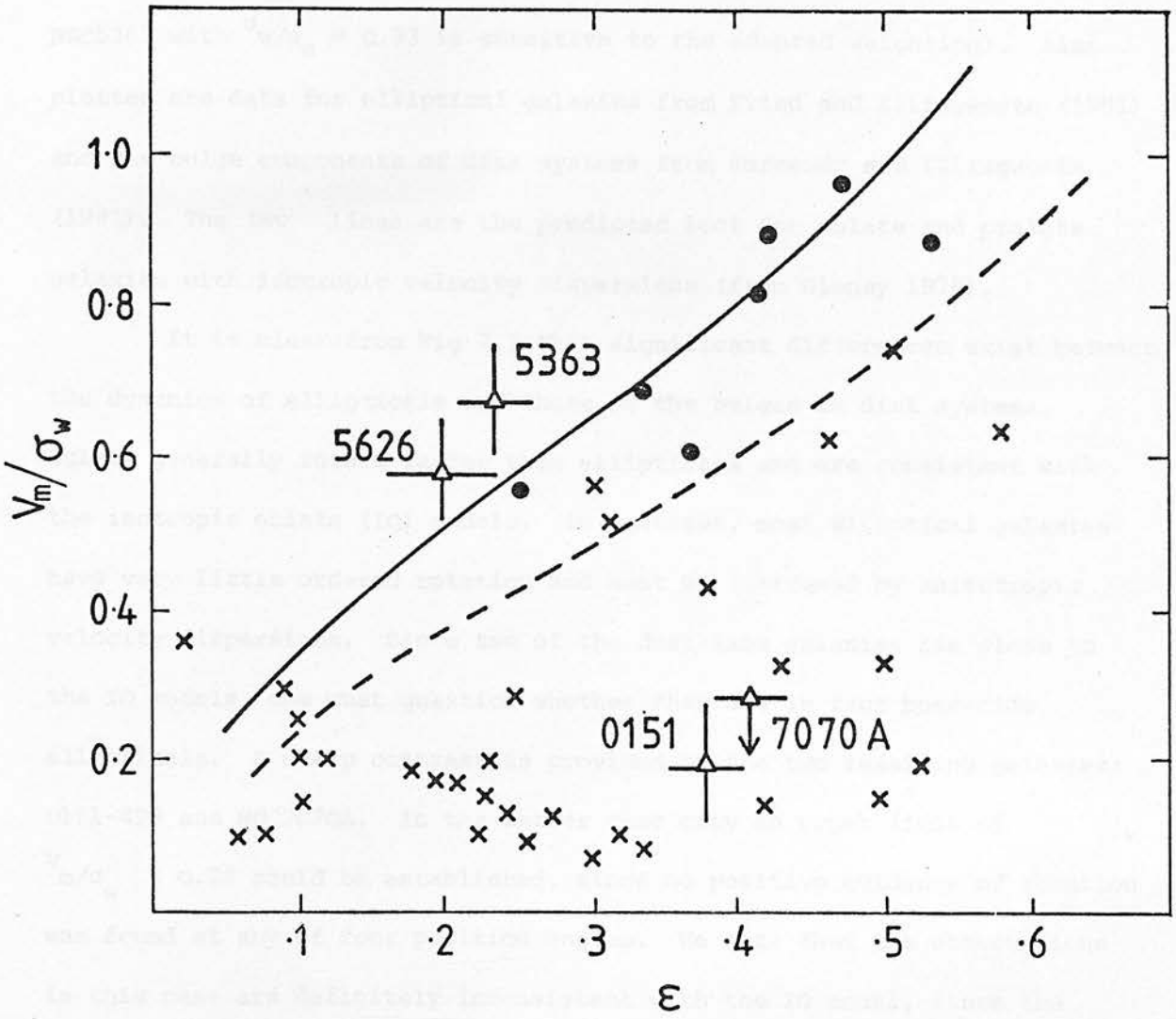

Figure 7.2 : The V_{max}/σ_w versus ellipticity diagram. Symbols used are as follows : triangles, dust-lane galaxies from this work ; filled circles, spiral bulges from Kormendy and Illingworth (1981) ; crosses, ellipticals from Illingworth (1981). The solid line is the locus of isotropic oblate models from Binney (1978). The dashed line is a prolate isotropic model (Binney 1978) viewed broadside-on from the plane of figure rotation. Although the predictions of the oblate models are largely insensitive to the orientation, this is not true in the prolate case.

NGC5363 with $^{\sigma}w/\sigma_o$ = 0.93 is sensitive to the adopted weighting). Also plotted are data for elliptical galaxies from Fried and Illingworth (1981) and the bulge components of disk systems from Kormendy and Illingworth (1981). The two lines are the predicted loci for oblate and prolate galaxies with isotropic velocity dispersions (from Binney 1978).

It is clear from Fig 7.2 that significant differences exist between the dynamics of ellipticals and those of the bulges in disk systems. Bulges generally rotate faster than ellipticals and are consistent with the isotropic oblate (IO) models. In contrast, most elliptical galaxies have very little ordered rotation and must be flattened by anisotropic velocity dispersions. Since two of the dust-lane galaxies lie close to the IO models, one must question whether they are in fact bone-fide ellipticals. A sharp contrast is provided by the two remaining galaxies: 0151-498 and NGC7070A. In the latter case only an upper limit of $V_{m/\sigma_w} < 0.28$ could be established, since no positive evidence of rotation was found at any of four position angles. We note that the observations in this case are definitely inconsistent with the IO model, since the effect of changing the inclination is to move the models parallel to the predicted locus.

7.2 DUST-LANE KINEMATICS

The spectroscopic configuration described in § 5.2 was optimized for the study of absorption-line kinematics. Efforts were also made, however, to include the emission lines of Hβ and [OIII]λλ5007, 4959 in the data window, in order to study the kinematics of the gaseous components in the four galaxies. Our principal aim in this respect was to investigate the rotation properties of the well-defined dust-lanes in NGC5363, NGC7070A and 0151-498. No prominent emission-line regions were found in NGC5626.

The spectra taken along the dust-lanes of these three galaxies revealed weak emission lines in each case. Generally only the [OIII]λ5007

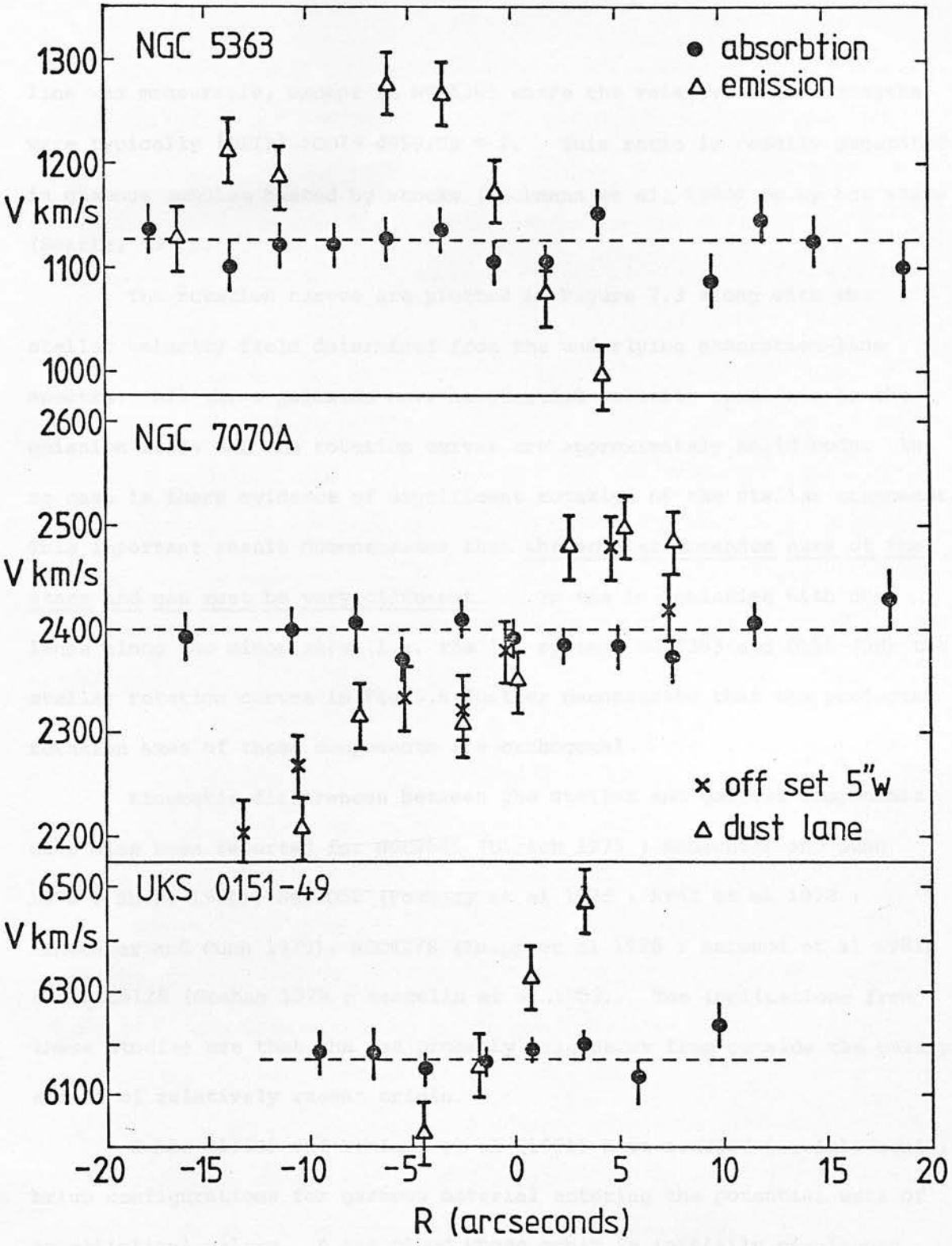

Figure 7.3 : The kinematics of the dust-lanes in NGC5363 (inner dust-lane), NGC7070A and 0151-498. In each case triangles are the emission line velocities and filled circles the absorption line velocities. The gas motions along the spectrum offset 5" W in NGC7070A are also plotted.

line was measurable, except in NGC5363 where the relative line strengths were typically [OIII] 5007 + 4959/Hβ ∿ 2. This ratio is readily generated in gaseous nebulae heated by shocks (Heckmann et al, 1980) or by hot stars (Searle, 1971).

The rotation curves are plotted in Figure 7.3 along with the stellar velocity field determined from the underlying absorption-line spectra. All three galaxies have substantial velocity gradients in the emission lines and the rotation curves are approximately solid body. In no case is there evidence of significant rotation of the stellar component. This important result demonstrates that the angular momentum axes of the stars and gas must be very different. In the two galaxies with dust lanes along the minor axis (i.e. the 'P' systems NGC5363 and 0151-498) the stellar rotation curves in Fig 5.6 further demonstrate that the projected rotation axes of these components are orthogonal.

Kinematic differences between the stellar and gaseous components have also been reported for NGC2685 (Ulrich 1975 ; Schechter and Gunn 1978 ; Shane 1980), NGC1052 (Fosbury et al 1978 ; Reif et al 1978 ; Schechter and Gunn 1979), NGC4278 (Knapp et al 1978 ; Raimond et al 1981) and NGC5128 (Graham 1979 ; Marcelin et al 1982). The implications from these studies are that the gas probably originates from outside the galaxy and is of relatively recent origin.

Tubbs (1980) and Tohline et al (1981) have studied possible equilibrium configurations for gaseous material entering the potential well of an elliptical galaxy. A gas cloud whose orbit is initially misaligned with the symmetry axis of the mass distribution, experiences a gravitational torque which causes the orbit to precess about the symmetry axis (Kahn & Woltjer 1959). Dissipative cloud-cloud collisions then work to destroy the component of angular momentum perpendicular to the symmetry axis, and

the clouds settle into a preferred plane of the galaxy on a timescale of typically 10^8-10^9 yrs (Tubbs 1980). This preferred plane depends only on the gross geometric shape of the galaxy : if the mass distribution is intrinsically prolate the angular momentum vector aligns with the longest axis, if the galaxy is oblate it will align with the shortest axis (Tohline et al 1981).

Our observations of NGC5363 and 0151-498 demonstrate that the projected rotation axis of the dust-lane is aligned with the major axis of the light distribution. This implies that the intrinsic geometry of the central regions of these galaxies is generically prolate. NGC7070A is less readily understood ; the chaotic appearance of the dust lane in Fig 5.1 suggests that in this case the dust lane may not yet have reached equilibrium.

7.3 NGC 5363

This galaxy is the brightest object in our sample, with B_T = 11.2 (RC2). It has been variously classified by previous workers as E_{pec} (Kormendy & Bachall 1974), SO (Krienke & Hodge 1974) & IO (Holmberg 1958 ; RC2), and is in a small group whose brightest members include NGC5338(SO), NGC5348(Sb), NGC5356(Sb), NGC5360(IO) and NGC5364 (Sb/c). The latter is a fine spiral at a projected distance of 14 arcminutes from NGC5363.

The rotation curves display a wide variety of structure not seen in the remaining galaxies. NGC5363 rotates rapidly along the major axis (Figs 5.5 and 5.6) reaching a maximum rotation velocity of 135 $\pm$ 10 kms^{-1} at a radius of 20 arcsec. There is a pronounced inflection in the rotation curve at r $\sim$ 40 arcsec, beyond which the velocities continue to rise. The measured angular velocity in the centre is 35 $\pm$ 5 kms^{-1} $arcsec^{-1}$ although it is probable that observations with higher spatial resolution would give an even larger value. NO evidence of substantial minor axis rotation is found in the present data.

The velocity dispersion profiles are unusual because of the rapid decrease in σ with increasing radius on the major axis. Between r = 0 and r = 25" this amounts to a drop of 40%, which may be compared with the decrease of 25% expected for a spherically symmetric $r^{1/4}$ mass distribution (Bailey and MacDonald 1981). Along the minor axis the gradient is much less marked over a similar range in distance. This behaviour would be expected of a thin inclined disc in which the radial component of velocity dispersion is higher than the tangential component (Kormendy 1981b), but the form of the velocity dispersion profile in a less-flattened anisotropic stellar system is difficult to predict a priori because of projection effects. A luminosity-weighted mean velocity dispersion has been derived using all the available observations with weights estimated from the IPCS counts : $\sigma_w = 199 \pm 15$ kms^{-1}. The ratio of maximum rotational velocity to mean dispersion $V_m/\sigma_w = 0.67 \pm 0.10$ places NGC5363 slightly above the predictions of the rotationally flattened oblate models (Fig 7.2). Kormendy (1981a) has shown that this property is characteristic of the triaxial bulge components in a sample of barred lenticular galaxies. Since the orientation of the nuclear dust-lane along the minor axis favours a prolate geometry for these regions (c.f. § 7.2), we compare the observed kinematics with some generically prolate models.

Lake (1981 a,b) constructed both analytical and numerical prolate models whose elongated shape came from suppressing the angular momentum about the symmetry axis. Because only classical integrals of motion were included in the distribution function, these models do not have any rotation along the major axis. Schwarzschild (1979) used linear programming techniques to build a self-consistent triaxial model from individual stellar orbits. The equidensity surfaces have axial ratios 2:1.25:1, so this model is in fact quite close to being prolate. However, all the

angular momentum is contained in tube orbits around the long axis, and the predicted minor axis rotation velocity is $V_m \sim 1.84\ \sigma_o \sim 125$ kms^{-1} using $\sigma_o = 215$ kms^{-1} for NGC5363. Clearly neither of these two models are representative of the results in Fig 5.6.

Miller and Smith (1979) consider the equilibrium configuration of a prolate stellar bar of intrinsic ellipticity $\varepsilon \sim 0.6$ tumbling about one of the short axes. The velocity and velocity dispersion fields and major axis rotation curve of this model are qualitatively similar to those of the inner regions of NGC5363. In particular, there are prograde streaming motions in the rotating frame of the bar, so the major axis rotation curve is non-linear and very much steeper than would be inferred from the pattern speed of the bar. The velocity dispersions are also highly anisotropic in the outer regions, leading to a rapid fall in the projected dispersion profile. There are two important differences between the model and our observations. First, the major axis velocity gradient in Fig 5.5 is considerably steeper than their model seen at any projection. Second, our offset slit position indicates a significant departure from the cylindrical velocity field exhibited by the model. The rapid rotation of the Miller-Smith bar ($V_m/\sigma_o \sim 1.67$) makes a detailed comparison difficult. Further N-body simulations to investigate the effects of introducing large density contrasts, similar to those found in the centres of real galaxies, would be very desirable.

We now consider some of the additional consequences of adopting a tumbling prolate model for the inner regions of NGC5363. Tohline and Durisen (1982) predict that there will be two preferred planes for gas flowing in such a potential. If the orbital period of the gas clouds is very much less than the tumble period of the bar (i.e. near the centre), the gas will effectively see a stationary prolate gravitational field and

will settle near to the equatorial plane. At large radii the gas clouds will be governed by a time-averaged field, which will therefore be oblate, and the gas clouds will settle into the 'inertial plane' in which the bar rotates. Van Albada et al (1982) and Heisler et al (1982) have made detailed studies of the stable orbits near the minor axis of a rotating bar-like potential. The Coriolis force causes these orbits to be tilted with respect to the equatorial plane ; for small angles this tilt is given by :

$$\tan\Theta \approx \left(\frac{\Omega}{\omega}\right)\left\{\frac{2}{1+(k/\omega)^2+(\Omega/\omega)^2}\right\} \qquad (7.9)$$

where Ω is the angular velocity with which the form of the galaxy rotates (i.e. the 'pattern speed'), ω is the angular velocity of the orbiting particles, and k is the gravitational 'spring constant' perpendicular to the equatorial plane. The tilt of the dust-lane with respect to the minor axis of NGC5363 can therefore be used to place constraints on the allowed pattern speeds.

We derive the spring constant 'k' using a mass model appropriate to a prolate galaxy obeying an $r^{1/4}$ law of surface brightness (Tubbs 1980). The density distribution of this model is given by

$$\rho(a) = \rho_o \left(\frac{\pi}{245.4}\right)^{\frac{1}{2}} \left(\frac{a}{a_c}\right)^{-7/8} \exp\left[-7.669\left(\frac{a}{a_e}\right)^{-1/4}\right] \qquad (7.10)$$

where a_e is the effective semi-minor axis, and

$$a^2 = r^2 + A^2 z^2 \qquad (7.11)$$

in a cylindrical co-ordinate system in which the z-axis is the axis of symmetry. The true axial ratio A is given in terms of the observed

(projected) value A_o by

$$A = \left[1 - (1 - A_o^{-2}) \sec^2 \zeta \right]^{-\frac{1}{2}} \qquad (7.12)$$

where ζ is the angle between the z-axis and the plane of the sky. Figure 7.4 shows that when this model is projected onto the sky it provides a good fit to the surface brightness distribution of NGC5363 with $a_e = 23"$. The ratio of z-oscillation period to rotation period for a gas cloud in circular orbit around the major axis is (Tubbs 1980) :

$$\frac{T_z}{T_{rot}} = \left\{ \frac{\int_o^r \rho(a) \left[1 + \left(\frac{a\varepsilon}{r} \right)^2 \right]^{-\frac{1}{2}} a^2 \, da}{\int_o^r \rho(a) \left[1 + \left(\frac{a\varepsilon}{r} \right)^2 \right]^{-3/2} a^2 \, da} \right\} \qquad (7.13)$$

where $A^2 = (1 + \varepsilon^2)^{-1}$. At the maximum radius of the dust-lane ($r \sim 5"$) we find

$$\frac{k}{\omega} = \frac{T_{rot}}{T_z} \sim 0.91 \qquad (7.14)$$

for $a_e = 23"$ and $A = 0.77$ (this value is very insensitive to the adopted values of A and r/a_e). Inspection of Fig 5.1 does not reveal any substantial tilt of the inner dust-lane with respect to the minor axis of NGC5363 ; we take $\Theta < 15^o$ as a conservative upper limit. The observed angular velocity in the dust lane (Fig 7.3) is $\omega = 39$ kms^{-1} arcsec^{-1}, so from equation 7.9: $\Omega < 0.9$ kms^{-1} arcsec^{-1}. At an adopted distance of D = 22.4 Mpc, the rotation period of the figure is therefore $\tau_f \sim 2.5\ 10^8$ yrs. This low value for the pattern speed is consistent with the lack of any pronounced features in the radial surface brightness profile of NGC5363, which might be expected to occur near principal resonances such corotation.

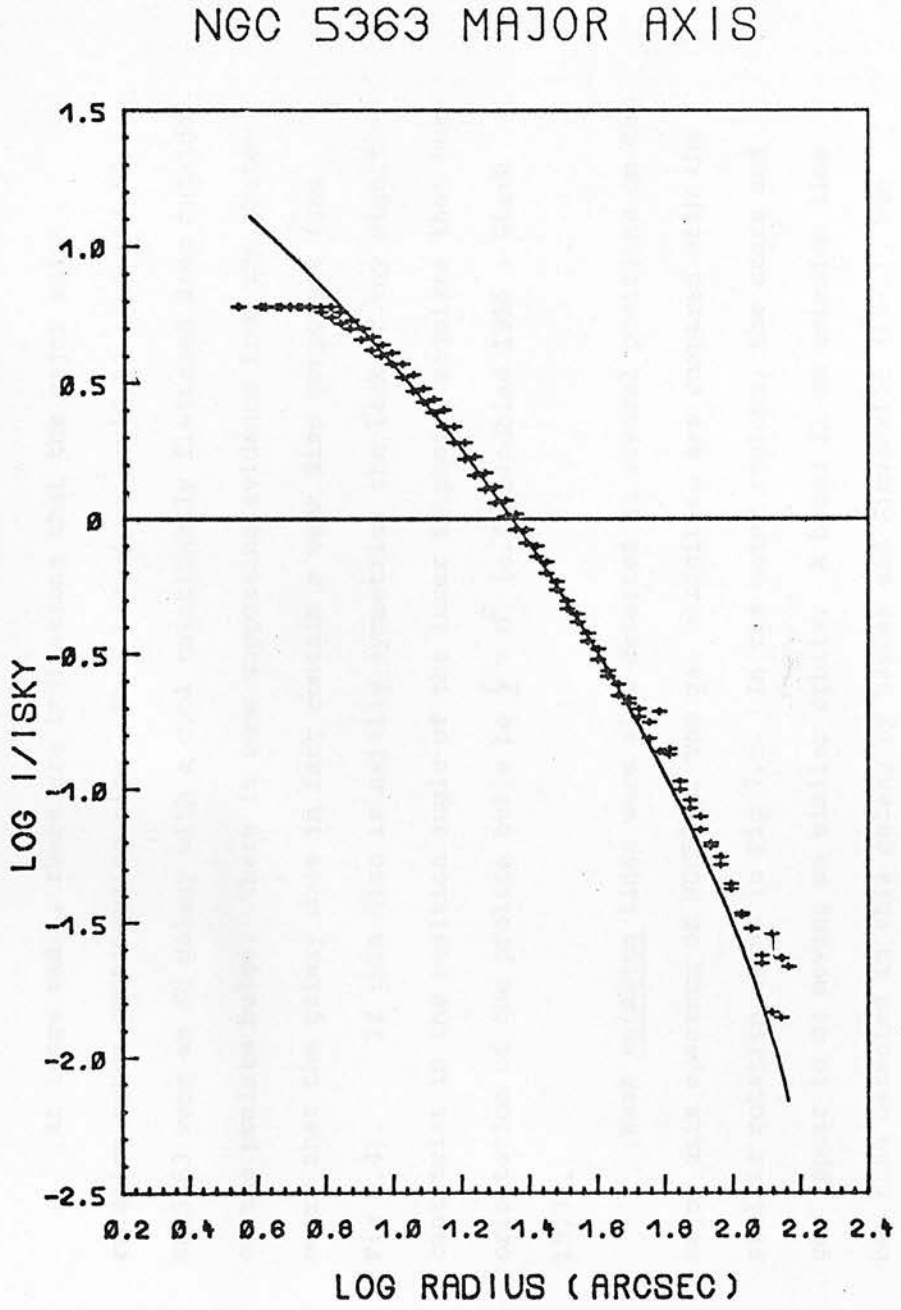

Figure 7.4 : The major axis luminosity profile of NGC5363 in the I band. Asymmetries due to diffuse dust absorption are minimised by using a red bandpass. The solid line is a numerical projection of the mass model from equation 7.10 onto the plane of the sky, and has been convolved with a Gaussian seeing profile of FWHM = 1.5 arcsec. At r < 8" the emulsion has become saturated and falls below the model predictions. At r > 45", there is a systematic excess of luminosity above that of the model ; since this corresponds closely with the position of the inflection in the major axis rotation curve in Fig 5.6, we identify this component with a rapidly rotating disc, contributing < 10% of the total light.

At large radii, there are indications that the major axis rotation curve continues to rise. This behaviour would be expected if NGC5363 were an SO galaxy with a cool rotationally flattened disc outside of the prolate bulge. There is some supporting evidence from the photometry that the galaxy does in fact contain a weak disc component (see Fig 7.4). If this disc is axially symmetric, the lack of any significant twist in the position angle of the inner isophotes requires that the orientation of the prolate bulge be $\zeta \sim 0^{\circ}$ (c.f. Lindblad 1956 ; Stark 1977).

Weak emission lines were also detected at several positions on the major axis spectrum of NGC5363. The gas velocities are compared with the stellar rotation curve in Fig 7.5. In the outer regions, the stars and gas appear to be moving on similar orbits. A broad 21 cm emission line has been detected in this galaxy by Haynes and Giovanelli (1981), who find a profile width of 605 kms^{-1} in a 3.9 arcmin beam, and a shape characteristic of the disc emission from early-type galaxies. Motions in the ionized gas near the centre of NGC5363 are chaotic, with line widths which appear somewhat greater than those in the outer regions. Our spectra do not constrain models of the ionization mechanism, however, so we cannot determine whether this is shock-heated gas similar to the turbulent, diffuse component in the elliptical body of NGC5128 (Phillips 1981). In one pixel, close to the nucleus of the galaxy, moderately strong Hβ emission is found. The Balmer-line emitting gas has a substantial positive velocity residual (100 ± 20 kms^{-1}) with respect to the systematic velocities defined by the [OIII] lines and the stellar velocity field. Haynes and Giovanelli (1981) found that the HI absorption in front of the compact radio source in the centre of this galaxy (Condon and Dressel 1978) is also asymmetrically distributed towards higher velocities. It is tempting to suggest that the HI absorption and Hβ emission-line regions are associated, and form a third

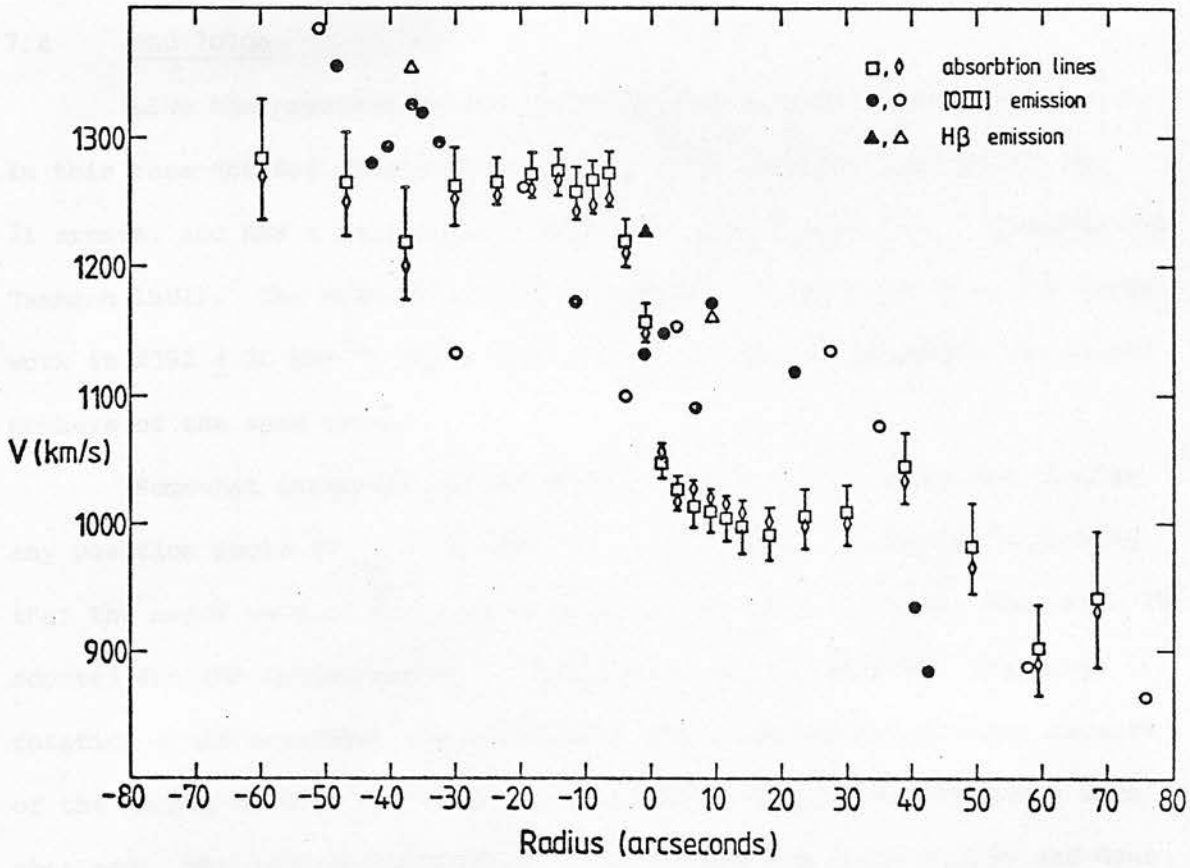

Figure 7.5 : The emission line regions on the major axis of NGC5363. Open squares and diamonds are the absorption line velocities from the cross-correlation and Fourier quotient methods respectively. Filled circles are [OIII] velocities, filled triangles are Hβ velocities. Open circles and triangles represent weak emission lines whose velocities are very uncertain. There is a difference between the Hβ and [OIII] velocities in the central pixel, probably because these two lines come from different regions.

gaseous component which is falling into the nucleus of NGC5363 (see also Thuan and Wadiak 1982).

7.4 NGC 7070A

Like the previous galaxy, NGC7070A has a bright spiral companion. In this case the Scd galaxy NGC7070 lies at an apparent separation of 21 arcmin, and has a heliocentric velocity of 2400 $\pm$ 50 kms^{-1} (Sandage and Tammann 1981). The mean heliocentric redshift of NGC7070A from the present work is 2392 $\pm$ 30 kms^{-1}, which indicates that the two galaxies are indeed members of the same group.

Somewhat surprisingly the stellar component shows no rotation at any position angle (V_{max} < 30 kms^{-1}). Our surface photometry indicates that the major axis of the isophotes is at PA = 8 $\pm$ 3° rather than PA = 29° adopted for the spectroscopy. It seems unlikely, however, that any rotation would have been observed along the isophotal major axis, because of the number of slit positions close to this at which observations were obtained. The velocity dispersion is also very low (c.f. § 7.2) and does not change with radius to within our observational errors (Fig 5.6). Taken together, the kinematic properties strongly favour the hypothesis that NGC7070A is a substantially flattened system seen almost face-on. Further support comes from the ellipticity profile (Fig 6.5) which shows that the galaxy becomes much less elongated at large radii. The inner regions have an apparent ellipticity of 0.4, so that their intrinsic geometry must then be triaxial or prolate.

Surface brightness profiles of NGC7070A (Fig 6.4) show a complicated structure. The major axis is dominated by the asymmetry of the dust lane, so the minor axis profile has been used to illustrate the interesting features of the overall light distribution. At r < 20" it can be well approximated by a de Vaucouleurs $r^{1/4}$ profile (Figure 7.6),

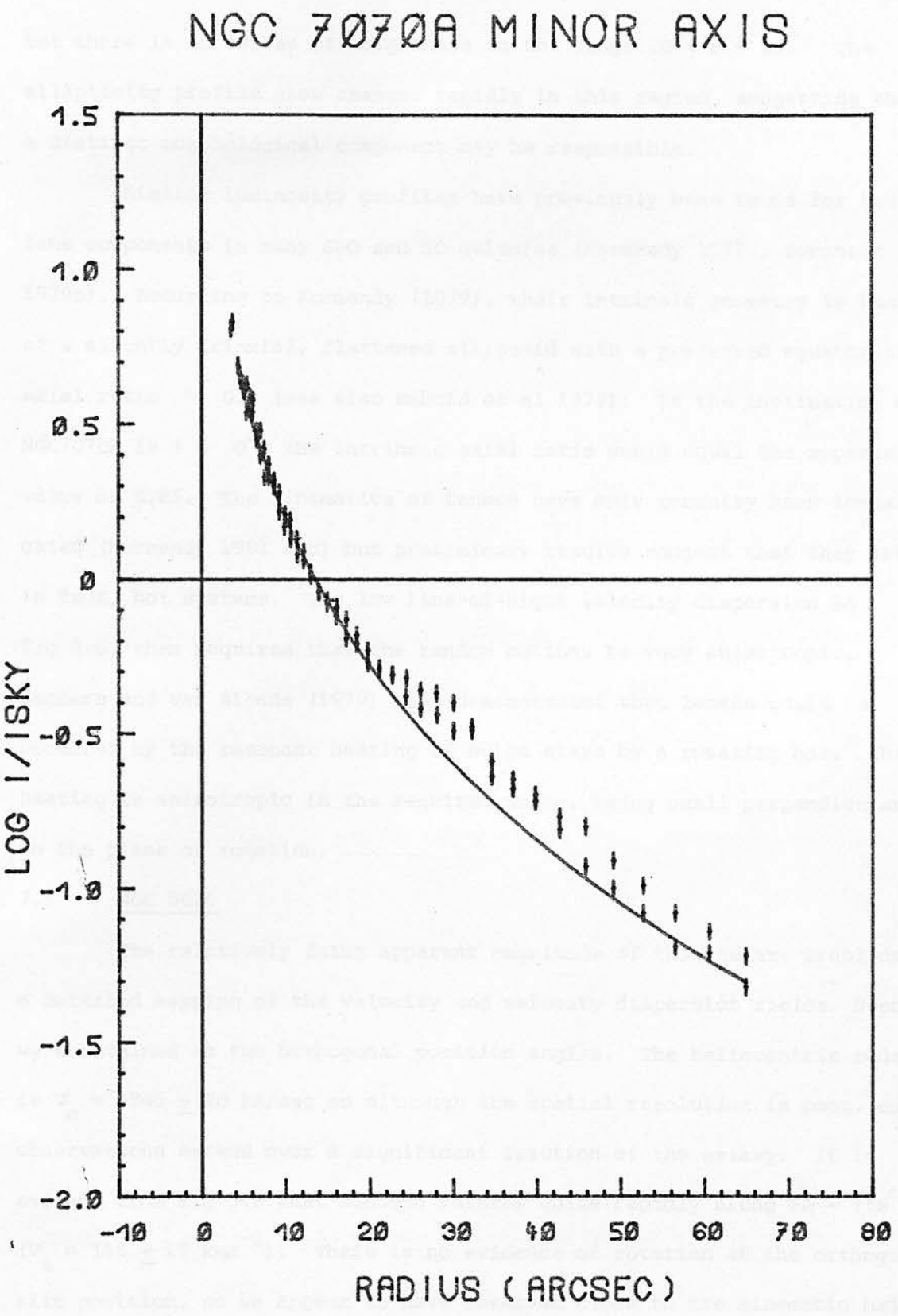

Figure 7.6 : Minor axis luminosity profile of NGC7070A. The solid line is a de Vaucouleurs $r^{1/4}$ profile with $r_e = 30.''5$ fitted to the inner regions.

but there is an excess of brightness in the range $20'' < r < 50''$. The ellipticity profile also changes rapidly in this region, suggesting that a distinct morphological component may be responsible.

Similar luminosity profiles have previously been found for the lens components in many SBO and SO galaxies (Kormendy 1977 ; Burstein 1979b). According to Kormendy (1979), their intrinsic geometry is that of a slightly triaxial, flattened ellipsoid with a preferred equatorial axial ratio $\sim$ 0.9 (see also Mebold et al 1979). If the inclination of NGC7070A is $i \sim 0^{\circ}$, the intrinsic axial ratio would equal the apparent value of 0.85. The kinematics of lenses have only recently been investigated (Kormendy 1981 a,b) but preliminary results suggest that they are, in fact, hot systems. The low line-of-sight velocity dispersion in Fig 5.6, then requires that the random motions be very anisotropic. Sanders and Van Albada (1979) have demonstrated that lenses could be produced by the resonant heating of bulge stars by a rotating bar. This heating is anisotropic in the required sense, being small perpendicular to the plane of rotation.

7.5 NGC 5626

The relatively faint apparent magnitude of this galaxy precluded a detailed mapping of the velocity and velocity dispersion fields. Spectra were obtained at two orthogonal position angles. The heliocentric redshift is $V_o = 6845 \pm 20$ km/sec so although the spatial resolution is poor, our observations extend over a significant fraction of the galaxy. It is evident from Fig 5.6 that NGC5626 rotates quite rapidly along PA = 135° ($V_m = 145 \pm 15$ kms^{-1}). There is no evidence of rotation at the orthogonal slit position, so we appear to have observed close to the kinematic major axis. Although the galaxy is quite round on the deep Schmidt plates (Hawarden et al 1981), the high resolution AAT plate in Fig 5.1 shows

that the inner regions are more elongated ($\varepsilon \sim 0.2$). There are large changes in the position angle of these isophotes (Fig 6.5), which may reflect an asymmetry in the dust distribution. The minor axis profile indicates that the disc is strongest in two well-defined rings at r = 6.5 and r = 10 arcsec. Only the latter is clearly visible near the foreground star in Fig 5.1.

The rapid rotation may indicate that NGC5626 is a lenticular galaxy with a large bulge/disc ratio. Observations of the dynamics of several luminous bulges by Kormendy and Illingworth (1981) have shown that all are rapid rotators and that the majority are consistent with rotationally flattened oblate models (§ 7.2). Because elliptical galaxies are <u>not</u>, in general, consistent with these models, the implication is that pure discless systems and the spheroidal components of disc galaxies undergo very different formation mechanisms. A serious difficulty in the comparison of elliptical and bulge properties, however, arises from their very different luminosity functions. Most of the observed bulges have much lower absolute magnitudes than those of normal ellipticals. Since recent observations of the dynamics of low-luminosity ellipticals (e.g. Tonry 1981 ; Fall 1982) have shown that rotational support plays a much more prominent role than at higher luminosities, further examples of rare high-luminosity bulges ($M_{B_T} < -21$) are urgently required.

Figure 7.7 illustrates a decomposition of the major axis surface brightness profile of NGC5626 into an $r^{1/4}$ bulge component and an exponential disc. The bulge/disc ratio is 1.30, which agrees well with a value of 1.45 obtained from an independent decomposition of the minor axis profile. Taking $B_T^o = 13.67$ from Table 7.1, the total absolute magnitude of the <u>bulge</u> component in NGC5626 is $M_{B_T^o}^{bulge} = -21.4 \pm 0.3$. The observations in Fig 7.2 therefore support the proposal that substantial

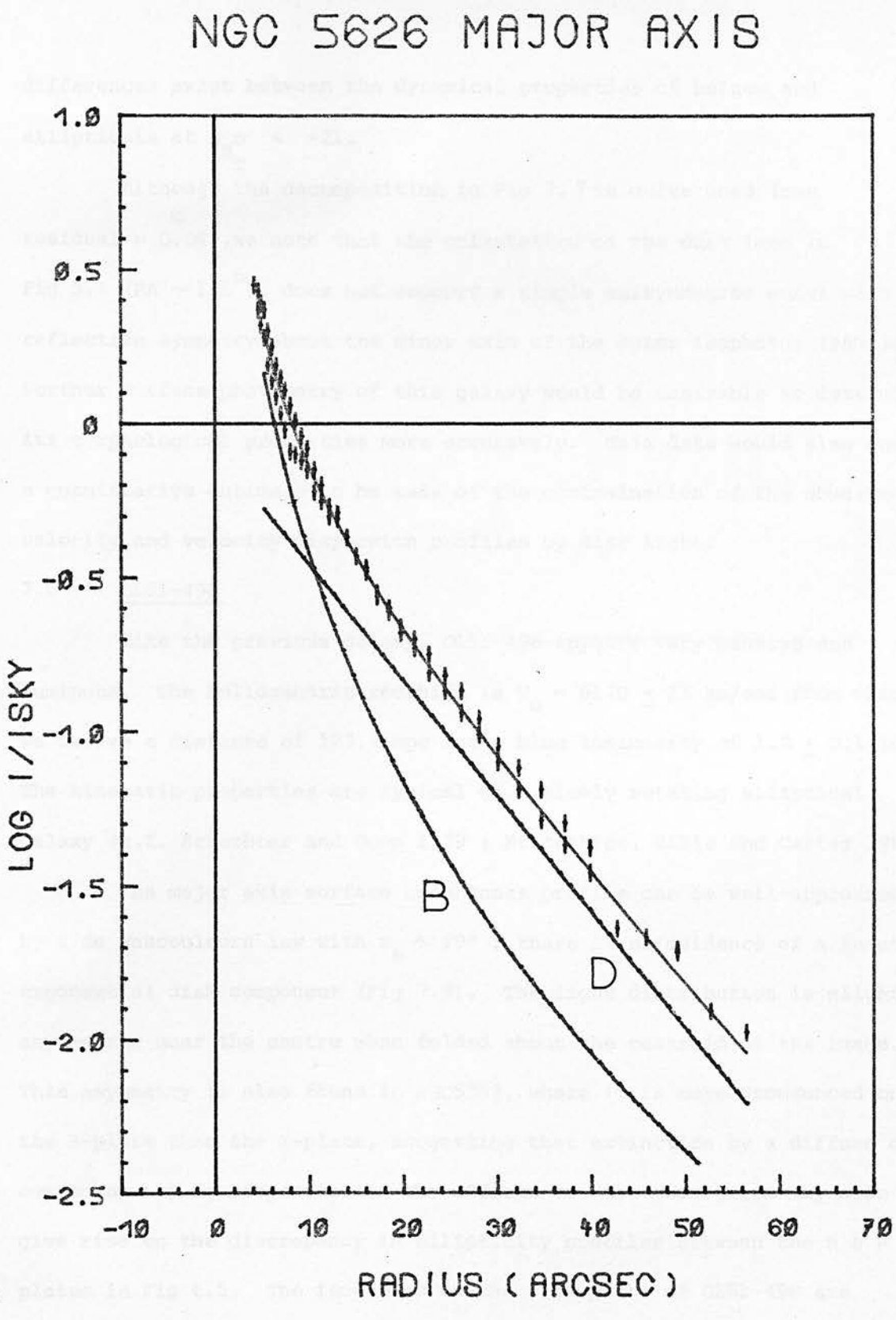

Figure 7.7 : Decomposition of the major axis profile of NGC5626 into an $r^{1/4}$ bulge (B) and an exponential disk (D). The solid line shows the sum of these two components. Scale lengths for this fit are r_e = 5" for the bulge and α = 11.5" for the disk.

differences exist between the dynamical properties of bulges and ellipticals at $M_{B_T}^o < -21$.

Although the decomposition in Fig 7.7 is quite good (rms residual = 0.04^m), we note that the orientation of the dust lane in Fig 5.1 (PA $\sim 135^\circ$), does not support a simple axisymmetric model with reflection symmetry about the minor axis of the outer isophotes (PA$\sim 180^\circ$). Further surface photometry of this galaxy would be desirable to determine its morphological properties more accurately. This data would also enable a quantitative estimate to be made of the contamination of the observed velocity and velocity dispersion profiles by disc light.

7.6 0151-498

Like the previous galaxy, 0151-498 appears very massive and luminous. The heliocentric redshift is $V_o = 6170 \pm 25$ km/sec from which we derive a distance of 123.4 Mpc and a blue luminosity of $1.0 \pm 0.1\ 10^{11}\ L_\odot$. The kinematic properties are typical of a slowly rotating elliptical galaxy (c.f. Schechter and Gunn 1979 ; Efstathiou, Ellis and Carter 1980).

The major axis surface brightness profile can be well-approximated by a de Vaucouleurs law with $r_e \sim 29"$; there is no evidence of a faint exponential disk component (Fig 7.8). The light distribution is slightly asymmetric near the centre when folded about the centroid of the image. This asymmetry is also found in NGC5363, where it is more pronounced on the B-plate than the I-plate, suggesting that extinction by a diffuse dust component may be responsible. The effects of dust absorption may also give rise to the discrepancy in ellipticity profiles between the B & R plates in Fig 6.5. The isophotes on the blue plate of 0151-498 are noticeably 'pear-shaped' (see Figs 5.1 and 6.2) which causes the apparent ellipticity to be overestimated when compared with the red plate. The origin of this asymmetric dust absorption is not understood. Heisler et al (1982) have proposed that the minor axis orbits in a rotating

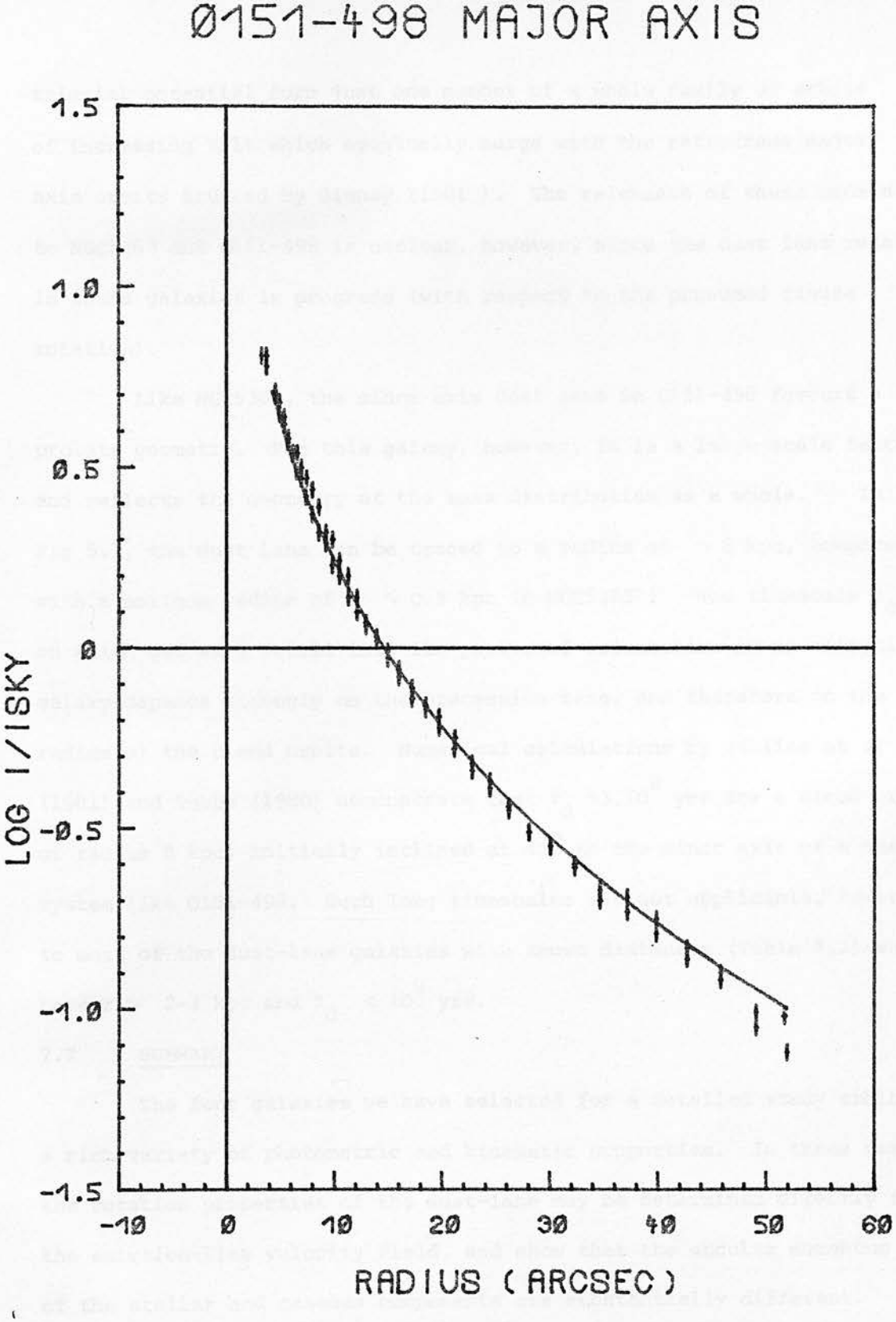

Figure 7.8 : Major axis luminosity profile of 0151-498, folded about the intensity-weighted centroid. The solid line is a de Vaucouleurs $r^{1/4}$ profile with r_e = 29". The asymmetry in the central regions can be seen more clearly in Fig 6.4.

triaxial potential form just one member of a whole family of orbits of increasing tilt which eventually merge with the retrograde major axis orbits studied by Binney (1981). The relevance of these models to NGC5363 and 0151-498 is unclear, however, since the dust lane rotation in these galaxies is prograde (with respect to the presumed figure rotation).

Like NGC5363, the minor axis dust lane in 0151-498 favours a prolate geometry. For this galaxy, however, it is a large-scale feature and reflects the geometry of the mass distribution as a whole. In Fig 5.1, the dust lane can be traced to a radius of $\sim$ 8 kpc, compared with a maximum radius of r $\sim$ 0.5 kpc in NGC5363 ! The timescale τ_d on which gas will settle into its preferred orientation in an elliptical galaxy depends strongly on the precession rate, and therefore on the radius of the cloud orbits. Numerical calculations by Tohline et al (1981) and Tubbs (1980) demonstrate that $\tau_d \sim 3.10^9$ yrs for a cloud orbit of radius 8 kpc, initially inclined at 45^o to the minor axis of a massive system like 0151-498. Such long timescales are not applicable, however, to most of the dust-lane galaxies with known distances (Table 4.2) which have r $\sim$ 2-3 kpc and $\tau_d < 10^9$ yrs.

7.7 SUMMARY

The four galaxies we have selected for a detailed study exhibit a rich variety of photometric and kinematic properties. In three cases the rotation properties of the dust-lane may be determined directly from the emission-line velocity field, and show that the angular momentum axes of the stellar and gaseous components are substantially different. The likelihood that the gas is the product of stellar mass loss is therefore exceedingly small.

The stellar kinematics of NGC5363 have been compared with a class of tumbling prolate models. It appears that this type of model can

qualitatively explain many of the observed properties if the pattern speeds are fairly low. NGC7070A is probably a face-on early-type disc galaxy with a prolate or triaxial bulge. The morphology of the dust-lane suggests that it is unlikely to be in equilibrium in this case. Our observations of NGC5626 are consistent with the dynamics of a rotationally flattened luminous bulge similar to those studied by Kormendy and Illingworth (1981). Combined with a preliminary optical zero-point for the photographic surface photometry, this supports recent suggestions that the dynamics of luminous bulges and those of ellipticals are substantially different. Perhaps the only bone-fide elliptical in the present sample is 0151-498. The low rotation velocities are characteristic of many morphologically normal ellipticals, but the orientation of the dust-lane favours a prolate geometry in this case.

The origin of the dust-lanes in these galaxies is not well understood. Accretion and merger events provide a possible explanation. Since two of the galaxies in our sample (NGC5363 and NGC7070A) have late-type spiral companions, tidal acquisition of the gas must also be considered. NGC7070 contains large amounts of neutral hydrogen, as expected, but no HI emission has been detected using a 15 arcmin beam at the position of NGC7070A (D. Carter, private communication). Haynes and Giovanelli (1981) detected a moderate amount of gas in NGC5363, but there is no evidence of any HI stream linking this galaxy to the gas-rich spiral NGC5364 (Haynes 1981). We conclude that there is no direct evidence, at the present time, to support a tidal origin for the dust and gas in these two galaxies.

CHAPTER 8

CONCLUSIONS AND PROSPECTS FOR FUTURE WORK

The final section of Chapter 1 contains a summary of several outstanding questions concerning the observable properties of elliptical and lenticular galaxies with dust-lanes. In this thesis are presented the results of new investigations, in the optical and infrared spectral regions, whose aim was to provide some of the answers to these questions and to put some of the more speculative theories on a sound factual basis.

The most detailed studies we have made are the spectroscopic and photographic measurements of four galaxies described in Chapters 5, 6 and 7. Although these galaxies were selected from a homogeneous survey of'elliptical-like' systems, in which no luminous discs were visible on the UK Schmidt survey plates, a more quantitative approach has shown the diversity of morphological and kinematic properties which may be found within this sample. It is likely that only one of the four galaxies is, in fact, a 'true' elliptical. Surface brightness profiles along the principal axes of the remaining three galaxies show an excess of light above the empirical $r^{1/4}$ law which provides a good fit to most morphologically normal ellipticals. Less ambiguous evidence comes from the kinematic data. Very few of the luminous elliptical galaxies studied by previous workers, rotate as rapidly as NGC5363 or NGC5626. In contrast, the bulge components in disc systems do seem to have a comparable fraction of rotational kinetic energy. NGC5626 is particularly important in this respect since it provides a very rare example of a high-luminosity bulge with $M_B < -21$. The discrepancy in dynamical properties between luminous bulges and ellipticals appears to be a serious problem for the classical

collapse picture of galaxy formation, which must contain enough dissipation to produce colour gradients in ellipticals (hitherto understood only on the basis of dissipative infall) without the formation of even a weak disc and hence a contradiction with the observed dynamics of large bulge/disc systems.

Until recently, the consensus of opinion held that the three-dimensional shape of elliptical galaxies was that of an oblate spheroid, although any theoretical justification for this idea had disappeared with the first observations of their low rotation velocities. The dust-lanes in NGC5363 and 0151-498, however, are more consistent with the morphological and kinematic properties of equilibrium gas discs in a prolate mass distribution. There is no minor axis rotation in the stellar component of these two galaxies, contrary to the predictions of some recent stellar dynamical models of prolate systems. Since the angular momentum properties of the dust-lanes are very different from those of the stellar component, it is also extremely unlikely that this material arises internal to the galaxy due to mass-loss from late-type stars. An explicit external source for the gas has yet to be identified in any individual case.

Further observations of the major axis stellar rotation curve in NGC5363 would allow us to determine the kinematic properties of the outer disc-like component more clearly, and to compare them with the rotation of the neutral and ionised gas. On the theoretical side, we urgently require N-body simulations which include the effects of near-singular central densities on the stellar streaming motions within the figure of a rotating bar. Work on this latter problem is now underway by various groups.

The aims of the infrared survey in Chapter 2, were to study the incidence of nuclear activity in dust-lane galaxies, as evidenced by excess infrared emission, and to identify individual cases worthy of further

observations at longer wavelengths. It is clear that a source of raw material is necessary to fuel any nuclear activity, whether interpreted as non-thermal emission processes or as recent star formation bursts, but an empirical test was required to determine if the presence of such a reservoir in these early-type systems materially increased the probability of such activity being observable. The results from Chapter 2 indicate that there is no large population of dust-lane galaxies with strong nuclear infrared emission. Optical spectra of the discless sample, presented in Chapter 4, also confirm that the fraction with emission lines is consistent with the 20-25% expected from previous surveys of morphologically normal galaxies. The prototype dust-lane elliptical, NGC5128, whose bright nuclear infrared source would be easily identifiable at the mean depth of the IR survey in Chapter 2, is clearly exceptional in these respects. The modest infrared excess found in a small proportion of the sample, appears to occur primarily in systems exhibiting at least weak signs of a luminous disc. A fair comparison of the colour distributions in this subsample awaits an unbiased survey of infrared-colours in early-type disc galaxies, since published data has been heavily biased by the selection procedures adopted.

The most peculiar object found in this survey is undoubtedly NGC7172, whose extreme infrared-excess was totally unexpected when the first observations were obtained at SAAO. It is pertinent to note that Piccinotti et al (1982) have recently included NGC7172 as the only normal galaxy in their complete HEAO-A2 hard X-ray sample ! The infrared variability and optical emission-line spectrum discussed in Chapter 3, both confirm the presence of an unusually active nucleus in this heavily obscured galaxy.

Obscuration can play a crucial role in the recognition of active nuclei, as evidenced by the tendency for optically-selected Seyferts to be

face-on and the absence of this effect in recent X-ray selected samples. NGC7172 is clearly a promising candidate for further study of the physical processes associated with an obscured active nucleus in a relatively nearby galaxy.

A completely different observational approach has been used in Chapter 4, where new photometric and spectroscopic observations have been combined with data from other sources to provide representative values for the mean optical properties of the discless galaxy sample as a whole. The normal UBV colours (for an old stellar population) imply that massive star formation in these galaxies was substantially complete some 10^9 years ago. There is no tendency for dust-lanes to occur preferentially in low-luminosity systems, so the fraction of all ellipticals containing large-scale dust features is likely to be < 0.1%. Since the timescale over which differential precession can align a dust-lane with one of the principal axes of the light distribution is $\sim 10^9$ yrs, the proposed accretion or merger events which provide the visible gas and dust in these galaxies need occur only infrequently. The cosmological implications of dust-lane galaxies lie in the importance of established cases of this scenario, for the evolution of early-type galaxies and the interstellar matter within them.

Velocities (V), dispersions (σ) and line strengths (γ) from the Fourier Quotient (FQ) and Cross-Correlation (CC) methods. V_o is the systemic velocity used to derive Figure 5.6 and ΔV the heliocentric correction. Radial distances are measured with the convention that negative radii have lower increment numbers. This can be related to the slit positions in Figure 5.1 by noting that position angles θ are measured N through E, and that when θ=0, increment 1 is N of increment 56.

R(")	V(CC)	V(FQ)	Err	σ(CC)	σ(FQ)	Err	γ(FQ)	Err
NGC 5363	Major Axis	PA=135	V_o=1119	ΔV=+1				
-59.8	1284	1270	47	...	...	..	...	...
-46.8	1267	1250	40	...	...	..	...	...
-37.7	1219	1201	43	...	...	..	...	...
-29.9	1263	1256	30	150	148	32	0.58	0.12
-23.4	1264	1257	17	125	132	20	0.76	0.12
-18.2	1272	1262	17	191	178	17	0.94	0.12
-14.3	1274	1270	17	164	160	18	0.96	0.13
-11.7	1257	1241	20	188	213	19	0.99	0.13
-9.1	1268	1245	18	199	194	17	1.15	0.11
-6.5	1274	1255	15	194	215	14	1.17	0.10
-3.9	1222	1213	15	209	211	14	1.07	0.09
-1.3	1155	1149	17	229	236	16	1.21	0.09
1.3	1048	1054	13	189	204	12	1.12	0.06
3.9	1025	1018	12	188	192	12	0.99	0.07
6.5	1013	1030	16	178	184	16	0.92	0.09
9.1	1012	1018	17	143	180	19	0.91	0.11
11.7	1006	1017	20	171	173	20	0.95	0.13
14.3	998	1009	18	152	180	20	1.07	0.15
18.2	993	1000	19	167	153	20	0.85	0.12
23.4	1004	1000	22	101	102	30	0.70	0.11
29.9	1008	1002	23	120	118	27	0.70	0.12
39.0	1046	1034	27	127	127	32	0.67	0.13
49.4	981	967	35	...	...	..	...	...
59.8	926	916	36	...	...	..	...	...
68.7	967	959	52	...	...	..	...	...
NGC 5363	Dust Lane	PA=45	V_o=1127	ΔV=+1				
-60.8	1072	1044	76	...	...	..	...	...
-49.1	1113	1125	50	...	...	..	...	...
-38.7	1108	1115	33	...	...	..	...	...
-29.6	1099	1130	30	141	174	33	0.88	0.14
-23.1	1154	1162	33	229	206	30	0.69	0.16
-17.9	1136	1131	18	189	173	18	0.86	0.12
-14.0	1092	1105	23	181	191	22	0.82	0.14
-11.4	1121	1123	23	221	191	21	0.84	0.13
-8.8	1114	1120	18	171	218	18	1.04	0.12
-6.2	1126	1133	19	201	244	18	1.03	0.11
-3.6	1135	1130	19	176	205	19	0.93	0.08
-1.0	1100	1108	16	201	241	15	1.24	0.08
1.6	1101	1102	17	219	221	16	0.99	0.07
4.2	1150	1157	21	...	...	..	...	...
9.4	1086	1084	25	202	188	24	0.69	0.11
11.9	1139	1148	21	248	216	19	1.00	0.15
14.6	1127	1125	24	195	191	23	0.98	0.16
18.5	1100	1100	25	198	197	23	0.86	0.13
23.7	1129	1163	37	272	205	32	0.66	0.16
30.2	1155	1154	38	174	169	38	0.69	0.14
39.3	1168	1168	34	...	...	..	...	...
49.7	1203	1222	51	...	...	..	...	...
60.1	1118	1137	55	...	...	..	...	...

R(")	V(CC)	V(FQ)	Err	σ(CC)	σ(FQ)	Err	ϒ(FQ)	Err
NGC 5363	Offset	Axis	PA=45	V_o=1125	ΔV=+1			
-49.1	1177	1150	37	...	...	..	...	...
-38.7	1154	1103	32	...	...	..	...	...
-29.6	1164	1169	25	...	...	..	...	...
-23.1	1174	1173	25	189	168	24	0.89	0.15
-17.9	1164	1160	28	182	165	27	0.83	0.13
-14.0	1189	1171	26	147	163	28	0.68	0.15
-11.4	1183	1185	16	193	172	16	0.98	0.14
-8.8	1219	1204	18	212	196	16	0.93	0.13
-6.2	1228	1219	19	199	192	18	1.07	0.11
-3.6	1229	1226	15	219	211	14	1.20	0.10
-1.0	1253	1244	11	224	223	11	1.24	0.09
1.6	1242	1228	14	218	231	13	1.25	0.10
4.2	1220	1210	12	207	196	12	1.15	0.10
6.8	1193	1197	17	190	212	17	1.17	0.13
9.4	1168	1171	19	197	208	18	1.15	0.14
12.0	1197	1183	23	216	221	21	1.12	0.17
14.6	1179	1171	21	161	166	22	1.07	0.16
18.5	1175	1177	25	169	190	25	0.92	0.14
23.7	1195	1209	33	177	202	32	0.82	0.18
30.2	1032	1055	44	...	...	..	...	...
39.3	1141	1144	41	...	...	..	...	...
49.7	1188	1190	42	...	...	..	...	...
NGC 5363	Skew	Axis	PA=90	V_o=1114	ΔV=+1			
-59.8	1264	1233	58	...	...	..	...	...
-46.8	1128	1166	48	...	...	..	...	...
-35.1	1264	1260	36	164	177	37	0.77	0.16
-26.0	1221	1216	30	167	188	30	0.85	0.16
-19.5	1221	1207	31	163	189	31	0.71	0.16
-14.3	1176	1191	28	157	209	29	0.82	0.14
-10.4	1171	1179	25	200	191	23	0.99	0.16
-7.8	1219	1215	22	229	245	20	1.07	0.16
-5.2	1209	1189	21	249	228	19	1.04	0.13
-2.6	1178	1188	23	224	208	21	0.91	0.12
0.0	1144	1150	19	193	207	18	0.85	0.09
2.6	1072	1079	15	185	193	15	1.03	0.07
5.2	1028	1029	12	213	192	11	1.15	0.08
7.8	1048	1049	13	160	193	14	1.04	0.09
10.4	1037	1033	16	133	160	19	0.93	0.10
13.0	1031	1059	23	218	210	21	1.18	0.14
15.6	1043	1045	20	220	192	18	1.05	0.15
18.2	1016	1034	26	160	182	27	1.00	0.16
22.1	1039	1049	20	201	184	19	1.00	0.13
28.6	1009	1003	22	141	127	25	0.76	0.12
36.4	1032	1041	28	161	158	28	0.98	0.15
45.5	998	1016	30	...	...	..	...	...
57.2	1029	1039	39	...	...	..	...	...

R(")	V(CC)	V(FQ)	Err	σ(CC)	σ(FQ)	Err	Y(FQ)	Err
NGC 5363	Dust Lane (excluding NaD line)					PA=45	V_o=1135	ΔV=+1
-60.8	1060	1045	66	...	...	..	...	...
-49.1	1119	1117	41	...	...	..	...	...
-38.7	1094	1095	28	...	...	..	...	...
-29.6	1088	1140	30	104	167	37	0.80	0.15
-23.1	1115	1163	29	134	207	31	0.75	0.15
-17.9	1162	1147	18	156	173	18	0.90	0.15
-14.0	1101	1121	19	167	188	19	0.80	0.15
-11.4	1140	1134	21	230	187	19	0.85	0.15
-8.8	1129	1121	18	141	205	19	0.90	0.15
-6.2	1124	1145	18	171	221	17	0.90	0.10
-3.6	1139	1135	18	147	177	19	0.75	0.10
-1.0	1100	1111	14	173	225	14	1.05	0.10
1.6	1101	1111	17	206	210	16	0.80	0.10
4.2	1140	1156	34	...	...	..	...	...
9.4	1090	1099	33	210	175	35	0.55	0.10
11.9	1137	1149	20	264	217	18	1.00	0.15
14.6	1131	1129	24	198	172	22	0.75	0.15
18.5	1101	1110	24	186	194	22	0.80	0.15
23.7	1248	1172	37	148	214	37	0.60	0.15
30.2	1176	1167	33	139	161	34	0.60	0.15
39.3	1166	1168	31	...	...	..	...	...
49.7	1222	1236	41	...	...	..	...	...
>60.1	1170	1189	80	...	...	..	...	...
NGC 5626	Minor Axis		PA=45	V_o=6855	ΔV=+4			
-21.1	6799	6826	43	...	...	..	...	...
-6.8	6870	6866	34	222	187	31	0.87	0.20
-2.9	6844	6838	21	268	219	19	1.04	0.15
-0.3	6857	6851	17	273	260	15	1.20	0.11
2.3	6867	6864	17	266	236	16	1.09	0.12
4.9	6833	6832	23	247	214	21	1.08	0.18
8.8	6876	6911	37	219	246	33	0.88	0.22
17.9	6890	6863	41	...	...	..	...	...
NGC 5626	Major Axis		PA=135	V_o=6836	ΔV=+4			
-21.6	7022	7014	38	...	...	..	...	...
-8.6	6951	6944	28	...	...	..	...	...
-4.7	6961	6930	23	270	270	20	1.19	0.20
-2.1	6860	6859	20	290	269	17	1.12	0.13
-0.5	6854	6840	17	263	272	15	1.17	0.11
3.1	6794	6805	22	298	255	20	1.20	0.15
5.7	6696	6727	32	323	251	28	1.01	0.22
9.6	6676	6683	35	...	...	..	...	...
22.6	6715	6720	29	...	...	..	...	...
NGC 7070A	Major Axis		PA=209	V_o=2352	ΔV=+39			
-26.5	2353	2351	27	...	...	..	...	...
-14.8	2361	2357	22	109	101	28	0.89	0.13
-8.3	2342	2338	22	105	117	29	0.82	0.14
-4.4	2356	2353	25	85	84	37	0.82	0.14
-1.8	2340	2340	16	102	98	22	0.99	0.11
0.8	2353	2350	16	105	114	22	0.98	0.11
3.4	2360	2358	16	134	119	18	0.93	0.13
6.0	2344	2341	22	114	112	27	0.76	0.14
9.9	2368	2358	20	63	61	37	0.75	0.11
12.7	2315	2312	30	89	85	42	0.61	0.13
30.7	2409	2391	58	...	...	..	...	...

R(")	V(CC)	V(FQ)	Err	σ(CC)	σ(FQ)	Err	Y(FQ)	Err
NGC 7070A Minor Axis PA=346 V_o=2351 ΔV=+39								
-25.2	2323	2333	32	92	89	44	0.80	0.13
-8.3	2342	2348	23	126	124	26	0.99	0.17
-5.7	2346	2345	20	145	152	21	1.13	0.20
-3.1	2346	2351	18	106	108	24	0.98	0.13
-0.5	2357	2359	14	117	116	18	1.11	0.11
2.1	2352	2346	18	90	91	26	0.87	0.11
4.7	2353	2347	18	115	129	22	1.00	0.15
8.6	2341	2343	22	66	60	39	0.67	0.12
22.9	2398	2392	29	77	113	45	0.79	0.14
NGC 7070A Bright Edge PA=346 V_o=2364 ΔV=+39								
-21.6	2369	2372	21	96	106	29	1.11	0.14
-12.5	2350	2353	21	58	55	41	0.78	0.13
-7.3	2362	2357	17	92	88	25	0.91	0.12
-3.4	2363	2363	20	82	86	30	0.86	0.15
-0.8	2345	2348	22	105	109	29	0.75	0.14
1.8	2384	2382	18	104	96	24	0.82	0.13
4.4	2365	2364	19	74	82	31	0.79	0.14
8.3	2371	2368	20	92	93	28	0.86	0.13
18.7	2368	2370	22	67	84	38	0.78	0.12
NGC 7070A Dust Lane PA=346 V_o=2362 ΔV=+39								
-35.1	2426	2408	50	...	...	..	...	...
-23.4	2362	2361	30	...	...	..	...	...
-16.9	2350	2351	27	95	93	36	0.69	0.14
-11.7	2364	2358	21	97	90	29	0.69	0.12
-7.8	2368	2366	25	101	123	33	0.92	0.16
-5.2	2332	2329	19	88	78	27	0.84	0.13
-2.6	2371	2375	16	119	130	20	1.08	0.12
0.0	2352	2350	15	98	104	21	1.01	0.08
2.6	2342	2343	14	91	101	21	0.99	0.09
5.2	2345	2346	18	90	91	27	0.96	0.13
7.8	2330	2334	22	63	77	41	0.81	0.14
11.7	2367	2365	22	98	98	30	0.96	0.14
18.2	2385	2396	26	98	115	36	0.89	0.16
26.0	2406	2404	37	...	...	..	...	...
37.7	2338	2344	35	...	...	..	...	...
NGC 7070A Skew Axis PA=256 V_o=2353 ΔV=+39								
-22.6	2343	2350	28	...	..	..	...	...
-8.3	2349	2351	17	99	101	24	0.95	0.13
-4.4	2359	2354	18	91	92	26	0.91	0.12
-1.8	2345	2348	14	88	92	21	0.98	0.09
0.8	2357	2353	12	97	96	18	1.04	0.09
3.4	2343	2345	15	95	97	21	0.82	0.11
6.0	2354	2352	16	98	94	23	0.84	0.13
9.9	2359	2358	23	61	81	42	0.73	0.13
22.9	2376	2371	34	...	...	..	...	...

R(")	V(CC)	V(FQ)	Err	σ(CC)	σ(FQ)	Err	γ(FQ)	Err
NGC 7070A Faint Edge PA=346 V_o=2338 ΔV=+39								
-30.2	2280	2275	47	...	...	..	...	...
-14.6	2363	2356	21	...	...	..	...	...
-6.8	2357	2359	22	95	105	30	0.84	0.14
-2.9	2335	2336	20	107	120	26	0.97	0.16
-0.3	2319	2319	15	104	102	20	0.98	0.12
2.3	2345	2347	15	100	101	21	0.98	0.13
6.2	2343	2341	22	113	107	27	0.91	0.13
12.7	2354	2351	21	81	93	32	0.91	0.13
25.7	2356	2350	25	...	...	..	...	...
UKS 0151-49 Dust Lane PA=270 V_o=6130 ΔV=+45								
-18.7	6110	6131	61	...	...	..	...	...
-9.6	6123	6139	38	298	237	33	1.08	0.25
-7.0	6120	6147	40	264	275	35	1.11	0.26
-4.4	6099	6095	28	298	292	25	1.26	0.19
-1.8	6115	6124	22	302	304	20	1.46	0.12
0.8	6134	6135	17	291	293	15	1.36	0.11
3.4	6155	6147	23	260	239	20	1.12	0.14
6.0	6086	6081	42	253	260	36	0.83	0.22
9.9	6186	6199	39	246	227	34	0.87	0.22
UKS 0151-49 Major Axis PA=180 V_o=6123 ΔV=+45								
-33.5	6016	6012	80	...	...	..	...	...
-19.2	6073	6078	31	...	...	..	...	...
-12.7	6090	6057	35	...	...	..	...	...
-8.8	6136	6116	34	267	229	30	0.98	0.21
-6.2	6120	6110	24	226	213	22	1.02	0.15
-3.6	6124	6112	19	287	283	16	1.40	0.14
-1.0	6103	6097	17	280	270	15	1.32	0.10
1.6	6148	6135	17	264	278	15	1.23	0.11
4.2	6155	6132	17	296	269	15	1.28	0.14
6.8	6161	6170	24	276	249	21	1.08	0.17
9.4	6172	6168	27	247	199	23	1.13	0.19
12.0	6196	6157	44	...	...	..	...	...
15.9	6177	6155	35	...	...	..	...	...
32.8	6151	6125	49	...	...	..	...	...

BIBLIOGRAPHY

AANESTAD, P.A., 1975, Astrophys. J., 200, 30.

AARONSON, M., 1977, Ph.D.Thesis : Harvard University.

AARONSON, M., FROGEL, J.A., and PERSSON, S.E., 1978a, Astrophys.J.,220,442.

AARONSON, M., FROGEL, J.A., and PERSSON, S.E., 1978b ,Astrophys.J., 223,824.

AARONSON, M., MOULD, J.R., and HUCHRA, J.P., 1980, Astrophys.J., 237, 655.

ALLEN, D.A., 1976, Astrophys. J., 207, 367.

ALLEN, D.A., and HYLAND, A.R., 1981,AAO Preprint No.152.

BAADE, W., and MINKOWSKI, R., 1954, Astrophys. J., 119, 215.

BABCOCK, T.A., 1976, AAS Photo-Bulletin No.13.

BAILEY, M.E., and MACDONALD, J., 1981, Mon.Not.R.ast.Soc.,194, 195.

BALDWIN, J.A., PHILLIPS, M.M., and TERLEVICH, R.,1981,Pub.Ast.Soc.Pacific, 93, 5 [BPT].

BALZANO, V.A., and WEEDMAN, D.W., 1981, Astrophys.J., 243, 756.

BECKLIN, E.E., FROGEL, J.A., KLEINMANN, D.E., NEUGEBAUER, G., NEY, E.P. and STRECKER, D.W., 1971, Astrophys.J.Lett., 171, L15.

BERTOLA, F., 1981, Sky & Telescope, 61, 380.

BERTOLA, F., and CAPPACCIOLI, M., 1975, Astrophys. J., 200, 439.

BERTOLA, F., and GALLETTA, G., 1978, Astrophys.J.Lett., 226, L115.

BINGGELLI, B., 1980, Astron.Astrophys., 82, 289.

BINNEY, J.J., 1976, Mon.Not.R.ast.Soc., 177, 19.

BINNEY, J.J., 1978, Mon.Not.R.ast.Soc., 183, 501.

BINNEY, J.J., 1980a, Mon.Not.R.ast.Soc., 190, 421.

BINNEY, J.J., 1980b, Mon.Not.R.ast.Soc., 190, 873.

BINNEY, J.J., 1980c, Phil.Trans.Roy.Soc.Lond.A, 296, 329.

BINNEY, J.J., 1981, Mon.Not.R.ast.Soc., 196, 455.

BINNEY, J.J., and de VAUCOULEURS, G., 1981, Mon.Not.R.ast.Soc., 194, 679.

BLACKMAN, C.P., 1979, Mon.Not.R.ast.Soc., 186, 1.

BLANDFORD, R.D., and REES, M.J., 1974, Mon.Not.R.ast.Soc., 169, 395.

BOKSENBERG, A., 1972, in 'Auxiliary Instrumentation for Large Telescopes' Proc.of the ESO-CERN Conference, eds. S. Lausten and A.Reiz, p.295.

BOKSENBERG, A., and BURGESS, D.E., 1973, in 'Astronomical Observations with Television-Type Sensors', ed. J.W.Glaspey.

BOLTON, J.G., STANLEY, G.J., and SLEE, O.B., 1949, Nature 164, 101.

BOLTON, J.G., WRIGHT, A.E., and SAVAGE, A., 1979, Aust.J.Phys.Supp., 46, 1.

BOTTINELLI, L., GOUGUENHEIM, L., and PATUREL, G.,1980,Astron.Astrophys.,88,32.

BRACEWELL, R.N., 1965, 'The Fourier Transform and its Applications' (New York: McGraw-Hill).

BRAULT, J.M., and WHITE, O.R., 1971, Astron.Astrophys.,13, 169.

BREGMAN, J.N., 1978, Astrophys. J., 224, 768.

BROCKLEHURST, M., 1971, Mon.Not.R.ast.Soc., 153, 471.

BUCKNELL, M.J., and PEACH, J.V., 1976, Observatory, 96, 61.

BURSTEIN, D., 1979a, AAS Photo-Bulletin No.20, p.6.

BURSTEIN, D., 1979b, Astrophys. J.Supp., 41, 435.

BURTON, W.B., 1976, Ann.Rev.Astron.Astrophys., 14, 277.

CALDWELL, C.N., and PHILLIPS, M.M., 1981, Astrophys. J., 244, 447.

CARTER, D., 1977, Mon.Not.R.ast.Soc., 178, 137.

CARTER, D., 1978, Mon.Not.R.ast.Soc., 182, 797.

CASSINELLI, J.P., 1979, Ann.Rev.Astron.Astrophys., 17, 275.

CHANDRASEKHAR, S., 1964, in 'Lectures in Theoretical Physics', Vol.6, eds. W.E.Britten and W.E.Chappell (Boulder:University of Colorado Press),p.1.

CHROMEY, F.R., 1973, Astron.Astrophys., 29, 77.

CHROMEY, F.R., 1974a, Astron.Astrophys., 31, 165.

CHROMEY, F.R., 1974b, Astron.Astrophys., 37, 7.

CONDON, J.J. and DRESSEL, L.L., 1978, Astrophys. J., 221, 456.

CONTOPOULOS, G., 1956, Astrophys. J., 39, 126.

COTTRELL, G.A., 1977, Mon.Not.R.ast.Soc., 184, 259.

COUSINS, A.J.W., 1973, Mem.R.ast.Soc., 77, 223.

DANZIGER, I.J., GOSS, W.M., and WELLINGTON, K.J., 1981, Mon.Not.R.ast.Soc., 196, 845.

DAVIES, R.L., 1981, Mon.Not.R.ast.Soc., 194, 879.

de BRUYN, A.G., and WILSON, A.S., 1978, Astron.Astrophys., 64, 433.

de VAUCOULEURS, G., 1959, Handbuch der Physik, 53, 275 (Berlin:Springer-Verlag).

de VAUCOULEURS, G., and CORWIN, H.G., 1977, Astrophys.J.Supp., 33, 219.

de VAUCOULEURS, G., de VAUCOULEURS, A., 1972, Mem.R.ast.Soc., 77, 1.

de VAUCOULEURS, G., and de VAUCOULEURS, A., 1964, 'Reference Catalogue of Bright Galaxies', (University of Texas Press) [RCBG].

de VAUCOULEURS, G., de VAUCOULEURS, A., and CORWIN, H.G., 1976, 'Second Reference Catalogue of Bright Galaxies' (University of Texas Press) [RC2].

DEMOULIN, M.H., 1969a, Astrophys. J., 157, 69.

DEMOULIN, M.H., 1969b, Astrophys. J., 157, 75.

DEMOULIN, M.H., 1969c, Astrophys. J., 157, 81.

DRESSLER, A., 1980, Astrophys. J., 236, 351.

EFSTATHIOU, G., ELLIS, R.S., and CARTER, D., 1980, Mon.Not.R.ast.Soc.,193,931.

EFSTATHIOU, G., ELLIS, R.S., and CARTER, D., 1982, AAO Preprint No.164.

EKERS, R.D., GOSS, W.M., KOTANYI, C.G., and SKELLERN, D.J., 1978, Astron.Astrophys. 69, L21.

ELVIS, M., MACCACARO, T., WILSON, A.S., WARD, M.J., PENSTON, M.V., FOSBURY, R.A.E., and PEROLA, G.C., 1978, Mon.Not.R.ast.Soc., 183,129.

FABER, S.M., 1977, in 'Evolution of Galaxies and Stellar Populations', eds. B.M.Tinsley and R.B.Larson (New Haven: Yale University Observatory) p.401.

FABER, S.M. and GALLAGHER, J.S., 1976, Astrophys.J., 204, 365.

FABER, S.M., and GALLAGHER, J.S., 1979, Ann.Rev.Astron.Astrophys., 17,135.

FABER, S.M., and JACKSON, R.E., 1976, Astrophys.J., 204, 668.

FABER, S.M.,BURSTEIN,D., and DRESSLER, A.,1977,Astron.J., 82, 941.

FALL, S.M., 1982, Preprint.

FELTEN, J.E., 1977, Astron. J., 82, 861.

FOSBURY, R.A.E., MEBOLD, U., GOSS, W.M., and DOPITA M.A., 1978, Mon.Not.R.ast.Soc., 183, 549.

FREEMAN, K.C., 1970, Astrophys. J., 160, 811.

FREEMAN, K.C., 1975, in 'Stars and Stellar Systems', Vol.IX, eds.A.Sandage and J. Kristian (University of Chicago Press), p.409.

FRIED, J., and ILLINGWORTH, G., 1981, in preparation.

FROGEL, J.A., PERSSON, S.E., AARONSON, M., BECKLIN, E.E., MATTHEWS, K., and NEUGEBAUR, G., 1975a, Astrophys.J., 195, 15.

FROGEL, J.A., PERSSON, S.E., and AARONSON, M., 1975b, Astrophys. J.Lett., 200, L123.

FROGEL, J.A., PERSSON, S.E., AARONSON, M., BECKLIN, E.E., and MATTHEWS, K., 1975c, in 'The Galaxy and the Local Group', RGO Bull. No.182, eds. R.J.Dickens and J.E.Perry, p.111.

FROGEL, J.A., PERSSON, S.E., AARONSON, M., and MATTHEWS, K., 1978, Astrophys. J., 220, 75.

GALLAGHER, J.S., and HUNTER, D.A., 1981, Astron.J., 86, 1312.

GALLAGHER, J.S., FABER, S.M., and BALICK, B., 1975,Astrophys.J.,202, 7.

GINSBERG, V., and SYROVATSKI, S., 1965, Ann.Rev.Astron.Astrophys, 3, 297.

GISLER, G.R., 1976, Astron.Astrophys., 51, 137.

GISLER, G.R., 1978, Mon.Not.R.ast.Soc., 183, 633.

GLASS, I.S., 1973, Mon.Not.R.ast.Soc., 164, 155.

GLASS, I.S., 1976, Mon.Not.R.ast.Soc., 175, 191.

GLASS, I.S., 1979, Mon.Not.R.ast.Soc., 186, 29P.

GLASS, I.S., 1981, Mon.Not.R.ast.Soc., 197, 1067.

GODWIN, J., 1976, Ph.D.Thesis, Oxford University.

GORDON, M.A., & Burton, W.B., 1976, Astrophys. J., 208, 346.

GOSS, W.M., DANZIGER, I.J., FOSBURY, R.A.E., and BOKSENBERG, A., 1980, Mon.Not.R.ast.Soc., 190, 23P.

GOTTESMAN, S.T., and WELIACHEW, L., 1977, Astrophys.J., 211, 47.

GRAHAM, J.A., 1979, Astrophys. J., 232, 60.

GRASDALEN, G.L., 1975, Astrophys. J., 195, 605.

GRASDALEN, G.L., and JOYCE, R.R., 1976, Astrophys. J., 208, 317.

GRIERSMITH, D., 1980a, Astron.J., 85, 1295.

GRIERSMITH, D., 1980b, Astron.J., 85, 1135.

GRIERSMITH, D., 1980c, Astron.J., 85, 789.

GRINDLAY, J.E., 1975, Astrophys. J., 199, 49.

GUNN, J.E. in 'Active Galactic Nuclei', eds. C.Hazard and S.Mitton (Cambridge: CUP), p.213 (1979).

GUNN, J.E., and GOTT, J.R., 1972, Astrophys.J., 176, 1.

GUNN, J.E., STRYCKER, L.L., and TINSLEY, B.M., 1981,Astrophys.J., 249,48.

HAWARDEN, T.G., ELSON, R.A.W., LONGMORE, A.J., TRITTON, S.B., and CORWIN, H.G., 1981, Mon.Not.R.ast.Soc., 196, 747.

HAYNES, M.P., 1981, Astron.J., 86, 1126.

HAYNES, M.P., and GIOVANELLI, R., 1981, Astrophys.J.Lett.,246, L105.

HAYNES, M.P., and ROBERTS, M.S., 1979, Astrophys.J., 227, 767.

HAYNES, R.F., HUCHTMEIER, W.K.H., SEIGMAN, B.C., and WRIGHT, A.E., 1975, 'A Compendium of Radio Measurements of Bright Galaxies' (Melbourne: CSIRO Division of Radiophysics).

HECKMANN, T.M., BALICK, B., and CRANE, P.C.,1980,Astron.Astrophys.Supp., 40, 295.

HEIDMANN, J., HEIDMANN, N., and de VAUCOULEURS, G., 1972,Mem.R.ast.Soc., 75, 85.

HEISLER, J., MERRITT, D., and SCHWARZSCHILD, M., 1982, Preprint.

HOHL, F., and ZANG, T.A., 1979, Astron.J., 84, 585.

HOLMBERG, E., 1958, Medd.Lund.Astr.Obs.Ser.II, 136, 1.

HUBBLE, E., 1926, Astrophys. J., 64, 321.

HUCHRA, J.P., 1977, Astrophys. J. Supp., 35, 171.

HUMASON, M.L., MAYALL, N.U., and SANDAGE, A.R., 1956, Astron.J.,61, 97.

HYLAND, A.R., and ALLEN, D.A., 1981, AAO Preprint No.152.

ILLINGWORTH, G., 1977, Astrophys. J. Lett., 218, L43.

ILLINGWORTH, G., 1981, in 'The Structure and Evolution of Normal Galaxies' eds. S.M.Fall and D.Lynden-Bell (Cambridge University Press),p.27.

JENKINS, C.R., 1981, Mon.Not.R.ast.Soc., 196, 987.

JOHNSON, H.L., 1966a, Astrophys. J., 143, 187.

JOHNSON, H.L., 1966b, Ann.Rev.Astron.Astrophys., 3, 193.

JOHNSON, H.L., 1968, in 'Stars and Stellar Systems' Vol.7, eds. B.M.Middlehurst and L.H.Aller (University of Chicago Press), p.167.

JOHNSON, D.W., and GOTTESMAN, S.T., 1979, in 'Photometry, Kinematics and Dynamics of Galaxies', ed. D.S.Evans (Austin:University of Texas Press), p.57.

JONES, T.J., and HYLAND, A.R., 1980, Mon.Not.R.ast.Soc., 192, 359.

JONES, T.W.,and STEIN, W.A., 1975, Astrophys.J., 197, 297.

JONES, T.W., O'DELL, S.L., and STEIN, W.A., 1974a, Astrophys. J., 188,353.

JONES, T.W., O'DELL, S.L., and STEIN, W.A., 1974b, Astrophys. J., 192, 261.

JURA, M., 1977, Astrophys. J., 212, 634.

KAHN, F.D., and WOLTJER, L., 1959, Astrophys. J., 130,705.

KEEL, W.C., 1980, Astron.J., 85, 198.

KING, I.R., 1966, Astron.J., 71, 64.

KING, I.R., 1978, Astrophys. J., 222, 1.

KLEINMANN, D.E., and WRIGHT, E.L., 1974, Astrophys.J., 191, L19.

KNAPP, G.R., KERR, F.J., and WILLIAMS, B.A.,1978, Astrophys.J., 222, 800.

KNAPP, G.R., KERR, F.J., and HENDERSON, A.P.,1979,ApJ. 234, 448.

KORMENDY, J., 1976, Ph.D.Thesis, California Institute of Technology.

KORMENDY, J., 1977, Astrophys. J., 218, 333.

KORMENDY, J., 1979, in 'Photometry, Kinematics and Dynamics of Galaxies', ed. D.S.Evans (University of Texas Press), p.341.

KORMENDY, J., 1981a, in 'Structure and Evolution of Normal Galaxies', eds. S.M.Fall and D.Lynden-Bell (Cambridge University Press),p.85.

KORMENDY, J., 1981b, Preprint.

KORMENDY, J., and BACHALL, J.N., 1974, Astron.J., 79, 671.

KORMENDY, J., and ILLINGWORTH, G., 1981, Preprint.

KOSKI, A.T., 1978, Astrophys.J., 223, 56.

KOTANYI, C.G., 1979, Astron.Astrophys., 74, 156.

KOTANYI, C.G., and EKERS, R.D., 1979, Astron.Astrophys., 73, L1.

KRIENKE, O.K., and HODGE, P.W., 1974, Astron.J., 79, 1242.

KRON, R.G., 1980, Astrophys. J. Supp., 43, 305.

LAKE, G., 1981a, Astrophys.J., 243, 111.

LAKE, G., 1981b, Astrophys. J., 243, 121.

LAMPTON, M., MARGON, B., and BOWYER, S., 1976, Astrophys.J.,208, 177.

LARGE, M.I., MILLS., B.Y., LITTLE, A.G., CRAWFORD, D.F., and SUTTON, J.M., 1981, Mon.Not.R.ast.Soc., 194, 693.

LARSON, R., TINSLEY, B.M., and CALDWELL, C. N., 1980,Astrophys.J., 237,692.

LAWRENCE, A., and ELVIS, M., 1981, Preprint.

LEACH, R., 1981, Astrophys.J., 248, 485.

LEBOFSKY, M.J., and RIEKE, G.H., 1979, Astrophys.J., 229, 111.

LEBOFSKY, M.J., and RIEKE, G.H., 1980, Nature, 284, 410.

LINDBLAD, B., 1956, Stockholm Obs.Ann., 19, No.2.

LO, K.Y., and SARGENT, W.L.W., 1979, Astrophys.J., 227, 756.

MALIN, D.F., and PETERSON, B.A., 1981, AAO Preprint.

MARCELIN, M., BOULESTEIX, J., COURTES, G., and MILLIARD, B.,1982,Nature,297,38.

MARCHANT, A.B., and OLSEN, D.W.,1979, Astrophys.J.Lett.,230, L157.

MARSHALL, F.E.,BOLDT,E.A.,HOLT, S.S.,MUSHOTZKY, R.F.,PRAVDO,S.H., ROTHSCHILD, K., and SERLEMITSOS, P.J.,1979,Astrophys.J.Supp.,40,657.

MARTIN, P.G., 1979, 'Cosmic Dust' (Oxford University Press).

MARTIN, R., and LUTZ, R.K., 1979, in 'Image Processing in Astronomy' eds. G. Sedmak, M.Cappaccioli and R.J.Allen (Observatorio Astronomico di Trieste), p.211.

MATTHEWS, W.G., and BAKER, J.C., 1971, Astrophys. J., 170,241.

McALAREY, C.W., McLAREN, R.A , CRABTREE, D.R., 1979, Astrophys.J.,234,471.

McHARDY, I.M., LAWRENCE, A., PYE, J.P., and POUNDS, K.A.,1981, Mon.Not.R. ast.Soc., 197, 193.

MEBOLD, U., GOSS, W.M., van WOERDEN, H., HAWARDEN, T.G., and SIEGMAN, B., 1979, Astron.Astrophys., 74, 100.

MICHARD, R., 1980, Astron.Astrophys., 91, 122.

MICHIE, R.W., 1963, Mon.Not.R. ast.Soc., 126, 499.

MIHALAS, D., and BINNEY, J.J., 1981, 'Galactic Astronomy' (San Francisco: Freeman), p.331.

MILLER, J.S., and MATTHEWS, W.G., 1972, Astrophys. J., 172, 593.

MILLER, R.H., and SMITH, B.F., 1979, Astrophys. J., 227, 785.

MILLS, B.Y., 1954, Observatory, 74, 248.

MINKOWSKI, R., 1954, Carnegie Yearbook, p.26.

MINKOWSKI, R., 1962, in 'Problems of Extragalactic Research', ed.G.McVittie (New York : Macmillan) p.112.

MINKOWSKI, R., and OSTERBROCK, D.E., 1959, Astrophys. J., 129, 583.

MOFFET, A.T., 1975, 'Stars and Stellar Systems', Vol.IX, eds.A. Sandage and J. Kristian (University of Chicago Press), p.211.

MORITA, K., and SAKASHITA, S., 1979, Prog. of Theor.Phys., 61, 94.

MORTON, D.C., and CHEVALIER, R., 1973, Astrophys. J., 179, 55.

MORTON, D.C., and ELMERGREEN, B.G., 1976, Astrophys. J., 205, 63.

MOULD, J.R., 1978, Astrophys. J., 220, 434.

NELDER, J.A., and MEAD, R., 1965, Computer J., 7, 308.

NEUGEBAUER, G., BECKLIN, E.E., OKE, J.B., and SEARLE, L., 1976, Astrophys.J., 205, 29.

NEUGEBAUER, G., OKE, J.B., BECKLIN, E.E., and MATTHEWS, K., 1979, Astrophys., J., 230, 79.

NILSSON, P., 1973, 'Uppsala General Catalogue of Galaxies' (Uppsala Astronomical Observatory).

OEMLER, A., and TINSLEY, B.M., 1979, Astron.J., 84, 985.

OKE, J.B., 1974, Astrophys. J.Supp., 27, 21.

OKE, J.B., and SANDAGE, A., Astrophys. J., 154, 21 (1968).

OKE, J.B., and SCHILD, R., 1971, Astrophys. J., 209, 214.

OSTERBROCK, D.E., 1960, Astrophys.J., 132, 325.

OSTERBROCK, D.E., 1974, 'Astrophysics of Gaseous Nebulae' (San Francisco: Freeman).

OSTERBROCK, D.E., 1977, in 'Active Galactic Nuclei', eds. C.Hazard and S. Mitton (Cambridge University Press), p.25.

OSTERBROCK, D,E., 1979, Astron.J., 84, 901.

PACHOLCZYCK, A.G., and WISNIEWSKI, W.Z., 1967, Astrophys.J., 147, 394.

PENCE, W.D., 1976, Astrophys. J., 203, 39.

PENSTON, M.V., PENSTON, M.J., SELMES, R.A., BECKLIN, E.E., and NEUGEBAUER, G., 1974, Mon.Not.R.ast.Soc., 169, 357.

PETROU, M., 1981, Mon.Not.R.ast. Soc., 196, 933.

PHILLIPS, M.M., 1979, Astrophys. J.Lett., 227, L121.

PHILLIPS, M.M., 1981, Mon.Not.R.ast.Soc., 197, 659.

PICCINOTTI, G., MUSHOTZKY, R.F., BOLDT, E.A., HOLT, S.S., MARSHALL, F.E., SERLEMITSOS, P.J., and SCHAFER, R.A., 1982, Astrophys.J.,253, 485.

POVEDA, A., 1958, Bol.Obs.Tonantzintla y Tacubaya, No.17.

POVEDA, A., ITURRIAGA, R., and OROZEO, I., 1960, Bol.Obs.Tonantzintla y Tacubaya, No.20.

PUSCHELL, J.J., 1981, Astron.J., 86, 16.

RAIMOND, E., FABER, S.M., GALLAGHER, J.S., and KNAPP, G.R., 1981, Astrophys. J., 246, 708.

REIF, K., MEBOLD, U., and GOSS, W.M., 1978, Astron.Astrophys., 67, L1.

RICHSTONE, D.O., 1979, Astrophys. J., 234, 825.

RIEKE, G.H., 1978, Astrophys. J., 226, 550.

RIEKE, G.H., and LEBOFSKY, M., 1979a, Ann.Rev.Astron.Astrophys., 17, 477.

RIEKE, G.H., and LEBOFSKY, M., 1979b, Astrophys. J., 227, 710.

RIEKE, G. H., and LOW, F.J., 1972, Astrophys., J.Lett, 176, L95.

RIEKE, G.H., LEBOFSKY, M., and KEMP, J.C., 1982, Astrophys. J.Lett., 252, L53.

RODGERS, A.W., 1978, Astrophys. J. Lett, 219, L7.

RUBIN, V.C., 1974, Astrophys. J., 191, 645.

SANDAGE, A.R., 1961, 'Hubble Atlas of Galaxies' (Washington : Carnegie Institution).

SANDAGE, A.R., 1973a, Astrophys.J., 183, 711.

SANDAGE, A.R., 1973b, Astrophys.J., 180,687.

SANDAGE, A.R., 1975, Astrophys. J., 202, 563.

SANDAGE, A.R., 1978, Astron.J., 83, 709.

SANDAGE, A.R., and TAMMANN, G.A., 1981, 'Revised Shapley-Ames Catalogue of Bright Galaxies' (Washington: Carnegie Institution).

SANDAGE, A.R., and VISVANATHAN, N., 1978a, Astrophys. J., 223, 707.

SANDAGE, A.R., and VISVANATHAN, N., 1978b, Astrophys.J., 225, 742.

SANDAGE, A.R., FREEMAN, K.C., and STOKES, N.R., 1970, Astrophys.J.,160, 831 [SFS].

SANDERS, R.H., 1980, Astrophys.J., 242, 931.

SANDERS, R.H., and VAN ALBADA, T.S., 1979, Mon.Not.R.ast.Soc., 189,971.

SARGENT, W.L.W., SCHECHTER, P.L., BOKSENBERG, A., and SHORTRIDGE, K., 1977, Astrophys. J., 212, 366 [SSBS].

SARGENT, W.L.W., YOUNG, P.J., BOKSENBERG, A., SHORTRIDGE, K., LYNDS, C.R., and HARTWICK, F.D.A.,1978, Astrophys. J.,221, 731.

SATOH, C., 1980, Pub.Ast.Soc.Japan, 32, 41.

SAVAGE, B.D., and MATHIS, J.S., 1979, Ann.Rev.Astron.Astrophys., 17, 73.

SCHECHTER, P.L., 1980, Astron.J., 85, 801.

SCHECHTER, P.L., and GUNN, J.E., 1978, Astron.J., 83, 1360.

SCHECHTER, P.L., and GUNN, J.E., 1979, Astrophys.J., 229, 472.

SCHWARZSCHILD, M., 1979, Astrophys. J., 232, 236.

SCHWEIZER, F., 1979, Astrophys.J., 233, 23.

SCHWEIZER, F., 1981, Astron.J., 86, 662.

SEARLE, L., 1971, Astrophys. J., 168, 327.

SERSIC, J.E., 1968. 'Atlas de Galaxias Australes' (Observatorio Astronomico Universidad Nacional de Cordoba).

SHANE, W.W., 1980, Astron.Astrophys., 82, 314.

SHUDER, J.M., 1980, Astrophys. J., 240,32.

SILK, J., and NORMAN, C., 1979, Astrophys. J., 234, 86.

SIMKIN, S.M., 1974, Astron.Astrophys., 31, 129.

SMYTH, R.J., 1980, Ph.D.Thesis, University of Edinburgh.

SMYTH, R.J., and STOBIE, R.S., 1980, Mon.Not.R.ast.Soc., 190, 631.

STARK, A.A., 1977, Astrophys.J., 213, 368.

STEIN, W.A., and WEEDMAN, D.W., 1976, Astrophys.J., 205, 44.

STEIN, W.A., GILLETT, F.C., and MERRILL, K.M., 1974, Astrophys.J., 187,213.

STRECKER, D.W,, ERICKSON, E.F., and WITTEBORN, F.C., 1979, Astrophys.J.Supp., 41, 501.

STROM, S.E., STROM, K.M., GOAD, J.W., VRBA, F.J., and RICE,W., 1976, Astrophys.J., 204, 684.

TELESCO, C.M., 1978, Astrophys.J.Lett., 226, L125.

TELESCO, C.M., and HARPER, D.A., 1980, Astrophys.J., 235, 392.

TERLEVICH, R., DAVIES, R.L., FABER, S.M. and BURSTEIN, D., 1981, Mon.Not.R.ast.Soc., 196, 381.

THUAN, T.X., and WADIAK, E.J., 1982, Astrophys.J., 252, 125.

TOHLINE, J.E., and DURISEN, R.H., 1982, Preprint.

TOHLINE, J.E., SIMONSON, G.F., and CALDWELL, N., 1981,
Astrophys. J.,252 , 92 (1982).

TONRY, J., 1981, Astrophys.J.Lett., 251, L1.

TONRY, J., and DAVIS, M., 1979, Astron.J., 84, 1511 [TD].

TONRY, J., and DAVIS, M., 1981a, Astrophys.J., 246, 666.

TONRY, J., and DAVIS, M., 1981b, Astrophys.J., 246, 680.

TOOMRE, A., and TOOMRE J., 1972, Astrophys.J., 178, 623.

TUBBS, A.D. 1980, Astrophys.J., 241, 969.

ULRICH, M.H., 1975, Pub.Astron.Soc.Pacific, 87, 965.

VAN ALBADA, T.S., KOTANYI, C.G., and SCHWARZSCHILD, M., 1982,
Mon.Not.R.ast.Soc., 198, 303.

VAN WOERDEN, H., 1977, in 'Topics in Interstellar Matter',
ed. H. Van Woerden (Dordrecht: Reidel), p.261.

VERON, P., LINDBLAD, P.O., ZUIDERWIJK, E.J., VERON, M.P., and ADAM, G.,
1980, Astron.Astrophys., 87, 245.

VISVANATHAN, N., and SANDAGE, A., 1977, Astrophys. J., 216, 214.

WADE, C.M., 1960, Observatory, 80, 235.

WARD, M.J., ALLEN, D.A., WILSON, A.S., SMITH, M.G., and WRIGHT, A.E.,
1981, AAO Preprint No.152.

WARD, M.J., WILSON, A.S., PENSTON, M.V., ELVIS, M., MACCACARO, T.,
and TRITTON, K.P., 1978, Astrophys.J., 223, 788.

WEEDMANN, D.W., 1977, Ann.Rev.Astron.Astrophys., 15, 69.

WEGNER, G., 1979, Astrophys.Space Sci., 60, 15.

WERNER, M.W., and SALPETER, E.E., 1969, Mon.Not.R.ast.Soc., 145, 249.

WESTERLUND, B.E., and SMITH, L.F., 1966, Aust.J.Phys., 17, 340.

WESTIN, B.A., 1980, Astron.Astrophys., 89, L11.

WHITFORD, A.E., 1958, Astron.J., 63, 201.

WHITFORD, A.E., 1971, Astron.J., 169, 215.

WHITMORE, B.C., KIRSCHNER, R.P., and SCHECHTER, P.L., 1979, Astrophys.J., 234, 68.

WILKINSON, A., and JAMES, R.A., 1982, Mon.Not.R.ast.Soc., 199, 171.

WILLIAMS, T.B., 1981, Astrophys.J., 244, 458.

WILLIAMS, T.B., and SCHWARZSCHILD, M., 1979, Astrophys.J., 227, 56.

WILLNER, S.P., BECKLIN, E.E., and VISVANATHAN, N., 1972, Astrophys.J., 175, 699.

WILSON, A.S., 1979, Proc.R.Soc.Lon.A., 366, 461.

WILSON, C.P., 1975, Astron.J., 80, 175.

WILSON, W.J., SCHWARTZ, P.R., NEUGEBAUER, G., HARVEY, P.M., and BECKLIN, E.E., 1972, Astrophys.J., 177, 523.

WOOLF, N.J., SCHWARZSCHILD, M., and ROSE, W.K., 1964, Astrophys.J., 140,853.

WRAY, J.D., and BENEDICT, S., 1974, Proc.Soc.Photo-Opt.Instr.Eng., 44, 137.

WYNN-WILLIAMS, C.G., et al, 1982, in preparation.

WYNN-WILLIAMS, C.G., and BECKLIN, E.E., 1974, Pub.Ast.Soc.Pacific, 86, 5.

YOUNG, P.J., SARGENT, W.L.W., BOKSENBERG, A., LYNDS, C.R., and HARTWICK, F.D.A., 1978, Astrophys.J., 222, 450.

ACKNOWLEDGEMENTS

I am extremely grateful to my supervisors, Andy Longmore and Mike Smith, who have provided advice, encouragement and criticism whenever required. Particular thanks must go to Andy for his continued enthusiasm for the project even when distanced by several thousand miles. The wealth of experience which I have been fortunate to be able to draw upon during our many observing runs has contributed greatly to the successful outcome of this work, even when the weather seemed determined to prevent such a conclusion.

On other occasions, I have had the pleasure of working at the telescope with Dave Carter, Tim Hawarden and Mauricio Tapia, who all provided good humour and common sense when most needed.

The extensive computing aspects of the spectroscopic and photographic work have benefitted from contacts with several people. I should particularly like to thank George Efstathiou, Dennis Kelly, Dave Carter, Clinton Blackman and Bernie McNally, for their valued help and contributions.

During my three years at Edinburgh, I was fortunate to have many useful discussions with Steve Heathcote, Becky Elson and fellow research students.

I am grateful to Mrs. S. Mellanby for her careful typing of the manuscript and to the staff of the ROE Photolabs for their incomparable photographic work.

Finally, I should like to thank Heather Scott for her painstaking labours on the diagrams and without whose understanding and support this thesis would never have been completed.